To my family

PROTON INDUCED X-RAY EMISSION AND ITS APPLICATION TO BIOMEDICAL ELEMENTAL ANALYSIS

by

NAWAL SHAFIG SHAKIR

DEPARTMENT OF PHYSICS

UNIVERSITY OF ASTON IN BIRMINGHAM

March, 1984

A dissertation submitted in fulfilment of
the requirements for the degree of
Doctor of Philosophy in Physics

University of Aston in Birmingham

SUMMARY

Proton Induced X-Ray Emission And Its Application To Biomedical Elemental Analysis

by

Nawal Shafig Shakir

Submitted for the degree of Ph.D. March 1984

A proton induced x-ray emission (PIXE) system has been used in elemental analysis of hair samples. The system utilises a 2.37 MeV beam of protons to excite characteristic x-ray emission in bombarded samples. A solid state Si(Li) detector, is used to detect a fraction of the emitted x-rays.

Calibration was accomplished using thin targets of standard foils. Calibration accuracy was also established in two independent comparisons using bovine liver Standard Reference Material 1577 and IAEA hair powder H H - 1.

An original computer program was written which calculates factors to be used to correct for the reduced x-ray yield in semi-thick or thick targets due to x-ray absorption and proton energy loss.

The wet digestion technique used for sample preparation is described in detail, and the use of liposomes as homogenisers is demonstrated.

The applicability of PIXE for multielement analysis is demonstrated. The method is used for the first time in a major systematic study on hair samples using one target analysis. The pathological states considered are hyperactive children and agitated elderly people. The main elements examined are S, K, Ca, Fe, Co, Ni, Cu, Zn, Se, Br, Hg and Pb. The minimum detectable limits are 1-10 ppm using 180 μg of dry hair and 25 μc irradiations for elements between K and Br. The significance of differences between the hair elements in control populations and in patients suffering from the pathological conditions are investigated.

Investigations of the possible linear and multiple-correlations between elements in each population are made. The work indicates that some elements do exhibit variation with pathological state, and that analysis of hair gives useful information about the subject. Conclusions and further suggestions are described for optimizing and extending the PIXE hair analysis.

Key Words: Analysis, Hair, Protons, X-rays, Hyperkinesis

ACKNOWLEDGEMENTS

I would like to express my extreme gratitude to my supervisor Dr.P.E.Francois, for his support, guidance and consideration at all times. Without his encouragement this work would not have been possible.

Thanks are also due to my associate supervisor Dr.D.Crumpton for his continual supervision of the work.

I wish to express my appreciation to Professor S.E.Hunt for extending the hospitality of his department.

Collaboration with numerous people from outside the Physics Department has been an especially rewarding aspect of this work. In particular I would like to acknowledge the following people: Dr.P.J.Barlow, Environmental Health Department in the University, who proved extremely helpful in supplying me with literature relevant to the hair analysis; Dr.L.G. Earwaker and the Dynamitron group, and Dr.J.Owen and Mrs.J.Blackband at the Radiation Centre.

The art work on the illustrations was expertly drafted by Mr.A.Marriott-Reynolds, and the manuscript was carefully and diligently typed by Mrs.A.Howell.

Finally, my deep gratitude to my husband, Wahib, and our

children, Nihad and Osama, for enduring so patiently the division of my attention during the time of this work.

This work was supported by the University of Khartoum, Sudan.

N.S.S.

CONTENTS

List of Tables

LIST OF FIGURES

CHAPTER I

INTRODUCTION

Over the last twenty years the importance of trace elements in various biological processes has been underlined. It has been shown that normal growth and health depend on the continuous and sufficient supply of certain elements, and the ability to assess levels of these elements is very important.

The biological effect of an element depends on its concentration in the organism, and these elements are sometimes present as parts-per-million or less, therefore, in sample analysis,factors like contamination, sample size, sample treatment, and the limits of detection are very important. Easily accessible biological samples that validly reflect the status of individuals are needed as well as sensitive and specific techniques for the assessment of levels. Proton Induced X-Ray Emission (PIXE) using hair as the biological sample could be a useful biomedical research tool.

The success and capability of proton induced x-ray analysis are illustrated by many authors who have reported the analysis of biological and medical specimens using a variety of sample preparation techniques. The method needs a proton accelerator of some MeV energy as well as nuclear equipment allowing one to detect

characteristic x-rays, but has several advantages. It is simultaneously multielemental and all elements of atomic number greater than 13 can be analysed, this makes PIXE valuable for studies requiring multielement information, as for example, in the study of trace element metabolism of patients or control populations where several elements may be of significance.

One can make use of nuclear reactions induced in the target by the incident beam to extend the analytical capability of the system to atomic number less than 13, Johansson et al (1976). It has high sensitivity, approximately ppm or less, which makes PIXE suitable for low elemental concentrations,and small sample masses may be used. It can be non destructive and the sample may be reanalysed using a different technique.

It is of interest to evaluate the capabilities of some competing techniques used in trace element analysis, for example, atomic absorption spectrometry (AAS), and nutron activation analysis (NAA).

AAS is one of the cheapest and most widely available techniques. It is more suited to the use of liquid samples, it is single element procedure but can be used to determine a series of individual elements in sequence. The technique is sensitive, many elements can be determined at the ppm level or less, it is suitable for most of the trace elements, but not for F and I (Hislop 1980).

In NAA the individual radioactivity in the irradiated sample can be measured in a number of ways, e.g. the emitted γ-radiation can be measured using an energy dispersive system, this has the advantage that a number of elements may be measured simultaneously. This technique with a larger sample mass gives practical concentration limits of 0.1 ppb or lower, Hislop (1980). The technique is suitable for most of the trace elements, but a number of elements are rather difficult to measure by NAA because unfavourable nuclear properties,for instance, F and Sn, Ryabukhin (1980)

Several interesting PIXE biomedical applications have appeared in the literature, some of these are given briefly as examples. In a project on blood serum from rheumatoid arthritis patients receiving gold salt treatment by Barrette et al (1979 a,b), abnormal concentrations of trace elements Cu and Zn were found in the patients. A systematic profile of the trace elements Cu, Zn and Au was established in rheumatoid arthritis at the onset and during the gold salt treatments.

PIXE analysis was applied to cancerous and normal sections of the same organ of patients, Maenhaut et al (1980). Substantial differences were observed between the trace element concentrations in cancerous and normal tissues with a marked decrease in the Cd concentration for all the malignant tissue sections, and increases in the K/Zn, Fe/Zn, Br/Zn and Rb/Zn ratios for cancerous sections

when compared with normal ones.

In an example of the use of hair analysis by PIXE for the determination of environmental contamination, Bodart (1978) used hair from 100 individuals in Mexico. Half of the samples showed higher Cr from individuals suspected of having Cr contamination, the other half were controls and had less Cr.

Several hair studies using different techniques for analysis have been reported, of those studies we mention the work by Barlow et al (1981) applying the AAS technique to the hair of a population of Downs Syndrome patients. They compared with a control group and found abnormally low levels of manganese, calcium and possibly copper in the Downs syndrome patients. The work by Johannesson et al (1981) used NAA in hair samples taken from 58 persons living inside and outside areas with known volcanic activities, where large amounts of Hg were known to be emitted. Hg, As, Cd, Se and Zn were determined, low levels of As and Hg were reported. They concluded that volcanic activity did not appear to increase the body burden of Hg in that population.

This thesis describes biomedical applications of proton induced x-rays technique to hair analysis.

The material which follows is divided into a further five chapters. Chapter II examines theoretical aspects

of particle induced x-rays emission, including a discussion of background sources of radiation. Chapter III discusses experimental aspects of PIXE in terms of the following topics data collection, data interpretation, system calibration, sample preparation, sensitivity, and accuracy and precision considerations. Chapter IV is a general survey of trace elements. Chapter V describes in detail a study of the use of hair elemental analysis by PIXE in a medical application. The pathological states considered are hyperactive handicapped children, with non hyperactive handicapped children as controls, and an agitated demented elderly population with a non agitated demented elderly group as control. The elements measured are S, K, Ca, Fe, Co, Ni, Cu, Zn, Se, Br, Hg and Pb. Tests of significance are applied to compare hair elemental concentrations between the groups. An attempt is made to investigate possible linear and multiple-correlations between hair elements in each population. Chapter VI gives a summary, conclusions and suggestions for future work.

CHAPTER II

THEORY

II.A Introduction

Proton Induced X-Ray Emission, PIXE, analysis is one of several methods utilising x-ray emission for the determination of sample element concentration. The methods are commonly called x-ray fluorescence techniques. The x-ray fluorescence process basically involves removal of inner electrons from sample atoms, followed by rapid decay of the excited atoms to lower energy states. The decay consists of refilling the inner electron shells by electron transitions within the excited atoms. This process, occurring in 10^{-14} S or less, Fink (1966), releases the energy associated with the change in binding energy of the transition electrons. The energy is released as an x-ray photon or in ejecting an outer-shell electron, Since atoms of each element have unique energy levels, x-rays thus emitted have energies characteristic of their element of origin. Measurement of these x-ray energies then identifies the element present in the sample.

A number of sample excitation and x-ray detection methods have given rise to various, useful analytical methods with differing capabilities. Most x-ray fluorescence techniques can detect all elements except those of low

atomic number. The exact light element limit depends on the apparatus in question but usually one can detect from Si upwards in the periodic table. The limit exists because x-ray energies decrease with lower atomic numbers and a point is reached at which the x-rays no longer have sufficient energy to penetrate air paths and detector windows. Concentrations ranging from percentage levels to sub-parts per million may be determined by most x-ray fluorescence techniques, Gouding and Jaklevic (1977), Scheer et al (1977), Gilfrich et al (1973), Jaklevic and Walter (1977).

The PIXE analysis method used for the work reported here involves sample excitation through 2.37 MeV proton bombardment and x-ray energy analysis with a Si(Li) energy dispersion detector. Since low-energy protons have a short range of penetration, PIXE samples are limited to very thin (several milligrams per square centimeter) matrices. The usual method used was to prepare the sample in a liquid solution and to deposit a drop on a thin backing. Once dry, the target can be bombarded with a proton beam. The resulting x-rays were counted for a suitable time and the x-ray spectrum was analysed by computer to identify peaks and to relate peak areas to elemental quantities.

A typical PIXE spectrum is given, fig.2.1, for a bovine liver standard sample. The elements in the sample can be identified by their characteristic x-ray lines. These

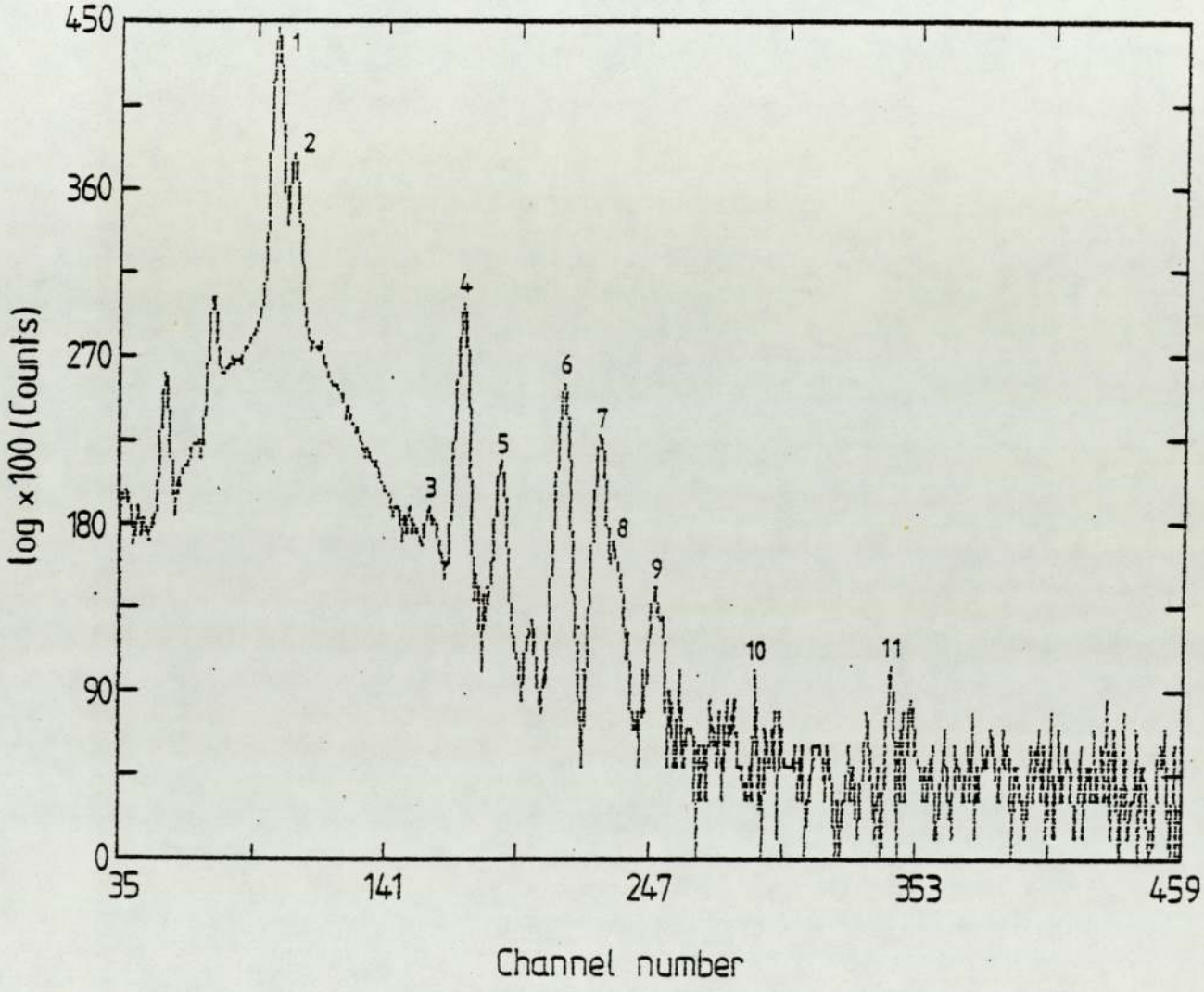

Fig 2.1 PIXE spectrum from the analysis of bovine liver.

1 - K (Kα)
2 - Ca (Kα)
3 - Mn (Kα)
4 - Fe (Kα)
5 - Fe (Kβ)
6 - Cu (Kα)
7 - Zn (Kα)
8 - Cu (Kβ)
9 - Zn (Kβ)
10 - Se (Kα)
11 - Rb (Kα)

lines are always superimposed on a broad smoothly varying x-ray bremstrahlung continuum. One can also see the interference between x-ray lines. The Kα and Kβ lines are in fact multiplets of two or more individual lines, but for the purposes of obtaining quantitative analysis of PIXE spectra, it is sufficient to treat K-line emission as two lines (Kα and Kβ).

It should be noted that in fig. 2.1 and in spectra to follow, the vertical axis represents the log of the x-ray counts multiplied by one hundred. As a consequence, the background and regions of a few counts are visually enhanced relative to the characteristic x-ray peaks.

The mechanism of x-ray production, can be viewed as a two step process involving first the creation of inner-shell vacancies by proton bombardment, and second the emission of characteristic x-rays as outer shell or free electrons drop in to fill the inner-shell vacancies, fig.2.2.

Details of each of these processes are discussed in the following sections.

II.B Interaction of Protons with Matter and Inner-Shell Vacancies Creation:

The description of the interaction of the accelerated protons with atoms is primary through Coulomb forces

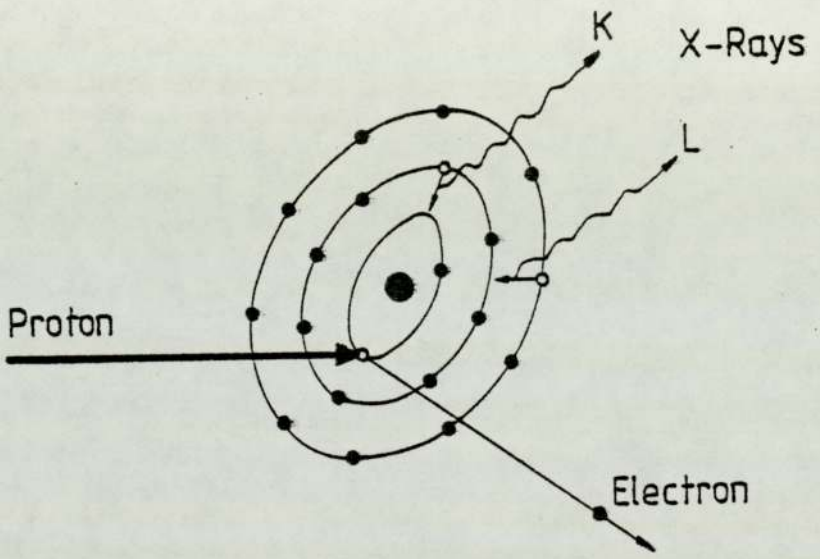

Fig 2:2 Production of Proton induced x-rays (schematic)

between their positive charge and negative charge of the orbital electrons within the atoms, although interactions of the protons with nuclei (as in Rutherford scattering or proton induced reactions) also are possible. Upon entering any absorbing target, the charged particle immediately interacts simultaneously with many electrons. In any one such encounter, the electron feels an impulse from the attractive Coulomb force as the particle passes its vicinity, Knoll (1979). Depending on the proximity of the encounter, this impulse may be sufficient to raise the electron to a higher lying shell within the absorber atom (excitation) or to completely remove the electron from the atom (ionization). The energy that is transferred to the electron must come at the expense of the charged particle, and its velocity is therefore decreased as a result of the encounter. It can be shown from conservation of momentum that the maximum velocity that an ion of velocity v can impart to a free electron is 2v; therefore the maximum energy, T_m, that an electron of mass m_o can receive from the impact of a proton with energy E_p and mass m is about $4 \frac{m_o}{m} E_p$. Because this is a small fraction of the total energy, the primary particle must lose its energy in many such interactions during its passage through the target. The products of these encounters are either excited or ionized atoms, each ionized atom is made up of a free electron and vacancy in the atomic structure. When the velocity of the ion has been reduced to a point at which it is comparable to the velocity of the valance electrons in an atom of

the target, the proton starts making elastic collisions with the atoms rather than exciting the atomic electrons, Friedlander et al (1981).

The inelastic collision between the charged particle and the electron may produce inner-shell ionization of the atom. The cross sections or the probabilities for inner-shell ionization by charged particle bombardment are relatively large.

Several different theoretical approaches have been used to describe the inner-shell ionization by charged particles from which the cross-sections and their variation with energy can be extracted. Early theoretical and experimental work has been summarised by Marzbacher and Lewis (1958), they presented a comprehensive quantum mechanical treatment of inner-shell ionization by protons in terms of the plane wave Born approximation (PWBA). This approach explains the dependence of ionization cross-sections on particle energy quantitatively at higher particle energies, while in the lower energy regions correction for the binding energy of the target atom electron and Coulombic deflection of the particle must be considered in order to obtain a quantitative description of the process, Basbas et al (1973), and Madison and Merzbacher (1975).

Quantum mechanical calculations of inelastic atomic processes are mathematically complicated. Consequently,

attention has been directed to a more simplified scheme of calculation that might be more manageable when carried to a higher order of approximations, the binary encounter approximation (BEA). Such a technique views the collision between a projectile and the complex atom as a binary encounter between the projectile and a particular active atomic electron. The rest of the target atom is regarded as a passive spectator in the collision, providing the environment in which the active electron moves, Garcia(1970). Madison and Merzbacher(1975), showed that at low energies the Born cross sections are about an order of magnitude larger than the binary encounter cross sections, so there is a disagreement of BEA when it is applied to ionization of specific subshells. Efforts by Hansen(1973), at improving the BEA, while retaining its fundamentally classical form, lead to computations which are as complicated as the quantum mechanical Born approximation.

Another approach is a semiclassical treatment (SCA) published by Bang and Hansteen(1959). Their approach treats the relative motion in terms of prescribed classical trajectories, while the atomic electrons have a fully quantum treatment, Hansteen(1973).

Brandt and Lapicki(1979) have pointed out that large discrepancies exist between experimental L-cross-sections and the plane wave Born approximation which can be accounted for by the CPSSR formulation of the plane wave Born approximation provided the projectile atomic number

is small compared to the target atomic number. This was accomplished by incorporating into the theory two effects not included into the PWBA. They are (i) the Coulomb repulsion (C) of the projectile by the target nucleus, and (ii) the increase in the binding energy of the inner shell electron to be ionized due to the proximity of the ionizing particle i.e. the polarization effect is incorporated in accordance with the perturbed stationary-state (PSS) approximation. This CPSS theory is developed further to include relativistic effects (R) of the target wave function through a procedure that reproduces the results of numerical calculations for heavy target atoms.

For detailed discussions of these various models one refers to current reviews by Madison and Merzbacher (1975), Garcia et al (1973), Hansteen (1975), and Brandt and Grzegorz Lapicki (1979). These are not sufficiently clear and easy to apply for practical PIXE analysis, from the practical view-point it is useful to know the behaviour of the cross-sections in terms of the energy and atomic number dependence. Khan et al (1977), Akselesson and Johansson (1974) have formulated empirical polynomial expressions based on experimental measurements which enables the cross-sections to be evaluated readily. The polynomials of Khan et al (1977) are based on their experimental measurements of K x-ray ionization cross sections of several elements between Z = 20 to 50 in the proton energy range 1 to 3 MeV. The equation for the

ionization cross-section, σ_{ion}, requires only the input of the atomic number, Z, and the proton energy, E_p, and is given by:

$$\ln(\sigma_{ion}) = (41.46 - 37.32E_p + 8.448E_p^2) - (12.212 - 21.242E_p + 4.864E_p^2)\ln Z - (0.0107 + 2.737E_p - 0.6551E_p^2)(\ln Z)^2 \qquad 2.1$$

Akselesson and Johansson (1974) derived an empirical formula for ionization cross section based on available thin target measurements. The K-shell cross-section data were fitted using a fifth degree polynomial curve given by:

$$\ln(\sigma_{k\,ion}\, I_k^2) = \sum_{i=0}^{5} b_i X^i \quad -3 \leq X \leq .8 \qquad 2.2$$

where

$b_o = 1.8451$ $\quad b_3 = 0.17481$

$b_1 = 0.60365$ $\quad b_4 = 0.11142$

$b_2 = -0.44481$ $\quad b_5 = 0.01941$

$X = \ln(10^{-3} E_p/I_k)$

I_k = the ionization energy in ev

E_p = the proton energy in ev

$\sigma_{k\,ion}$ = K-shell ionization cross-section in 10^{-14} cm^2

Johansson and Johansson (1976) developed a semi-empirical

formula for ionization cross section, the function for fitting is the same as used by Akselesson, the use of many more data points changes the coefficients slightly.

The calculation of cross sections production using Khan et al and Johansson and Johansson expressions are represented in fig.2.3 for proton energy 2.37 MeV. There is good agreement in the region of interest, $24 < Z < 32$, for lower Z Johansson is higher while for high Z Khan is higher with maximum difference of 10%.

Expressions 2.1 and 2.2 are particularly useful in calculating ionization cross sections at arbitrary projectile energies E_p. For example in order to obtain quantitative results for PIXE analysis of "thick" samples (i.e. samples in which the incident proton beam loses a significant fraction of its initial energy) correction must be applied to the observed x-ray yields to account for the changing x-ray emission cross-sections as the proton beam loses energy in the sample (Sec.IIIC.2). Table 2.1 contains useful values calculated from expression 2.2 for K-shell x-ray ionization cross sections for selected elements and proton energy 2.37 MeV. For energies between 1-3 MeV the ionization cross sections are represented graphically in fig.2.4.

For use in chemical analysis, the x-ray production cross section rather than the ionization cross sections is of interest. The ionization cross sections must be corrected

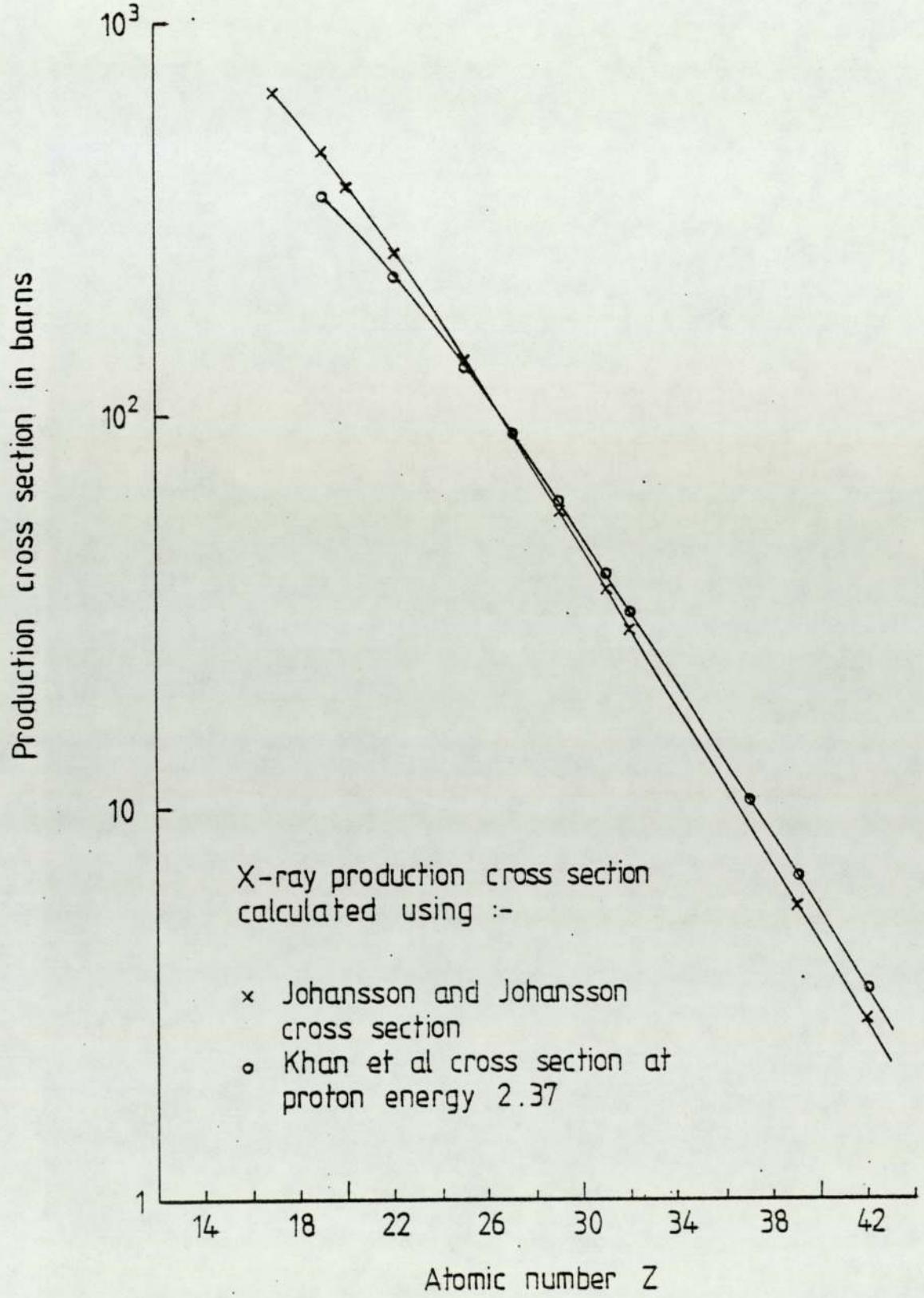

Fig 2:3 X-ray production cross section for 2·37 MeV

Table 2.1: Results of calculated ionization and production cross sections using equations 2.2 and 2.3

Element	Z	E_K keV	σ^{ion} barns	ω_K	σ^{pro} barns
Mg	12	1.303	48108.5	0.030	1443.26
Si	14	1.838	21293.4	0.050	1064.67
P	15	2.142	14598.3	0.063	919.69
S	16	2.470	10110.0	0.078	788.58
Cl	17	2.819	7070.9	0.097	685.88
K	19	3.607	3456.3	0.140	483.88
Ca	20	4.038	2434.9	0.163	356.89
Ti	22	4.964	1236.4	0.214	264.59
V	23	5.463	888.6	0.243	215.93
Cr	24	5.988	641.7	0.275	176.47
Mn	25	6.537	466.3	0.308	143.62
Fe	26	7.111	340.8	0.340	115.87
Co	27	7.709	250.7	0.373	93.51
Cu	29	8.980	138.1	0.440	60.76
Zn	30	9.66	103.1	0.474	48.87
Ga	31	10.368	77.4	0.507	39.24
Ge	32	11.103	58.4	0.535	31.24
As	33	11.863	44.3	0.562	24.897
Se	34	12.652	33.8	0.589	19.908
Br	35	13.475	25.8	0.618	15.94
Rb	37	15.2 1	15.3	0.667	10.205
Y	39	17.03	9.3	0.71	6.60
Mo	42	20.002	4.506	0.765	3.447

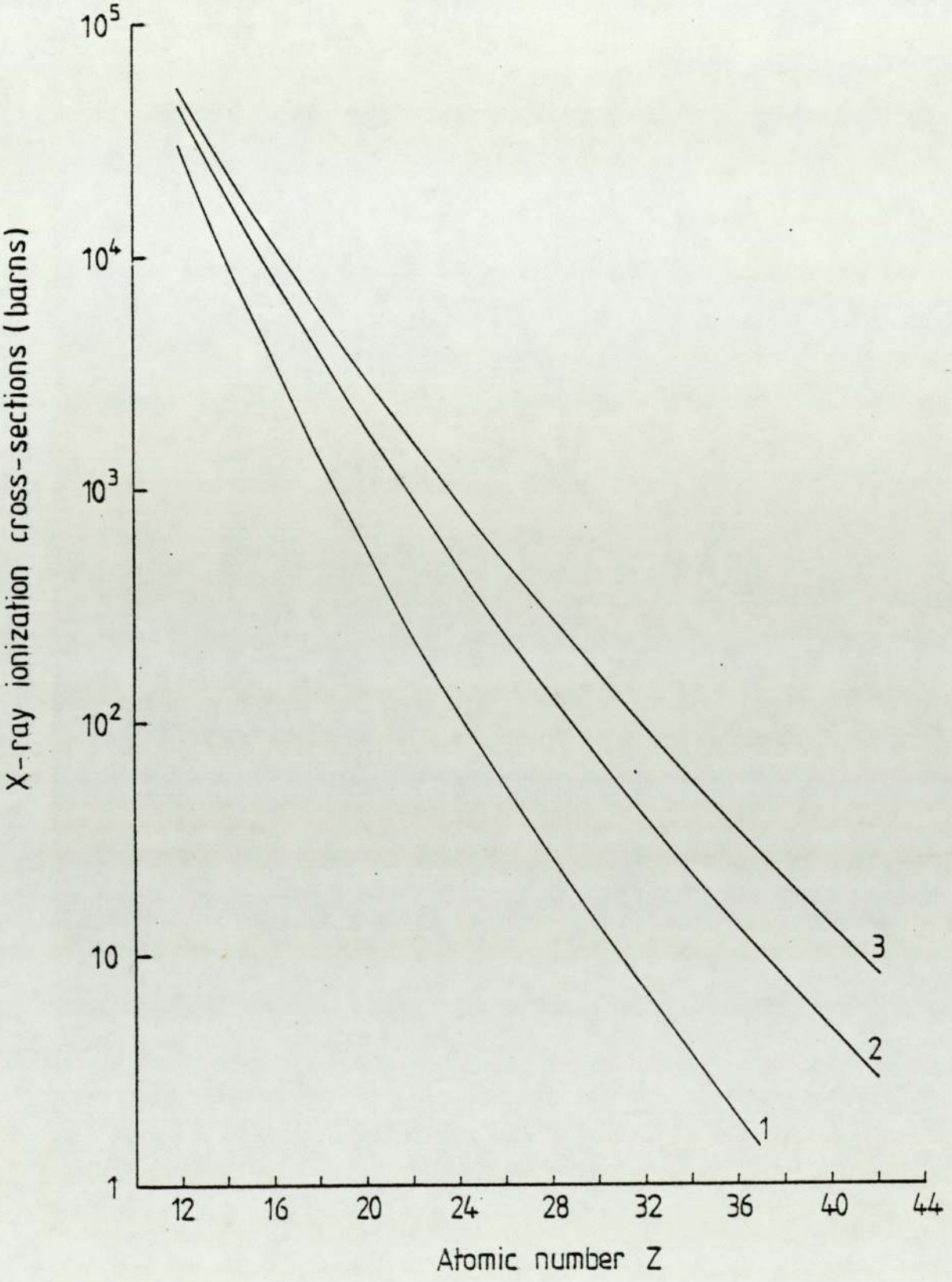

Fig 2:4 Calculated K x-ray ionization cross sections versus Z for proton energies 1·0, 2·0 and 3·0 MeV. Calculation are from equation 2.2

by fluorescence yield factors (sec.II.D) when compared with x-ray production data.

II.C X-Ray Production:

If a vacancy is created in one of the inner shells of an atom, an electron from an outer shell will fill the vacancy and the energy will be emitted as a characteristic x-ray photon or Auger, whose energy is given by the energy difference between the initial and final states.

For example, on creation of a K-shell vacancy in a heavy atom, a succession of spontaneous electron transitions follows; each fills a vacancy in a lower level with resultant emission of an x-ray photon, but also creates a vacancy in a level further out. The result of such processes in large numbers of atoms is the simultaneous emission of K, L and M...series of x-ray spectrum of that element. Fig.2.5 shows schematically all K, L, M, N and the first five O levels, giving for each n, l and j quantum numbers and their orbital x-ray notation, at the top of the figure are approximate relative intensities, and photon energies of the lines for gold, Bertin (1978). Since these electron transitions correspond precisely to the difference in energy between two atomic orbitals, the emitted x-ray photon has energy characteristic of this difference and thereby of the atom and element, for example in fig.2.5 for gold:

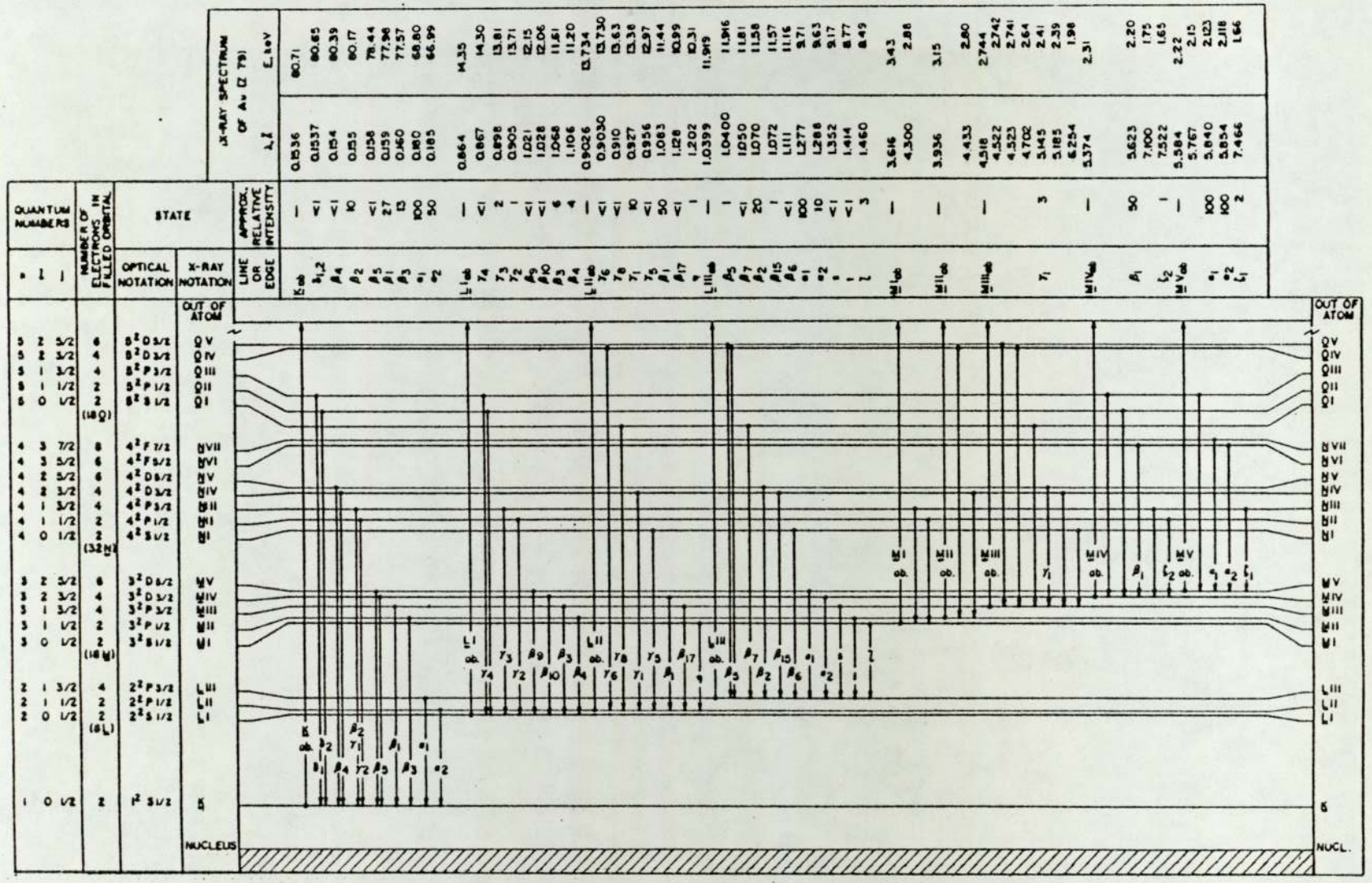

Fig 2:5 Origin of x-ray spectra · electron transitions leading to the characteristic x-ray spectrum (for Au Z=79)

K state	⟶	L III state	+	$K\alpha_1$
80.71		11.92		68.80 keV

K state	⟶	M III state	+	$K\beta_1$
80.71		2.74		77.98 keV

Electron transitions cannot occur from any higher to any lower orbital. Only certain transition are "permitted" by the radiative transition selection rules, which are given in column 5 of table 2.2.

Thus an L III → L I transition would violate the first rule, an M IV (l=2) → L I (l=0) transition would violate the second rule, and M V (j=5/2) → L II (j=1/2) transition violate the third rule. X-ray spectral lines that "obey" the selection rules are known as diagram lines, those which do not as forbidden lines. An example of a forbidden line in fig.2.5 is $L\beta_9$, M V → L I (l=2 to l=0, and j=5/2 to j=1/2).

A third type of x-ray lines - satelite lines or non diagram lines - arise in atoms having two or more inner-shell vacancies. A specified electron transition emits a slightly different energy in such atoms compared with singly ionized atoms. An example is the Si $SK\alpha_3$ line, which arises from an L III → K transition in an atom having both K and L vacancies; its energy is 1.752 keV, compared with 1.74 keV for diagram Si Kα Bertin (1978).

Table (2.2): Quantum Numbers

From Valcovic (1973)

Quantum number	Symbol	Significance	Allowed Values	Transitions
Principal	n	Principal binding energy indicates shell	n = 1,2,3,4,.... K,L,M,N,....	$\Delta n \neq 0$
Orbital angular	l	Orbital angular momentum determines shape of orbit	l = 1,2,3,...(n-1) s,p,d,...	$\Delta l = \pm 1$
Spin	s	Angular momentum due to spin of electron around its own axis	$\pm \frac{1}{2}$	-
Total angular	j	vector sum of l and s	$l \pm \frac{1}{2}$; if $l=0, j=\frac{1}{2}$	$\Delta j = 0, \pm 1$

Some additional features of characteristic x-ray spectra can be discussed with reference to fig.2.1, showing interferences due to overlapping x-ray lines from different elements. Since each transition occurs with an intrinsic probability which is constant for a given Z and which determines the relative intensities of the emission lines observed for a given element, the intensity ratio, $K\beta/K\alpha$, of an element is expected to remain constant irrespective of the mode of ionization. The intensity ratios, $K\beta/K\alpha$, are essential in being able to resolve interferences due to overlapping x-ray lines. Fig.2.6 plots $K\beta/K\alpha$ intensity ratios versus Z using values calculated by Scofield (1974) and the experimental fit of Khan and Karimi (1980).

II.D K-Shell Transition Probabilities:

It has been known that once the atom is excited its de-excitation can occur not only by emission of electro-magnetic radiation but also by some other processes. The fluorescence yield of an atomic shell is the probability that a vacancy in that shell will be filled through a radiative transition. For the K-shell the competing process is the emission of Auger electrons. In this decay two electrons are involved. One fills the initial vacancy, and the other is ejected into the continuum. It is a direct energy transfer process, but it can be assumed that a photon is produced, in the first instance, However, the photon does not leave the atom of its origin,

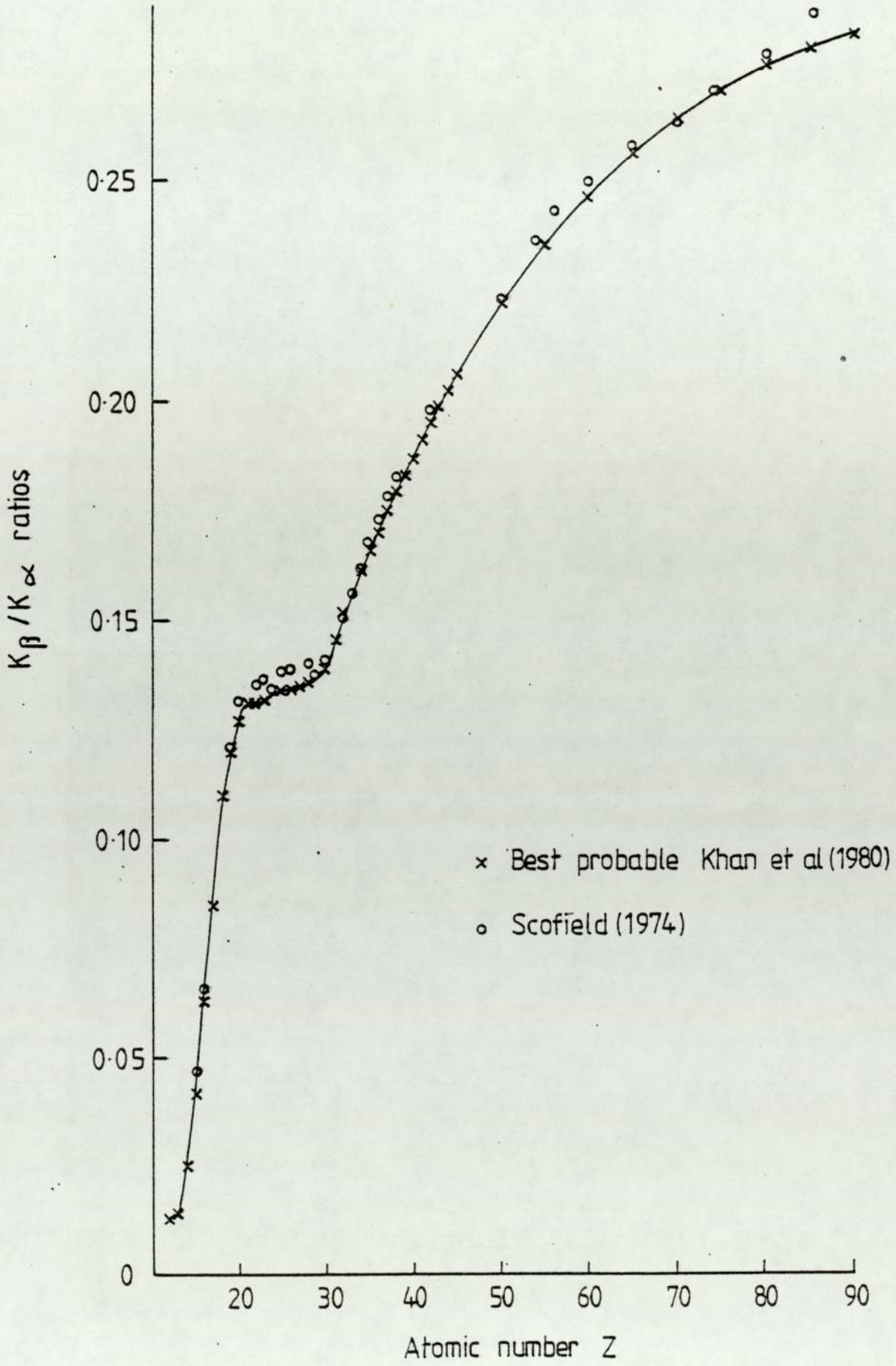

Fig 2:6 Plot of K_β / K_α intensity ratios versus atomic number Z

but is absorbed within the atom with consequent expulsion of another electron. This results in emission of an Auger electron rather than an x-ray photon, and leaves the atom doubly ionized, i.e. with two orbital electron vacancies, The one created by the filling of the initial vacancy and the one created by the Auger process.

The Auger effect is more common in elements of low atomic number because their atomic electrons are more loosely bound and their characteristic x-ray photons more readily absorbed. The effect is more common for L series than for K series for the same reason. A detailed discussion of this phenomenum and the appropriate theory can be obtained from Bambynek et al (1972), Burhop et al (1972), and Krause (1979).

The measure of the relative probabilities for K x-ray emission and radiationless transition is the fluorescence yield factor, ω_k, defined as the ratio of K x-ray quanta emitted per primary K-shell vacancy created, Fig.2.7 plots values for the K-shell fluorescence yield, ω_k versus Z. Values for ω_k are taken from Krause (1979). The behaviour of ω_k's is seen to be smoothing increasing function of Z, contributing significantly to reduce the x-ray emission for low Z elements, which is a major limitation to sensitivity for elements in this region.

In PIXE analyis, the x-ray production σ_{pro}, rather than ionization cross section σ_{ion}, is of interest. For a K

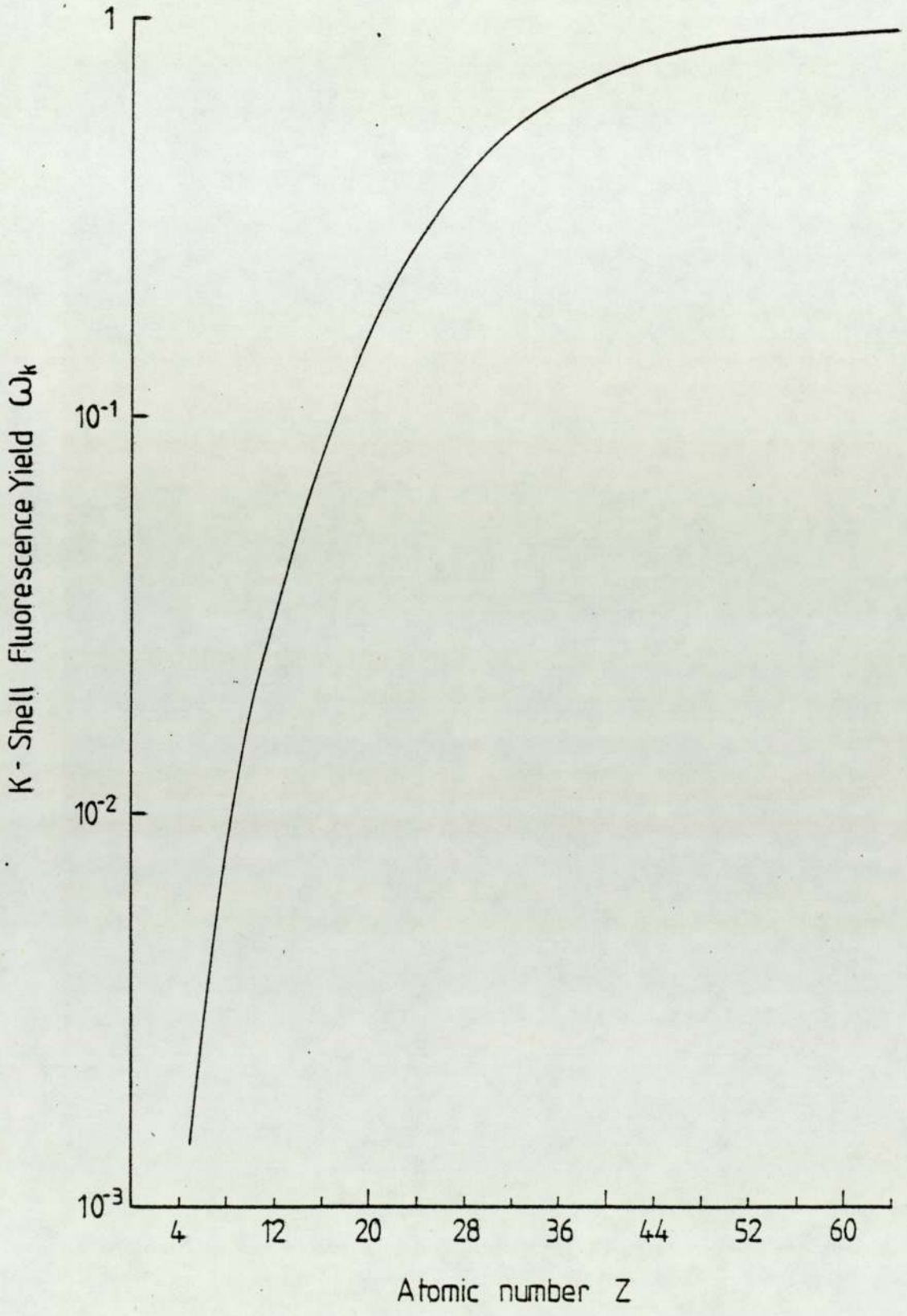

Fig 2:7 K - shell fluorescence yield ω_k versus atomic number. Krause (1979)

line in a spectrum $\sigma_k$pro is obtained by:

$$\sigma_k\text{pro} = \sigma_k\text{ion}\ \omega_k \qquad 2.3$$

The calculated values for $\sigma_k$pro using equations 2.2 and 2.3 are represented in fig.2.8.

II.E Background Production Processes:

The x-rays registered by the detector in fig.2.1 are not only characteristic x-rays from the elements but also background radiation from the target matrix. This consists of a continuous distribution peaked at rather low energy and having a high energy tail. The continuous background observed can be attributed to:

1. bremsstrahlung radiation due to secondary electrons ejected from target atoms by the proton beam;
2. bremsstrahlung radiation from the protons themselves;
3. Compton scattering of nuclear γ-rays;
4. charging of the sample.

II.E.1 Bremsstrahlung Radiation:

The first two types of background are always present when one employs protons for generating the x-radiation, and constitute the limiting factor irrespective of type of the detector used for measuring the x-rays. Folkman et al (1974 a) have made calculations of the x-ray background due to bremsstrahlung produced in an organic

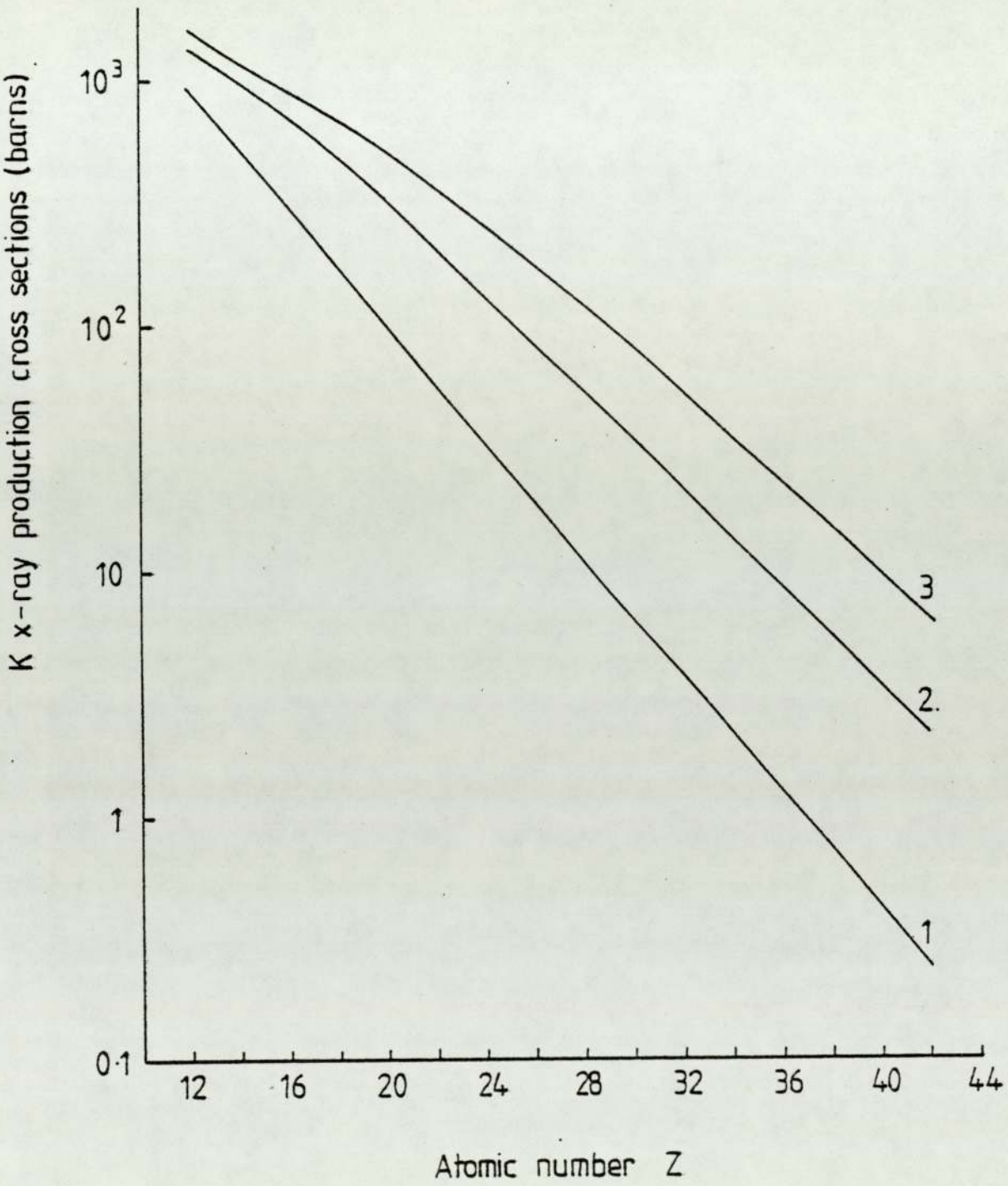

Fig 2:8 K x-ray production cross sections versus Z for proton energies 1,2 and 3 MeV

matrix by the incident beam itself and due to the electrons that have been knocked out by the beam. The expected contribution of these two bremsstrahlung sources is represented by solid curve in fig.2.9 for the 2 MeV proton. Fölkmann et al also measured the background levels and these results are shown by the broken curve in fig.2.9. The bremsstrahlung from the electrons, that interact inside the matrix, is the dominant source of background x-rays at low energies, while the high energy bremsstrahlung is due to the protons themselves.

The production of bremsstrahlung by secondary electrons is essentially a two step process consisting firstly of the ejection of electrons from matrix atoms by the incident protons, and secondly, of the radiative collision of these ejected electrons with the nuclei of matrix atoms resulting in bremsstrahlung. In order to estimate the intensity of this radiation, one must consider the probabilities associated with both mechanisms of the two step process. The probability that a proton of energy E_p and mass m will eject electron of energy E_o and mass m_o is characterised by a sharp decline for $E_e \geq T_m$ (T_m is defined in sec.II.B). For a proton with 2.37 MeV, used in this work, $T_m \sim 5.2$ KeV which falls in the region of Cr Kα. The probability for ejection of a secondary electron with $E_e > T_m$ decreases as $\sim E_e^{-10}$ (Fölkmann,1974 a). It is advantageous in terms of minimizing electron bremsstrahlung to make T_m as small as practically possible.

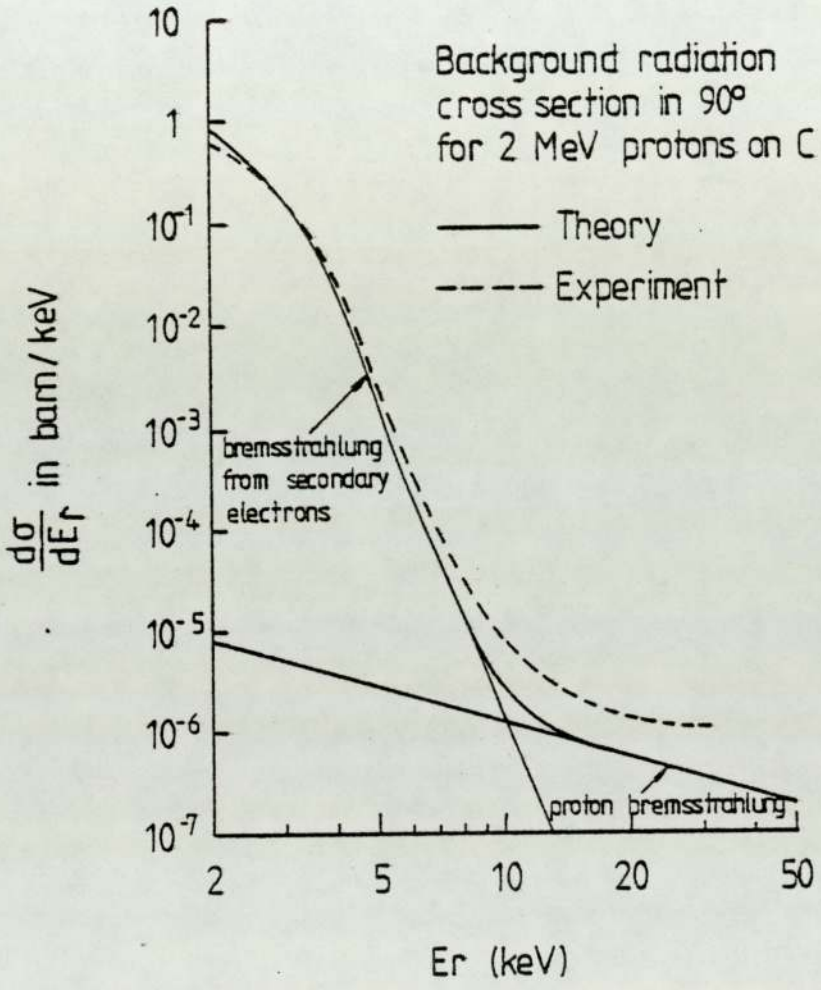

Fig 2:9 Experimental and theoretical background radiation cross sections for a thin sample. Falkman et al (1974a)

This could be achieved by reducing the proton energy E_p, but one suffers a corresponding decrease in the characteristic x-ray yield. There is little that can be done to reduce the secondary electron bremsstrahlung, the use of extremely thin targets may lead to the escape of the secondary electrons from the sample before suffering any radiative collisions with the target nuclei. Johansson (1976) has concluded that the thickness required to realize any significant gains are impractically small.

Some reduction in the background intensity at low energies can be achieved by exploiting the angular distributions of the secondary electron bremsstrahlung. Kaji et al (1977) measurements show clearly that the secondary electron bremsstrahlung peaked in at forward angles. Campbell et al (1981) however, showed that the decrease in electron bremsstrahlung afforded by the 135^{o} angle detector relative to the more widely used 90^{o} could be offset by the loss of efficiency.

The large accelerations which occur during close collisions between the proton (Z, A, E_p) and the nuclei (Z_1, A_1) of the matrix atoms result in a direct production of bremsstrahlung which becomes of interest at higher radiation energies, fig.2.8. The cross section of the process is given by:

$$\frac{d\sigma}{dE_x} = C \frac{A Z^2 Z_1^2}{E_p E_x} \left(\frac{Z}{A} - \frac{Z_1}{A_1} \right)^2 \qquad 2.4$$

where C is approximately constant (Alder et al 1956).

Bremsstrahlung from equation 2.4 is a slowly decreasing function of E_x and E_p in contrast to the very rapid decrease in secondary electron bremsstrahlung with E_x.

II.E.2 Compton Scattering of Nuclear γ-Rays:

The third type of radiation is as fundamental as the first two in the sense that the proton beam has a probability of exciting elements in the target which have a particular high cross section for excitation of low energy nuclear levels, such ^{19}F and ^{23}Na, which through their decay will give rise to γ-radiation. For low Z material the dominant interaction of γ-rays with matter is Compton scattering which converts the γ-rays to a continuous background in the x-ray region. In addition, γ-rays can also be produced in the nuclei of any other material that the beam strikes.

Estimates of the intensity of the Compton background are in general difficult to make. The probability for nuclear excitation is sensitive to the projectile, its energy, and the particular target composition; and the probability for Compton scattering in the detector is a function of the detector composition and geometrical configuration.

Several studies have been made in an effort to measure the significance of the Compton background under different experimental conditions, Fölkmann et al (1974 b); Cahil

et al (1974); Herman et al (1973). Measurements by Falkmann indicate that for proton energies below approximately 2 MeV, the Coulomb barrier of carbon and heavier nuclei cannot be penetrated.

II.E.3 Charging of the Sample:

Background contribution from target charge-up could be seen both when thick and thin insulating targets are used. The thin targets used in this work were usually mounted on pure aluminium frames, when perspex frames were used instead of aluminium such an effect was seen. Fig.2.10 represents two spectra of a digested blood serum sample. The spectra have been measured using a proton beam of 2.37 MeV and 20 μm aluminium absorber in front of the detector. One spectrum has been taken for a 10 μL digested blood sample mounted on a perspex frame, the other of 20 μL mounted on an aluminium frame. The difference in background is illustrated clearly.

Under proton bombardment an insulated target is charged positively by the ions stopped in it and by knock-off electrons which leave the target. Then a high voltage is built up, leading eventually to an electric break-down. At high target potentials, before breakdown occurs, electrons can be attracted from the surroundings towards the target. Upon striking the target surface these electrons may produce additional bremsstrahlung which causes the increased background extending sometimes to

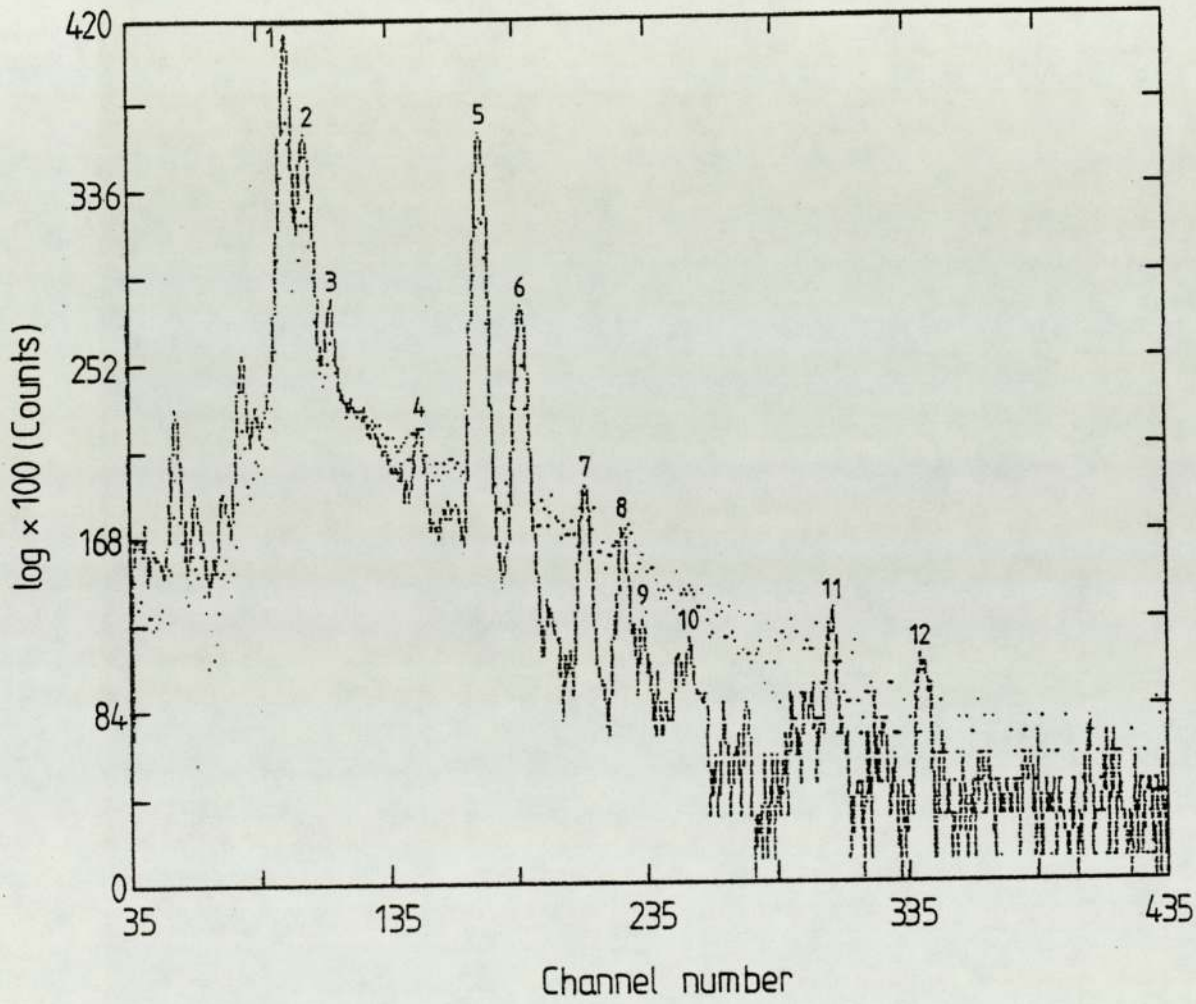

Fig 2.10 PIXE spectra of digested blood serum sample demonstrating the improvement gained by using Al frame to eliminate the target charging.
····· 10 μL using perspex frame, —— 20 μL using Al frame

1 - K (Kα)	7 - Cu (Kα)
2 - Ca (Kα)	8 - Zn (Kα)
3 - Ca (Kβ)	9 - Cu (Kβ)
4 - Cr (Kα)	10 - Zn (Kβ)
5 - Fe (Kα)	11 - Br (Kα)
6 - Fe (Kβ)	12 - Rb (Kα)

several tens of KeV, Van Zon et al (1981). Such a high background may significantly reduce the minimum limits for detection of trace element concentrations. Various techniques have been proposed to eliminate this charging of thick insulating target, these include:

1. evaporation of a thin conducting layer over the face of the sample, which is simple and quite satisfactory. Papper et al (1978) successfully employed this approach to reduce the charging of their thick blood samples. They evaporated 200^{o}A of pure carbon onto the surface which resulted in a considerable reduction in background affording an enhanced sensitivity.

2. mixing a conducting powder with the sample before pressing it into a pellet,which has a risk of contamination, non uniform mixing and even changing the matrix sample Jopson et al (1962).

3. irradiating under low vacuum Ahlberg et al (1975), or in air, Huda et al (1979), produces uncertainties in terms of contamination. For this reason high purity nitrogen is used by Van Zon et al (1981) in eliminating the target charging

4. a heated filament in the target chamber to spray electrons into the target which gave a good result, Ahlberg et al (1975) and Willis et al (1977). Ahlberg used electron gun with a commercial carbon filament. Tungsten filaments were also tried but found to contaminate the sample when heated.

5. another technique has been used by Chandhri and Crawford (1981), by placing a thin foil of a suitable material, 1-2 cm in front of the target, and monitoring the back scattered particles from it with a surface barrier detector. The incident beam of charged particles produces sufficient number of electrons in the forward direction from this foil, to neutralize the positive charge accumulating in the target.

In the present work this effect is eliminated by using a thin target mounted on an aluminium frame.

CHAPTER III

EXPERIMENTAL

The present chapter discusses the experimental aspects of PIXE in terms of the following topics.

A. Data Collection,

B. Data Interpretation,

C. System Calibration,

D. Sample Preparation,

E. Sensitivity Considerations,

F. Precision and Accuracy Considerations.

III.A Data Collection:

III.A.1 Introduction:

The equipment arrangement used in this work is shown schematically in fig.3.1. A proton beam of energy 2.5 MeV, determined to approximately ± .02 MeV is obtained from the 3 MeV Dynamitron accelerator at the Joint Birmingham Radiation Centre. The protons are produced in the ion source. The ion source is placed at an angle to the acceleration column, and the protons bent into the line of the accelerator by a permanent magnet. After acceleration the beam is taken through an angle in one of the bending magnets and directed onto a 5 micron thick pure aluminium foil which serves as a diffuser (sec.III.A.2), located approximately 118 cm from the irradiation target. This diffuser and a set of two collimators result in a

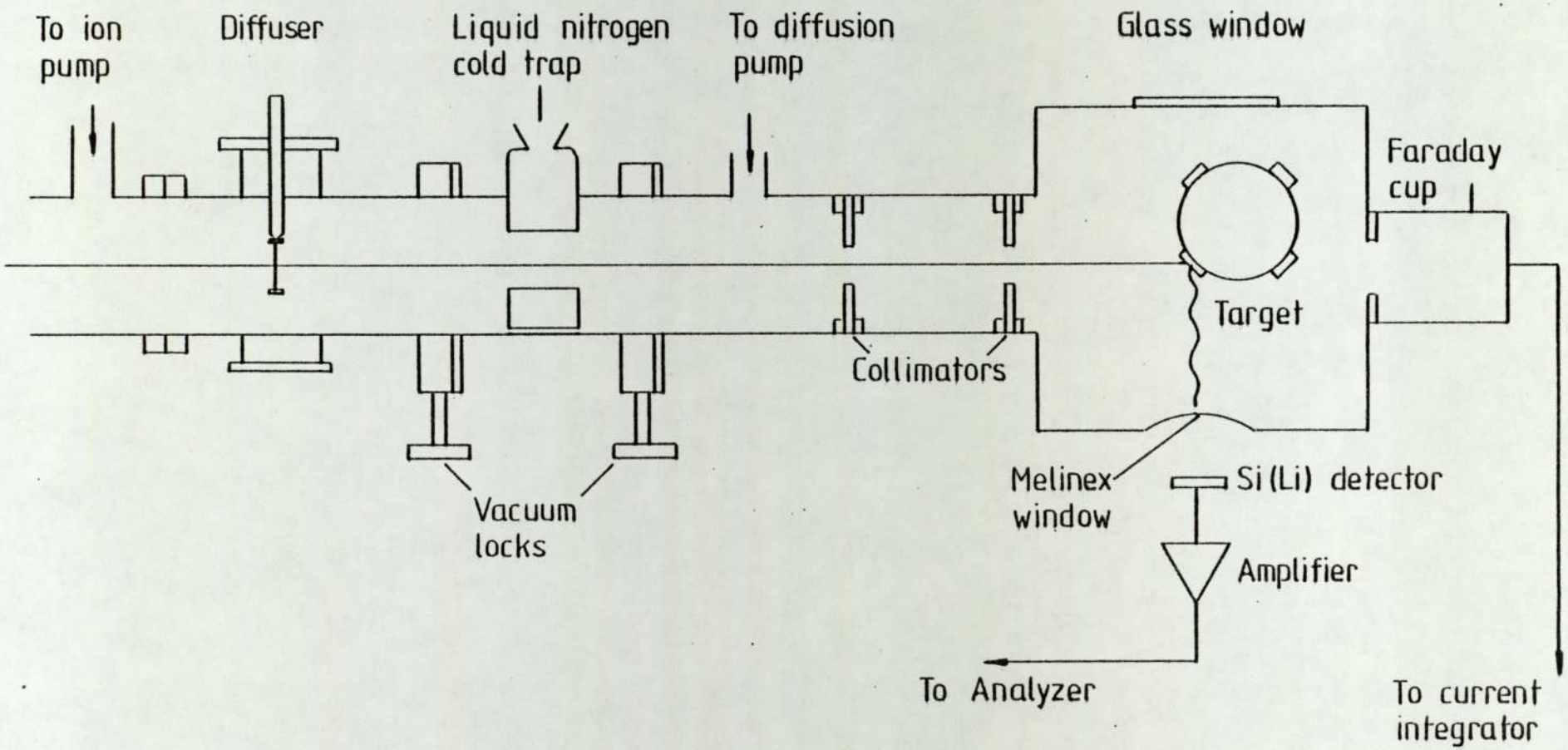

Fig 3:1 Target irradiation facility

beam spot on the target which is approximately 0.255 cm^2 in area. The beam is stopped, after passing through the thin target in the Faraday cup, F.C., which serves to count the number of protons passing through the target. A fraction of the x-rays excited in the sample leave the target chamber through a 50 micron Melinex window to the Si(Li) detector. Details of the instrumental considerations are discussed in the following section.

III.A.2 Instrumental Considerations:

1) Beam transport: The arrangement of the Aston beam room in the basement of the Radiation Centre needs the beam to pass into the first bending magnet in the magnet room, where it bent through 45^o and onto a second bending magnet, which caused the beam to bend through a further 45^o to serve the basement Aston beam room, Weaver(1980). The magnets also separate out the other particles such as H_2^+ ions. This accelerated beam travels in evacuated tubes, the pressure in the beam tubes throughout the system was maintained near 10^{-5} torr or less using triode ion pumps, Weaver(1980).

2) Diffusion foil: For quantitative analysis of a sample (giving trace elements in absolute amounts) one must apply a homogeneous beam with constant intensity distribution. This can be achieved if the beam passes through a thin metal foil from which the small angle scattering of the ions produces approximate homogeneity

of the beam, Bearse et al (1974), Falkmann (1975). The degree of uniformity achieved by this procedure depends on the characteristics of the diffuser, on its relative distance from the target, and on the beam focalisation, Montenegro et al (1979b). They described the procedure in detail and established a criterion for the choice of the diffuser by relating the uncertainty in the mass determination due to the beam distribution, to the diffusing film thickness.

Bauman et al (1979) compared the physical characteristic for nickel, gold and tungsten. They concluded that high Z materials have minimum energy loss per collision leading to longer foil lifetime.

Akselsson and Johansson (1979) obtained a homogeneous beam by letting it pass through a 1.7 mg/cm^2 Al diffuser foil. The distance between this foil and the sample was about 60 cm.

The diffuser foil used in this work was 5 micron thick pure aluminium, obtained from Good Fellow Metals, Cambridge, England, and is mounted on a rotating rectangular support which permitted the rotation of the diffuser without breaking the vacuum. The proton energy loss in the diffuser foil is about 130 keV.

3) Collimators: A set of two collimators preceding the target chamber served to define the diffused beam,

selecting the central and most uniform portion of the beam. The collimators are two circular tantalum sheets with circular holes of 2 and 4 mm diameters. They are placed 25 cm apart in the horizontal beam pipe, with the 4 mm diameter aperture nearer the target chamber, at 16.5 cm from the target. The second collimator effectively skimmed any spray of particles scattered from the aperture edges of the first collimator. Clearly the size of the irradiation area can be conveniently adjusted by changing the beam collimators.

A uniform intensity distribution of the proton beam spot is essential in obtaining quantitative and reproducbile measurement. The foil diffuser is a satisfactory method for obtaining a uniform beam spot, while one can achieve similar results by sweeping a narrow beam over the irradiation area with a pair of parallel deflector plates with rapidly oscillating voltages, Johansson et al (1972), Campbell et al (1975), or with a defocussing quadrapole magnet, Falkmann (1975).

4) Target chamber: The initial target chamber was a stainless steel rectangular box of dimensions 26 x 16.5 x 14 cm^3, with a glass window on one side to allow visual positioning of the target. The chamber housed a target arm having circular disk for mounting four targets. The target's angular position was controlled by a stepping motor, the targets are always at 45^o to the beam direction. To improve efficiency of collection of x-rays a new

chamber was constructed. The chamber consists of $\approx$ 1.5 cm thick cylindrical tube with diameter 37.5 cm and 40 cm height. This chamber houses the chassis of a Kodak Carousel projector and its frame changer which can hold up to 80 frames, the targets, prepared in the same fashion as described in sec.III.D are mounted on 5x5 cm^2 pure aluminium frames. These frames are then placed in the slide changer of the Kodak projector whose chassis is suitably transformed to position the targets, one by one, in line with the beam. A complete target replacement is easily done by opening the chamber, removing the frame changer and inserting a new one containing a fresh batch of targets. A photograph, fig.3.2, shows detailed views of the target chamber and Carousel frame changer. Seven tubes, also cylindrical, are connected to the previous part (central chamber), the first one forms part of the system for changing the targets, the second tube has a glass window for visual inspection of the central chamber interior (e.g. target position), the third, has a Faraday cup for beam integration,aligned with the entrance one, the fifth and sixth tubes are entrance windows for the x-ray detector at two different angles, finally the last tube is part of a Rutherford backscattered proton system. All these parts were made of stainless steel. The target chamber is electrically insulated from the rest of the beam line so that the beam current entering the target chamber can be monitored. The irradiation of the sample takes place under vacuum in the target chamber, two hand operated vacuum locks isolated the chamber from the

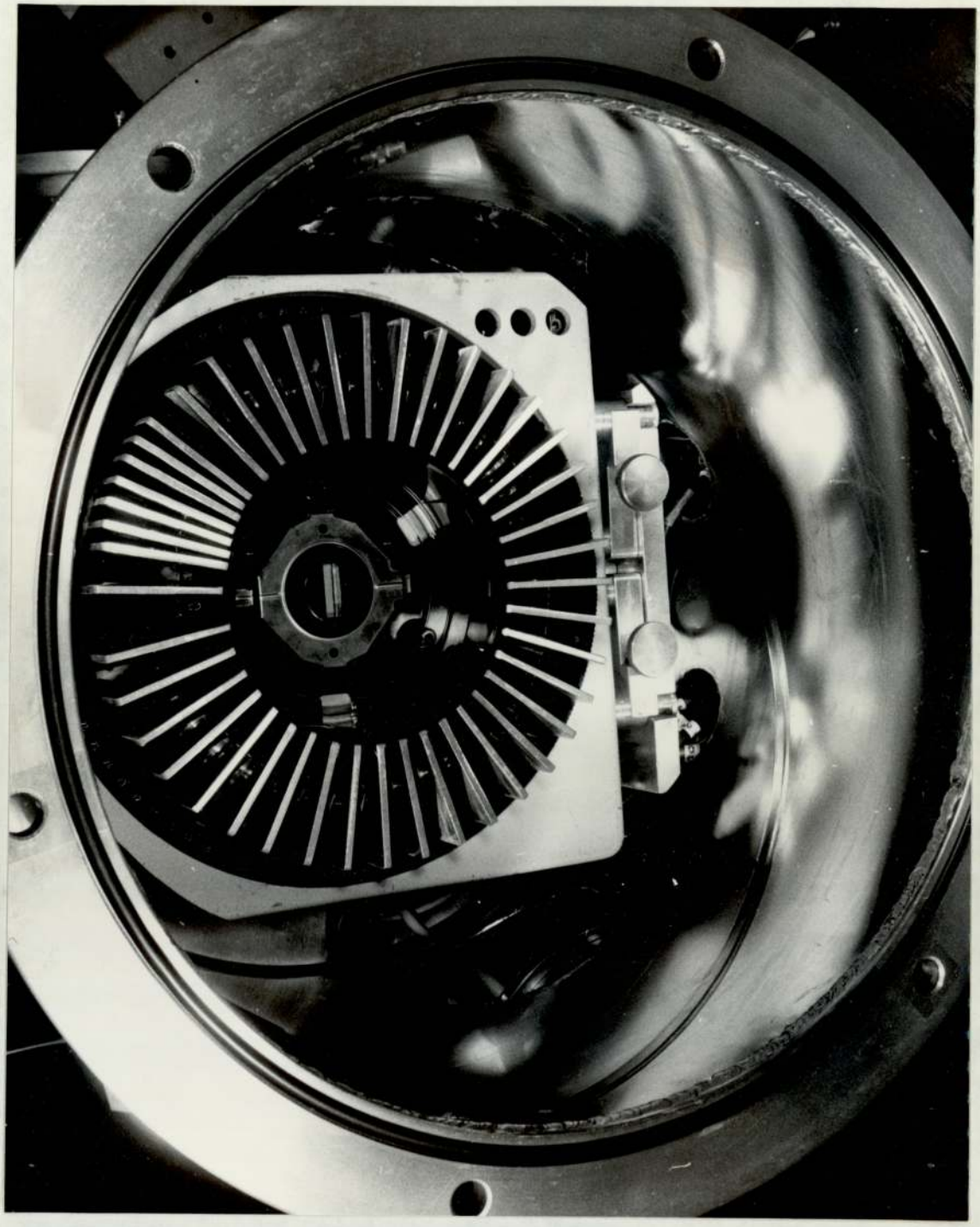

Fig.3.2 Target chamber and Carousel frame holder

accelerator vacuum system. A liquid nitrogen cold trap is located between the two locks to condense any vapours in the chamber which might contaminate the beam. The isolated system is pumped down initially through a rotary pump and is then opened to the diffusion pump. To replace the targets, i.e. when letting the target chamber up to atmospheric pressure, dry nitrogen is supplied from a cylinder rather than letting in air; this is done to speed the process of pumping out again as water vapour adsorbed on to the walls of the line can make it very difficult to start the ion pump even though an apparently good roughing pressure has been achieved, Weaver (1980).

5) Faraday Cup: The emergent proton beam passing through the thin target is dumped onto a 40 cm long stainless steel tube, 15 cm behind the target which forms a Faraday Cup. This distance was reduced to 11 cm in the case of the big chamber.

6) Detector: The x-rays that are emitted from the target are detected with a 30 mm^2 lithium drifted silicon detector placed perpendicular to the proton beam direction. The x-rays pass from the vacuum chamber, through a 50 micron Melinex window, through 3.2 cm of air before entering the 12.5 micron thick Be window of the detector. Keeping the detector in air is a mere convenience, some PIXE systems designed to measure x-rays emitted from light elements operate with a detector which

protrudes into the evacuated region, Hansen (1973).

7) X-Ray Filter: For biological samples, an x-ray filter of pure aluminium is usually inserted between the target chamber and the detector in order to reduce to a tolerable level the flux of low energy x-ray into the detector. The use of x-ray filters is demonstrated in Fig.3.3 which shows the effect of two different thickness Al filters on spectra obtained from a blood sample. The effect of the thicker Al filter in the low-z region is quite obvious.

A general view of the beam line with the big chamber is shown in fig.(3.4).

III.A.3 Signal Processing Electronics:

For quantitative analysis, the measured quantity of interest is the number of x-ray counts detected (of a given energy) per unit number of proton charge accumulated on the sample. The total amount of proton charge on the target comprised the charge collected on Faraday Cup plus any charge which may have been collected on the walls of the scattering chamber or on the target rod due to protons which were scattered after interacting with the sample. The total current collected is fed into a current integrator (Keithly electrometer). This provided a range of inputs with the accuracy required. It also supplies a voltage level which is proportional to the

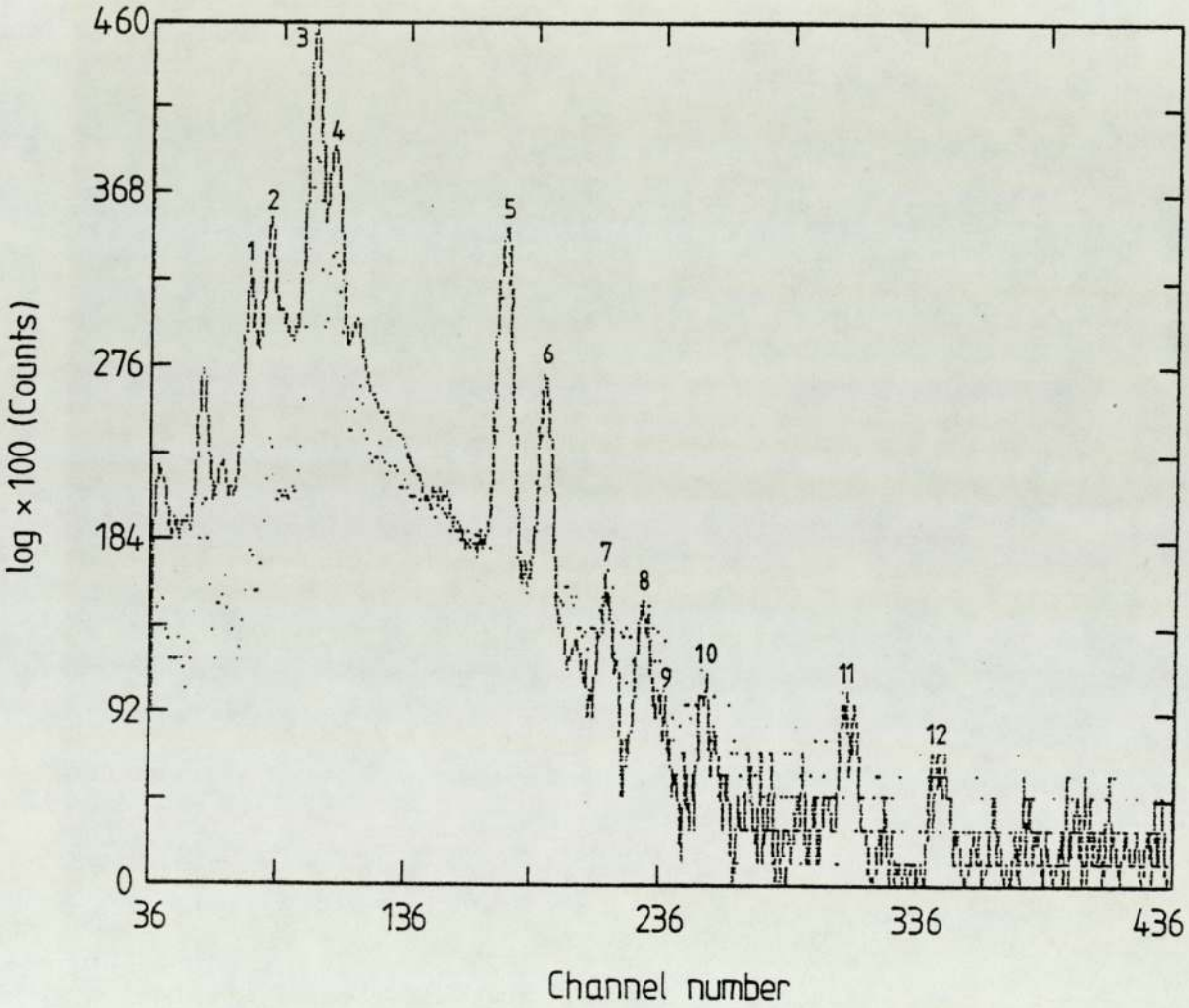

Fig 3.3 PIXE spectra of a digested blood obtained with —— 5 and ····· 20 μm Al absorbers.

1 - S (Kα + Kβ)	7 - Cu (Kα)
2 - Cl (Kα + Kβ)	8 - Zn (Kα)
3 - K (Kα)	9 - Cu (Kβ)
4 - Ca (Kα)	10 - Zn (Kβ)
5 - Fe (Kα)	11 - Br (Kα)
6 - Fe (Kβ)	12 - Rb (Kα)

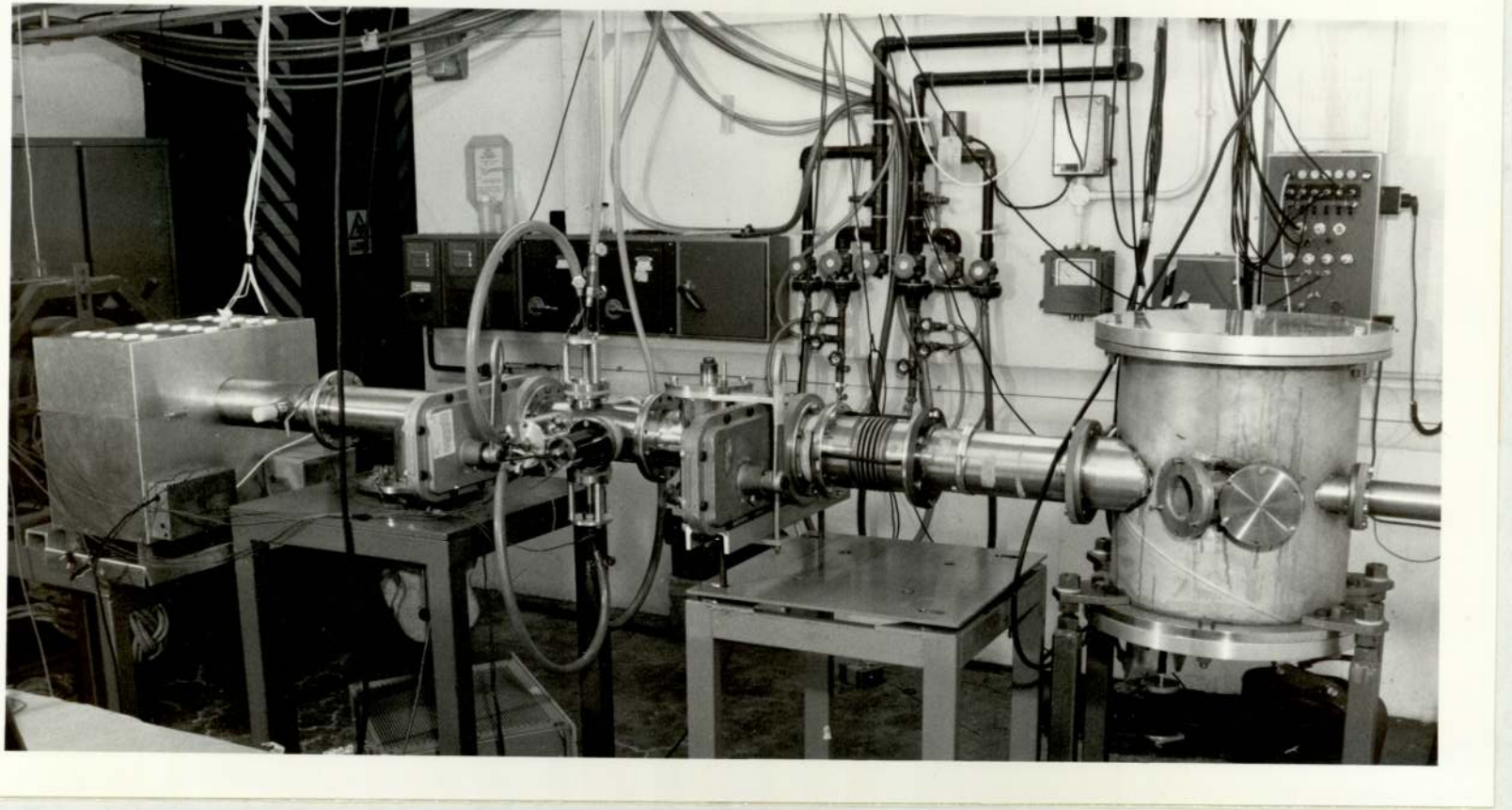

Fig.3.4 General view of the beam line

meter deflection and is 1 V for a full scale deflection (F.S.D.). The output is fed to a voltage-to-frequency converter, V.F.C., which produces a pulse chain of 10^5 Hz for 1 V input. The output of the V.F.C. is fed to a scaler through a decade dividing circuit providing outputs which are suitable for counting, fig.3.5. The scaler and the divider are controlled by an automatic start, stop, or reset device. Typical example used in this work is that counting for 250000 pulses (preset) under current 10 nA (F.S.D.) using division factor = 1000 is equivalent to counting for charge = 25μc collected on the target, where

$$\text{Charge } (\mu c) = \text{F.S.D.}(\mu A) \times \frac{\text{division factor}}{10^5} \times (\text{preset counts}) \quad \ldots\ldots 3.1$$

The components, of x-ray count detector, are:

a. Solid state Si(Li) detector, Kevex 3201 cryogenic subsystem,
b. 2002 Kevex preamplifier with pulsed optical feed-back system,
c. 4500 p pulsed optical feed-back amplifier,
d. Analog-to-digital converters, ADC model 5416 A.

X-rays entering the Si(Li) detector interact with atoms of the Si primarily via photoelectric and Compton scattering processes. These photons lose energy by producing ionization in the form of free holes and electrons. The free charges are swept away by the

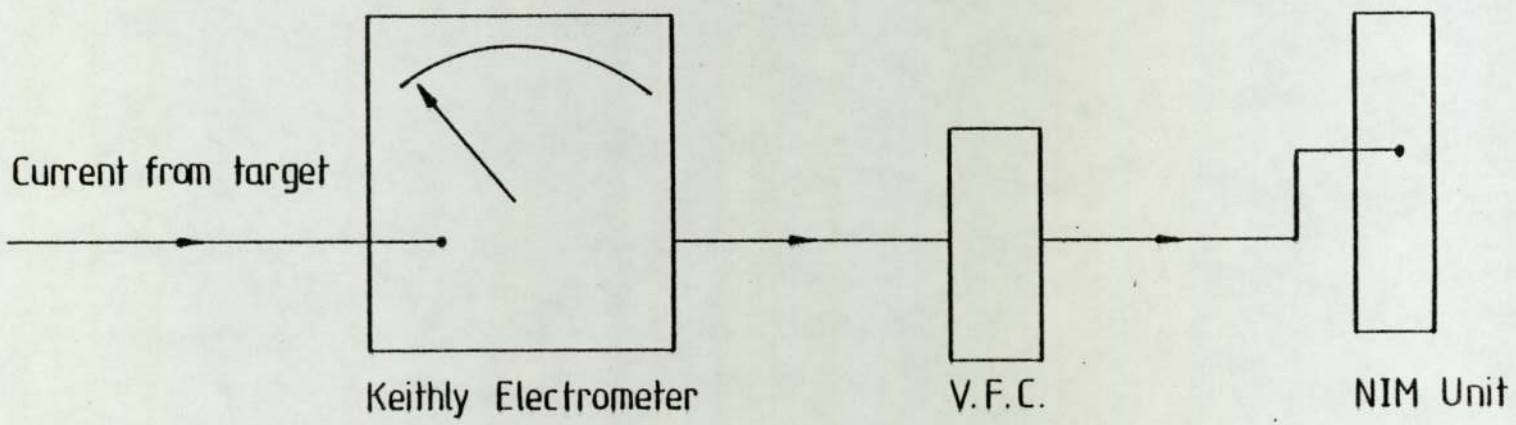

Fig 3:5 Current Integrator

applied bias and collected. Since a well-defined average energy is required to produce an electron-hole pair in a particular semiconductor material, the total number of charges produced is directly proportional to the energy of the absorbed x-ray (assuming total x-ray energy absorption). The first stage of the preamplifier is mounted in contact with the detector and maintained at a low temperature in the cryostat, it integrates each detector charge signal to produce a voltage step proportional to the charge, the Kevex 2002 preamplifier gives an output with negative reset pulses. The input charge conversion is approximately 4.5 mV per 10 keV Khan (1976). This pulse is then amplified and shaped in a series of differentiating stages to make them compatible with the subsequent data analysis and storage system. The maximum output is +10 V direct coupled. The output pulses are flat topped and 2 μs in duration. The resulting shaped pulse is then passed into an analog-to-digital converter ADC. The input is dc coupled and accepts inputs between +0 V to +10 V. The ADC sorted the input signals by pulse height into 2048 channels, thus building up a spectrum of counts versus channel number, or counts versus x-ray energy, since channel number is proportional to energy. The count rate in the biological samples is $\sim$ 600 c/s, under normal running conditions. A block diagram is shown in fig.3.6. At the end of the analysis the data are stored on magnetic tape for analysis at a later time.

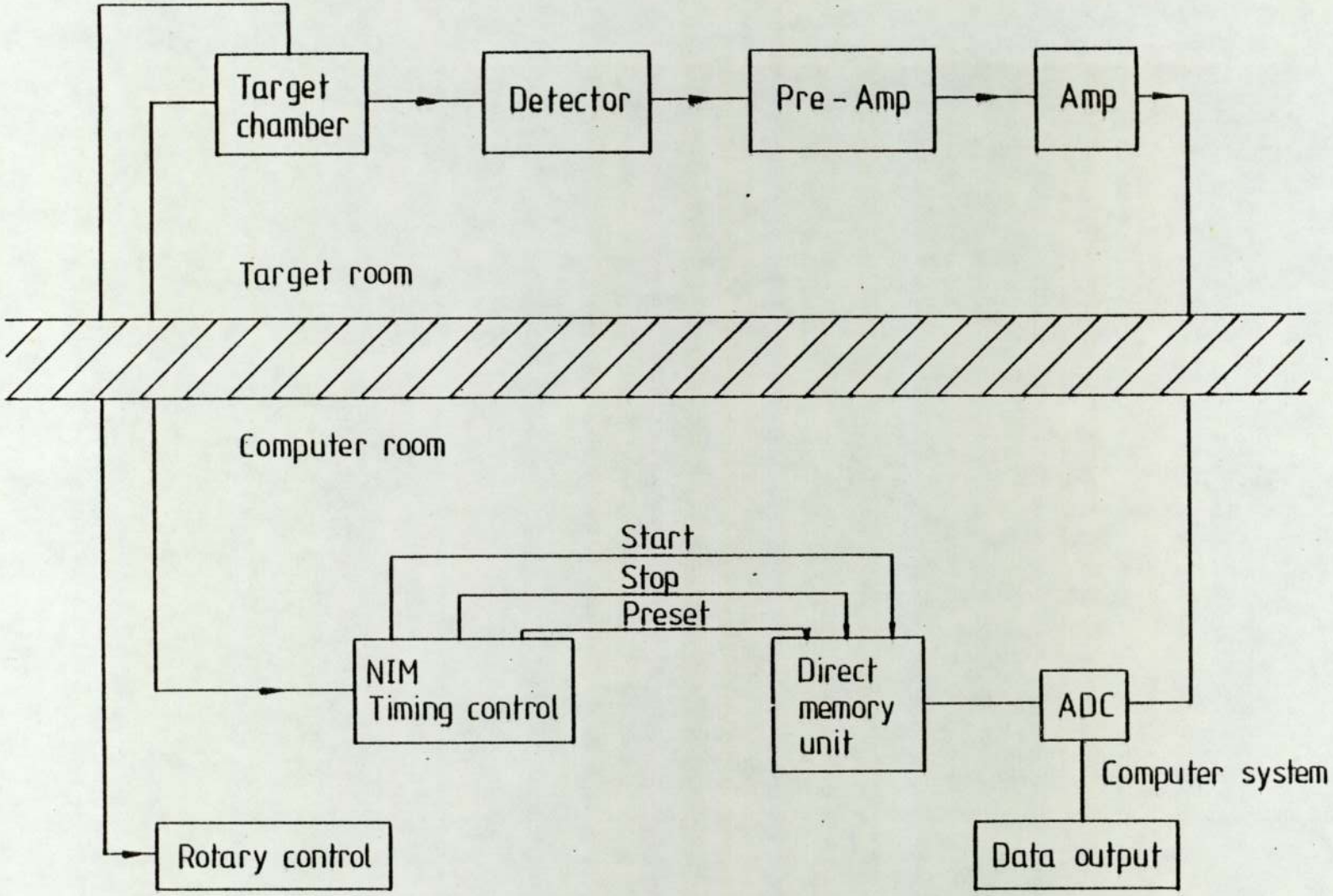

Fig 3:6 Block diagram for experimental arrangement

The ability to detect x-rays of many elements simultaneously is the primary attraction of energy dispersive x-ray analysis. The key component of the energy dispersive system in this work is the Si(Li) solid state detector and its electronic parts.

Two parameters which relate to the performance of the Si(Li) detector are the detector resolution, and the detector efficiency. The energy resolution of the detector is determined partly by electronic noise but also by statistical fluctuation in the number of electron-hole pairs generated by a monoenergetic x-ray line. The deviation caused by these two sources of fluctuation can be expressed as quadratic sum of two components:

$$(FWHM)^2_{overall} = (FWHM)^2_{noise} + (FWHM)^2_{intrinsic} \quad ....3.2$$

where $(FWHM)_{noise}$ is the electronic noise contribution determined by the input amplifier stage and by detector leakage current. Operating the detector at low temperature is essential to reduce the latter component. The statistical spread, $(FWHM)_{intrinsic}$, can be represented by:

$$(FWHM)^2 = (2.35)^2 \epsilon FE \quad .....3.3$$

where E is the x-ray energy, ϵ is the average energy required to produce an electron-hole pair, and F is the Fano factor which corrects for the departure of the energy-loss process from a Poisson distribution, Knoll(1979). The definition of detector resolution, for peaks whose

shape is Gaussian with standard deviation σ, the FWHM = 2.35 σ is given by

$$\text{Resolution} = \frac{\text{FWHM}}{Ex} = \frac{2.35\sigma}{Ex} \qquad \ldots\ldots 3.4$$

Table 3.1 represents resolution calculated using equation 3.4 and σ's for the standards used to calibrate the system, as a function of x-ray energy Ex, is represented graphically in fig.3.7, which illustrates typical energy resolution capabilities, for the detector used in this work, as a function of x-ray energy over the range of interest. The dominant importance of energy resolution in the analysis is illustrated in fig.3.8 which shows the Z and energies of characteristic K x-rays versus the channel number. The relative separations of the Kα lines of adjacent elements as Z changes, and also the relative separation of the Kα line of an element from the Kβ line of the next lower Z element are represented in table 3.2, shown in fig.3.9. When those results are compared with the energy resolution curve, it becomes obvious that complete separation of the Kα line of adjacent element for very light elements is not possible, even more important, interference between the Kβ line of an element and Kα line of the next higher Z element is serious for higher values of Z. Fortunately, the analysis of the whole spectrum, taking into account the known x-ray line structure of various elements, can accommodate a reasonable level of such interference.

Table 3.1:

σch	σeV	F.W.H.M	Resolution %	Ex keV	Standard
1.21	49.3	115.86	5.02	2.307	S
1.26	51.3	120.56	4.60	2.621	Cl
1.37	55.8	131.13	3.96	3.312	K
1.42	57.8	135.83	3.68	3.690	Ca
1.53	62.3	146.41	3.25	4.508	Ti
1.70	69.2	162.62	2.76	5.895	Mn
1.78	72.5	170.38	2.46	6.925	Co
1.90	77.4	181.89	2.26	8.041	Cu
1.94	79.0	185.65	2.01	9.243	Ga
2.00	81.5	191.53	1.94	9.876	Ge
2.32	94.5	222.08	1.66	13.370	Rb
2.44	99.4	233.59	1.57	14.933	Y
2.61	106.3	249.81	1.43	17.443	Mo

Energy resolution capabilities for detector used in this work as a function of x-ray energy over the range of interest.

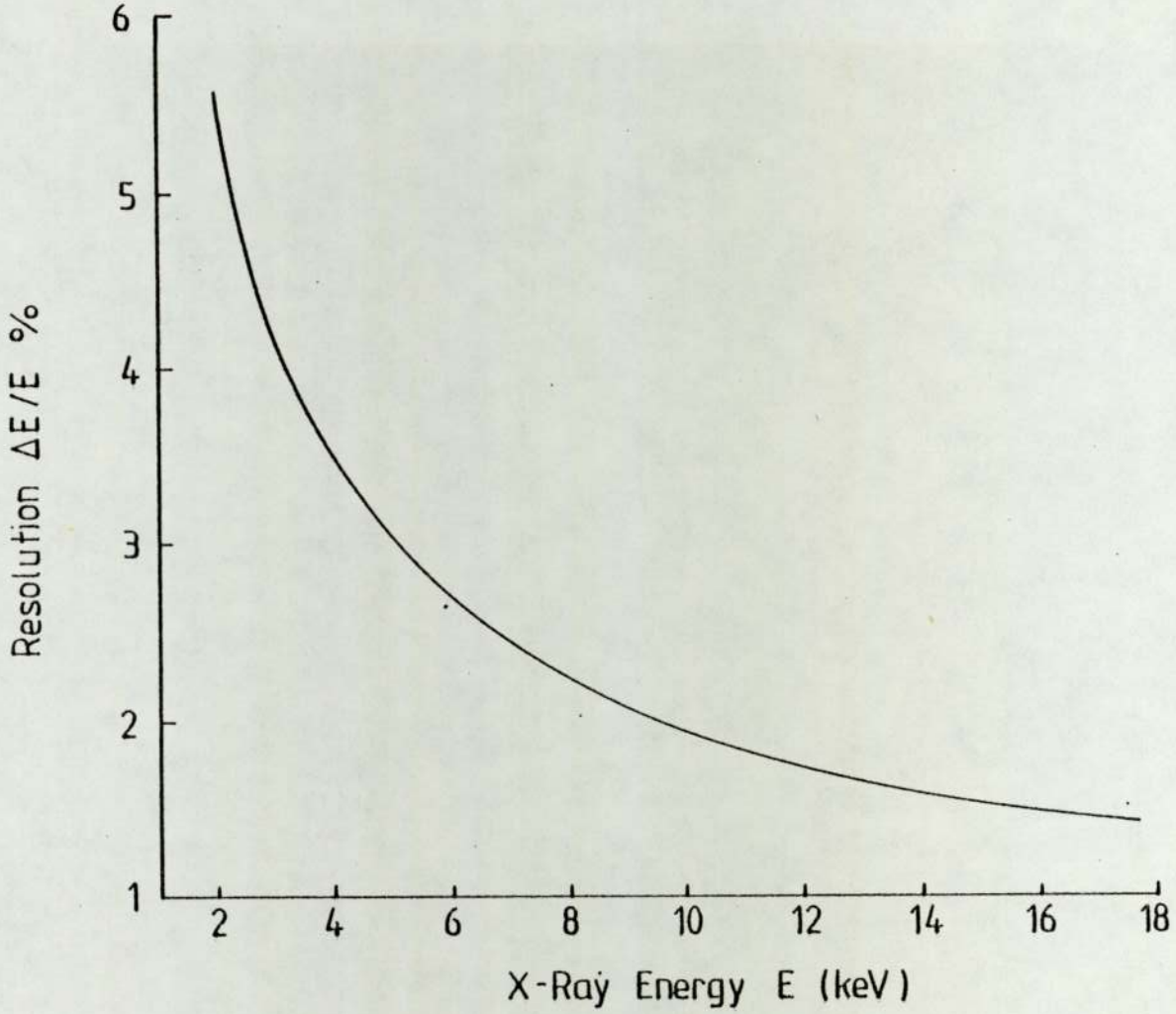

Fig 3:7 Typical resolution for Si(Li) detector used in this work

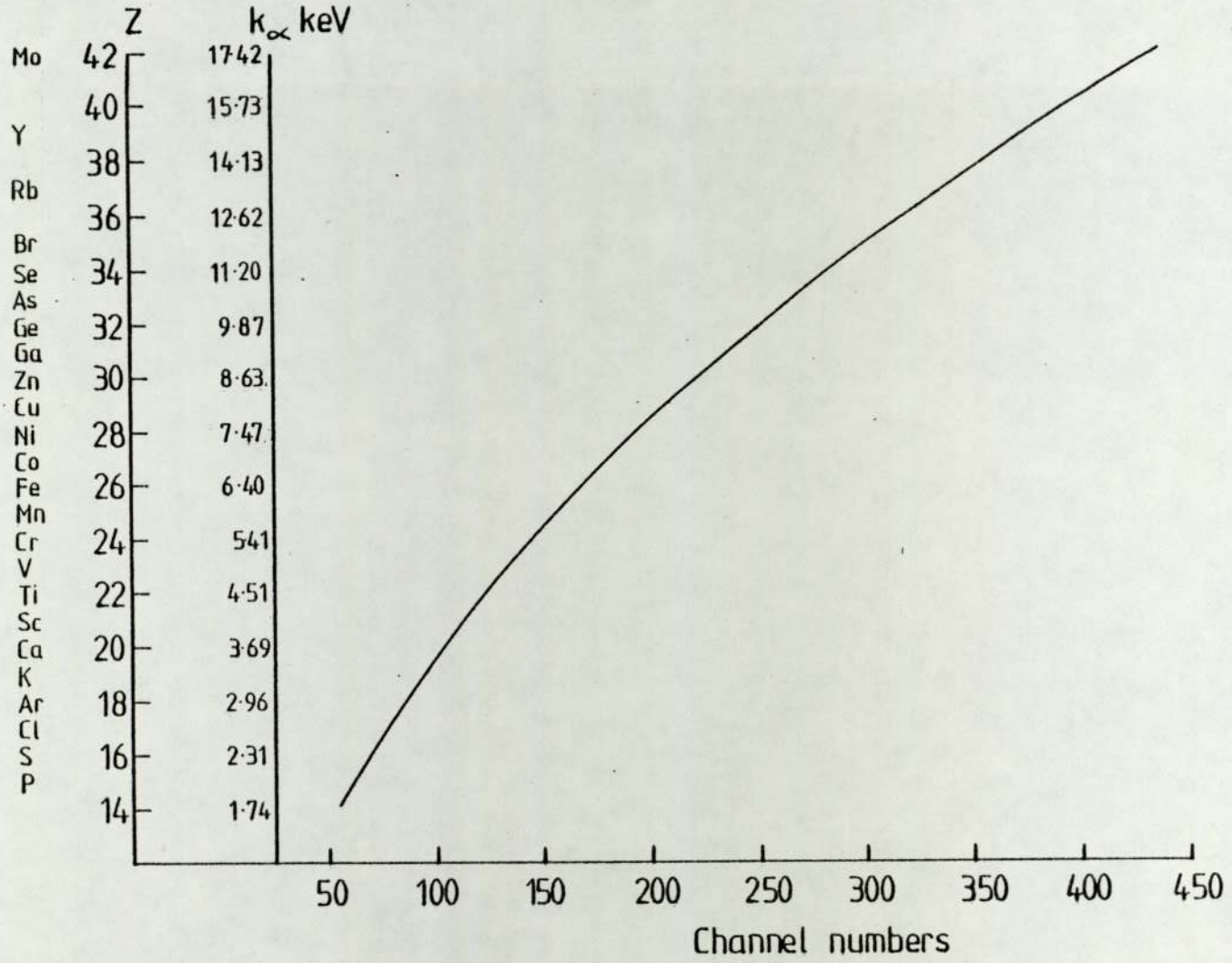

Fig 3:8 Calibration curve. The atomic numbers and energies for elements of interest as a function of channel number

Table 3.2

$E_\alpha(z)$ keV	$[E_\alpha(z+1)-E_\alpha(z)]/[E_\alpha(z)]$ %	$[E_\beta(z-1)-E_\alpha(z)]/[E_\alpha(z)]$ %
2.015	14.52	-9.05
2.307	13.63	-7.41
2.621	12.78	-5.99
3.312	11.4	-3.62
3.690	10.77	-2.74
4.508	9.78	-1.04
5.895	8.57	0.92
6.925	7.90	1.95
8.041	7.33	3.22
9.243	6.795	4.03
9.876	6.64	4.50
13.370	5.73	6.34
14.933	5.45	6.96
17.443	5.41	7.81

Relative energy difference between adjacent x-ray lines of some elements.

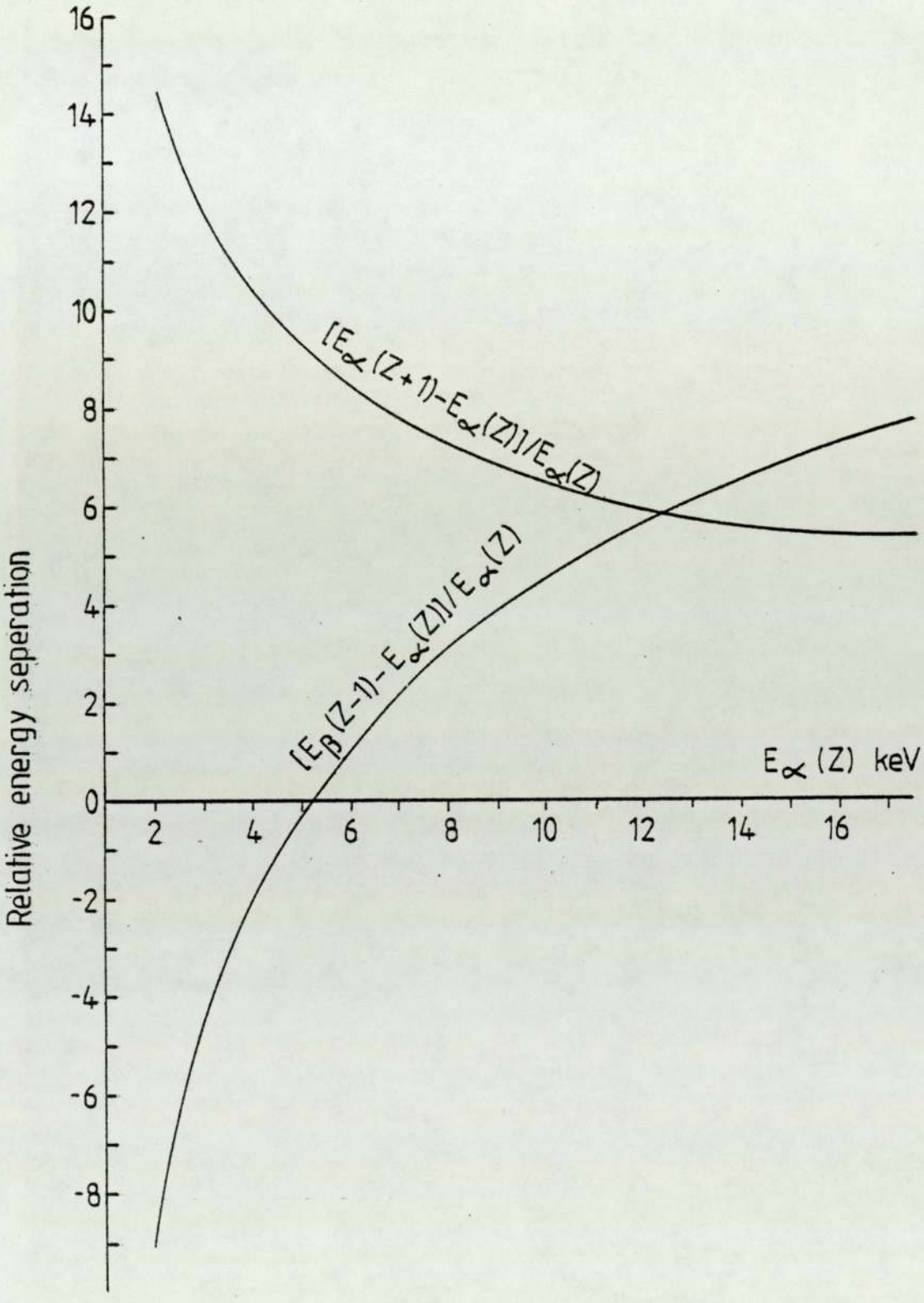

Fig 3:9 Relative energy difference between adjacent x-ray lines of elements.

In order to relate the number of pulses counted to the number of photons incident on the detector, it becomes necessary to estimate the detector efficiency. It is convenient to subdivide counts efficiencies into two classes, absolute and intrinsic. Absolute efficiencies are defined as:

$$\varepsilon_{abs} = \frac{\text{number of pulses recorded}}{\text{number of quanta emitted by source}} \quad \ldots 3.5$$

and are dependent not only on detector properties but also on the details of the counting geometry (primarily the distance from the source to the detector).
The intrinsic efficiency is defined as:

$$\varepsilon_{int} = \frac{\text{number of pulses recorded}}{\text{number of quanta incident on detector}} \quad \ldots 3.6$$

The two efficiencies are simply related for an isotropic source by:

$$\varepsilon_{int} = \varepsilon_{abs} \cdot \frac{4\pi}{\Omega} \quad \ldots . 3.7$$

where Ω is the solid angle of the detector seen from the actual source position, Knoll (1979)

The efficiency of a Si(Li) detector to x-rays, depends on the energy of the x-ray, detector thickness, and the entrance windows employed. Since the x-ray absorption obeys an exponential attenuation low, the approximate detection efficiency can be calculated using the expression:

$$\varepsilon_{int} = \left(1 - e^{-\mu_{si} x_{si}}\right) e^{-\sum_i \mu_i x_i} \quad \ldots . 3.8$$

where x_{si} and x_i are the thickness of the detector and windows respectively, μ_{si} and μ_i are the appropriate energy dependence absorption coefficients.

The estimated efficiency as a function of x-ray energy using equation 3.8 is shown in fig.3.10 for a 3 mm thick Si(Li) detector with a 12.5 micron Be window, together with the resulting calculated efficiency for the x-ray passed through 50 micron Melinex window and 3.2 cm air before entering the Be window of the detector. The detector is approximately 100% efficient for detecting incident x-ray with energies between 7 and 16 keV, the efficiency at low energies is critically dependent on the thickness of window materials. For very soft radiation, even a few centimeters of air between the source and detector can lead to significant attenuation, Fig.3.10. At higher energies, the peak efficiency begins to fall-off rapidly, reflecting the similar fall-off of the photoelectric cross section in silicon.

In an ideal detector the total charge is completely collected for each detector event and the response of the system to monochromatic photons is a single peak with zero counts elsewhere in the spectrum, Freund et al (1972). Processes in the detector which results in only partial deposition of an x-ray's energy or incomplete charge collection give rise to undesirable background features in the x-ray spectrum. These features include low energy tailing, pulse pile up, and Si escape peaks.

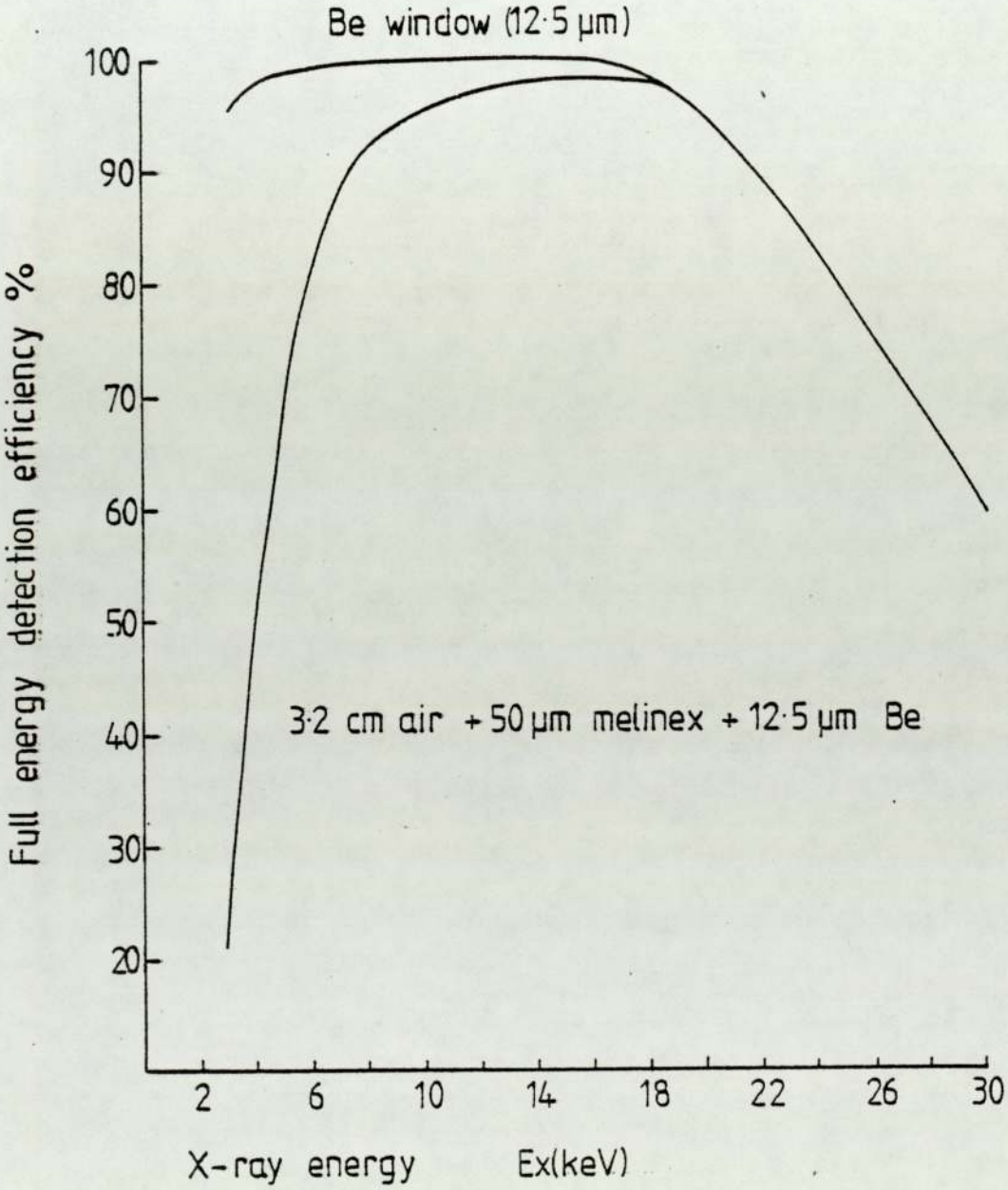

Fig 3:10 Calculated efficiency for a 3mm thick Si (Li) detector

Investigations of the nature of low energy tailing background have established that its origin is the distortion of internal electric fields caused by the detector surfaces present in most geometries, Jaklevic and Goulding (1972), Goulding (1977). Fig.3.11(a) shows a cross section of a typical detector, Jaklevic (1972), the shaded portions indicate areas in which the internal field lines do not terminate at the electrical contact formed by the metal surface barrier, but, instead, terminate on the ill-defined surface. Events occurring within this region experience incomplete collection of charge signal resulting in a smaller signal than should be produced.

The magnitude of this background can be reduced by collimating the incoming radiation to avoid the shaded region, a lead collimator of 4 mm diameter is used in this work. Another approach is to use the guard-ring detector fig.3.11(b), here a guard ring is added on the lithium-diffused side and the signal is taken from the central area while the outer ring serves to maintain uniform internal field lines in the detector, Jaklevic. The other detector background below the principal peak is established by the escape of secondary photons from the detector surface. Photoelectric absorption of an x-ray in the detector ejects an electron from one of the Si atoms shells creating a vacancy which subsequently fills with accompanying emission of Si characteristic x-rays. To produce a full-energy signal, the whole energy

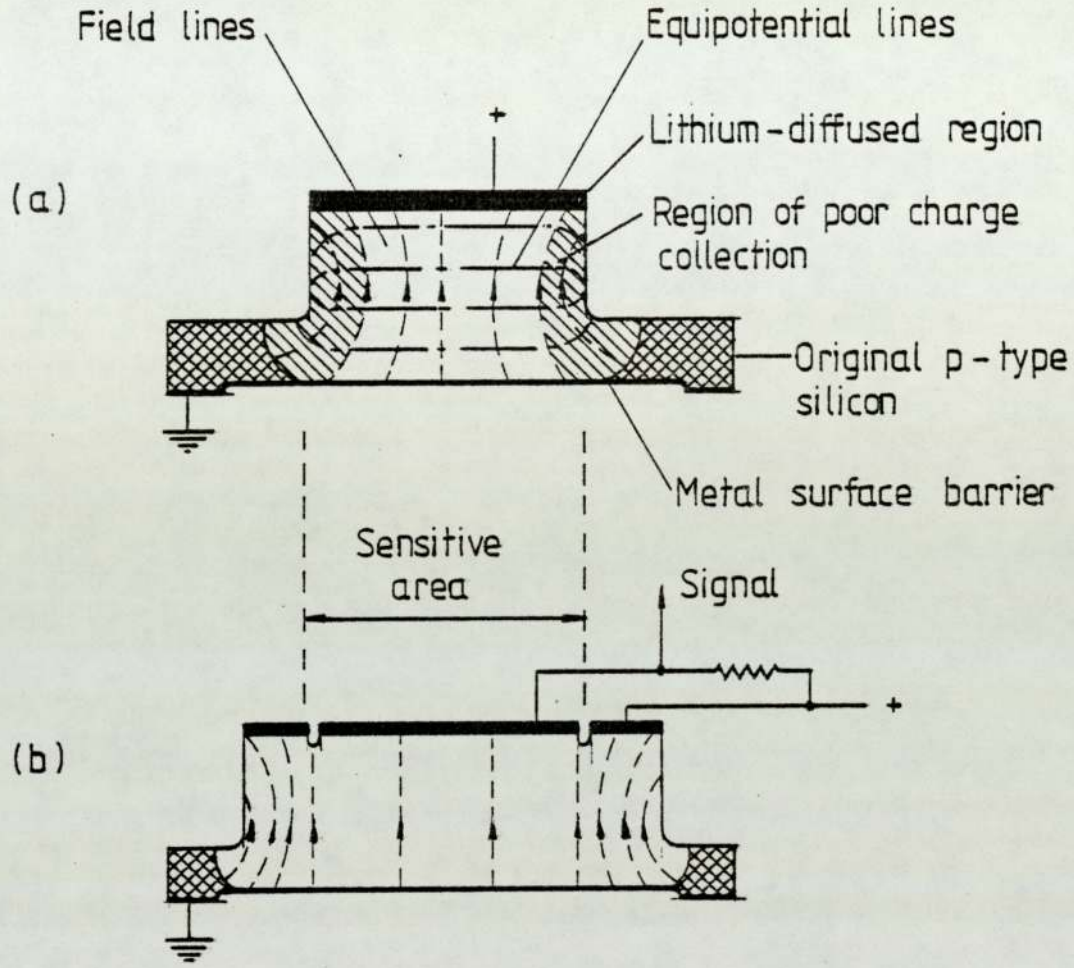

Fig 3:11 Cross sections of (a) a top-hat detector geometry and (b) a guard-ring detector showing the internal field distributions taken from Jaklevic and Goulding (1978)

of the initial photoelectron and that of the secondary radiation produced must be absorbed in the sensitive region of the detector. Any loss of energy will cause a signal smaller than desired resulting in detector background. This type of background depends only on the characteristics of the detector material and on its geometry. The escape of a characteristic x-ray of the detector material subtracts a definite energy from an event, and such events produce discrete 'escape' peaks in the background distribution at energies slightly below the main peaks. In the case of Si, the K escape causes a peak at an energy 1.74 keV less than the full-energy peak, Jaklevic and Goulding (1978). The probability for escape of the Si Kα x-ray as a function of the energy of the parent x-ray has been measured by Woldseth (1973) and increases for decreasing x-ray energies. This behaviour can be understood since the softer x-rays interact nearer the detector surface increasing the probability for Si Kα escape. In hair analysis, the elemental concentrations are not enough to generate significant escape peaks, and they are not seen.

In order to achieve the minimum possible resolution contribution due to electric noise sources it is necessary to filter the output signals to enhance the signal relative to noise, The first stage of the preamplifier is mounted with the detector and maintained at low temperature in the cryostat, the amplifier uses a long shaping time for efficient noise suppression.

But longer pulse shaping times increase the probability that a second pulse may arrive while the first pulse is being processed, resulting in an overlap of the two pulses in the main amplifier, pulse pile up, Khan(1976). This long pulse-shaping time places a limit on the maximum allowable counting rate. Fig.3.12, taken from Jaklevic (1978), is a plot of the counting rate characteristics of a semiconductor detector system operated at various pulse-shaping times, where the best resolution is achieved at 17 μs. However, the output rate at high input counting rates is higher for lower values of shaping time. The probability of pile up can be diminished by reducing the shaping time constant of the amplifier which is accompanied, however, by a corresponding loss of resolution, or by reducing the counting rate which thereby increases the analysis time required to obtain the same statistical accuracy. Depending on the application, a compromise value can be employed. Typical parameters for this work include shaping time constant of 8 μs and a counting rate of about 600 counts per second.

III.B Data Interpretation:

The elements present in a sample can be quickly identified from the appearance of multiple characteristic x-ray lines spectra and the energy calibration curve fig.3.8. To go from the easy rough qualitative estimate to the quantitative analysis requires more than additional practice;

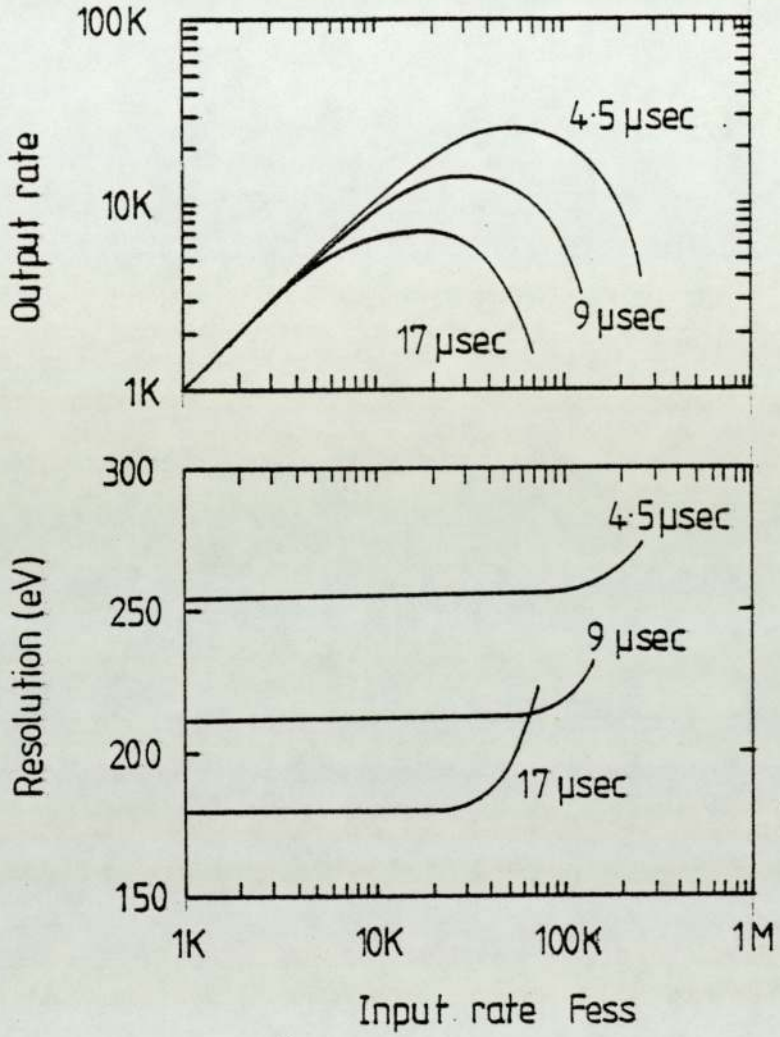

Fig 3:12 Output-counting and energy-resolution rate as a function of input counting rate for a pulsed optical-electronic processor employing pile-up rejection, taken from Jaklevic and Goulding (1978)

it requires mathematical data treatment, perhaps as simple as preparation of calibration curve sec.III.C.1, or as complex as computer calculations of elaborate matrix effects sec.III.C.2. Data interpretation can be optimised if one understands why it is necessary and how detailed it needs to be for different kinds of application or degree of reliability. The next section will consider individually the several factors which one needs to account for.

III.B.1 Spectral Analysis:

Once each peak has been located, the next step normally involves a sequential examination of the data in the immediate vicinity of individual peaks to determine their area. Intensities of the single lines can then be calculated from the number of counts in the peak, peak area. Various automated techniques for determining peak area in multichannel spectra have been compared in Baedecker (1971), Kokta (1973), and Hertogen et al (1974). The methods can be subdivided into two groups: those which obtain the area from a fitted analytical function, and those which carry out a direct summation of the data points between prescribed limits. In either approach, the contribution of the continuum upon which the peak is superimposed must be subtracted. The data in the channels on either side of each peak are normally used to define the continuum, and an assumed linear or quadratic curve is fitted to produce an estimated continuum

in the region under the peak. Channel-by-channel subtraction of the continuum then produces corrected data for the following steps.

In the direct summation method, some criteria must be preselected for the number of channels over which the data will be summed. In principle, the summation should extend over all channels which are significantly above the continuum. In practice, it is normally limited to a given number of channels on either side of the peak centroid, depending on the detector resolution. A number of alternative schemes are discussed in Kokta (1973).

A more common procedure is to use the area obtained from an analytical fit to the data points comprising the peak. Most assumed shapes involve a primary Gaussian peak with a small additive component to represent tailing on low-energy side of the peak, caused by incomplete charge collection within the detector. The primary contribution to the photopeak in a semiconductor detector is a Gaussian distribution arising from the statistical fluctuation in the division of absorbed energy between ionization and heating of the crystal lattice (Fano factor). The degree to which the experimental data deviate from this fundamental description is dependent on the quality of detector, associated electronics, and other experimental considerations. Least-squares methods are normally used to fit the function, and the area is then derived from the fitted

shape parameters. Examples of a number of complex fitting functions applied to Ge(Li) and Si(Li) detector photo-peaks are given in Roberts et al (1975), McNelles and Campbell (1977).

If the complicating effects of background continuum and peak tailing are not significant or can be subtracted out, most spectral peaks can be treated as a simple Gaussian

$$Y(x) = Y_o \exp\left[-(x - \mu)^2 / 2\sigma^2\right] \qquad \ldots.3.9$$

where Y(x) is the amplitude of the Gaussian at channel x, Y_o is its maximum, μ is the centroid, and σ is the standard deviation. In this case, the iterative procedures normally required for more complex fitting function can be replaced by simple direct process, Mukoyama (1975), Abondanno et al (1977), Mukoyama (1981).

Several computer programs which are available in the Radiation Centre computer system permit individual peak areas, centroids, and standard deviations to be determined, those used in this work are, PEAK routine, NEIB, and J J Fit.

The PEAK routine, applies the first method, it calculates the sum of counts, centroid, and standard deviation of the peak. Two or more channels each side of a complete peak are used in a linear background calculation.

The NEIB routine, applies the second method, it fits a simple Gaussian to a specified number of channels, two or more channels on each side of the peak are used in computing the straight line approximation to the background.

JJ Fit is a non linear least square technique which can fit for a single line peak or double (over lapping) peaks. (Documentation of program JJ Fit).

The calibration factors, sec.III.C.1, used in the analysis to convert x-ray counts into elemental abundances are generated from the experimental values for standard foils. The x-ray calibration factor for each element is extracted from the peak area of the reference line for that element. For all elements the spectral lines from these standards are fitted to a single Gaussian line shape, NEIB, and the method of direct summation, the PEAK routine, in order to obtain the peak area, centroid, and standard deviation yielding the best fit. The resulting standard deviation as a function of energy, for the two routines, is represented in fig.3.13. It is found that resulting areas using PEAK and NEIB routines at these standard deviation are nearly the same. The resulting standard deviation for each element, Fig.3.13, is used to extract the best fit for the element in biological samples. An example of NEIB fit together with the PIXE line is represented in fig.3.14. In small peaks only PEAK routine is applied.

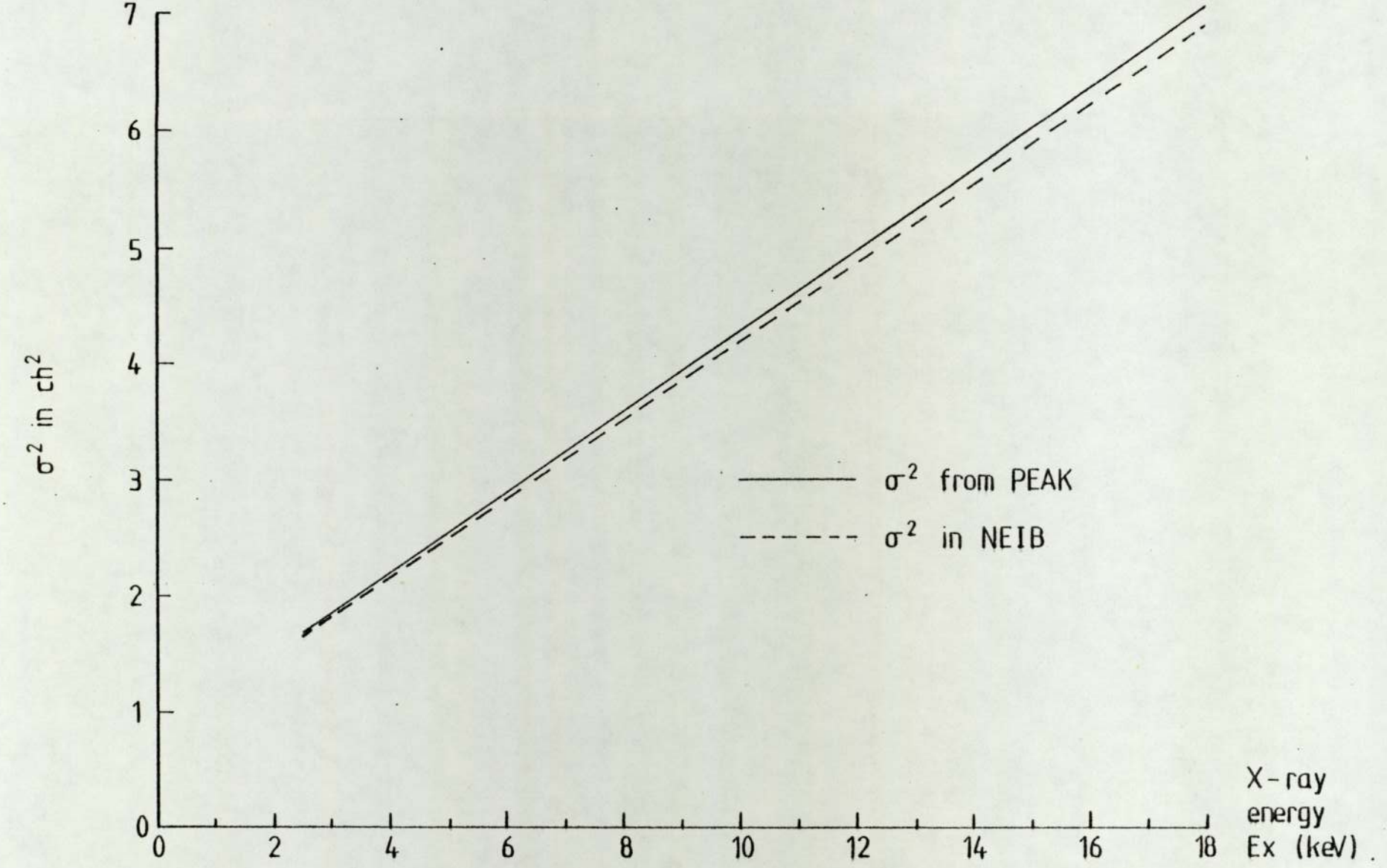

Fig 3:13 The resulting standard deviation as a function of x-ray energy for the PEAK and NEIB routines

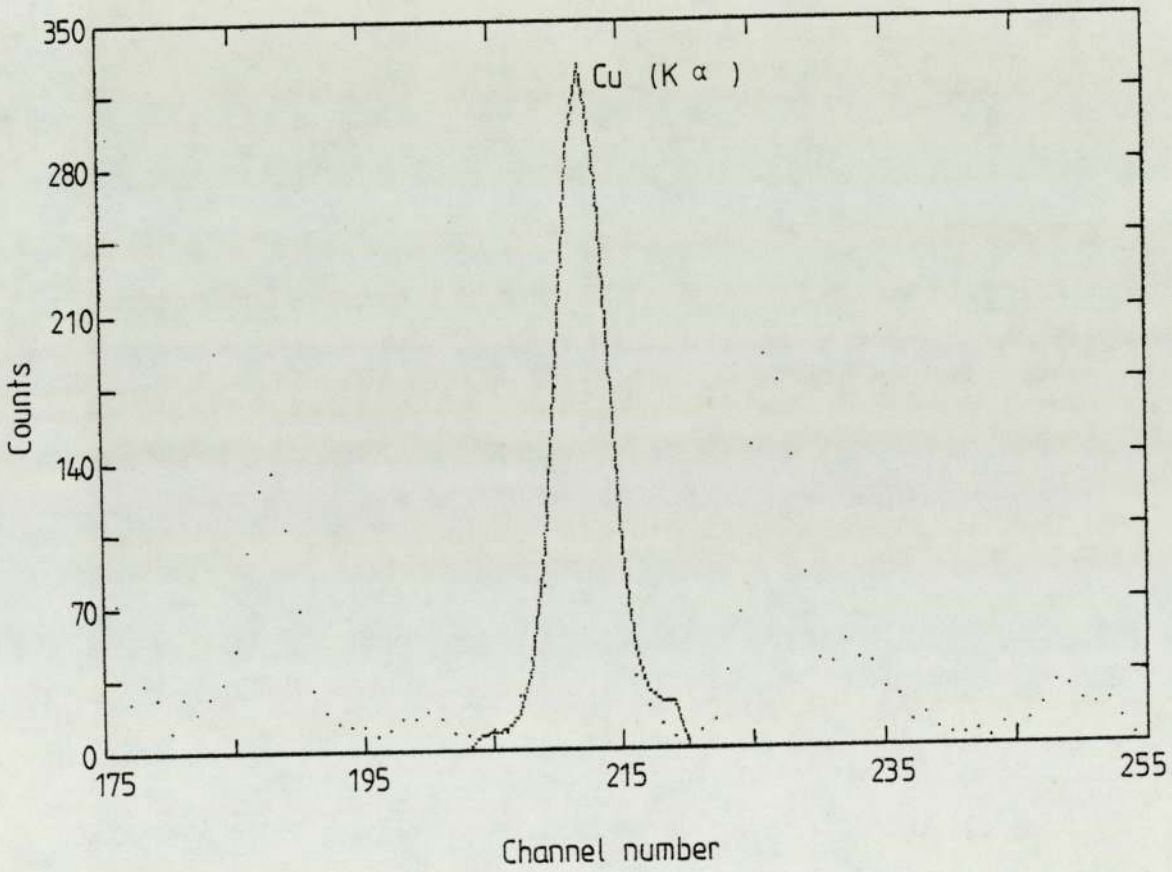

Fig 3.14 Gaussian fit NEIB to Cu line on PIXE spectrum from bovine liver. ····· Bovine liver, —— NEIB.

III.B.2 Background:

Fig.2.1, reproduced in fig.3.15, helps to illustrate the complexity of the problem of background in spectral analysis. The spectrum is obtained from a deposit of 3 μL of digested bovine liver (SRM 1577) on a kimfoi backing, affixed with 2 μL low-Z glue (sec.III.D.1). An aluminium filter, 5 micron, is inserted between the chamber and the detector.

The signal to be related to composition is the characteristic line for each element. As seen in fig.3.15, and as discussed before, sec.II.5.1, there is always some background intensity, and this must be subtracted from the total intensity at each line position. Because the 5 μm aluminium filter attenuate the lowest x-ray energies, and because the detector efficiency drops at low energies, the observed background appears to fall off below channel 96. The effect of the absorption and the bremsstrahlung shape causes a broad hump around channel 96 with the 5 micron aluminium filter, in this region it is very difficult to define the x-ray line intensity. The proton bremsstrahlung becomes significant around channel 200 and is responsible for the levelling off of the counts in channels above 220. These backgrounds arise in both the target material and its backing. In addition however, there is the "chamber background". This arises from charged particles which are scattered and impinge on material other than the sample. Fig.3.16 is the chamber

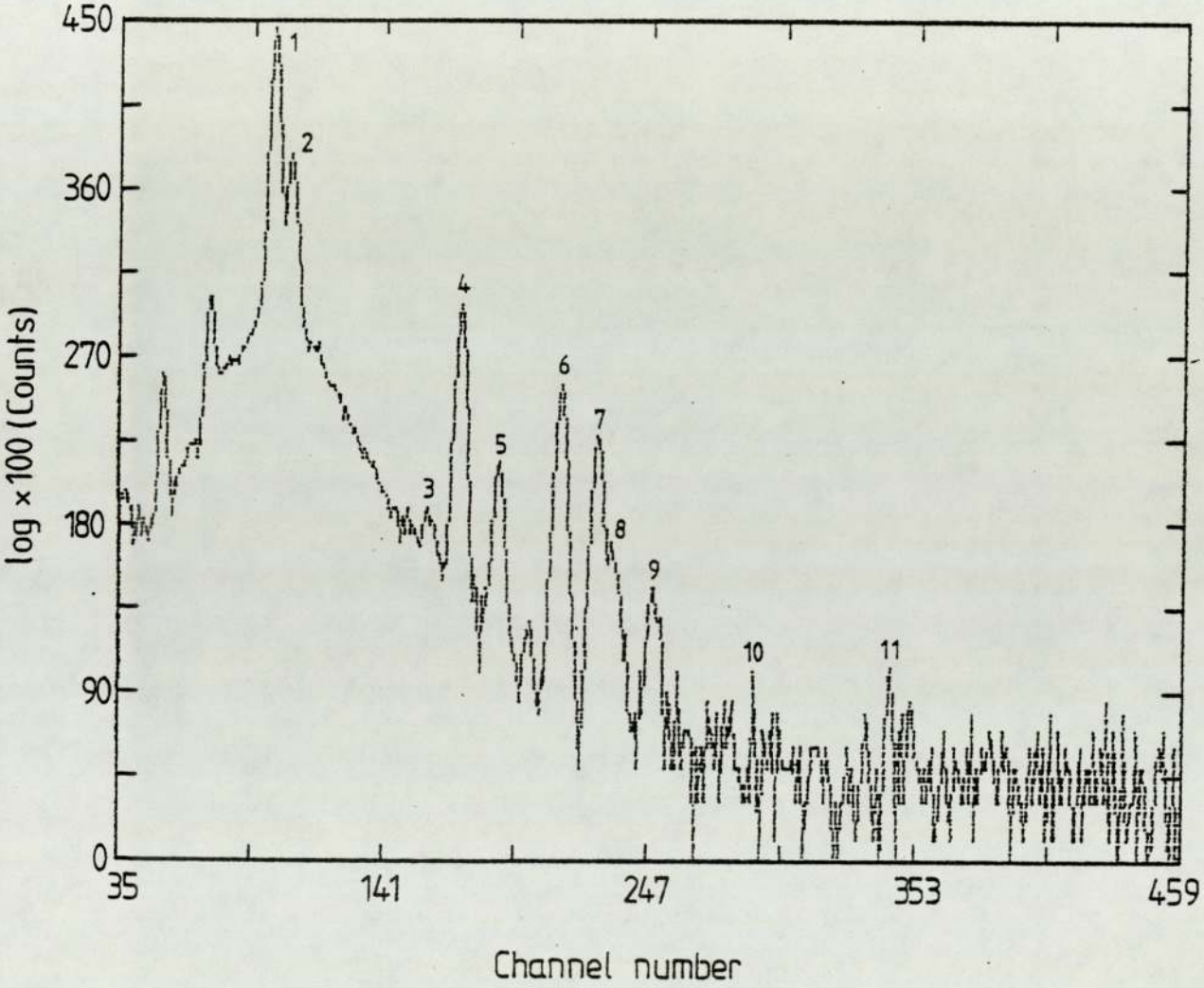

Fig 3.15 PIXE spectrum from the analysis of bovine liver.

1 - K (K α)
2 - Ca (K α)
3 - Mn (K α)
4 - Fe (K α)
5 - Fe (K β)
6 - Cu (K α)
7 - Zn (K α)
8 - Cu (K β)
9 - Zn (K β)
10 - Se (K α)
11 - Rb (K α)

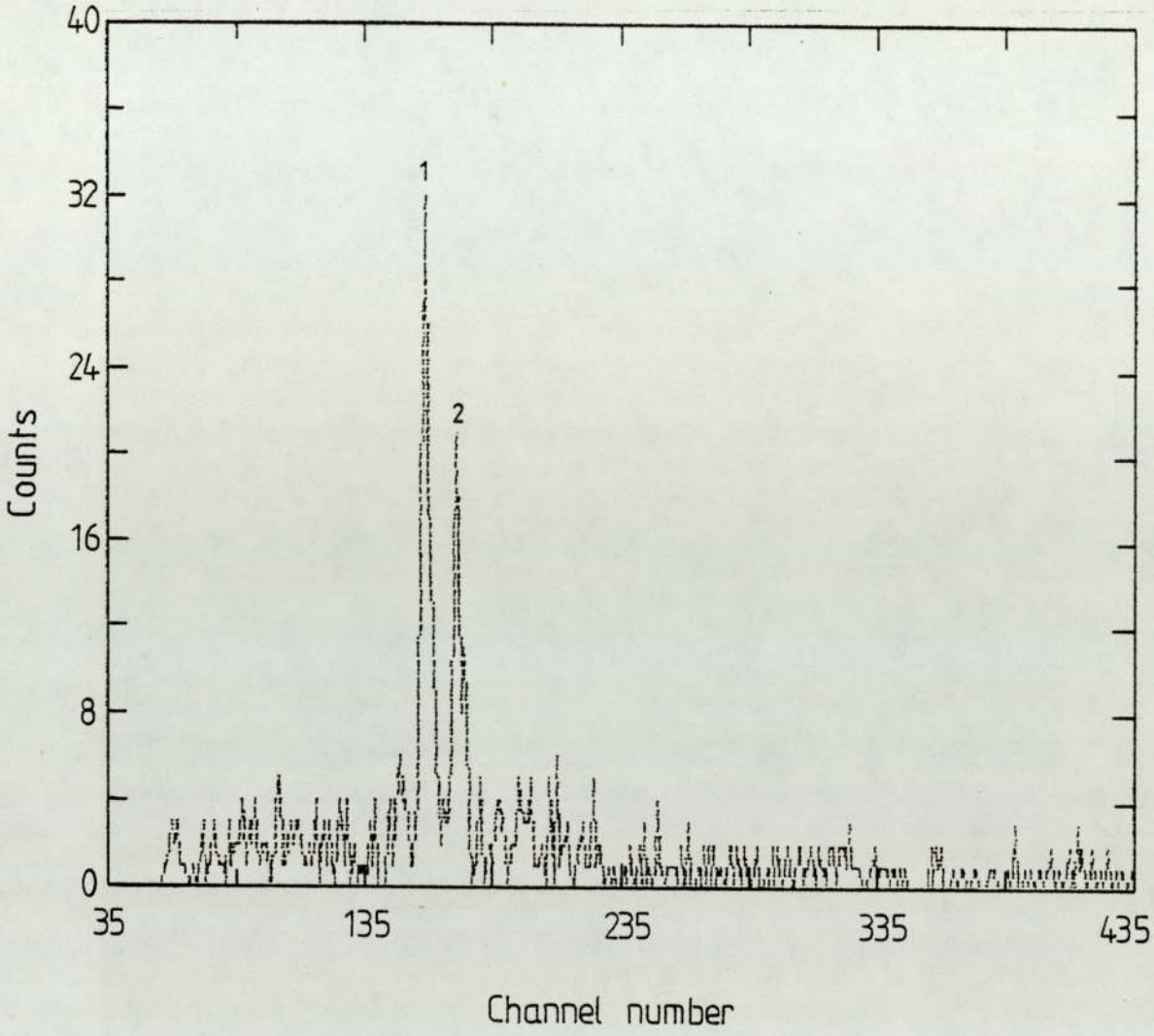

Fig 3.16 PIXE spectrum for the background from the chamber.

1 - Mn (K α)
2 - Fe (K α)

background, obtained from a 2.37 MeV proton beam, employed on the frame, with no target or backing, for 25 μc. It is clear therefore, that any specific analysis performed with the technique must be preceded by an investigation of the chamber background, and backing material impurities, and of their intensities relative to the x-rays intensities from the actual samples. Unless this is done and subtracted, there is no guarantee that the calculated areas represent faithfully the constitution of the specimen. To investigate this, a blank kimfoil with 2 μL glue only on it, is irradiated under the same condition as the sample under investigation. The resulting background, fig.3.17, is subtracted from the total intensity before the spectral analysis, since the PEAK and NEIB fit is more reliable with the background removed, especially in the region where the background is largest.

III.B.3 Line Interference:

The large number of x-ray lines and the limited resolution power of Si(Li) detectors makes line interferences unavoidable. Fortunately, in most analytical situations there are methods to handle these problems, and to correct the x-ray characteristic lines for interference. Refering to fig.3.15, where the Cuβ line interferes with the Znα line, but there is no interference with the Cuα line. The fractional contribution of Cuβ at the Znα is measured, simply the Cuα intensity is

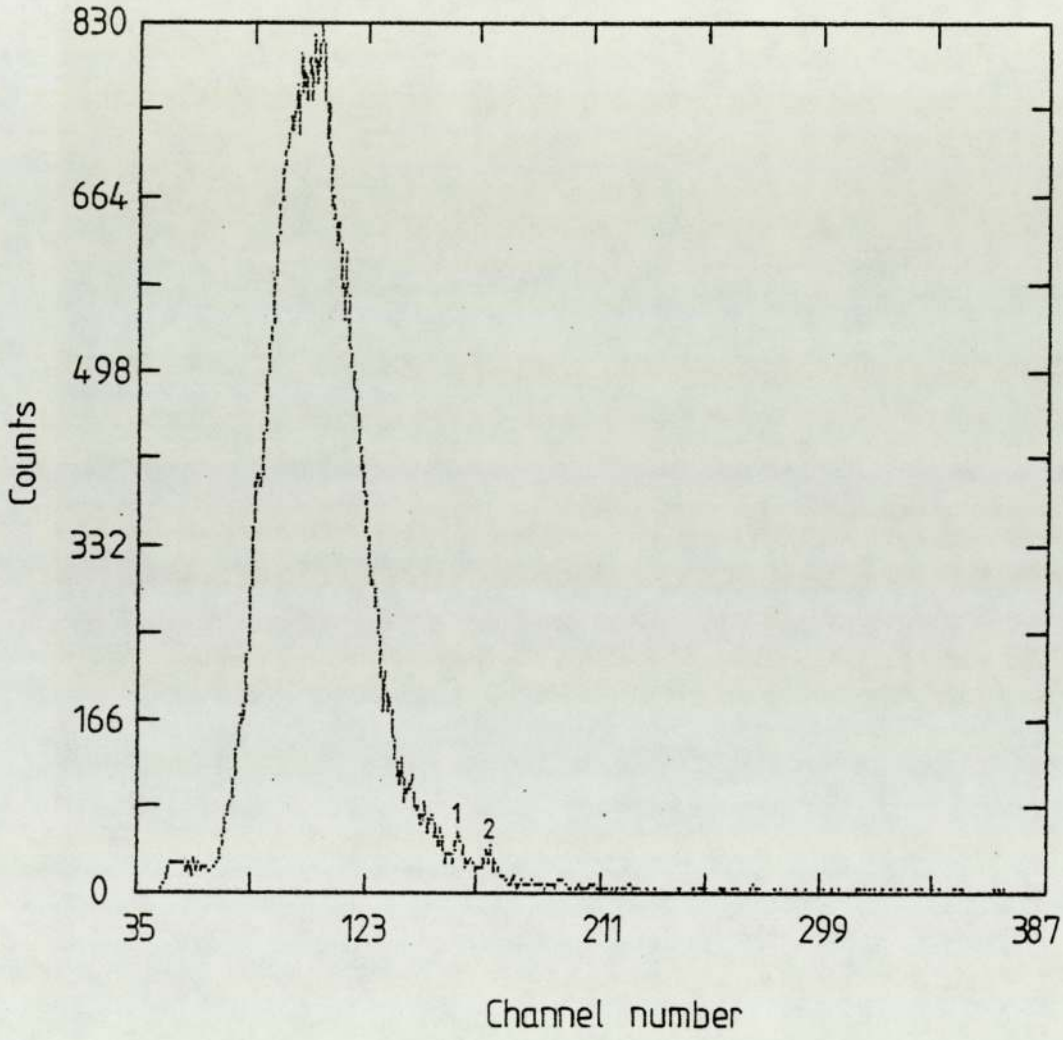

Fig 3.17 PIXE spectrum from Kimfol backing with 2 μm glue on it.

1 - Mn (K α)
2 - Fe (K α)

measured first, then using the ratio $K_\beta/K\alpha$ for Cu, the intensity of Cu_β can be estimated. Using the PEAK routine the area under the combined peak of $Zn\alpha + Cu_\beta$ is determined and $Zn\alpha$ intensity is found by subtracting the Cu_β intensity from the total.

In order to obtain a more reliable value for the area of interest the JJ Fit is applied for the overlapping peaks and the best fit to data obtained by searching the parameter space for the point which minimises χ^2 (Documentation of JJ Fit taken from Bevington 1969). What is more important is when $Co\alpha$ as well as Co_β is interfered with by Fe_β and $Ni\alpha$ lines, shown in fig.3.18 for H H-1 hair spectrum, but there is no interference with $Fe\alpha$. Then the intensities $I_{Co\alpha}$ and $I_{Ni\alpha}$ are determined by solving the equations:

$$I_{Co\alpha} = I_{Co\alpha+Fe\beta} - (K_\beta/K\alpha)_{Fe} \cdot I_{Fe\alpha} \quad ....3.10$$

$$I_{Ni\alpha} = I_{Ni\alpha+Co\beta} - (K_\beta/K\alpha)_{Co} \cdot I_{Co\alpha} \quad ....3.11$$

The steps followed to extract the peak area are represented by flow-chart fig.3.19. Table 3.3 gives the x-ray lines investigated and the interferences subtracted.

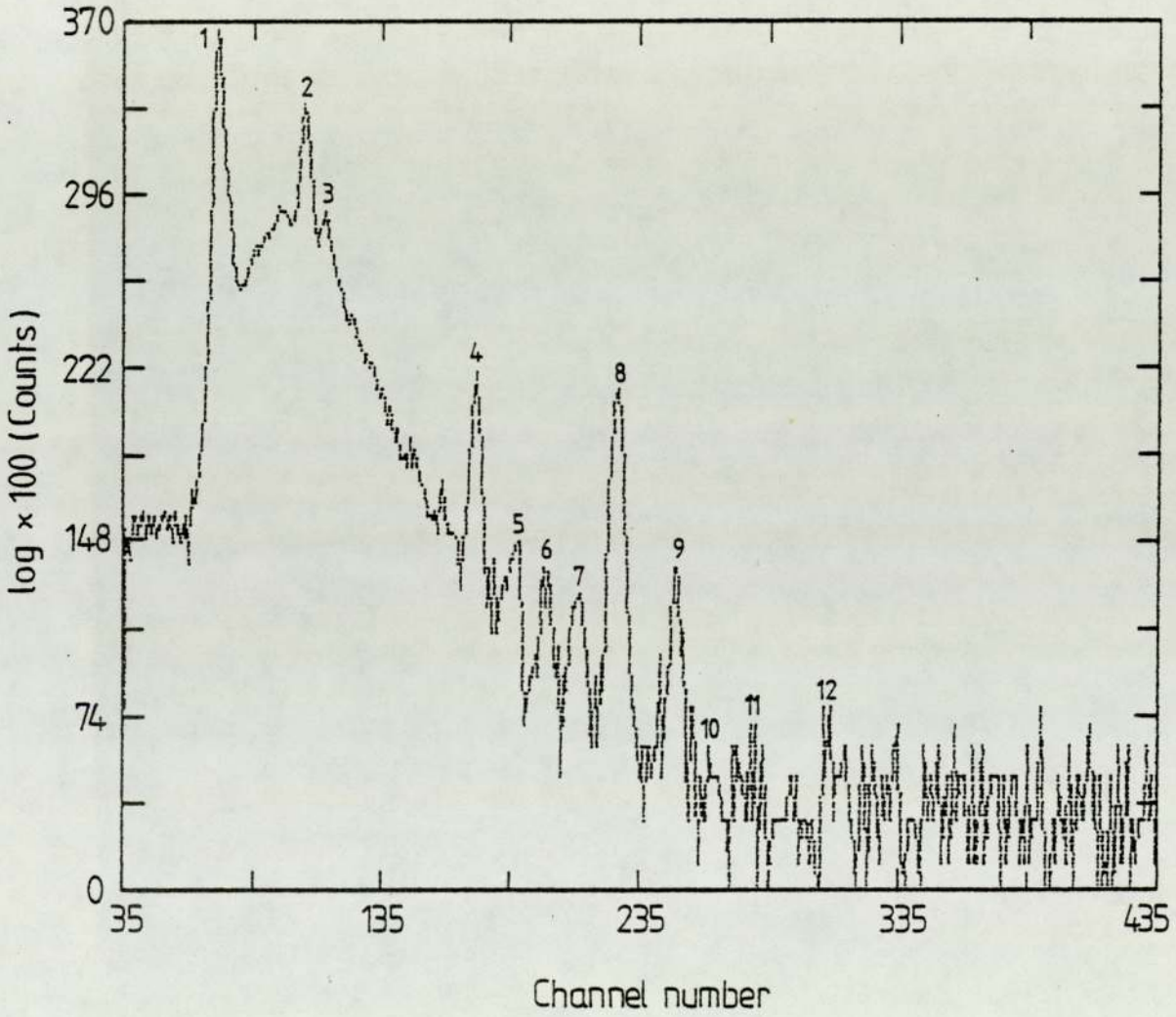

Fig 3.18 PIXE spectrum for hair HH-1, IAEA hair sample.

1 - S (Kα + Kβ)	7 - Cu (Kα)
2 - Ca (Kα)	8 - Zn (Kα)
3 - Ca (Kβ)	9 - Zn (Kβ)
4 - Fe (Kα)	10 - Hg (Lα)
5 - Fe (Kβ)	11 - Pb (Lα)
6 - Ni (Kα)	12 - Br (Kα)

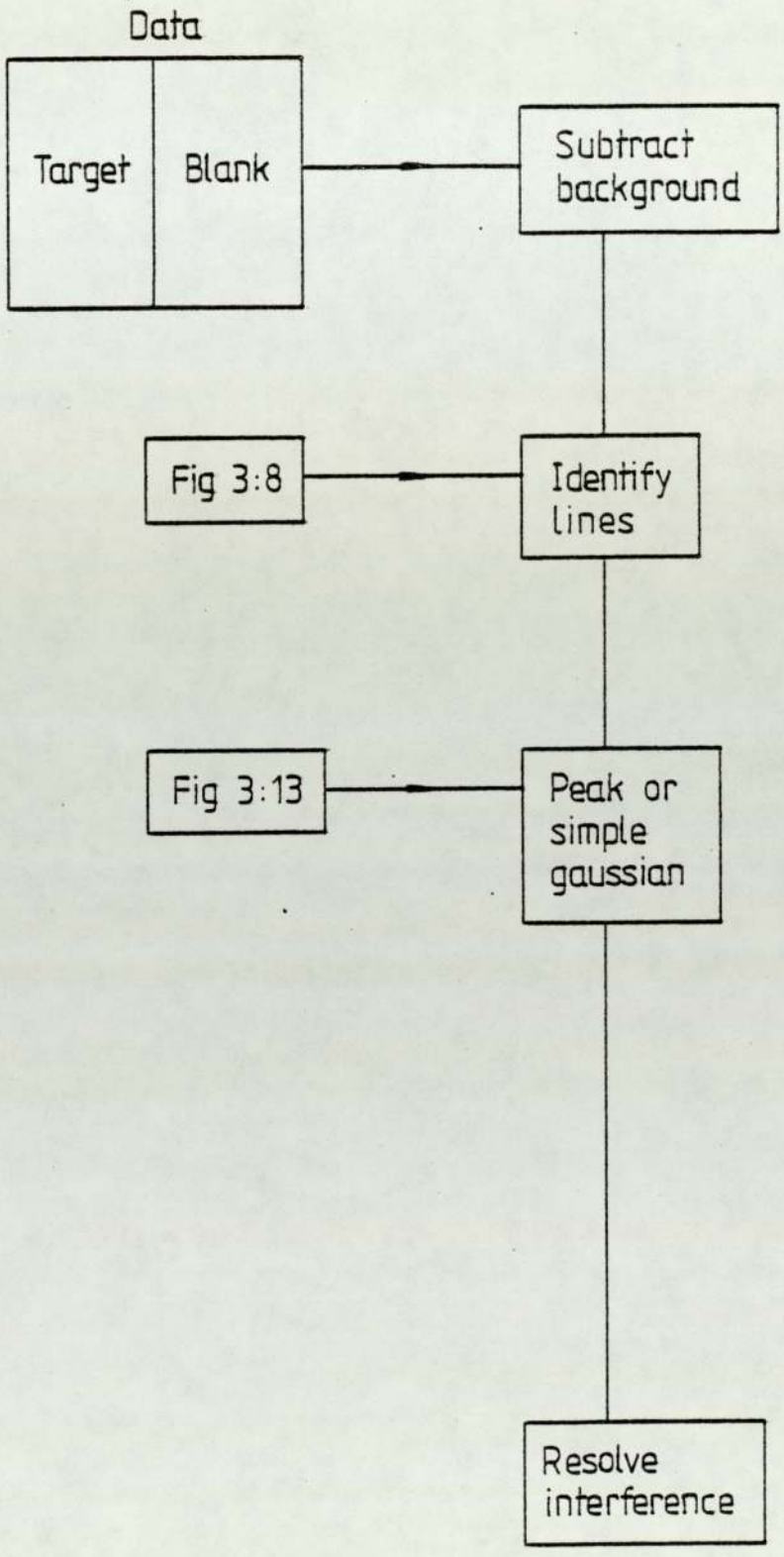

Fig 3:19 Flow-chart for extracting the peak area

Table 3.3:

X-ray lines and interferences line subtracted in the analysis:

Element	PEAK used	Interference Peak
S	$K\alpha + K\beta$	non
K	$K\alpha$	non
Ca	$K\alpha$	K $K\beta$
Ti	$K\alpha$	non
Mn	$K\alpha$	Cr $K\beta$
Fe	$K\alpha$	Mn $K\beta$
Co	$K\alpha$	Fe $K\beta$
Ni	$K\alpha$	Co $K\beta$
Cu	$K\alpha$	Ni $K\beta$
Zn	$K\alpha$	Cu $K\beta$
Se	$K\alpha$	non
Br	$K\alpha$	Hg $L\beta$
Rb	$K\alpha$	Br $K\beta$
Mo	$K\alpha$	non
Hg	$L\alpha$	non
Pb	$L\alpha$	non

III.C System Calibration

All of the factors discussed up to this point are merely to eliminate background and interferences so that the true intensity of a given characteristic x-ray line can be stated unambiguously and quantitatively. We now come to the important calibration which must be made so that x-ray intensity can be converted to chemical composition i.e. to determine from x-ray intensity of element Z and a given target, one or more of the following:

1. the absolute mass of element Z in the irradiated fraction of the target $M_Z(g)$;
2. the areal density ($\rho_z t$) of element Z of the target (g/cm^2);
3. the concentration (ppm) of element Z in the target.

Calibration of a PIXE system requires that the experimentally observed quantity (number of Z x-rays observed (Y_Z) per unit proton charge (Q) collected on the target) be related to the physical quantity of interest (M_Z, $\rho_z t$, or ppm) for all elements of interest. This relation is expressed in the following formula, for a beam area greater than the target area Willis(1977), Khan and Crumpton(1981):

$$M_Z(\mu g) = \left[\frac{A_Z \cdot e \cdot 10^6}{N_o \cdot \sigma_Z^{pro}(E_o) \cdot \frac{\Omega}{4\pi} \cdot \varepsilon_{int}}\right] \cdot \frac{C(Z) \cdot Y_Z \cdot A_B}{C_{Al} \cdot Q}$$

$$= \frac{F(Z)^{-1} \cdot C(Z) \cdot Y_Z \cdot A_B}{Q \cdot C_{Al}} \qquad 3.12$$

where

M_Z = mass of the element Z (μg) in the irradiated region of the target,

Y_Z = number of x-ray counts appearing in a selected x-ray line of element Z,

Q = total proton charge incident on the target (μc)

A_B = cross sectional area of proton beam (cm^2),

A_Z = atomic weight of element Z,

$\sigma_Z^{pro}(E_o)$ = x-ray production cross section for element Z, proton energy E_o, and the atomic shell K of interest (cm^2/atom),

No = Avogadro's number (mol^{-1}),

e = unit of charge (μc),

Ω = solid angle by the detector at the source position in steradians,

ε_{int} = intrinsic detector efficiency,

C_{Al} = absorption losses in aluminium x-ray filter,

C(Z) = correction factor to account for proton energy loss and x-ray attenuation in the target,

F(Z) = thin target calibration factor for element Z (counts/μc.μg.cm^{-2}).

It is, however, initially necessary to establish a reliable calibration of the analytical system, and to secure good stability of the experimental arrangement by periodically analysing samples sensitive to any significant changes in the system. The calibration may be performed in different ways. One approach is to procure accurate values of all the individual physical parameters of the

system. Another way is to determine the calibration factor for each element of interest by a calibration curve obtained from experimental values.

It is convenient in the following discussion to distinguish between certain types of targets, three types of targets can be considered: thin targets, moderately thick targets, and thick targets.

III.C.1 Calibration of Thin Targets:

Equation 3.12 is simplified if $C(Z) \simeq 1$. This condition will be satisfied if target thickness cause:

(i) negligible proton energy loss, so that the x-ray production cross-section, which is energy dependent, can be taken as constant throughout the sample, and

(ii) negligible absorbtion of x-rays, produced from the element of interest, in the sample matrix. Such a target is defined as a thin target. In the case of thin metallic samples x-ray absorption is the dominant criterion which determines the thickness and thin samples have areal densities typically 20-100 $\mu g/cm^2$. For biological samples the variation of cross-section with energy determines the thickness, and, thin biological samples are typically 1 mg/cm^2 thick, Khan and Crumpton(1981).

With $C(Z) = 1$, the thin target calibration is determined by a calibration function $F(Z)$ which is matrix independent.

That is, the same calibration is valid for all thin target analysis regardless of matrix composition. This is not the case for intermediate or thick targets because the value C(Z) depends on the chemical composition of the particular target matrix.

In the present experiments, commercially available standard foils of known areal density from MicroMatter Co., were used which consist of a thin layer of the element of interest evaporated onto a Nuclepore filter. According to the manufacturer the accuracy in the areal density is better than 5%.

The standards were analysed using 0.25 cm^2 beam area and no external x-ray absorber except for the chamber window (Melinex) and detector (Be) vacuum window, the count rates were all kept below 1000 c/s to reduce pile-up peaks in the spectrum and the time of analysis was chosen to give a statistical error below 2%.

Eleven different standard foils of thickness ranging from 15-71$\mu g/cm^2$, were analysed for their K-lines, the x-ray peak areas measured and normalized to the incident proton charge and the areal density of the element of interest. The resulting calibration factors, F(Z),

$$F(Z) = \frac{Y_Z}{Q \rho_Z t} \quad \text{counts}/\mu c.\mu g.cm^{-2} \qquad 3.13$$

are plotted as a function of their atomic numbers to

give calibration curves shown in fig,3.20, thus achieving a calibration factor F(Z), counts/$\mu c.\mu g.cm^{-2}$, for all elements in the region $16 \leqslant Z \leqslant 45$ with an accuracy of better than 6%.

A preliminary calibration was made, F(Z) was determined for each element and x-ray transition of interest by direct evaluation of the expression

$$F(Z) = \frac{No \ \sigma_z^{pro}(E_o) \ \Omega \ \varepsilon_{int}}{4 \pi \ Az \ e \ 10^6} \qquad 3.14$$

typical example of the detail followed in this calculation is given below, for Cu:

$$\sigma_z^{pro}(E_o) = \sigma_z^{ion}(E_o) \ . \ \omega_k$$

$\sigma^{ion}(E_o)$ x-ray ionization cross section calculated from polynomial by Khan et al(1977).

$$^{e}\log \ \sigma_z^{ion}(E_o) = [41.46 - 37.32E_o + 8.448E_o^2] - [12.212 - 21.242E_o + 4.864E_o^2](^{e}\log Z) - [0.0107 + 2.737E_o - 0.6551E_o^2](^{e}\log Z)^2$$

$\sigma_z^{ion}(E_o) = 136.605$ at proton energy $E_o = 2.37$MeV

$\omega_k = 0.44$ taken from Bambynek(1972)

$$\varepsilon_{int} = (1 - e^{-\mu_{si} (\rho t)_{si}}) . e^{-\sum \mu_i X_i}$$

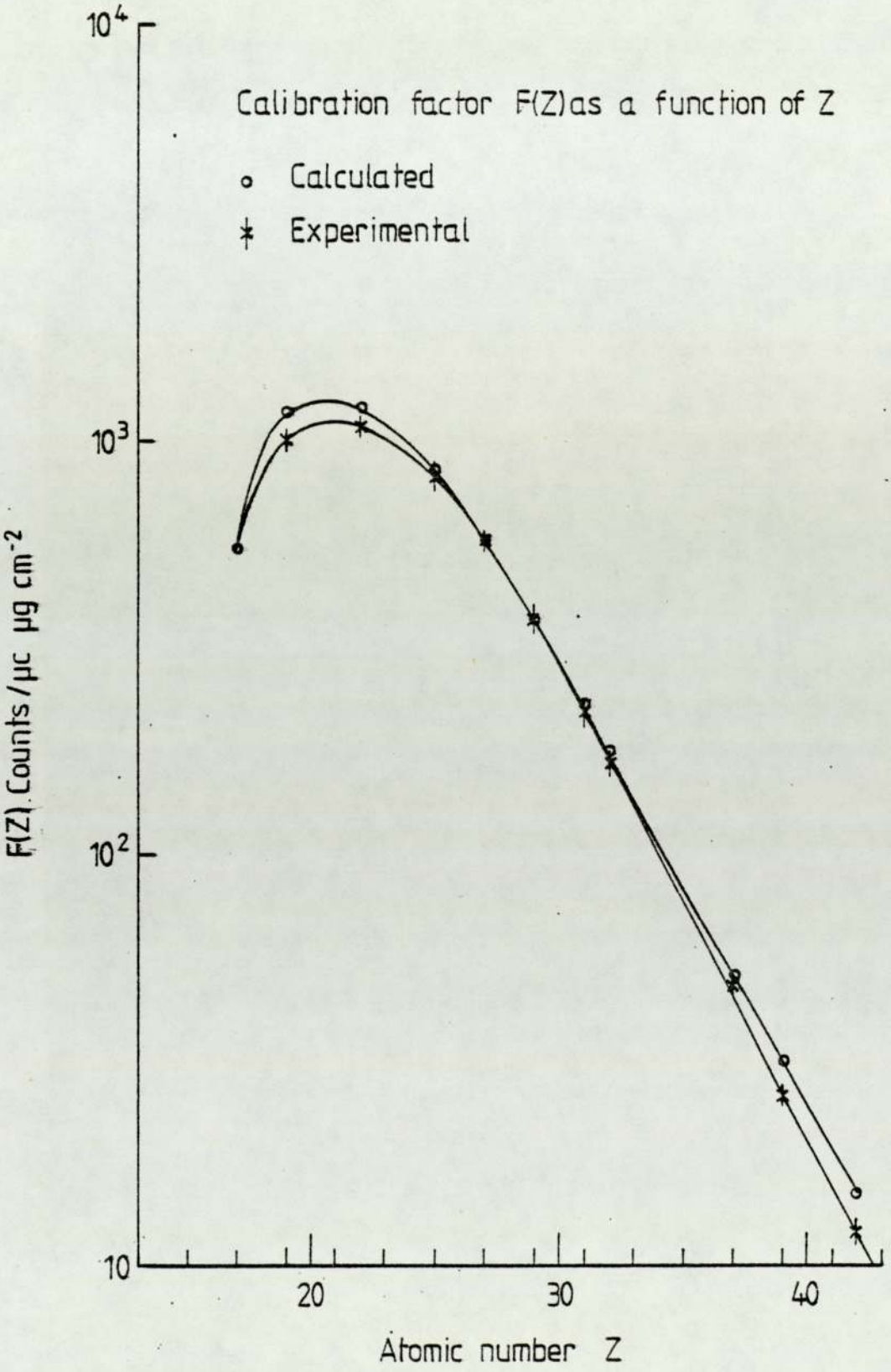

Fig 3:20 Calibration curve for 2·37 MeV proton induced x-ray emission

where $e^{-\Sigma \mu_i X_i}$ are the correction for x-ray absorption in air, melinex and Be windows = $e^{-[\mu_{air}(\rho t)_{air} + \mu_{Be}(\rho t)_{Be} + \mu_{me}(\rho t)_{me}]}$ Melinex is a compound of $C_{10}H_8O_4$. Air is 78% N, 21% O, and 1% argon, therefore, using Bragg additivity rule

$$\mu_{Me} = 0.625\mu_C + .04197\mu_H + .3329\mu_O,$$

$$\mu_{air} = 0.78\mu_N + 0.21\mu_O + .01\mu_{ar}$$

mass absorption coefficients μ_i were taken from Storm and Israel(1970). The fraction of x-ray transmitted through 50 μm Melinex, 3.2 cm air, 12.5 μm Be, and 0.3 cm Si. The x-ray absorption in the gold-layer and silicon dead-layer is negligible,

$$\varepsilon_{int} = 0.92$$
$$N_o = 6.023 \times 10^{23}$$
$$A_{Cu} = 63.54$$
$$\Omega = 1.42 \times 10^{-3}$$
$$e = 1.6 \times 10^{-13}$$

resulting in F(Z) = 370.8 counts/μc.μg.cm^{-2} for Cu. The uncertainty in F(Z) calculation varies from 8% to 20%, depending on the element. This uncertainty is due to uncertainty on the production cross section data, on solid angle determination, and x-ray absorption coefficients. The uncertainty on the production cross section data is estimated by the authors to be not more than 10% for Y and Ti, and less than 6% for all other elements.

Results of the Calculated F(Z) values, together with the experimental measurements for thin foils are given in Table 3.4, the last column represents the ratio of the comparison, the ratios have a Standard deviation of 0.1. In practice in the present work we have used the experimental calibration via thin standard foils rather than through reliance on ionization cross sections, fluorescence yields, detector efficiencies, or window absorption.

There is a possibility that beam conditions or target geometry may alter slightly so that specimens and standards encounter different conditions. This may be guarded against by adding a known quantity of one specific element to the specimen; and if necessary the previously determined calibration curve, fig.3.20, may then be normalized to the sensitivity of this internal standard (Sec.III.C.3).

The target calibration curves fig.3.20 for the detection of $K\alpha$ x-rays are seen to have a peak in the region $18 \leqslant Z \leqslant 24$. The system response calibration factor drops rapidly on both the low Z and high Z sides, the low energy fall off is due to the combined effects of :

1. increased absorption losses of soft x-rays in absorbing windows and air,
2. decreasing values for fluorescence yield fig.2.7, and
3. the falling detector efficiency fig.3.10.

TABLE 3.4

System calibration results for thin targets

Element	F(Z) Counts / $\mu C \mu g\ cm^{-2}$		
	Experimental	Calculated	Ratio (exp/ther)
Cl	568 ± 34	542 ± 59	1.05 ± 0.12
K	1009 ± 56	1168 ± 127	0.86 ± 0.10
Ti	1066 ± 58	1197 ± 135	0.89 ± 0.11
Mn	826 ± 46	841 ± 66	0.98 ± 0.08
Co	569 ± 33	569 ± 43	1.00 ± 0.09
Cu	376 ± 21	371 ± 28	1.01 ± 0.09
Ga	211 ± 12	229 ± 18	0.92 ± 0.09
Ge	165 ± 8	178 ± 14	0.93 ± 0.08
Rb	48.9 ± 2.9	51.5 ± 3.8	0.95 ± 0.09
Y	25.8 ± 1.4	31.8 ± 3.2	0.81 ± 0.10
Mo	12.1 ± 0.7	15.1 ± 1.1	0.80 ± 0.09

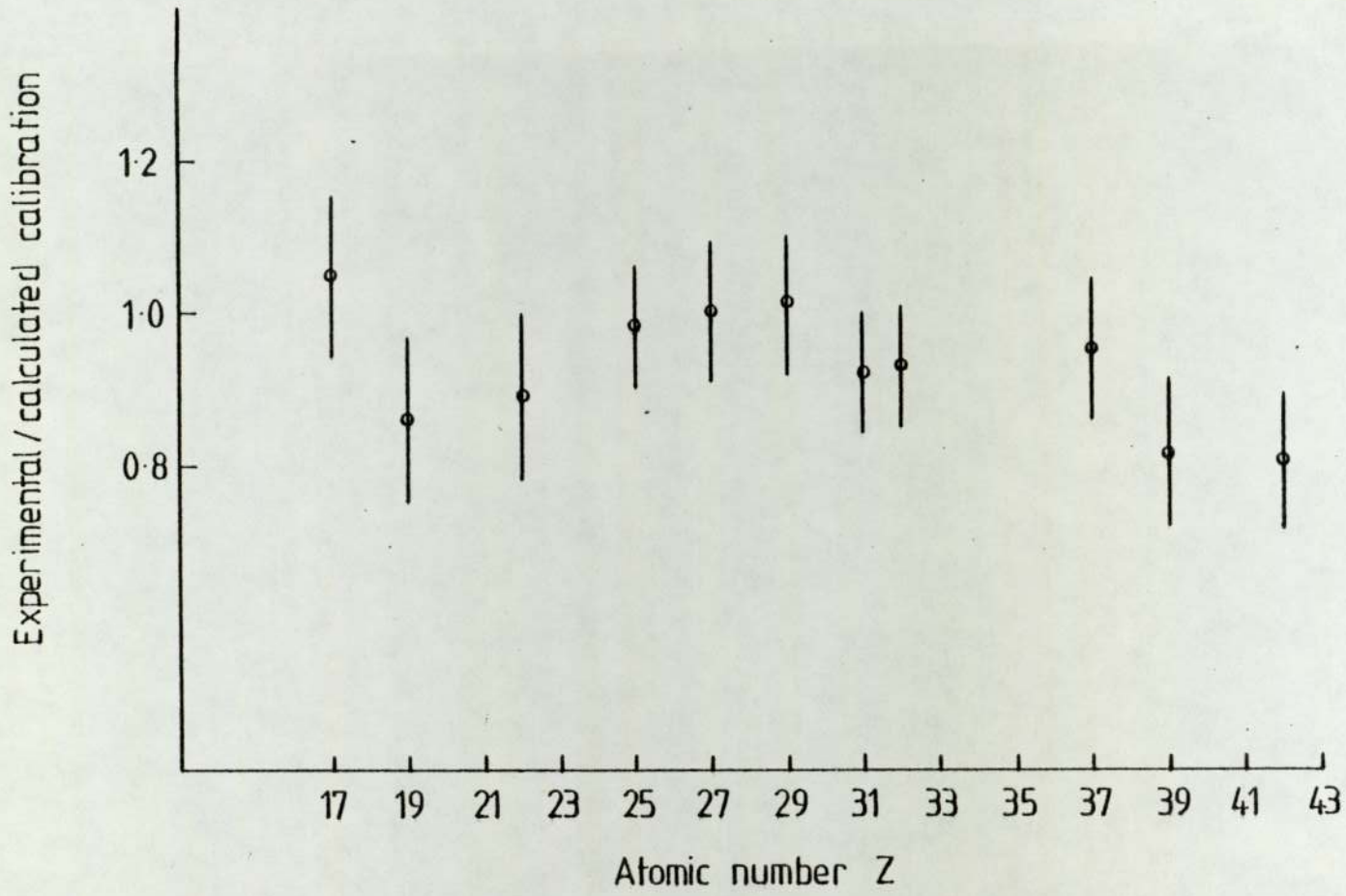

Fig 3:21 Ratio of experimental calibration / calculated with the standard deviation

The high energy fall-off in system calibration is due to rapidly decreasing x-ray production cross-section fig.2.8, and decreasing detector efficiency.

Quantitative analysis for thin targets can be carried out using equation 3.12 with the appropriate experimental values for F(Z).

III.C.2 Moderate Thick and Thick Target Calibration

The aspect of attenuation of the emitted x-rays within the target has been avoided by assuming the targets are thin enough that the absorption of the x-rays of interest is negligible. Likewise, the decrease in characteristic x-ray production as the particle beam loses energy in penetrating the target is also avoided for thin targets. Because of the interrelation between these two effects, it will simplify matters to discuss the latter one first. Here we will limit the description to a 2.37 MeV proton beam; used in the PIXE analysis for this work, other energies or types of particles can be handled in a similar fashion.

From stopping powers calculated by the formula of Andersen and Ziegler(1977), a 2.37 MeV proton falls in energy to about 2.263 MeV in passing through a 1 mg/cm^2 thick target comprised predominantly of NO_3. From calculations of Akselsson and Johansson(1974) the Mo x-ray production cross section of 2.263 MeV is about 0.89

of the 2.37 MeV production. Thus the averaged production per unit mass for a 1 mg/cm^2 target would be down by $\simeq$ 5% from that for an extremely thin target. Therefore, to within 5% a target NO_3 as thick as a 1 mg/cm^2 can be considered to be thin, Willis et al(1977), defined for proton energies of 3 MeV, the dividing line between thin and thick targets of biological materials at about 1 mg/cm^2. Campbell(1977) adopting a more formal definition of a thin specimen as one where the effective mean cross section is not more than 5% less than $\sigma(E_o)$.

In a 1 mg/cm^2 matrix, the average absorption, Montenegro et al(1978), of 6.92-KeV x-ray (Co Kα) is $\sim$ 0.5% and for 3.31-KeV x-ray (K Kα) is $\sim$ 6%. So, for elements heavier than Co, the correction for Kα absorption will be negligible in a 1 mg/cm^2 NO_3 matrix and for elements below K a correction needs to be applied if one is to attempt to achieve an accuracy of better than 6%. If the target is thicker than 1 mg/cm^2, one can continue to use the necessary correction factors, table 3.5, prepared for 21 different elements at 6 different thicknesses.

The correction factor for an element Z in a homogeneous target, C(Z) in equation 3.12, is taken as the ratio of x-ray yield $Y_z(E_o)$, "calculate by assuming no proton energy loss or x-ray absorption effect" to the measured x-ray yield $Y_z(E)$, Fig.3.22. It is shown in the appendix that

$$C(Z) = \sigma_z(0) \cdot t \cdot \left\{ \int_o^t \sigma_z(x) \cdot e^{-\mu_z x} \, dx \right\}^{-1} \qquad 3.15$$

Table 3.5

Correction factors for different target thickness for NO_3 matrix

	C(Z) for NO_3					
Element	1 mg/cm^2	2 mg/cm^2	3 mg/cm^2	4 mg/cm^2	5 mg/cm^2	6 mg/cm^2
Mg	2.121	3.609	5.276	7.004	8.748	10.497
Si	1.492	2.096	2.795	3.561	4.370	5.206
P	1.335	1.73	2.18	2.678	3.213	3.776
S	1.236	1.505	1.806	2.138	2.498	2.882
Cl	1.171	1.362	1.573	1.805	2.056	2.326
K	1.103	1.214	1.337	1.47	1.616	1.774
Ca	1.085	1.177	1.278	1.388	1.509	1.641
Ti	1.066	1.138	1.216	1.303	1.4	1.506
Cr	1.058	1.122	1.193	1.271	1.359	1.457
Mn	1.057	1.119	1.188	1.265	1.351	1.447
Fe	1.056	1.117	1.186	1.262	1.347	1.443
Co	1.055	1.117	1.185	1.261	1.347	1.443
Ni	1.056	1.118	1.187	1.263	1.349	1.446
Cu	1.056	1.118	1.187	1.265	1.352	1.450
Zn	1.057	1.12	1.19	1.268	1.357	1.456
As	1.059	1.125	1.198	1.28	1.373	1.477
Sl	1.06	1.127	1.201	1.284	1.378	1.484
Br	1.061	1.129	1.204	1.289	1.385	1.493
Rb	1.063	1.133	1.211	1.299	1.398	1.510
Y	1.065	1.137	1.217	1.308	1.411	1.527
Mo	1.068	1.144	1.229	1.325	1.434	1.557

incident proton energy = 2.37 MeV target angle 45^o

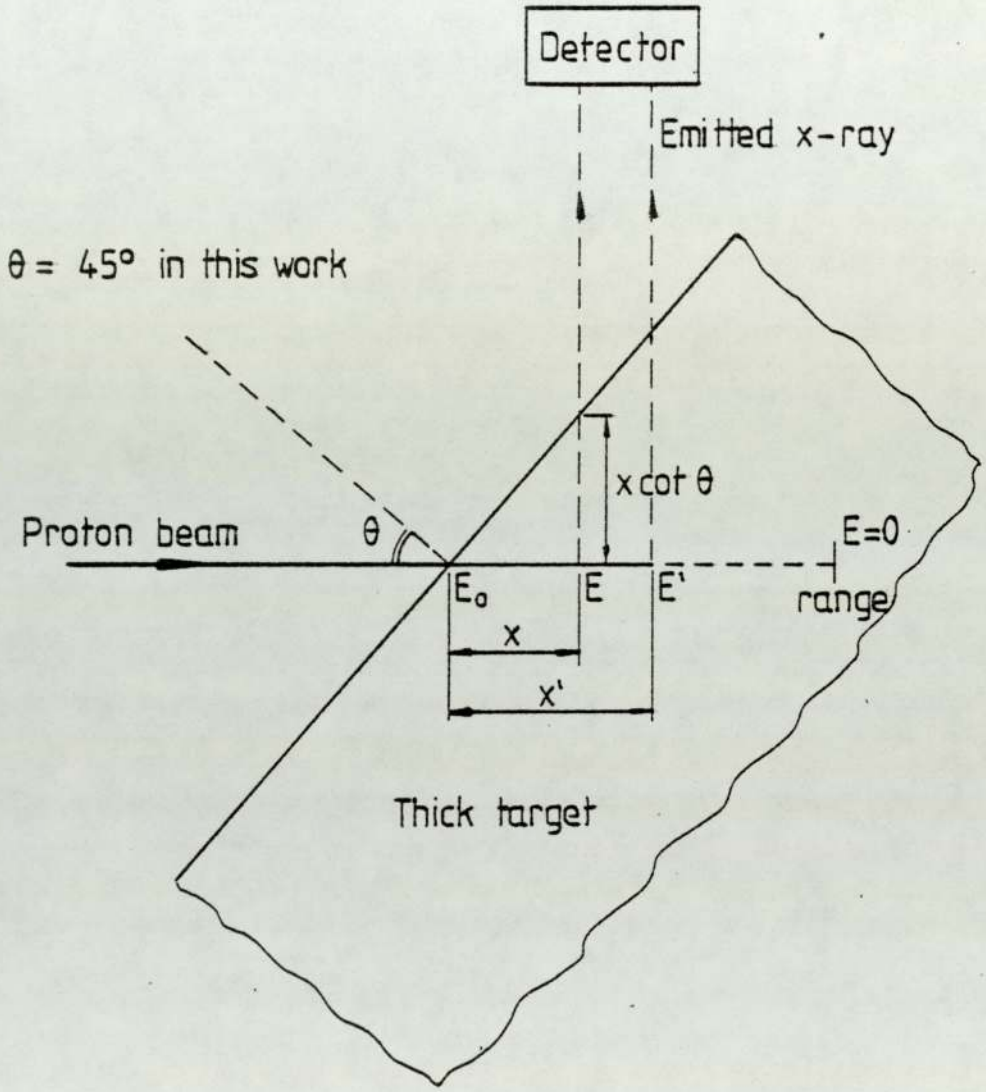

Fig 3:22 Meaning of parameters used in the derivation of correction factor for thick target

t in this expression is the thickness in (mg/cm^2) as presented and as seen by the detector i.e. t = cosec θ actual target thickness for moderately thin target or equal to range of proton for thick targets, $\sigma_z(x)$ represents the K ionization cross section for element Z at depth x in the target, and μ_z is the mass attenuation coefficient in (cm^2/mg) for the measured x-ray line in the target material. The integral in the denominator of equation 3.15 is evaluated numerically. The depth x in this integral is related to the decreasing proton energy E by the stopping power formula $S(E) = -(\frac{dE}{dx})$. The stopping powers for different targets are calculated as those for the major elements using the formula of Andersen and Ziegler(1977). The semiempirical formula by Akselsson and Johannson(1974) is used to calculate the cross section $\sigma_z(x)$. The mass attenuation coefficients μ_z are determined using the fitted polynomial by Montengro et al(1978).

It is apparent from equation 3.15 that the value C(Z) depends upon the bulk chemical composition of the target being analysed, each different target type requires a different set of values of C(Z), and in order to determine the minor and trace constituents in a given target, the major composition of the target must be known or estimated, an elementary experiment is made to estimate the major composition of targets prepared from digested blood in nitric acid, the mass attenuation coefficient μ_z is determined at a few selected energies by transmission experiments, the experimental results compared with

the mass attenuation coefficient for C, N and NO_3 in fig. 3.23, results showed that the dominant matrix composition is closer to NO_3.

A computer program, described in the appendix, has been written for calculating moderately thick or thick target correction factor C(Z) for 21 elements K lines given the following input: (i) the bulk composition of the target, (ii) the incident proton energy, and (iii) the target thickness.

A set of C(Z) values for C, NO, NO_3 for 1 mg/cm^2 is represented in table 3.6.

Fig.3.24 shows calculation of C(Z) for NO_3 matrices of several different thicknesses. The curves are observed to reach minima near Z = 27.

In fig.3.25, the individual contributions to C(Z) due to proton energy loss and x-ray absorption are shown for a 3 mg/cm^2 thick carbon target. The x-ray absorption effect dominates the total correction factor for very light elements ($Z \leqslant 20$), while for medium and heavy elements ($Z \geqslant 30$), the proton energy loss term is most important.

With calculated values of C(Z) inserted into equation 3.12 one can obtain the thick target calibration. The influence of matrix effects was investigated by measuring the yield for selected elements in dried digested blood serum

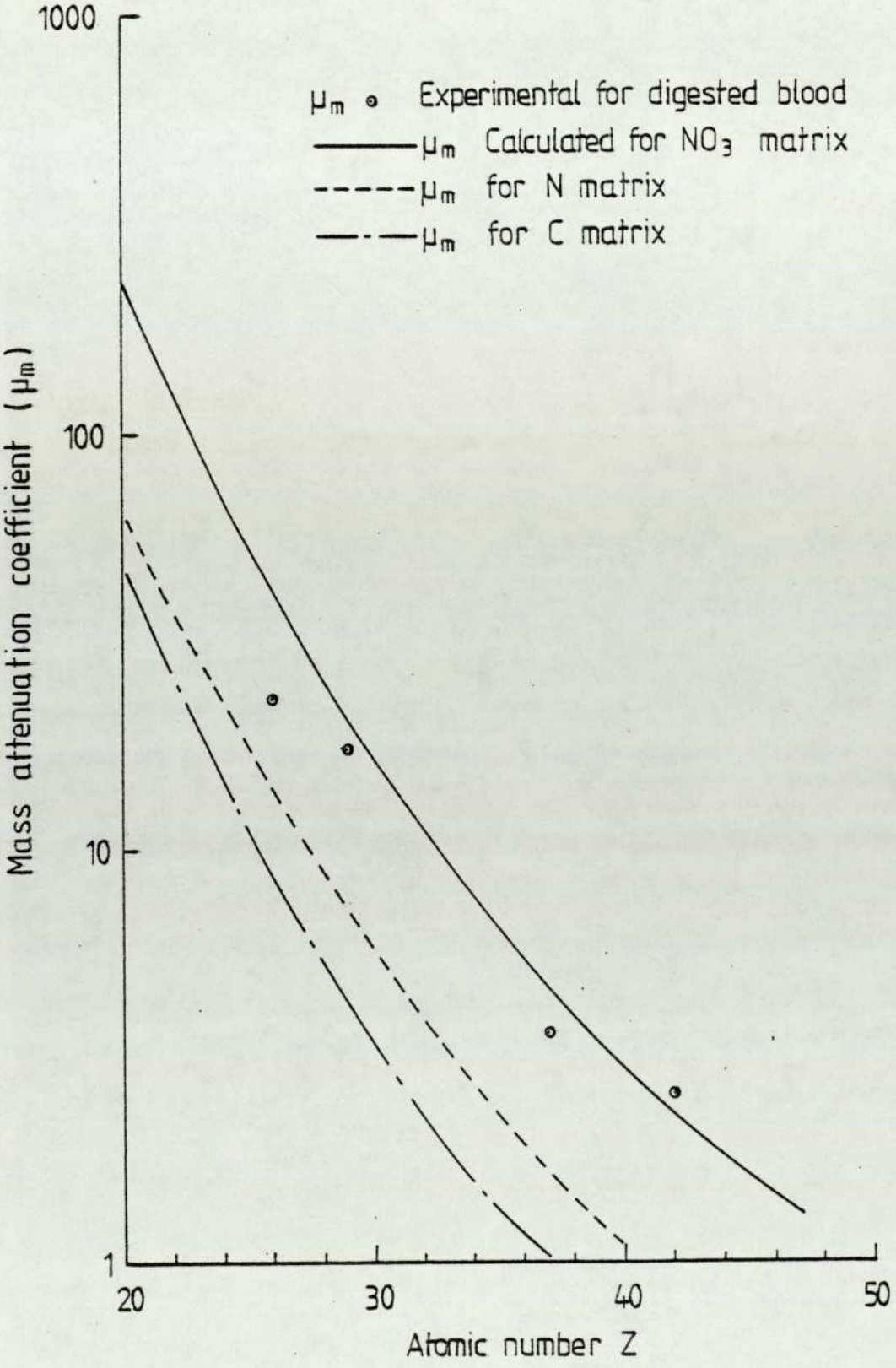

Fig 3:23 Mass attenuation coefficient for digested blood serum target

Table 3.6

Target correction factors for 3 different matrix composition with 1 mg/cm^2 thickness

	Correction factor C(Z)		
Element	Carbon	NO	NO_3
Mg	1.510	1.920	2.120
Si	1.239	1.410	1.490
P	1.168	1.280	1.330
S	1.123	1.199	1.240
Cl	1.093	1.146	1.170
K	1.064	1.090	1.100
Ca	1.0575	1.076	1.080
Ti	1.052	1.061	1.066
Cr	1.0515	1.056	1.058
Mn	1.052	1.055	1.057
Fe	1.053	1.054	1.056
Co	1.054	1.0546	1.0555
Ni	1.056	1.0555	1.056
Cu	1.056	1.056	1.056
Zn	1.058	1.056	1.057
As	1.061	1.059	1.059
Se	1.062	1.060	1.060
Br	1.064	1.061	1.061
Rb	1.066	1.064	1.063
Y	1.068	1.065	1.065
Mo	1.072	1.069	1.068
Incident Energy = 2.37 MeV			

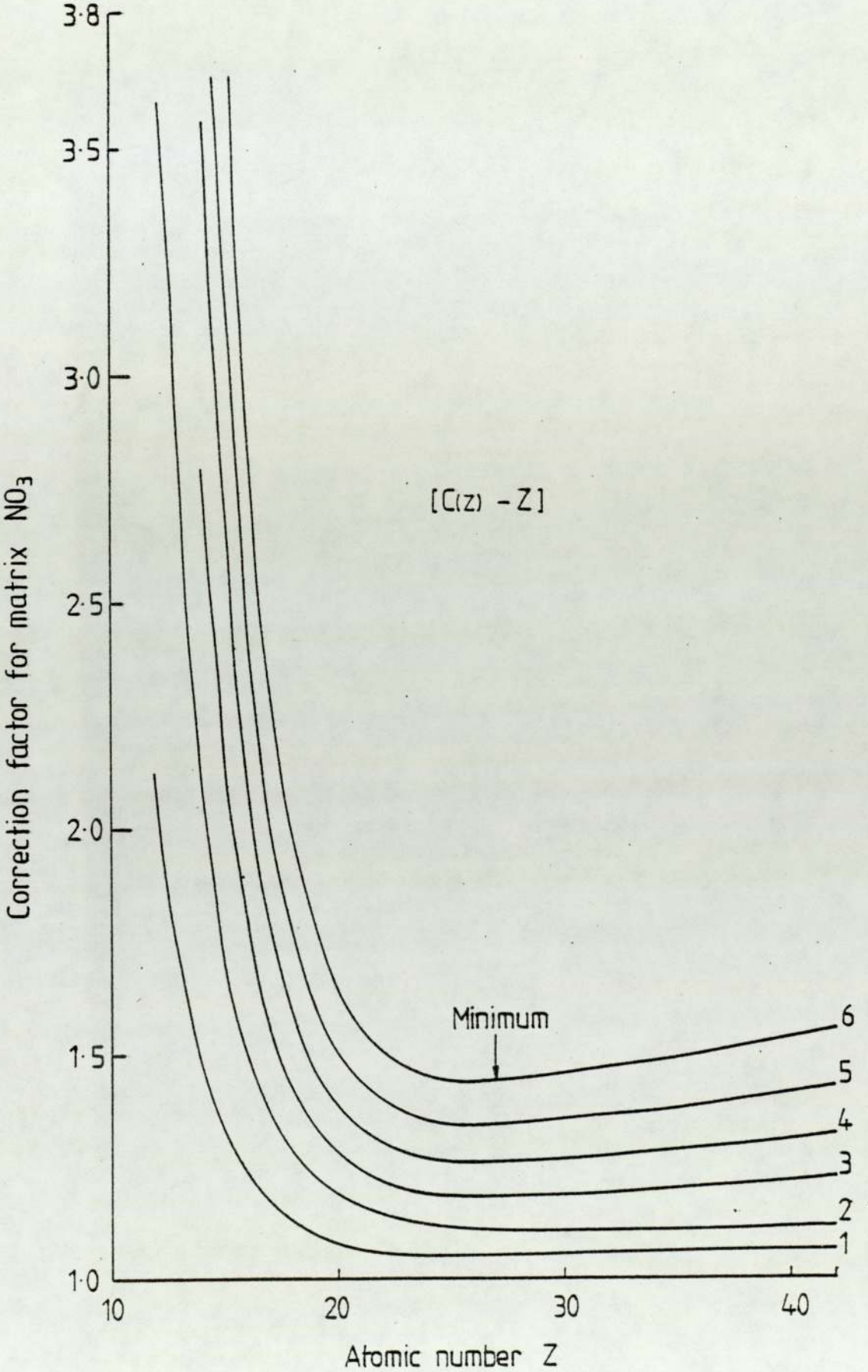

Fig 3:24 Correction factor for matrix NO_3 for 6 different thicknesses in mg / cm^2

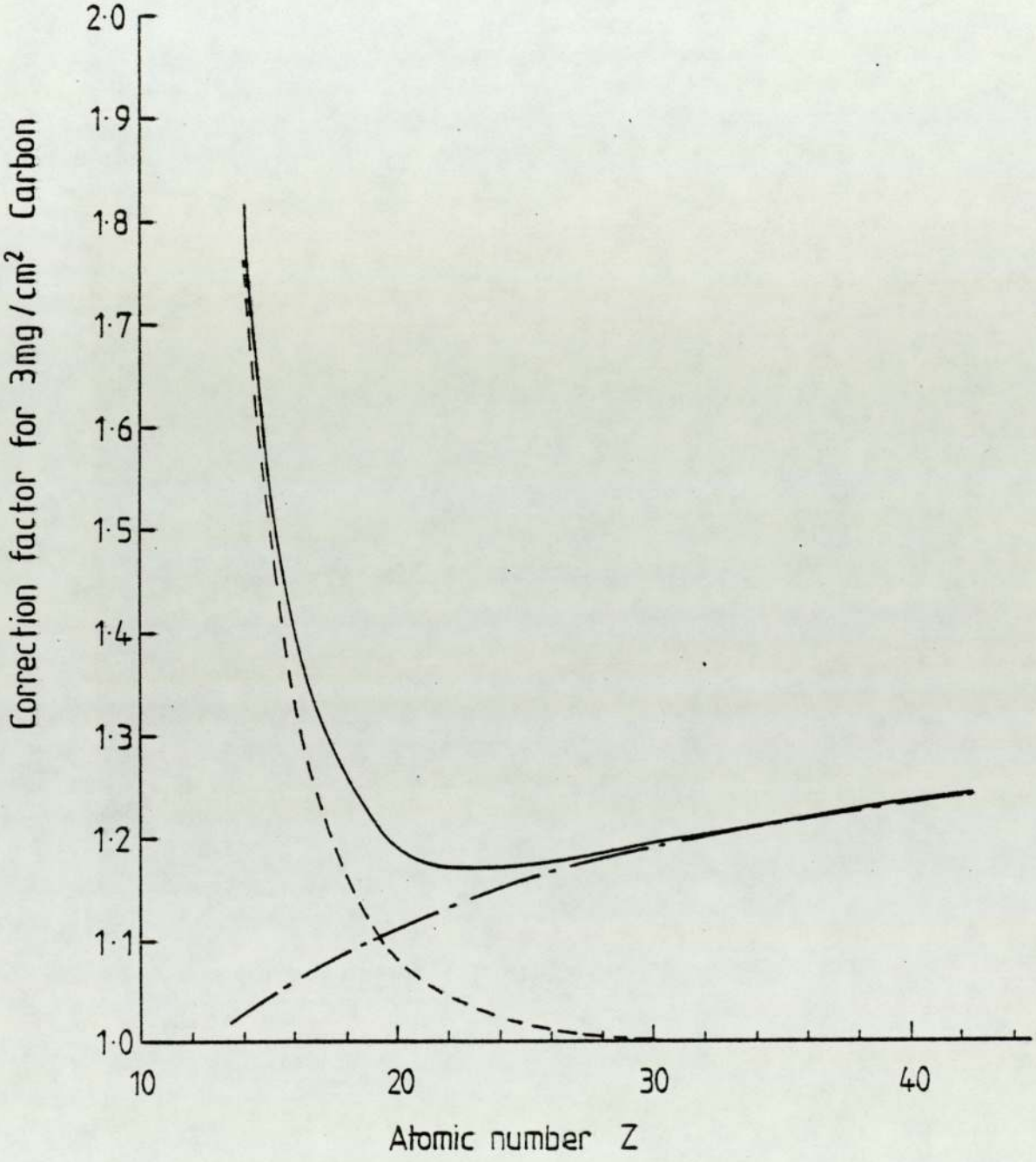

Fig 3:25 Correction factor for Carbon, thickness 3mg / cm²

——— Total correction for Carbon
------ X-ray absorption correction
—.-— Proton energy loss correction

target for two thicknesses. As expected the corrected data for the two thicknesses agree, table 3.7.

The correction factor assumes a homogeneous distribution of the element throughout the matrix. Several workers Willis et al(1977), Van Der Kam(1977), Patnaik and N.Dhere(1975), Reuter et al(1975, Montenegro et al(1980), Garten et al(1981), Richter and Watjen(1981)) have made calculations of the correction by various ways. In thick targets, the possibility of enhanced x-ray yields due to secondary excitation cannot be ignored, Reuter et al(1975). The only source of importance according to Ahlberg(1977) for secondary excitation is primary induced x-rays. Maximum enhancement occurs for elements whose K-shell absorption edge lies immediately below the energy of the primary radiation.

Another problem which could be added is the surface irregularities, the effect of the degree of nonuniformity of the matrix composition and matrix thickness is discussed by Montenegro et al(1979ø), the amount of a particular element present in a sample associated with a number of characteristic x-rays observed may be different for different arrangements of this element in the matrix and for different particle beam distribution, as a result of the loss of energy of the incident particle beam and x-ray absorption in the sample. Therefore there are elemental distributions for which the number of atoms associated with a definite number of observed

Table 3.7

Blood Serum Results for Sample (4D P9):

Calculation of ppm using the correction factors:

Element	20 μl			30 μl			mean ppm ± 1s.d
	Y_Z	C(Z)	ppm	Y_Z	C(Z)	ppm	
Zn	166	1.144	1.40	226	1.201	1.33	1.37 ± 0.04
Br	66	1.154	1.73	103	1.215	1.90	1.82 ± 0.09
Rb	51.5	1.164	2.17	67	1.229	1.98	2.08 ± 0.10

characteristic x-rays will be a maximum or minimum, Montenegro et al(1979a). They used these two extremes to define the uncertainty in the amount of the element measured. A criterion to associate the number of atoms of an element with a definite number of characteristic x-rays observed is established from the knowledge of these two limits.

The dominant uncertainties in the correction factor calculation are attributable to uncertainties in the values assumed for the x-ray production cross sections, the proton stopping powers, and the x-ray attenuation coefficients. Akselsson and Johansson(1974) analyse sources of errors in their x-ray cross section data and these are probably representative of cross section data in general. If all these errors are additive the total % error would be 6-16.5%. Andersen and Ziegler(1977) believe that their stopping power for high energy is accurate to 1%. Montenegro et al(1978) state that for elements, Ti-Sn, their absorption coefficients agree within 4% with experimental data from Millar and Greening(1974), and from semiempirical results of Hubbell et al(1974).

In order to provide independent checks on the system calibration described in the previous sections, it has been found useful to employ several additional calibration procedures. These are: the use of NBS Standard Reference Materials, international laboratory comparisons, and

relative calibration via internal standard.

III.C.3: Standard Reference Materials

In recent years there has been a significant increase of interest in evaluating the role and effects of trace elements in the biomedical problems. Often when researchers have attempted to compare their results with those of other laboratories they find disconcertingly wide discrepancies. It has become apparent that it is necessary to establish criteria and to have available for use, standard materials for which both the degree of homogeneity from sample to sample and the various trace element concentrations are known. The National Bureau of Standards, NBS, makes available a number of Standard Reference Materials (SRM's) suitable for providing checks for analytical systems. The concentrations of the major and minor elemental constituents of these reference materials are certified by the NBS. Certification of a concentration value requires that agreeing values be obtained by at least two independent analytical techniques, or by two different analysts using a recognised "referee" technique whose bias, if any, is well known. La Fleur(1974),H.J.M.Bowen(1974).

The Reference material which has been found most useful for providing a check on system calibration, testing the modification of the technique, comparing results with other laboratories is the bovine liver (SRM 1577). It is

available in the form of a finely ground, homogeneous powder. The NBS specifies a minimum sample size of 250 mg as constituting a representative sample. Their targets were prepared by digesting a representative sample of bovine liver (Sec.III.D) and depositing 3μL of the digested solution onto kimfol backing, resulting in an area smaller than the beam spot. Each target was irradiated with a proton current of 10 nA, and a total charge 25μC. Several workers have analysed the bovine liver, among them Saied(1981), Pallon and Malmqvist(1981), Willis and Walter(1977), Jolly et al(1978), Maenhaut et al(1980). Their results together with the results of this work are represented in table 3.8. The results in table 3.8 represent the mean value of three targets with the standard deviation given. The agreement between these values and the values reported by the NBS and the other workers is reasonable.

On working with well characterized sample materials, much valuable information has been learned about advantages and disadvantages of different target preparation techniques; analysis of SRM's has helped locate some of the difficulties associated with the computer analysis of complex spectra; and finally, SRM's serve as an accurate check by comparison of results from different laboratories.

Table 3.8

Elemental abundances (ppm) in NBS SRM 1577 bovine liver

Element	Present work	Jolby (1978)	Maenhaut (1980)	Pallon (1981)	Saied (1981)	Willis (1977)	NBS
K	10050 ± 596	10208 ± 480	5000 ± 700	8594 ± 352	7700 ± 1400		9700 ± 600
Ca	120 ± 17	-	90 ± 13	178 ± 21	-		123
Mn	10.3 ± 1.3	10.9 ± 1.5	8 ± 1	10.24 ± 0.3	9.63 ± 0.83	9.0 ± 2.2	10.3 ± 1.0
Fe	290 ± 38	272 ± 12	248 ± 16	242 ± 9	262 ± 18	293 ± 21	270 ± 20
Cu	193 ± 11	174 ± 14	179 ± 16	170 ± 4	182 ± 13	194 ± 13	193 ± 10
Zn	136 ± 10	126 ± 11	116 ± 18	120 ± 9.2	132 ± 10	144 ± 12	130 ± 10
Se	0.94 ± 0.88	0.98 ± 0.15	1.0 ± 0.2	0.9	1.05 ± 0.16	0	1.1 ± 0.1
Rb	18.7 ± 1.0	15.0 ± 2.5	9.9 ± 1.6	17.5 ± 1.0	18.3 ± 2.0	20.9 ± 2.5	18.3 ± 1.0

III.C.4 International Laboratories Comparisons

Intercomparison of trace and other elements in IAEA powdered human hair, HH-1:

The primary objective of the intercomparison is to evaluate the precision and accuracy in this work and to offer some comparison with other accepted methods. The HH-1 interlaboratory comparison involved the participation of 66 laboratories representing 8 different analytical techniques. Each participating laboratory benefited from intercomparison by learning how its results compared in an absolute basis with the mean values, certified by IAEA, and how the laboratory fared in the intercomparison relative to the other laboratories using the same or different analytical techniques.

The HH-1 powdered hair material was prepared from samples of head hair collected from 15 patients due to undergo skull operations at the General Hospital of the City of Vienna. Details such as age, sex, health of the donors are not available.

The samples were sent to the participants and results requested. The data received from the laboratories were processed by a computer program specially written by the IAEA analytical Quality Control Service, and they were stored on a computer file. This program analyses the results for each element in turn, treating each

laboratory mean as a single unweighted value. Various outlier tests were then applied at the 5% confidence level. Any laboratory mean identified as an outlier by one or other outlier tests is subsequently excluded from further computations. The remaining accepted laboratory means were then combined, without weighting, to provide estimates of the overall mean and its associated standard deviation.

Thin targets of HH-1 material were prepared by digesting 100 mg of the hair powder in 3.5 ml nitric acid (Sec.III.D) and 5 μL of the digested solution was deposited onto kimfoil backing, resulting in a spot of about 2 mm in diameter. Each target was irradiated with a proton current of 10 nA, total charge 25 μC, and a typical spectrum for one of the four hair samples used in the analysis is shown in fig.3.26. The results reported in this work are compared with the overall average and these are summarised in table 3.9 and seen in fig.3.27. Each point represents the average of four targets measurements carried out from one sample. The results of the analysis table 3.9 are in general in quite good agreement with the average values, with the exception of Fe and Mo they are within 15% of the mean values.

Thirty three elements are listed as present in this powder reproduced in table 3.10 with their averages and standard deviations. The elements below P are too low in energy to be detected with the present technique, their

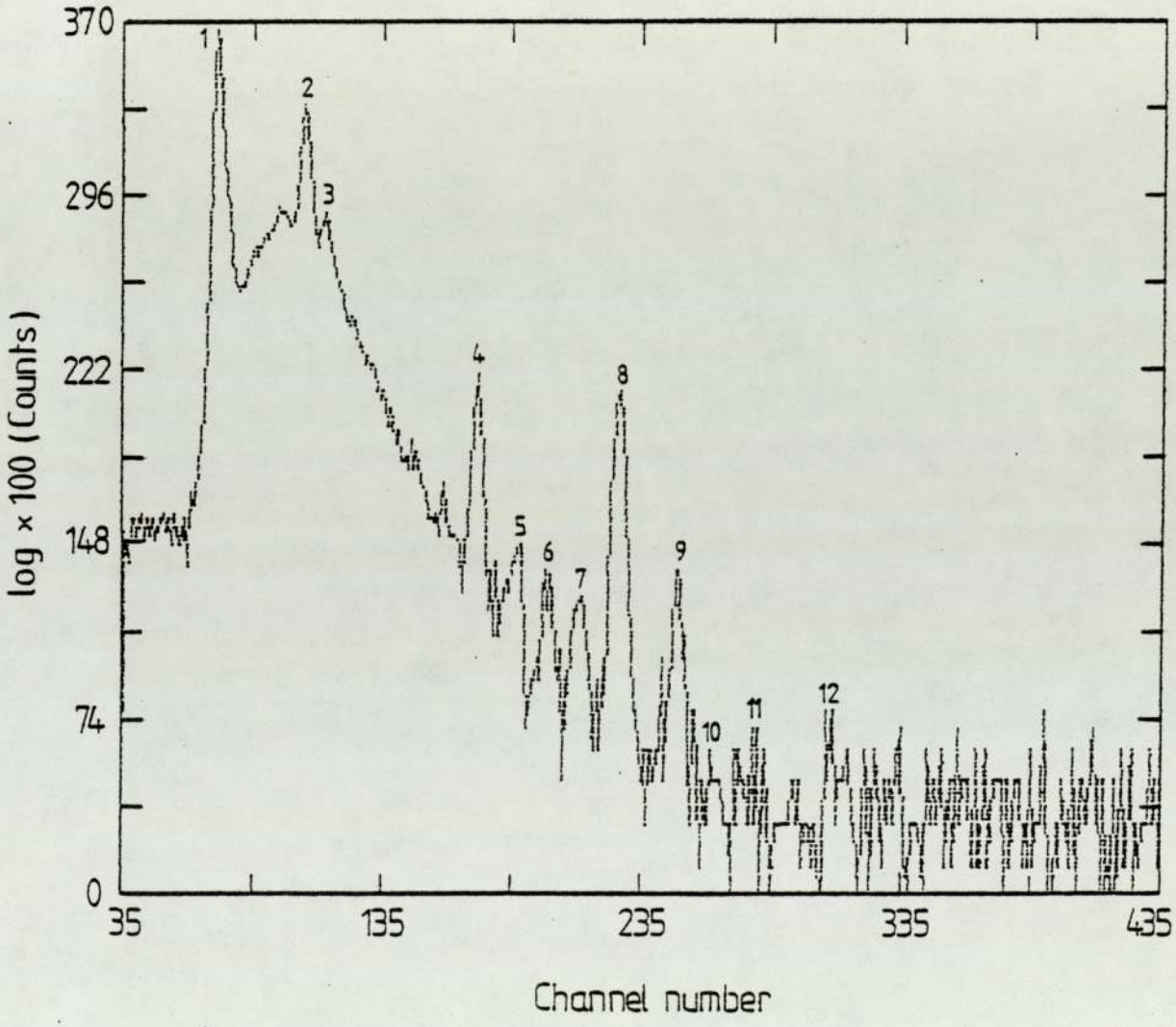

Fig 3.26 PIXE spectrum for hair HH-1, IAEA hair sample.

1 - S (Kα + Kβ)	7 - Cu (Kα)
2 - Ca (Kα)	8 - Zn (Kα)
3 - Ca (Kβ)	9 - Zn (Kβ)
4 - Fe (Kα)	10 - Hg (Lα)
5 - Fe (Kβ)	11 - Pb (Lα)
6 - Ni (Kα)	12 - Br (Kα)

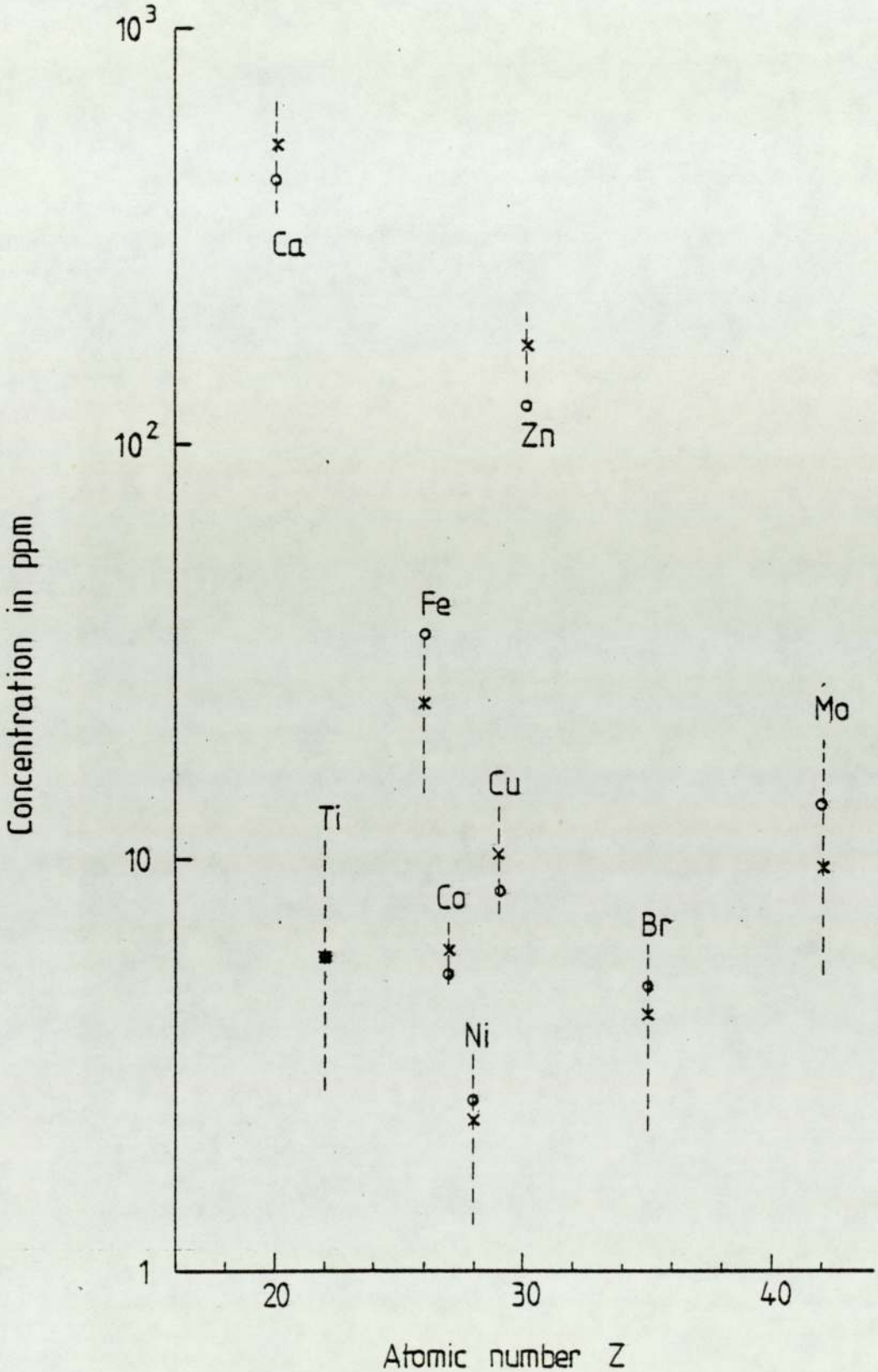

Fig 3:27 Concentration for HH-1 in ppm
(⊹) IAEA mean value with the standard deviation
(∘) this work

Table 3.9

Results in (μg/g dry weight)
for hair HH-1

Element	Present work	IAEA average	IAEA Accepted range
Ca	435.0 ± 46	522.0 ± 160	246.0 - 712
Ti	5.7 ± 0.6	5.81 ± 5.5	0.55 - 11.1
Fe	35.0 ± 6.1	23.7 ± 9.8	0.44 - 50.0
Co	5.3 ± 0.6	6.0 ± 1.2	2.70 - 8.05
Ni	2.6 ± 0.5	2.33 ± 1.14	0.52 - 4.00
Cu	8.3 ± 1.9	10.2 ± 3.2	1.89 - 19.05
Zn	122.0 ± 13.5	174.1 ± 31.5	91.0 - 265
Br	4.9 ± 1.2	4.2 ± 2.1	0.37 - 8.42
Mo	13.5 ± 5.2	9.5 ± 12.3	0.06 - 23.70

Table 3.10

Elements measured in HH-1 by different techniques as given in IAEA Report

Elements present in HH-1	Mean ppm ± standard deviation	Remarks
F	1082.50 ± 265.2	
Na	12.64 ± 4.77	These x-rays are too low in energy to be detected in the present techniques. They are absorbed in air, Be and melinex windows and 5 μm Al absorber
Mg	62.01 ± 9.58	
Al	5.50 ± 2.58	
P	148.11 ± 2.84	
S	48707.13 ± 15017.61	
Cl	2265.29 ± 478.28	
K	9.21 ± 5.15	
Ca	522.03 ± 160.22	
Ti	5.81 ± 5.51	
V	0.14 ± 0.15	below the detectable limit
Cr	0.27 ± 0.16	
Mn	0.85 ± 0.25	
Fe	23.70 ± 9.76	
Co	5.97 ± 1.21	
Ni	2.33 ± 1.14	
Cu	10.23 ± 3.17	
Zn	174.08 ± 31.51	
As	0.05 ± 0.02	below the detectable limit (Sec.III.E)
Se	0.35 ± 0.04	
Br	4.16 ± 2.09	
Rb	0.94 ± 0.09	
Sr	0.82 ± 0.16	
Mo	9.47 ± 12.32	
Ag	0.19 ± 0.06	below the detectable limits
Cd	0.26 ± 0.13	
Sb	0.03 ± 0.01	
I	20.25 ± 8.91	
Ba	1.83 ± 2.52	
La	0.01 ± 0.01	
Au	0.03 ± 0.01	
Hg	1.70 ± 0.24	
Pb	2.73 ± 1.40	

x-rays are absorbed in the air, the Be and melinex window, and the 5μm Al absorber used in this analysis. In the medium and high energy region, the low concentration and drop of production cross sections are responsible for the unmeasured elements.

III.C.5 Relative Calibration Via Internal Standards

From the analyst's viewpoint, whatever the technique, the use of internal standards is the most desirable means of effecting calibration, Ishii et al(1975), Agarwal et al (1975), Alexander et al(1974), Valcovic et al(1974), Campbell(1975), Ong et al(1974), Barrette et al(1976). The target and beam areas need not then be measured, and there should be some gain in precision since the uncertainties in relative measurements are certainly smaller than those in absolute values. Incorporation of internal standards may not be possible or practical with some types of targets. Microtome slices of tissue certainly do not lend themselves to this approach. With the smaller powder samples used by most workers, it is rather impractical, since the achievement of uniform mixing of the very small masses of standard elements in powder samples prior to deposition is not trivial. Clearly the use of solutions as prepared here is the method most compatible with internal standardisation. Yttrium, (always missing in biological samples) in the form of yttrium nitrate, ($Y(NO_3)_3.3H_2O$) was chosen to give the yttrium calibration peak in our spectra, since it is

highly soluble in water, the nitrogen and oxygen x-rays will not be seen in the spectra as, due to their low atomic numbers, they are absorbed in melinex and Be windows, and will not interfere with sample x-rays.

A 185 mg quantity of $Y(NO_3)_3.3H_20$ yields 50 mg of yttrium, and when thoroughly mixed in deionized water to give 25 ml of solution results with an yttrium concentration of 2 mg/ml. In this way any sample can be doped with a precise amount of yttrium by adding the proper volume of yttrium solution. For instance in the hair samples analysis for agitated and control groups (se.V.B), 1 ml of the digested sample was put in a plastic bottle and doped with 30μL of the yttrium standard solution. After the digested sample and the standard solution were well mixed, a drop was deposited on a backing kimfol, which was previously mounted on Al frame. Fig.3.28 shows the resulting spectrum from a hair sample doped with yttrium. From equation 3.12 the unknown mass of the element of interest, M_Z, and the standard, M_{St}, are

$$M_Z = \frac{Y_Z . C(Z) . A_B}{F(Z) . Q . C_{AL}(Z)} \qquad 3.16$$

and

$$M_{St} = \frac{Y_{St} . C(St) . A_B}{F(St) . Q . C_{AL}(St)} \qquad 3.17$$

where Z and St refer to element of interest and standard. Since the standard and unknown element constitute the same sample

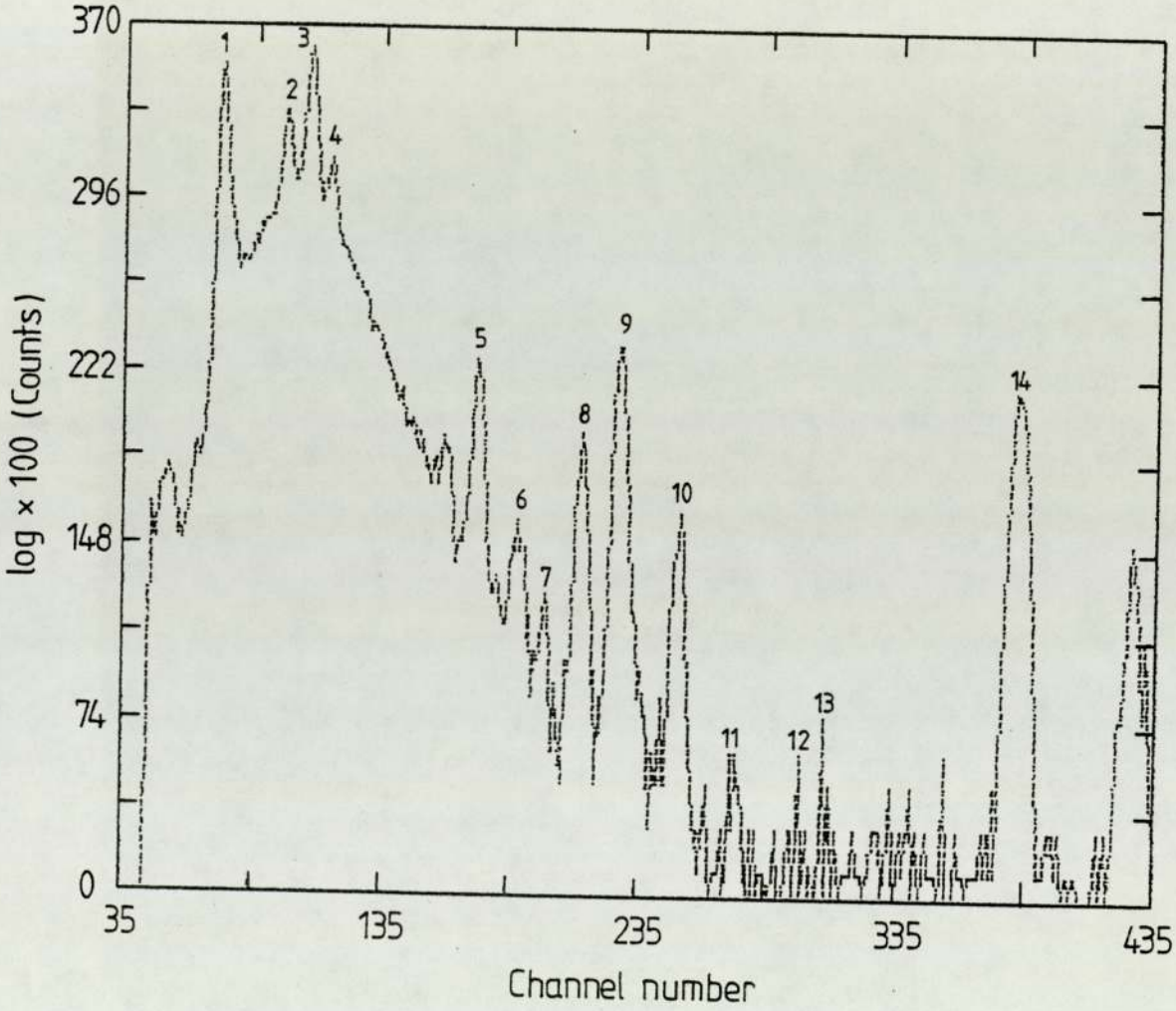

Fig 3.28 PIXE spectrum from one hair doped with Yttrium.

1 - S (K α + K β)	8 - Cu (K α)
2 - K (K α)	9 - Zn (K α)
3 - Ca (K α)	10 - Zn (K β)
4 - Ca (K β)	11 - Pb (L α)
5 - Fe (K α)	12 - Se (K α)
6 - Fe (K β)	13 - Br (K α)
7 - Ni (K α)	14 - Y (K α)

$$M_Z = M_{St} \frac{Y_Z}{Y_{St}} \cdot \frac{F(St)}{F(Z)} \cdot \frac{C(Z)}{C(St)} \cdot \frac{C_{Al}(St)}{C_{Al}(Z)} \qquad 3.18$$

for a thick target

and

$$M_Z = M_{St} \frac{Y_Z}{Y_{St}} \cdot \frac{F(St)}{F(Z)} \cdot \frac{C_{Al}(St)}{C_{Al}(Z)} \qquad 3.19$$

for a thin target

The values of C(Z) for Ca, Fe, Zn and Y taken from table 3.5, for different thicknesses together with their ratios to the yttrium are represented in table 3.11 and are shown in fig.3.29. Using the internal standard the correction due to x-ray production cross sections and x-ray absorptions are now replaced by their ratios, which are much smaller values. The conclusion is that more precision is achieved, and rather thicker targets may be tolerated if an internal standard is used.

In the agitated and control groups hair analysis, (sec.V.B), the yield relative to the yttrium R.F(Z) calibration curve as determined for the 2.37 MeV proton beam with 7 μm aluminium absorber is shown in fig.3.30. These curves were obtained by bombarding targets prepared from digested bovine liver doped with yttrium, compared with the yield obtained from the standard foils including yttrium and other elements to cover the region of interest. Table 3.12 represents the results of this analysis, the agreement between both sets of data, is better than 2% for elements higher than Ca. The reason for the 9%

Table 3.11

Correction factors for some elements and their ratios to the yttrium

Correction factor C(Z)	Ca	Fe	Zn	Y
1 mg/cm^2	1.085	1.056	1.057	1.065
Ratio	1.019	1.009	1.008	1
2 mg/cm^2	1.177	1.117	1.120	1.137
Ratio	1.035	1.018	1.015	1
3 mg/cm^2	1.278	1.186	1.190	1.2175
Ratio	1.050	1.027	1.023	1
4 mg/cm^2	1.388	1.262	1.268	1.308
Ratio	1.061	1.036	1.032	1
5 mg/cm^2	1.509	1.351	1.387	1.411
Ratio	1.069	1.044	1.017	1
6 mg/cm^2	1.641	1.443	1.456	1.527
Ratio	1.075	1.058	1.049	1

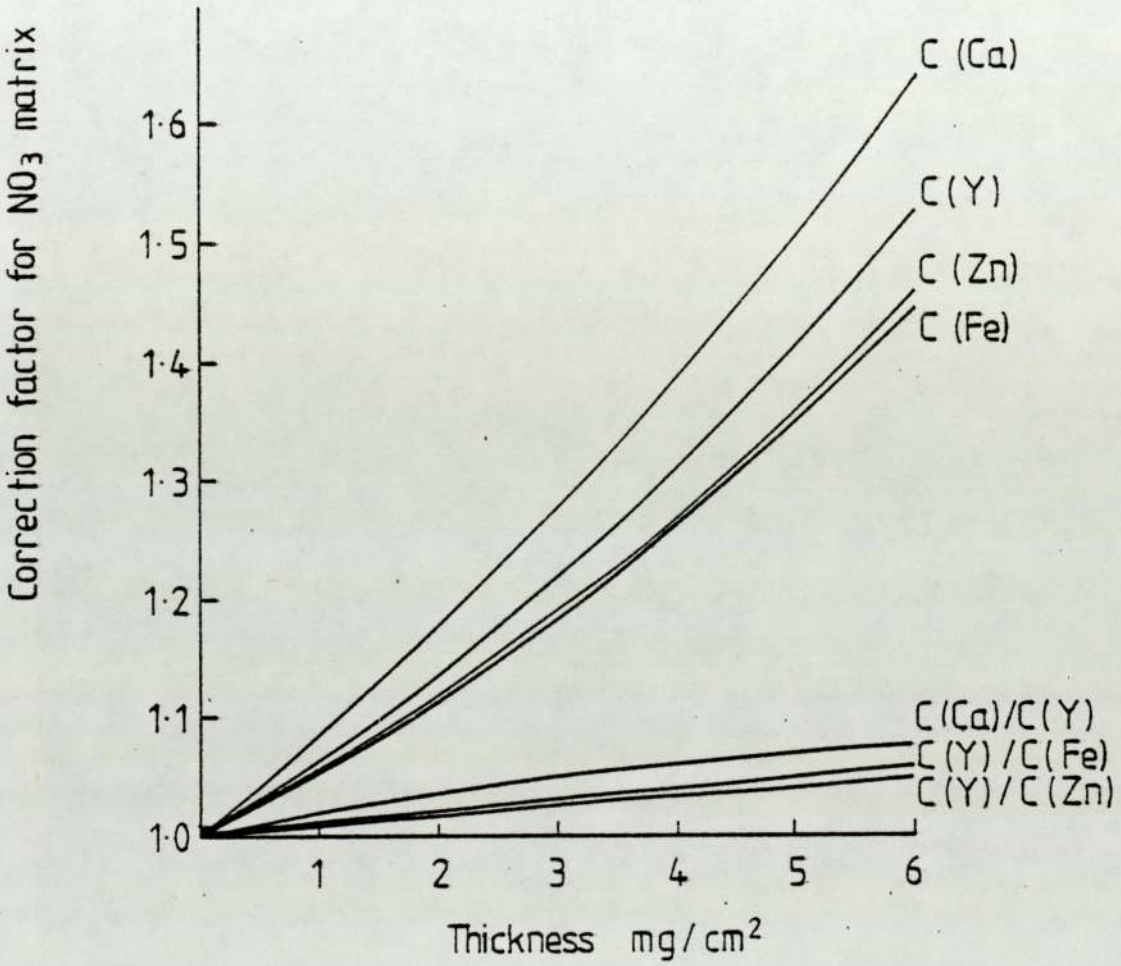

Fig 3:29 The effect of using internal standard on the correction factors.

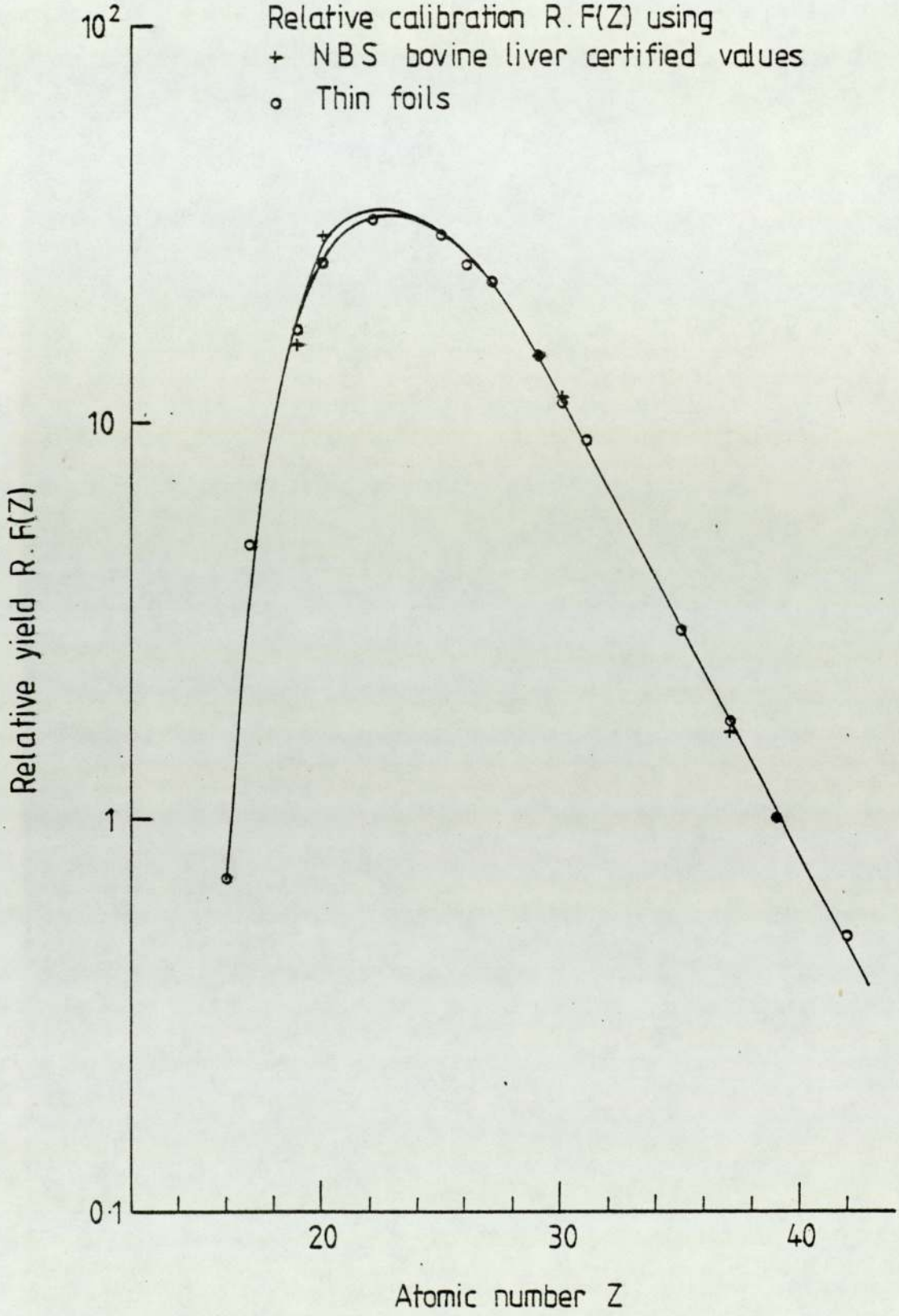

Fig 3:30 Relative x-ray yield for proton beam 2·37 MeV 7 μm aluminium absorber

Table 3.12

Relative yield results R.F(Z) from the NBS SRM 1577 and thin standard foils

Element	R.F(Z) using the standard foils	R.F(Z) using bovine liver
S	0.71 ± 0.05	---
Cl	5.20 ± 0.38	---
K	17.30 ± 1.2	15.7 ± 0.9
Ca	27.80 ± 1.9	30.7 ± 2.9
Ti	32.20 ± 2.2	---
Mn	29.50 ± 2.1	29.9 ± 3.3
Fe	25.50 ± 1.8	25.8 ± 1.7
Co	22.70 ± 1.6	---
Cu	14.70 ± 1.0	14.9 ± 0.8
Zn	---	11.6 ± 0.8
Ga	9.00 ± 0.6	---
Ge	6.60 ± 0.6	---
Rb	1.76 ± 0.13	1.8 ± 0.3
Y	1.00 ± 0.05	1.0 ± 0.03
Mo	0.50 ± 0.04	---

difference in K is the low yield in bovine liver, suggesting partial volatization in this element, since the target stays under vacuum for three days in the big chamber.

The internal standard procedure has the virtue that any systematic errors in the calibration or in data collection process which affect the standard and the element of interest by the same amount e.g. improper determination of integral beam charge, are effectively cancelled out in equation 3.12. The internal standard procedure is not without serious drawbacks however; the standard must be (1) free of contamination; (2) it must not cause precipitation of any element in the sample; (3) the standard must be distributed uniformly throughout the sample; (4) it should not volatilize during proton bombardment; (5) finally, the validity of the internal standard technique for thick targets requires that the standard and the element of interest have similar atomic numbers, i.e. if a broad range of elements are of interest; several standards should ideally be added to the sample, so that one of them will be close in atomic number to each element of interest.

III.D Sample Preparation Techniques:

III.D.1 Introduction:

Since sample preparation is an all important factor in the ultimate accuracy of PIXE analysis, many papers have been published describing a number of methods for sample handling. As several excellent review articles are available in the literature, Campbell et al (1975), Willis (1977), Mangelson et al (1977), Campbell (1977), and Mangelson et (1981), the content of the following section will be restricted to a general summary of methods which have been used for blood serum analysis, and hair analysis by PIXE, and only the adopted technique will be discussed in detail.

III.D.2 Blood Serum Analysis:

Two general approaches have been used:

(1) irradiation of serum with no concentration,

(2) preconcentration of the sample.

(1) Some projects employed thin target with no concentration beyond drying, Barrette et al (1976), (1979 a,b), (1981), Vis et al (1977), Chen and Anderson (1979), Chen (1981), Li Ming et al (1981 a,b), and Glazur et al (1981 a,b). Of these Chen (1981) prepared specimens by evaporating 30 μL of serum to dryness on

2.5μm stretched Mylar. The quantitative calibration was done by adding to the serum known quantities of several elements. A Se level down to 0.03 ppm was measured and Ni down to 0.01 ppm. He found that Se concentrations in serum of acutely ill Legionnairs patients are significantly lower than in their matching convalescent-phase serum. Barrette et al (1976) had to add 11 spectra each 1.5 h exposure to be able to detect Se. Clearly analysis without concentration requires rather lengthy analysis time or high current which can cause target damage.

(2) Freeze-drying, dry ashing and wet ashing are the methods used for preconcentration of serum samples. In freeze-drying serum is frozen and then the freezing chamber is evacuated and pumped for a relatively long period of time to sublimise the ice, this leaves a solid residue which can be thoroughly powdered to ensure uniformity of elements throughout. Campbell (1977) found that freeze-drying enabled the mass of the sample to be concentrated by a factor of 5. 110 g of serum was lyophilized and homogenized by Maenhaut et al (1980), 0.1 to 0.2 g of the powdered serum then doped with $AgNO_3$, two doped serum samples were prepared, one was again converted to powder by lyphilization and the other was used in the liquid form for target preparation.

In the ashing process, the elemental concentration of elements of intermediate atomic number is increased by

the removal of low atomic number elements, the process results in a homogenous sample. Dry ashing or dry oxidation can be done either at low or high temperatures. Weber et al (1980) lyophilized and ashed serum in a low temperature oxygen plasma (LTA), the residue was dissolved in pure acid. 20μL of this resulting solution and 20μL of $Y(NO_3)_3$ internal standard were pipetted onto the 4μm polypropylene backing, after addition of 20μL of lipsomes (homogenizer). The resulting droplet was dried in vacuum for one hour in order to avoid an excessive spread of the sample due to the use of the lipsomes. Mangelson et al (1977), Pallon and Malmqvist (1981) both used freeze-drying first, the resulting powder was low temperature ashed, and then resulting ash was dissolved in nitric acid. A drop of the resulting solution was used to prepare the target. Berti et al (1977) added 20% of powdered graphite to ashed serum before pelletizing, this improved the thermal conductivity so much that they could use 80 nA. Low temperature ashing is a useful technique for blood samples, it reduces the detectable limit by a factor of 3, Campbell et al (1981), increases the possibility of analysing elements such as Ni, Se, and Pb, but increases the cost and time of preparation.

In wet ashing procedures a specific amount of sample was digested with a suitable digestion agent, with or without heating. Campbell (1977) employed the wet digestion method, dissolving 0.25 mL serum in 1 mL ultra pure acid, one drop of the acidic solution was then

deposited on carbon foils to dry. In this work 400 mg of blood serum was digested in 1.2 mL of nitric acid "Aristrar" with heating sec.III.D.4. Wet digestion is useful in blood analysis, the difficulty of flaking off in vacuum of direct target preparation, Spoelstra et al (1981), is overcome and the breakage of the foils as the deposit dries is negligible.

The concentration of trace elements in blood serum are very low compared with the rest of the body, especially hair. They are, for most techniques, near the limits for good precision. When ashing is used, however, the precision is improved and also the MDL. High temperature dry ashing should be avoided unless it is absolutely necessary as volatile elements are frequently lost in the process, Gorsuch (1970). Also if samples are to be prepared by depositing a drop of digested solution onto foils and evaporating to dryness then the use of sulphuric acid as one of the digesting acids should be avoided as its high boiling point makes evaporation to dryness difficult, Khan and Crumpton (1981).

III.D.3 Hair Analysis:

Four general approaches have been used: (1) irradiation of hair strands, (2) scan of the length of strands, (3) scan of hair cross-section, and (4) homogenized samples.

The first approach was a direct analysis of hair. In the

measurement performed by Valcovic et al (1974) a single hair from a female head was cut into pieces approximately 3 cm in length. The sample was washed, dried, and mounted on an aluminium holder with a central hole 1.5 cm in diameter. Randic et al (1976), Ludi et al (1978), Henley (1976), Henley et al (1977), Jones et al (1979), and Bacsó et al (1982) also irradiated hair directly. Problems are encountered in the direct analysis of hair by particle irradiation because individual hair strands are thick with respect to the particle energy usually employed and some of the light element x-rays are attenuated to a considerable extent, variation in linear density along a given hair can cause a change in x-ray intensity which does not reflect elemental concentration changes. Russell et al (1981a)found a factor of ~5 in linear density hairs from different subjects. Whitehead (1979) represented the difficulties for direct hair analysis if absolute elemental concentration was required, and the main four factors suggested by Whitehead were:

a) The composition of hair with respect to the major elements is of uncertain variability. This is important because the assumptions for composition is used in calculating x-ray absorption. b) the x-ray production cross-sections are not known with great precision. c) the hair cross-section is assumed to be circular, but this is known to be only approximate. d) hair is not homogeneous, especially in the outer layers of hair.

Attempts to get around these by measuring the scattered proton, or the intensity of the sulphur x-ray peak, or by calculation were not successful. These problems can, however, be overcome by dissolving a weighed amount of hair in hot nitric acid adding an internal standard and preparing a thin target from the digested sample.

The second approach was scanning proton microprobe to map out the spatial distribution of a given element (or elements) along the hair described by Horwitz et al (1976). A hair was cemented to a rigid strip of Kapton with Kodak Micro Resist 747, then scanned repeatedly with the proton microbeam. Proton induced x-rays corresponding to each element of interest were detected and stored in a multichannel analyzer as a function of position. Thus are simultaneously obtained graphs of the abundances of a number of elements versus position along the hair. Jolley et al (1974), Grodzins et al (1976) also measured trace element distribution along human hair to study the history of exposure of the donor to toxic trace metals. Their results reflect the possible application of the proton microprobe to problems in biology and medicine.

Cookson and Pilling (1975), and Houtman et al (1979) used the proton induced x-ray method with a finally focussed beam to measure the distribution of trace elements across the diameter of human hairs in the hope that this will throw light on the origin of the trace elements in hair. Cookson (1975) embedded unwashed hair

in a block of epoxy-resin which was then machined to expose the section of hair of roughly circular shape and diameter between 70-100 μm. The beam of 3 MeV protons was focussed into a spot approximately 7 μm by 15 μm which arranged to cross a section of the hair and the x-ray yield from elements of interest determined. A comprehensive review is given of the development and use of beam of protons with spot size as small as 2 μm, Cookson (1979) and Cookson (1981). Micro-beam PIXE has the ability to determine how the trace elements are distributed in hair.

The last approach listed was to use physical or chemical means of breaking down the structure of the hair sample in order to provide a homogenized sample. Homogenized samples require several operations but are able to provide the most reliable analytical results barring contamination in the preparation process. All information relating element concentration to hair structure was lost in the process. Bodart (1978), and Khan (1979) analysed hair pellets by PIXE, Bodart prepared hair samples by freezing in liquid nitrogen and grounding in an agate mortar. The ground material was pressed into a pellet, making a thick target. Hill et al (1980), and Chen Jian-Xin et al (1981) had ashed hair in an oxygen plasma and dissolved the ash samples in acid. The method of dissolving hair sample in nitric acid was used by Whitehead (1979), Saied (1981), and Baptista et al (1981). Of these Baptista et al (1981) dissolved 60 mg of hair in 1 mL pure nitric acid to which 20 μL of a solution

containing strontium was added. The target itself was prepared by dripping 5 μL of the final solution onto a Nuclepore backing having 0.4 μm pore size mounted on an aluminium frame 1.2 cm in diameter. Comparing this method with the direct analysis of 8 selected hair strands, they found that dissolving the hair sample in nitric acid and adding internal standard to the solution proved to be more convenient when a large number of samples had to be analysed, since thin target can be obtained with a larger mass of hair, the time of irradiation was reduced, and the time consuming selection of hair strands with the same diameter was avoided.

Ashing provides a means of concentrating non-volatile metals in the sample by removing most of the organic compounds. Targets with a higher concentration of elements can then be fabricated with a much smaller total mass. This decrease in mass reduces the amount of background due to secondary electron bremsstrahlung, thus improving detectability limit, Bearse et al (1974). In discussing ashed specimens, one should also stress the fact that high temperature dry ashing is extremely likely to cause losses of several elements, Gorsuch (1970). Wet digestion using ultra-high purity reagents is a long established technique (Gorsuch) used prior to analysis by several conventional methods such as atomic absorption spectrometry.

Wet digestion offers a number of potential advantages

over other preparation techniques:

1. Converts the organic matter to solution, provided it was complete, ensures representative sampling;
2. targets can be kept thin for best quantitative results and to minimize beam heating and charge accumulation problems;
3. It is possible to concentrate the sample, thereby improving the sensitivity;
4. addition of an internal calibration is made easier for samples prepared in solution;
5. concentration of each element is determined from the total hair mass.

The disadvantages are:

1. Contaminations - contamination by extraneous trace metals can be minimized by using ultra high purity acid, during storage the high acidity of the solution minimizes losses to container walls, and the use of teflon or polyethylene containers avoids dissolution of trace metals from the container walls;
2. loss of volatile elements, this can be kept to a minimum using sealed teflon vessels in stainless steel jackets;
3. formation of crystals in the dried deposits of all biological specimens (sec.III.D.6) which makes the thickness of the target non uniform;
4. migration of the elements towards the outer edge of the target, Baum et al (1977) freeze dried the targets

to prevent migration of the elements. Uniformly distributed beam, covering the target is essential.

The choice of a particular technique of preparation is governed by considerations of the required accuracy, precision and sensitivity of the target analysis, as well as the time and cost limitations of the various preparation methods. The ideal target for PIXE analysis would have the following properties, Willis et al (1977 a):

1. Thinness,to avoid beam energy loss and x-ray absorption and minimize self-fluorescence effects;
2. homogeneity;
3. high electrical and heat conductivity;
4. stability in vacuum;
5. stability to beam damage;
6. sufficient concentration so that elements of interest can be detected; and
7. minimal sample preparation.

Wet digestion with suitable backing goes some way towards this goal. Preparation of biological sample by acid digestion bomb was followed in the present work with the digestion repeated three times, in the manner reported by Saied (1981).

III.D.4 Acid Digestion Bombs and Target Preparation:

Acid digestion bombs have added a new alternative to the task of preparing analytical samples for analysis. By combining the unique chemical inertness of teflon with the advantages of a sealed stainless steel pressure vessel, these convenient bombs offer a rapid procedure for sample dissolution or digestion which has several important advantages over more traditional methods of sample preparation. By providing a convenient means for holding strong acids at temperature well above normal boiling points, these sturdy digested bombs will:

1. Accelerate digestions which otherwise would proceed slowly if conducted in an open container at atmospheric pressure;
2. permit the use of strong acids, which will attack conventional containers;
3. dissolve the analytical samples without losing trace elements and without adding unwanted contaminations;
4. obtain complete digestion of samples which react slowly or incompletely when treated by other methods.

With this capability, these bombs are particularly useful for preparing biological samples for analysis by proton induced x-rays or for other instrumental methods in which trace elements must be identified. Each of these bombs (Digby bombs) has a thick-walled teflon linear cup which completely isolates the sample from

the supporting metal body. These liners are easily removed and can be emptied while outside the bomb to further eliminate any possible contamination from acid contact with the metal parts.

Different organic materials, hair and bovine liver powders, hair strands, heart muscle, and blood serum liquid, were treated satisfactorily in Digby digested bombs in the present work. In all cases the size of the sample and the amount of acid used must be carefully controlled. For nitric acid digestions the dry weight of organic matter placed in the bomb is about 0.1 gram. The amount of concentrated nitric acid around 3 mL, otherwise the disc in the bomb head will blow out and release the excess pressure with some loss in the sample. The sample does not have to be dried before it is placed in the bomb, but the amount used about 0.1 gram when converted to dry weight basis. The operating temperature and pressure are $\sim 170^{\circ}C$ and 1200 psig respectively. The bombs can be heated in an oven which should be cooled slowly. A safety rupture disc in the bomb head is designed to blow out and release the pressure through an opening in the cover at higher pressure. The various steps of sample preparation have been checked for possible contamination by trace elements during handling of the samples. Since there is no method that will completely eliminate possible contamination, it was decided to follow the same procedure in preparing all the samples. This procedure is described in the

following paragraphs:

Dishes, teflon cups, and bottles are washed once in "tot" detergent, twice in water, kept in high purity dilute "Analar" nitric acid for two hours, and rinsed thrice in deionized water. After washing, they are left to dry for about half an hour on a clean filter paper in a dust free oven.

About 100 mg dry weight of the sample was transferred to the cooled teflon cup, the liner was slid into its stainless steel container and 2 mL of concentrated nitric acid "Aristar" was added gradually drop by drop. This step was done in a fume cupboard to exhaust the toxic gases which could be released during addition of the acid. The top part was added and the bomb was properly tightened. The bomb was heated in an oven at 150^{o}C for two hours, this was the first digestion, it was allowed to cool for about three hours. Carefully the top part was opened and another 1 mL of the acid was added and the sample was kept at the same temperature in the oven for another one hour, this was the second digestion. After cooling the third digestion was performed by adding a further ½ mL of the acid. These steps need about twelve hours for each sample, the bomb was left over night to cool at room temperature. A 5 mL clean pipette was used to collect the digested sample and to give the exact volume of the resulting digested sample. The digested sample was kept in a clean labelled 10 mL polythene bottle.

Bovine liver, hair powder HH-1, heart muscle, blood serum, and hair strands have been digested, quantities of specimen material and acid used in digesting the specimens are given in table 3.13. In order to get representative samples several digestions have been made and the products pooled. The reproducibility of the resulting digested sample volume is better than 2%. Typical results from a group are represented in table 3.14 where 3.5 mL nitric acid is added to each sample for digestion, the reproducibility expressed as the S D in this group is 1.15%.

In the case of the samples doped with an internal standard, 1 mL of the digested sample was put in a polyethylene bottle and doped with a specific volume of an internal standard solution, containing certain concentrations of yttrium, the exact figures are given with each application, section V.A.3 and V.B.

After the sample and the standard solution were well mixed, an Oxford adjustable sampler, Micropipetting system (2-10 µL) (Oxford Laboratories International Corporation Athy, Co.Kildare, Ireland) was used to deliver a drop of the exact target volume onto a 5 µm thick kimfoi backing which had previously been mounted on a target frame. This target frame consists of a 5 X 5 cm^2 pure aluminium square with ~1.6 cm diameter circular aperture. The kimfol backing was held across the hole with the aid of a ring which is slightly smaller

Table 3.13: Typical quantities in wet digestion

Sample	Sample mass mg	Volume of added nitric acid mL
bovine liver	250	~ 6.0
hair sample HH-1	100	3.5
heart muscle	180	3.0
blood serum	400	1.2
hair strands	110	3.5

Table 3.14: Results of digestion on a group of samples, the non-agitated control group see sec.V.B , 3.5 mL nitric acid added to each sample

Sample	mass of hair strands mg ± 0.2	resulting volume of digested hair mL ± 0.02
PT 1	110.7	3.06
PT 2	116.2	3.18
PT 3	112.2	3.12
PT 4	114.1	3.18
PT 5	112.1	3.11
PT 6	110.8	3.10
PT 7	114.8	3.13
PT 8	116.4	3.05
PT 9	115.65	3.14
PT 10	115.2	3.15
PT 11	114.1	3.12
PT 12	108.3	3.14
PT 13	111.6	3.16
PT 14	115.6	3.10
PT 15	114.6	3.25
PT 16	114.25	3.08
PT 17	112.5	3.13
PT 18	113.1	3.05
PT 19	109.0	3.09
PT 20	110.5	3.17

than the hole so that it could be pressed into it and clamp the backing, a simple design seen in the photograph, Fig.3.31, was used to deliver the digested drop at the centre of the backing foil. To improve sampling precision, the following steps were followed:

1. The same speed of intake and delivery was affected for all targets. Smooth depression and release of the plunger knob will give most consistent results.

2. The plunger knob was always depressed to the proper stop before insertion of the tip into the solution. Depression of the plunger knob after insertion may cause the formation of an air bubble in the tip and result in a filling error.

3. The instrument was held vertically and the tip was inserted approximately the same depth into the sample each time.

4. A new tip was used for each target and never touched the backing.

The targets were allowed to dry in a clean dissicator. A very dilute low Z "glue" was prepared by dissolving 125 mg of polystyrene (Polysciences, Inc., Warrington, Windsor Laboratories Limited, Bedford Avenue, Slough, Berks) in 3.8 mL "Analar" benzine. The dried targets were stuck to the kimfoi backing with a 2μL of the prepared glue and allowed to dry; no observable x-rays arise from the glue residue, Fig.3.17. A photograph showing the

Fig.3.31 Instruments used in the target preparation

equipment used in the target preparation is shown in Fig.3.31.

PIXE spectra obtained from 4 μL target of digested heart muscle and 20 μL digested blood serum using these techniques are given in Fig.3.32 and Fig.3.33 respectively.

The matrix effect, correction factors (sec.III.C.2), can be applied if the target thickness is known. An electrobalance Model Cohen 25 was used to measure the target thickness prepared from digested hair samples. The Cohen 25 electrobalance is a closed loop electromechanical system in which a mass is weighed by a directly proportional current flowing through a torque motor. It is a very sensitive weight and force measurement instrument. It is sensitive to weight changes as small as 100 nanograms. The average mass of 5 μL digested hair was found to be 56 ± 4 μg, as an average of 20 targets, which gives a target thickness of ~ 0.8 mg/cm^2.

III.D.5 Backing Material:

In the present work, from the viewpoint of quantitative analysis, thin targets were prepared throughout the work, the sample was deposited in liquid form into a thin kimfol backing. The choice of backing material for PIXE analysis at certain energy was guided by several considerations. The backing must consist of low-Z material and contain minimal amounts of higher-Z impurities in

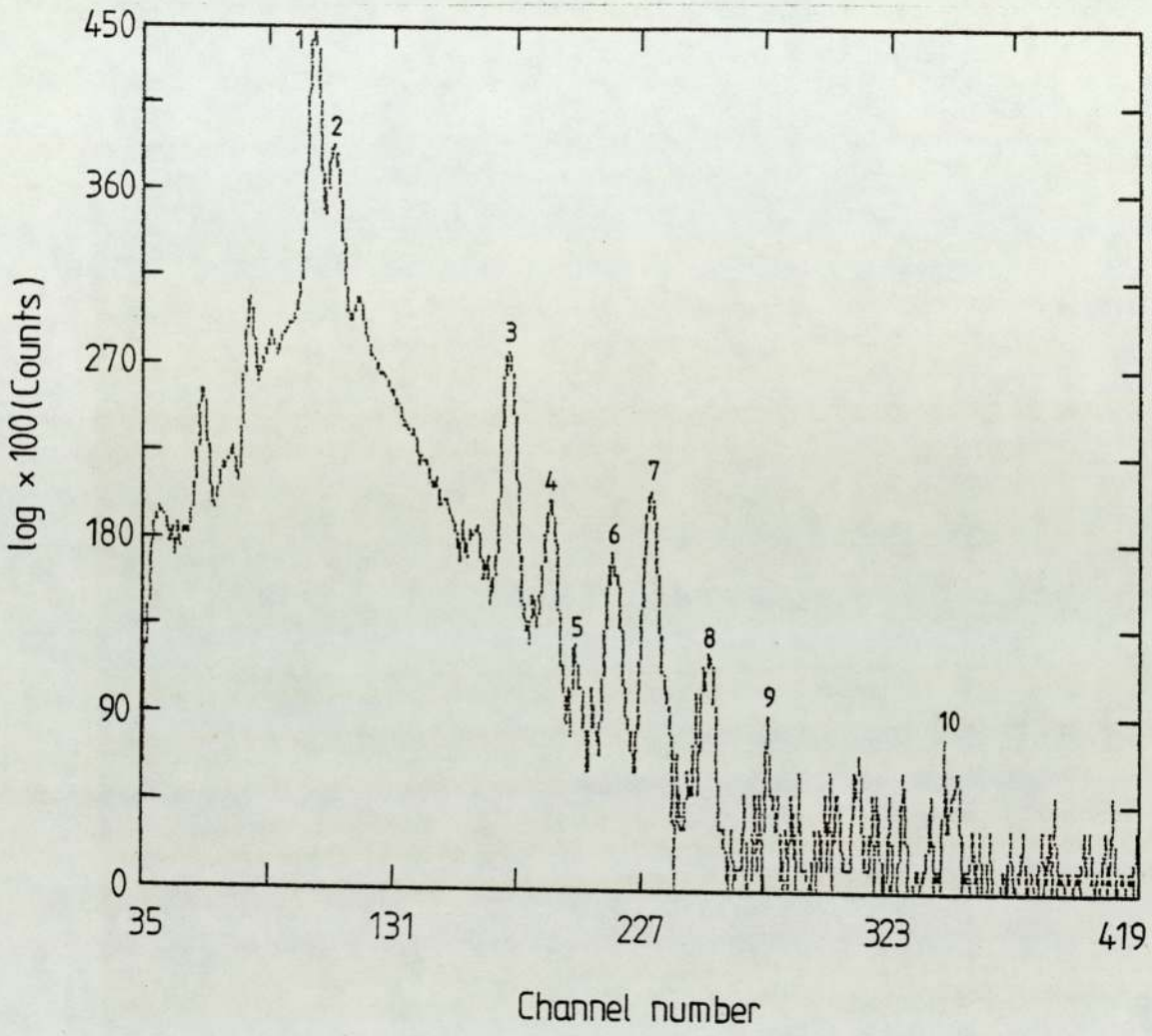

Fig 3.32 PIXE spectrum from 4 μm heart sample.

1 - K (K α)	6 - Cu (K α)
2 - Ca (K α)	7 - Zn (K α)
3 - Fe (K α)	8 - Zn (K β)
4 - Fe (K β)	9 - Pb (L α)
5 - Ni (K α)	10 - Rb (K α)

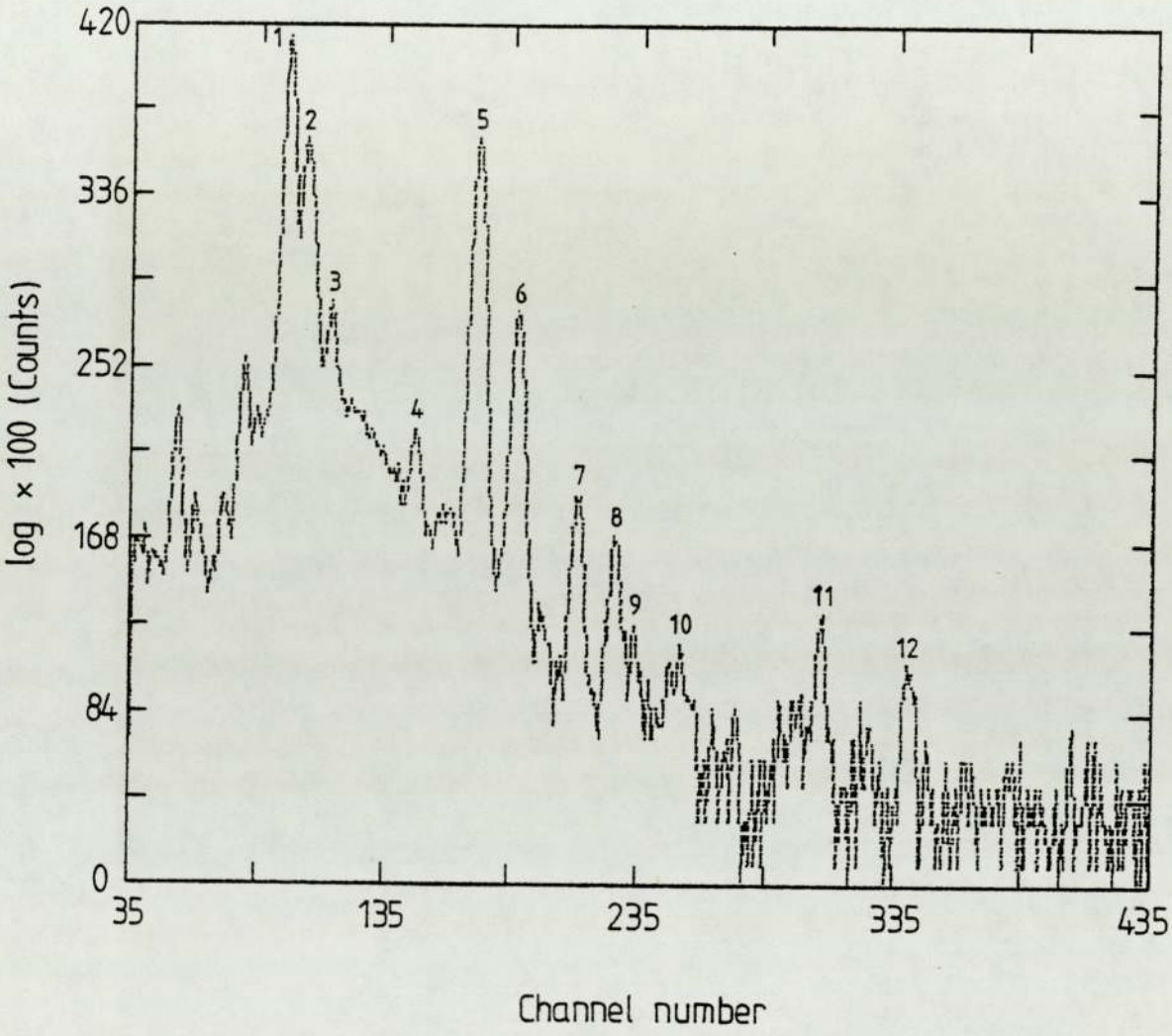

Fig 3.33 PIXE spectrum from 20 µl blood serum sample.

1 - K (K α)	7 - Cu (K α)
2 - Ca (K α)	8 - Zn (K α)
3 - Ca (K β)	9 - Cu (K β)
4 - Cr (K α)	10 - Zn (K β)
5 - Fe (K α)	11 - Br (K α)
6 - Fe (K β)	12 - Rb (K α)

order to avoid peak interferences for the elements to be analysed. Also, backing ought to be thin to minimize the x-ray background and thus increase sensitivity. Finally, the strength of the backing is of prime importance for its ability to withstand irradiation, handling, and target preparation precedures. Information on x-ray backgrounds, continuous and characteristic, from different backing foils bombarded by various ion beams is scattered throughout the literature. Many materials have been used for backing, some information on commonly used materials are given below.

Carbon foils have the advantages of commercial availability high heat conductivity, another significant advantage is that they are not attacked by acids; this is very useful where specimens are prepared by digestion in concentrated acid. Carbon foils can withstand very intense beams and are thus excellent for the analysis of very small amounts but are fragile and are less suited for work involving great numbers of samples or extensive sample handling, the use of carbon is much more expensive than any other material. Herman et al (1973b)prepared carbon foils from a wide variety of commercial carbon rods, and compared PIXE spectra. The Fe, Cu, Zn and Ni levels observed varied greatly. Due to these impurities Kaji et al (1977) suggested that carbon foils are not convenient as backing. For measurements requiring high sensitivity, 20$\mu g/cm^2$ carbon foils had been used by Johansson et al (1972). The Yissum Corporation had made

extensive improvements to its carbon impurities noticed by Campbell (1977). Russell et al (1981b) investigated different backing, 30 $\mu g/cm^2$ carbon foils from Yissum Corporation being one of them, they concluded that carbon foils are competitive with the most attractive commercial foils for PIXE, in terms of continuum background and Fe, Zn content; their heat conduction and resistance to acid are added advantages, offset by increased cost relative to the polymers.

Thin user made polymer films ($\sim$20 $\mu g/cm^2$) such as polystyrene and Formvar are used quite widely and offer the lowest available continuum background; however, their preparation can be time-consuming and they are easily broken. Many authors had published recipes for preparation of thin polymer films, for use in a great variety of applications. Grader et al (1971) discussed Monsanto Formvar or polyvinyl formal $(C_5H_7O_2)_x$, with suitable withdrawal rates they prepared films 15-50 $\mu g/cm^2$ in thickness. Bearse et al (1974) used the method described by Grader, and achieved thickness of 10 $\mu g/cm^2$. The foils withstood a 150 nA beam of 3.75 MeV protons, no metallic impurities are mentioned. Walter et al (1974) found Formvar backings are fragile and probably not practical for wide spread use, they observed Mn, Fe, Cu and Zn background impurities. Valcovic et al (1974) evaporated 100 $\mu g/cm^2$ of aluminium onto 50 $\mu g/cm^2$ polymer film, these backings withstood 150 nA of 3 MeV protons, they observed no characteristic x-ray peaks from the foils.

Johansson et al (1975) had used 4% polystyrene $(CH)_x$ in benzine. These films withstood 3.7 MeV protons beam, of intensity 1 nA/mm^2. Kubo (1974) had used Collodion $(C_{12}H_{11}O_{22}N_6)_x$ in PIXE work, these foils could only withstand 0.05 nA/mm^2. Microtome tissue sections were wrapped in sandwich fashion to withstand higher current.

There has been a trend recently to widespread use of commercial polymer foils, due to the ease of preparation that they afford; which is an important factor since PIXE now handles large numbers of specimens. Of these foils Kapton (polyimide), Mylar (polyster), Hostaphan (polyster) and Kimfol (poly carbonate) are most frequently mentioned. These foils have the advantages of cheapness, convenience and strength, but they produce a much more intense bremsstrahlung background than do the thin foils discussed before. Flocchini et al (1972) have examined commercial Mylar, Kapton and Teflon foils, the thickness varied between 0.7-8.0 mg/cm^2, with 30 and 50 MeV of particles. They found that Kapton and Mylar produce similar background for the same thickness, while Teflon gives a more intense background. Gordon and Kramer (1972) used 5 MeV protons to examine four backings, including Kapton and thin carbon, and recommended carbon foils as the most suitable. Barrette et al (1976) had selected Kapton as backing for their targets. Kaji et al (1977) have observed Cu, Fe and Zn in small amounts when analyzing 10 μm Mylar foil. Chu et al (1977) used 3.5 MeV protons for a comparison of 4-10 μm Mylar, very thin

carbon, and Formvar foils, the latter being coated with aluminium; they found Mylar superior on grounds of purity and strength.

Nucleopore backings are heavily used in PIXE analysis. Nucleopores have been used successfully by Nelson et al (1976) to absorb acid solutions of human tissue, these targets withstood proton beams of density up to 3.5 nA/mm^2. Campbell (1977) shows that Nucleopore are good backings. A study, presented by Russell et al (1981), covering the major commercial plastics that find use, in addition to commercial carbon foils and user-made polystyrene films. Their results of comparison at 2 MeV protons beam is represented in table 3.15, for most of the currently used backing foils, which would facilitate choice among available materials and lay down well-defined standard data against which new candidates might be judged. They concluded, kimfol and stretched polypropylene, normalized to equal thickness emerge overall as the most attractive commercial foils for PIXE.

The optimum choice of backing depends on the analytical situation as all parameters cannot be optimized simultaneously. Kimfol was chosen as backing for thin targets used throughout this work. Selection of Kimfol is based on the following:

The major application in this work is biomedical and needs the handling of large numbers of samples, Kimfol

Table 3.15: Results of 60-μc irradiations of a 21-mm^2 portion of various foils

Foil	thickness mg/cm^2	continuum counts (11-16 keV)	bremsstrahlung height at 5 keV	Elemental masses, ng/cm^2			
				Ca	Fe	Cu	Zn
Blank		24		0.14 ± 0.08	0.005 ± 0.01	-0.001 ± 0.02	-0.005 ± 0.02
Polypropylene	2.25	530	734	13.9 ± 3	27.8 ± 0.3	0.01 ± 0.1	0.8 ± 0.1
Kapton	1.08	441	460	23.8 ± 2.5	7.7 ± 0.3	2.7 ± 0.2	3.8 ± 0.2
Mylar (S)	1.06	494	585	438 ± 5	12.0 ± 0.4	5.3 ± 0.4	41.2 ± 0.8
Mylar (C)	0.21	136	145	1370 ± 8	2.3 ± 0.3	0.5 ± 0.2	15.7 ± 0.5
Spectro-film Mylar	0.53	222	280	927 ± 6	2.0 ± 0.2	0.2 ± 0.2	13.6 ± 0.5
Hostaphan	0.35	159	190	91.1 ± 2.4	2.19 ± 0.15	0.14 ± 0.08	-0.17 ± 0.08
Makrofol	0.30	127	136	11.4 ± 0.2	3.2 ± 0.2	0.4 ± 0.15	0.2 ± 0.2
Kimfol	0.24	122	124	3.6 ± 1.1	0.3 ± 0.1	0.08 ± 0.05	0.14 ± 0.05
Polystyrene	0.085	99	46	2.9 ± 0.7	0.6 ± 0.05	0.06 ± 0.05	0.18 ± 0.05
Polypropylene (S)	0.055	53	31	6.9 ± 0.7	1.27 ± 0.08	-0.04 ± 0.04	0.12 ± 0.04
Carbon	0.030	66	18	20.8 ± 0.9	0.29 ± 0.06	0.75 ± 0.08	0.25 ± 0.07
Nucleopore	9.0			0.1	90.0	3.0	6.0

affords ease of preparation. Kimfol is not attacked by acids, this is very useful since samples are prepared by digestion in concentrated nitric acid, they have good mechanical strength, a low level of high Z impurities, for optimum sensitivity thinner foils, 2.0 μm can be used. The drawback of these foils is the problem with the flaking of sample deposits, this problem is overcome by gluing the sample to the backing as described in sec.III.D.4.

To study the reproducibility in detail for the Kimfol roll that is adopted for use throughout this work, three targets were prepared from Kimfol only, mounted on the aluminium frame as described in sec.III.D,4. The replicate foils were taken from different points on the roll. The three Kimfol targets and a blank (aluminium frame present without foil) were irradiated with 2.37 MeV protons for 25 μc. Fig.3.34 compares typical spectra from Kimfol and a blank. The spectrum from the blank consisted of a weak continuum and two small peaks at Mn and Fe K lines. The metallic impurities of the three targets are indicated in table 3.16, these data were obtained using the equation

$$\frac{\text{mass}}{\text{unit area}}\ (\text{ng/cm}^2) = \frac{\text{Counts Kα x-ray} \cdot 10^3}{\text{Charge}(\mu\text{C}) \cdot F(z)(\text{counts}/\mu\text{c}.\mu\text{g cm}^{-2})} \qquad 3.20$$

to convert Kα x-ray intensity into elemental mass per unit

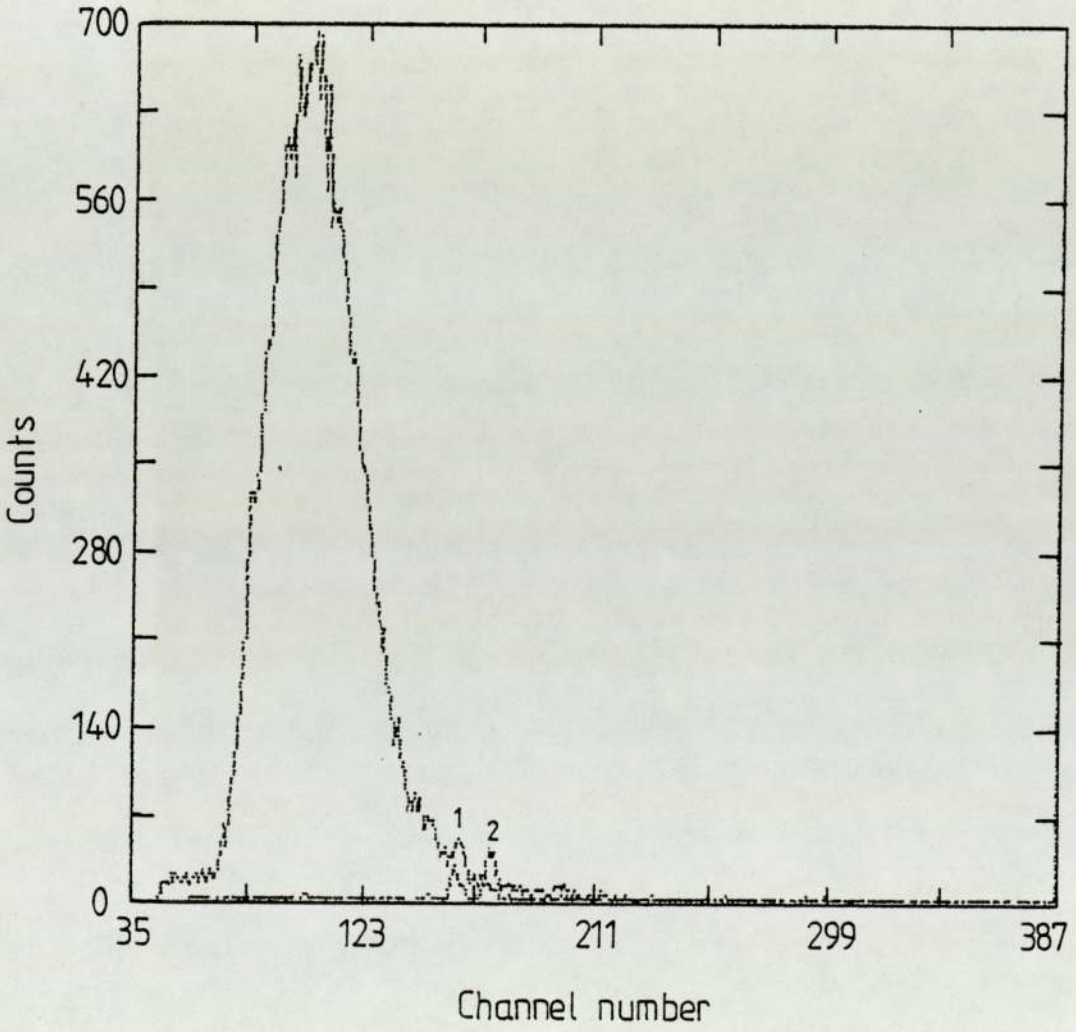

Fig 3.34 PIXE spectra from Kimfol backing and the chamber background.

1 - Mn (K α)
2 - Fe (K α)

Table 3.16: Trace element content with statistical counting error of replicate Kimfol targets, 5 μm thick, proton energy 2.37 MeV, charge 25 μc.

Target	continuum counts at (11-16) keV	bremsstrahlung counts at 5 keV	Elemental masses, ng/cm^2			
			Ca	Fe	Cu	Zn
blank Kimfoil	103	2	0.1 ± 0.1	1.4 ± 0.1	0.1 ± 0.1	0.1 ± 0.2
(1)	136	147	4.3 ± 1.4	0.9 ± 0.3	0.0 ± 0.2	-0.3 ± 0.2
(2)	136	112	6.0 ± 1.4	2.9 ± 0.2	1.0 ± 0.2	4.0 ± 0.2
(3)	93	154	4.6 ± 1.4	2.0 ± 0.3	0.6 ± 0.2	0.6 ± 0.2
mean ± σ	122 ± 20	138 ± 18	5.0 ± 0.7	1.7 ± 0.4	0.5 ± 0.4	1.0 ± 2.5
mean in ppm ± σ			8.3 ± 1.2	2.9 ± 0.7	0.9 ± 0.6	1.7 ± 4.2

area. The first row in table 3.16 presents data for blanks; such data have been omitted in most published discussions of PIXE backing foils. In the absence of such information the possibility is left open that a significant fraction of the background continuous and characteristic radiations, ascribed to any given foils may in fact arise from sources other than the foil. From the results in table 3.16 one can notice the high levels for all elements investigated in target number 2, compared with others, which shows that Kimfol is not reproducible in the levels of their impurities, especially in the Zn. From the numerical results, table 3.16, one can estimate roughly the importance of these contaminants for a given sample. For example, the foil Fe, Cu and Zn will add only a 1% or less to Fe, Cu, and Zn K x-ray peaks from hair samples having levels >20 ppm of these elements. The problem becomes more serious when elements in the sample are at ~ 1 ppm levels; as is the case in serum analysis; and the problem is more serious if these levels are variable. The major application of the present work is on hair analysis, where the levels are $\gg$ ppm and therefore it was possible to use Kimfol throughout the work as backing material without introducing large errors, and the average impurities were subtracted from the peaks as described in sec.III.B.2.

III.D.6 Use of Liposomes to Improve the Homogeneity of Biological Targets:

Thin targets were prepared by depositing a droplet of a digested sample on a Kimfol backing. After drying, some crystals were formed, whose thickness may be large. Owing to the close proximity of different elements in the crystal the so called enhancement-absorption effect may happen and lead to systematic error in the quantitative analysis. M.Ahlberg et al (1976) calculated the correction to be applied for this effect. Furthermore, this effect is generally considered to be negligible when the sample thickness does not exceed 1 mg/cm^2 of uniformly distributed material on the backing, the case in this work. Another way to minimize this phenomenon is to use homogenizing products. Some of these products were mentioned in the literature, Chung (1976). Robaye et al (1980) demonstrated the lowering of enhancement-absorption effects by using liposomes (synthetic phospholipid bilayer vesicles) as homogenizers in the preparation of thin targets. The mixture lecithin + cholesterol + phosphatidic acid (molar ratio 7:2:1 respectively) on a 3 mg/cm^2 cellulose filter Gelman G A-6 was used in sample preparation for biomedical analysis, Robaye et al (1981).

In an attempt to avoid little crystallization on the target prepared in this work, the liposomes mixture was adopted. It is commercially available from Lipid Products,

Nutfield Nurseries, Crab Hill Lane, South Nutfield, Red Hill, Surrey, RH1 5PC, U.K., it is inexpensive and easy to prepare. Hair targets were prepared with and without the liposomes, the target with liposomes was prepared as follows: A drop (5 μL) of a digested hair doped with yttrium, was deposited on a 5 μm Kimfol backing immediately after having received a 2 μL quantity of liposomes in benzine as an homogenizer. After drying, a large spot target, thin and homogeneous, was obtained where local crystallization was avoided. The target without liposomes was prepared in the usual way, 5 μL of the doped digested hair was deposited on the Kimfol An electron microscope was used to illustrate the difference existing between the two targets made of the doped hair with and without the addition of liposomes. Micrographs of the two targets are represented in Fig.3.35 and Fig.3.36. In Fig.3.36 the crystalization can be seen while in Fig.3.35 very small crystals are distributed over a much larger area.

To reduce the large spread of the deposited digested hair sample with the liposomes, a third target was prepared on 1 mg/cm^2 Nucleopore filter with 8 μm pore size receiving 2 μL of liposomes, which because it is porous reduces the spread.

To study the purity of the liposomes, two targets were prepared, one of Kimfol only, the other Kimfol onto which 2 μL liposomes was deposited. Beam of protons

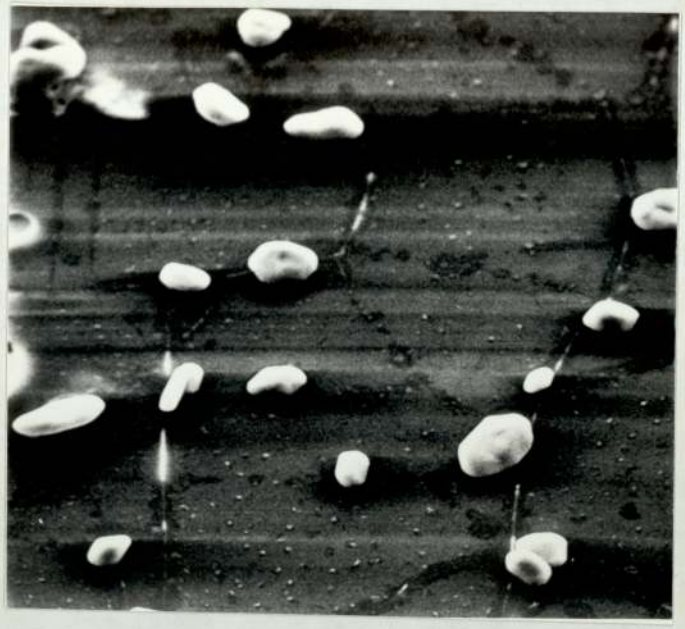

Fig.3.35 Micrograph 1000 magnification for target without liposomes

Fig.3.36 Micrograph 1000 magnification for hair target with liposomes

2.37 MeV, 10 nA were used to irradiate the target with 25 μc. The Si(Li) detector was placed at 90° to the incident beam, received the x-rays from the target through 7 μm aluminium absorber. Fig.3.37 shows the background obtained by bombarding the Kimfol with and without the liposomes, the absence of any different peaks on the bremsstrahlung and continuum proves the purity of the lecithin used. The spectra obtained by bombarding the three hair targets represented in Fig.3.38, Fig.3.39 and Fig.3.40. Counts in the Y Kα peak, with the ratio for [Cu (Kα counts)/Y (Kα counts)] are given in table 3.17. The poor statistics for targets with liposomes, due to the very large spread of the sample is clear. The use of Nucleopore with its porous surface and larger thickness improved the counts to some extent but it is offset by the higher level in the bremsstrahlung region. One can avoid too large a spread of the digested sample on the Kimfol, by drying under vacuum but this involves running the risk of contamination and losing volatile elements.

With liposomes on Kimfol the foil was destroyed when one tried to fix a larger quantity of the acidic digested sample to improve the counts. Robaye et al (1981) used a 3 mg/cm^2 cellulose filter Gelman, which is less sensitive to the acidity in order to increase target mass and thus improve the counts, but clearly it is not competitive when the ultimate in background is required.

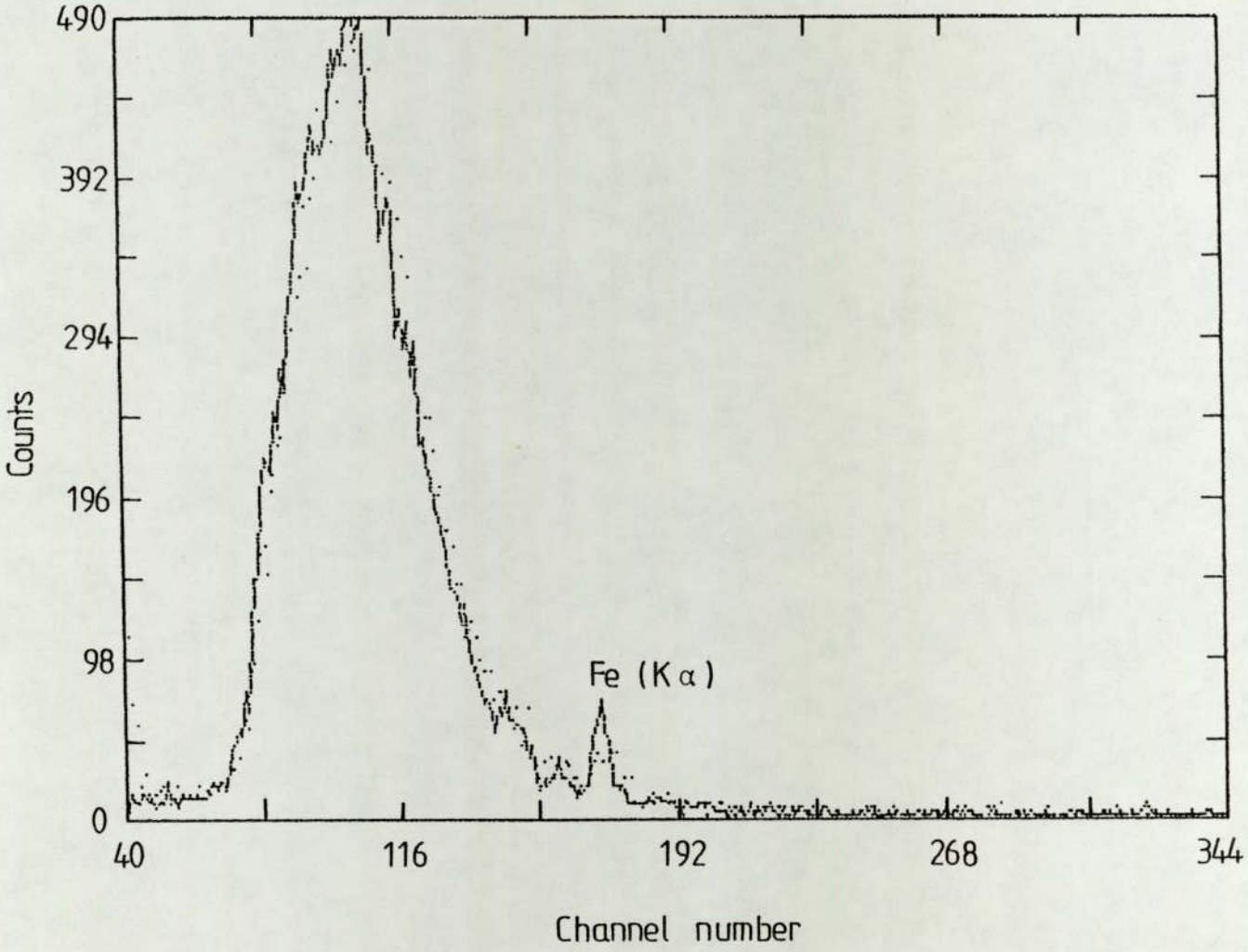

Fig 3.37 PIXE spectra from Kimfol only and Kimfol with liposomes on it.
..... Kimfol only on linear, —— Kimfol with liposomes on linear.

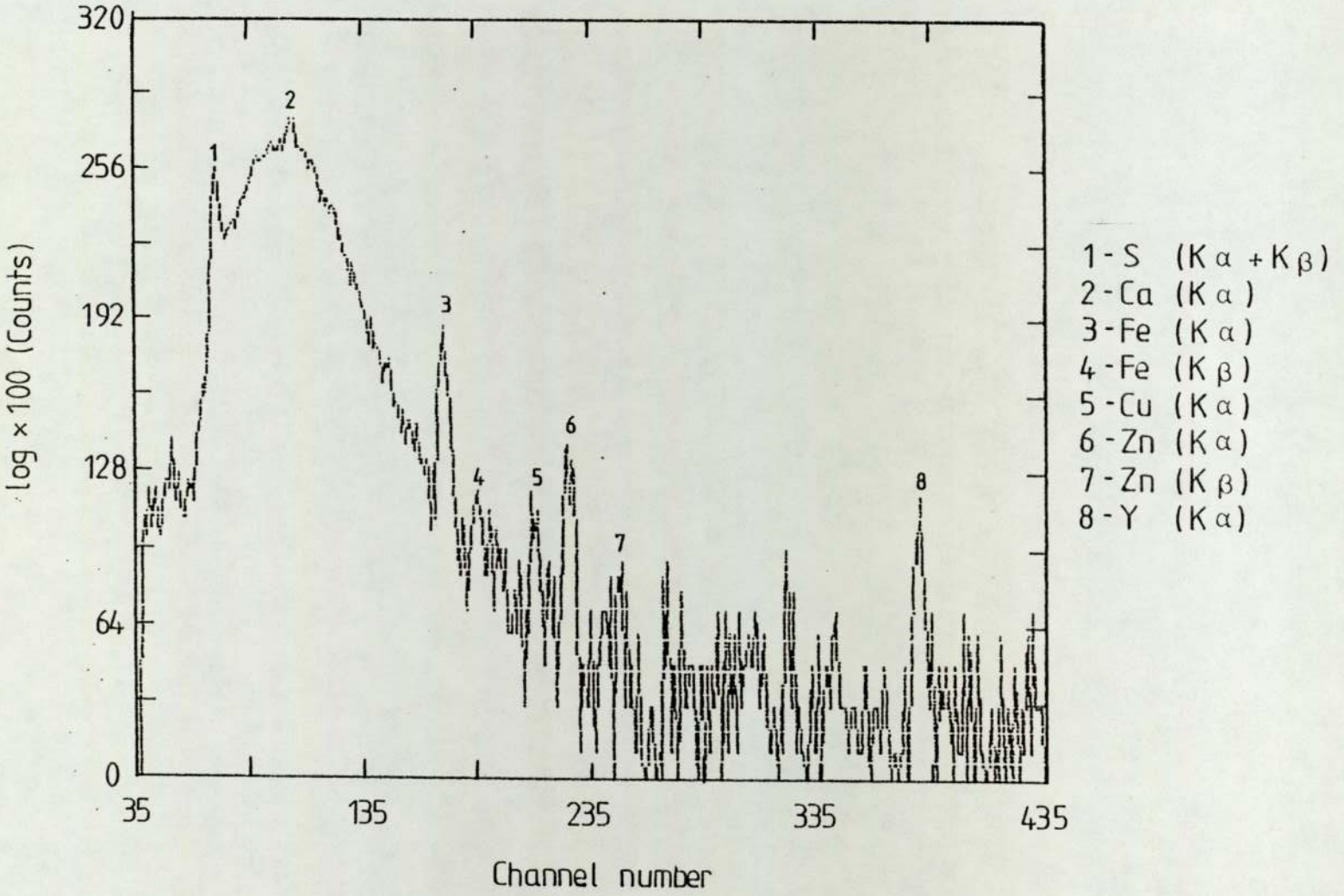

Fig 3.38 PIXE spectrum from hair sample with liposomes on Kimfol backing.

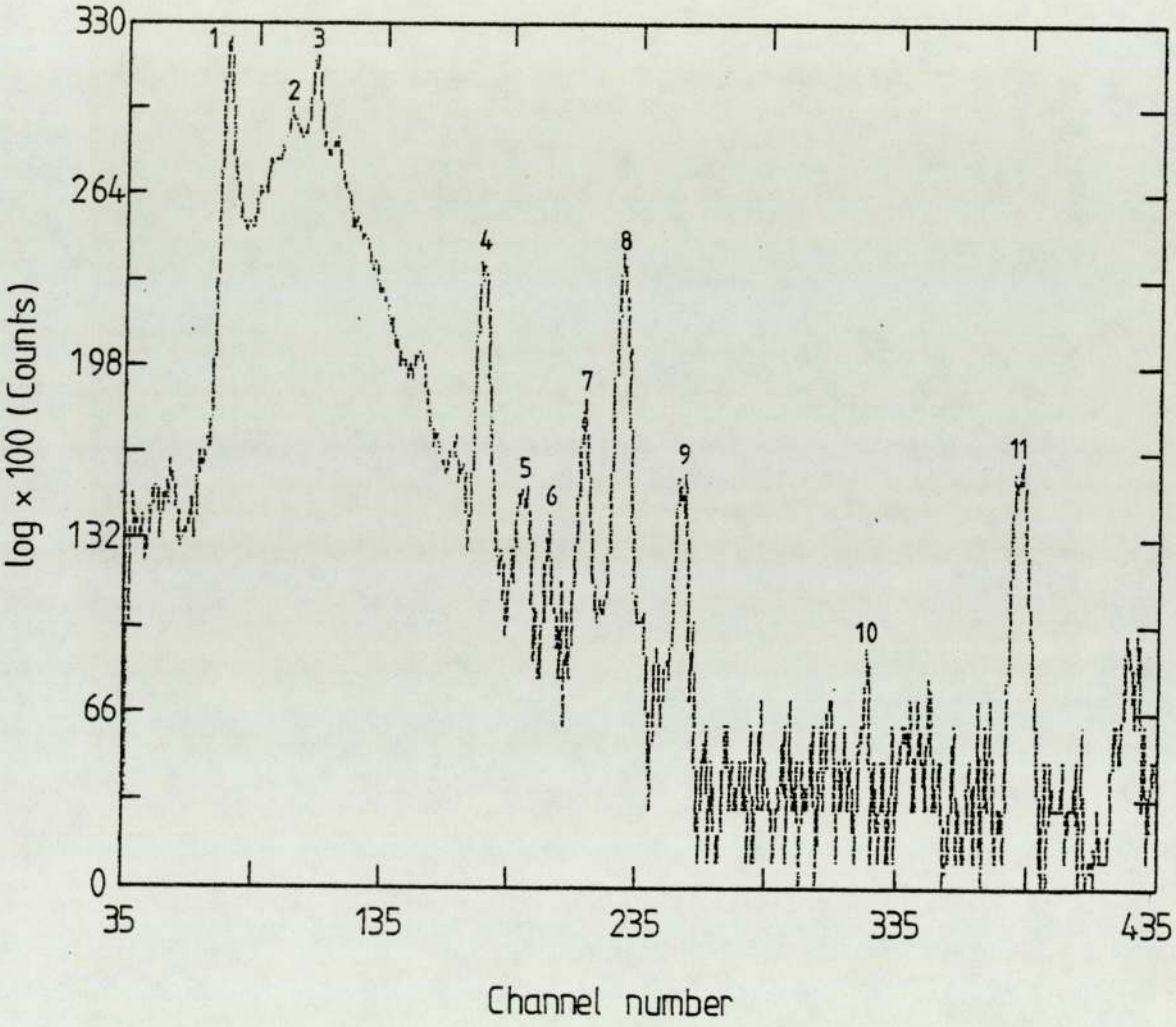

Fig 3.39 PIXE spectrum from hair sample on Kimfol without liposomes.

1 - S (K α +K β)
2 - K (K α)
3 - Ca (K α)
4 - Fe (K α)
5 - Fe (K β)
6 - Ni (K α)
7 - Cu (K α)
8 - Zn (K α)
9 - Zn (K β)
10 - Br (K α)
11 - Y (K α)

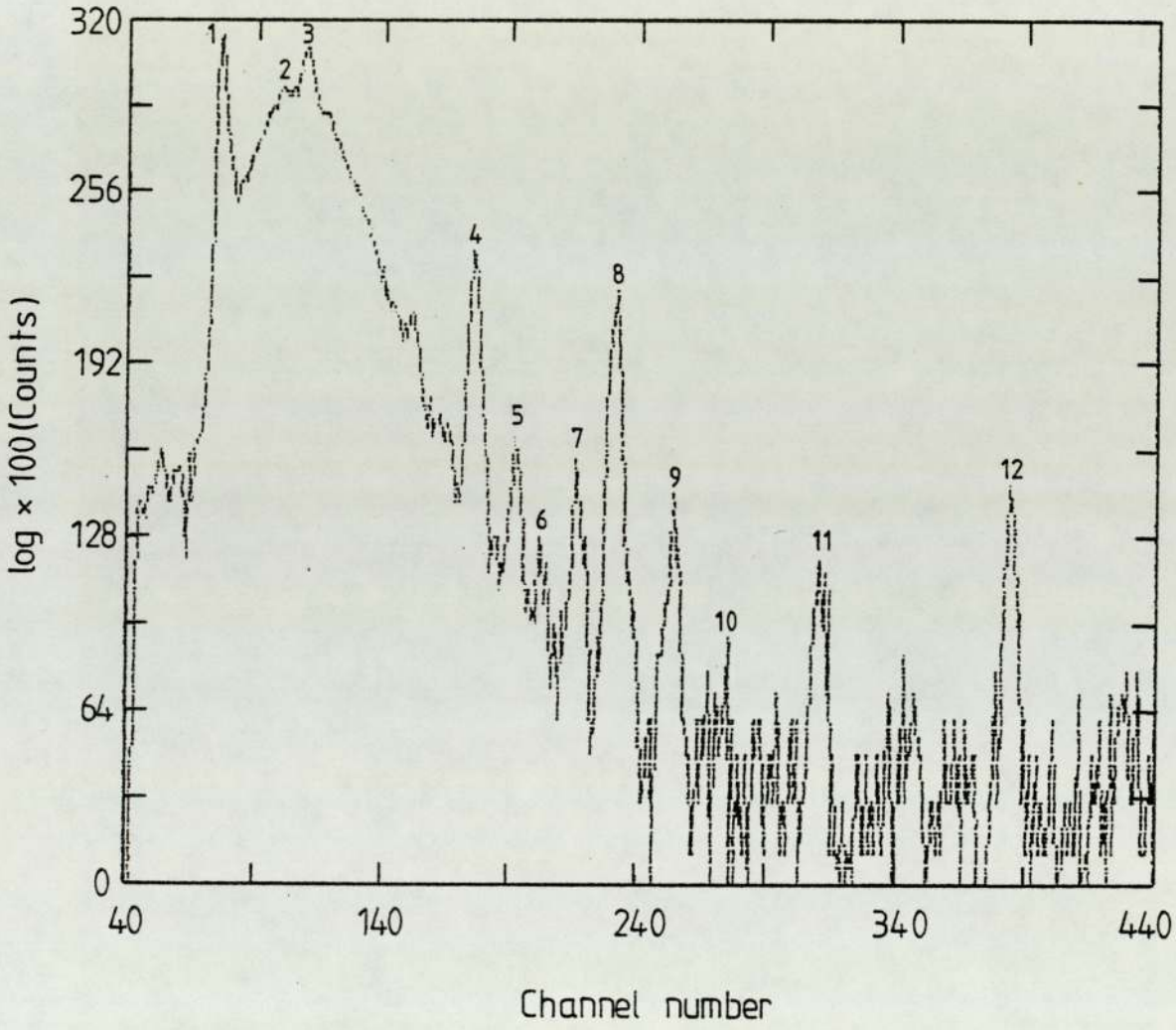

Fig 3.40 PIXE spectrum from hair sample on Noedepore with liposomes.

1 - S (K α +K)	7 - Cu (K α)
2 - K (K α)	8 - Zn (K α)
3 - Ca (K α)	9 - Zn (K β)
4 - Fe (K α)	10 - Pb (L α)
5 - Fe (K β)	11 - Br (K α)
6 - Ni (K α)	12 - Y (K α)

Table 3.17: Counts from the three different targets prepared to study the use of liposomes

Target	Y-Kα counts	$\frac{\text{Cu Kα counts}}{\text{Y Kα counts}}$
hair on Kimfol without liposomes	206	1.00
hair on Kimfol with liposomes	60	0.95
hair on Nucleopore with liposomes	120	0.96

The figures represented, and the results in table 3.17 lead to the conclusion that the use of liposomes as an homogenizer is a suitable technique for preparing very homogeneous thin targets where crystalization was avoided, the liposomes are free from impurities, but the drawback is the large spread of the sample,and the foil was destroyed when one tried to fix a larger quantity of the digested solution. Since the targets employed in the present work are thin targets irradiated with a beam of area bigger than the target, it was decided to use targets without liposomes for better statistics.

III.E PIXE Sensitivity

One of the main advantages of the PIXE method is its high sensitivity. It is therefore of considerable importance to discuss in more detail what sensitivity can be obtained and how it depends on the various experimental parameters.

There are several ways of defining the sensitivity of an analytical method. A complete discussion of sensitivity by Currie (1968) suggested that specific definitions are needed corresponding to each of the different parameters which can be measured.

In the present work, the problem is to measure small amounts of various trace elements in a certain matrix. The most basic definition of the sensitivity is therefore the minimum detectable concentration, MDL.

The trace elements to be measured are, however, always contained in their organic matrix. As described in sec. II.E a background arises inevitably in the interaction of the incident particles with the matrix atoms, this background sets a limit to the sensitivity which can be obtained since in order for the characteristic x-ray peak to be discerned, it must rise above the background in a statistically significant way. If the criterion is set such that a significant signal is taken as one which corresponds to a 95% probability, and if a set of targets

containing the minimum detectable amount are measured, 19 of 20 would be correctly identified. Samples whose concentration is more than the minimum detectable amount are reported with probability at least 95%. As an alternative a number of authors including Cahill et al (1974), Johansson and Johansson (1976), and Willis (1977) have employed a criterion for the detection limit given by

$$Y_{MDL} = 3\sqrt{Y_B} \qquad 3.21$$

where Y_B is the number of counts in the background under the peak interval having a width equal to FWHM of the peak, while Ahlberge et al (1976) and Mommsen et al (1978) used peak interval having 2 FWHM, Y_{MDL} is expressed as x-ray counts above background. Knowing the calibration function F(z) sec.III.C.1, one can calculate the amount of trace element needed to satisfy relation 3.21 through equation 3.12, that is for thin target,

$$M_{MDL} = \frac{3\sqrt{Y_B} \cdot A_B}{Q \cdot F(z)} \qquad 3.22.$$

where M_{MDL} is the minimum detectable mass of the element of interest, once it is known one can calculate the minimum detectable concentrations of various elements knowing the mass, M_S, of that part of the sample which is irradiated by the particle beam, using the equation

$$MDL\ (ppm) = \frac{3\sqrt{Y_B} \cdot A_B \cdot 10^6}{Q \cdot F(z) \cdot M_S} \qquad 3.23$$

The results of such a calculation depend on the experimental conditions. Cahill (1974), Johansson (1976), and

Falkmann (1975) have shown that the following parameters have influenced the sensitivity: the solid angle of the detector Ω , the detector resolution ΔE, collected charge Q, and target thickness t. It is easy to show that sensitivity scales with these factors as

$$(\Delta E)^{\frac{1}{2}} \quad (\Omega \cdot Q \cdot t)^{-\frac{1}{2}} \qquad 3.24$$

Suggestions for optimizing the sensitivty are offered based on these scaling properties. In practice, the improvements in sensitivity are limited by practical considerations. For example, sensitivities can be improved by accumulating more charge on the sample or equivalently counting for a longer period of time. But limits are imposed by the financial costs of longer runs and the target damage due to excessive beam heating.

Some gains in sensitivity are possible by moving the detector closer to the target, thus increasing the solid angle Ω. Moving the detector closer to the target is limited by counting rate limitations and physical limitations. More gains in sensitivities are possible by manipulating the count rate. For a typical sample, the majority of x-rays entering the detector are low-energy x-rays. The use of a low Z filter to reduce this often excessive counting rate, effectively improves sensitivity for more energetic x-rays. Optimal performance at high counting rate is obtained by employing triggered beam pulsing, Cahill (1975), Koening et al (1980).

Sensitivity for thin targets can be improved by increasing the target thickness, t, within the constraint that ($t \leqslant 1\ mg/cm^2$). The question of relative sensitivity of thick-target versus thin-target analysis has been investigated by Folkmann (1976) who calculated the minimum concentration giving a peak to background ratio of one. His results indicate that in favourable circumstances, thick targets provide better sensitivities for light elements ($17 \leqslant Z \leqslant 30$) while thin targets yield better sensitivities for heavier elements.

Experimental PIXE detection limits data obtained in the present work are represented in table 3.18 for eleven elements in hair samples. The eleven elements listed cover most of the detectable range of elements. The detection limits quoted in table 3.18 are based on:

1. an accumulated charge of 25 μc at 10 nA which is typical for a PIXE run;

2. 7 μm aluminium filter inserted between the detector and the irradiated target;

3. the value of Y_B was calculated from the original spectrum by drawing a smooth line under the characteristic x-ray peaks, assuming there is no interference between the elements and also that there are no impurities from the backing materials and therefore the results are somewhat better than would be expected for samples which present interference problems.

Table 3.18 PIXE detectability limits for 25μc charge of 2.37 MeV protons in thin hair sample having a dried mass of 180.3μg, beam area 0.24 cm^2.

Element	Minimum Detectable Limit	
	ng/cm^2	ppm
K	7.1	9.5
Ca	5.1	6.8
Ti	2.3	3.1
Cr	1.2	1.5
Mn	1.0	1.3
Fe	0.8	1.1
Ni	0.8	1.0
Cu	0.8	1.1
Zn	1.0	1.4
Br	1.9	2.6
Rb	3.0	4.0

4. using the criterion $3\sqrt{Y_B}$ taken within 2 FWHM, 2 FWHM was selected since the elemental concentration was measured using area under the full peak;

5. the quantitative calculation was carried out using the experimental values of F(z).

From results in table 3.18, a minimum detectable concentration of 1 ppm represents a detected mass of $\leqslant 10^{-9}$ g in hair mass of $\sim 180\mu g$ with a beam area of $0.24\,cm^2$. By using a focused microbeam, much smaller quantities can be detected.

Comparison of MDL produced with a $5\mu m$ Kimfol backing for different charges, employing the $3\sqrt{Y_B}$ criterian, is shown in fig.3.41 illustrating the improved detection limit for the $105\mu c$ over the $25\mu c$. But limits are imposed by the financial costs of longer runs.

Some gains in sensitivity are possible by moving the detector closer to the target, increasing the solid angle Ω, this effect has been demonstrated for Ω = 1.4 st. in the old system using $5\mu m$ aluminium x-ray absorber, and Ω = 2.73 st. using the new chamber with a $7\mu m$ Al absorber, and is represented in fig.3.42. The detection limits calculated are based on an accumulated charge of $25\mu c$ with 10 nA proton current at 2.37 MeV energy onto $5\mu m$ Kimfol, the improvement is clear.

Important features in the sensitivity curves, fig.3.41

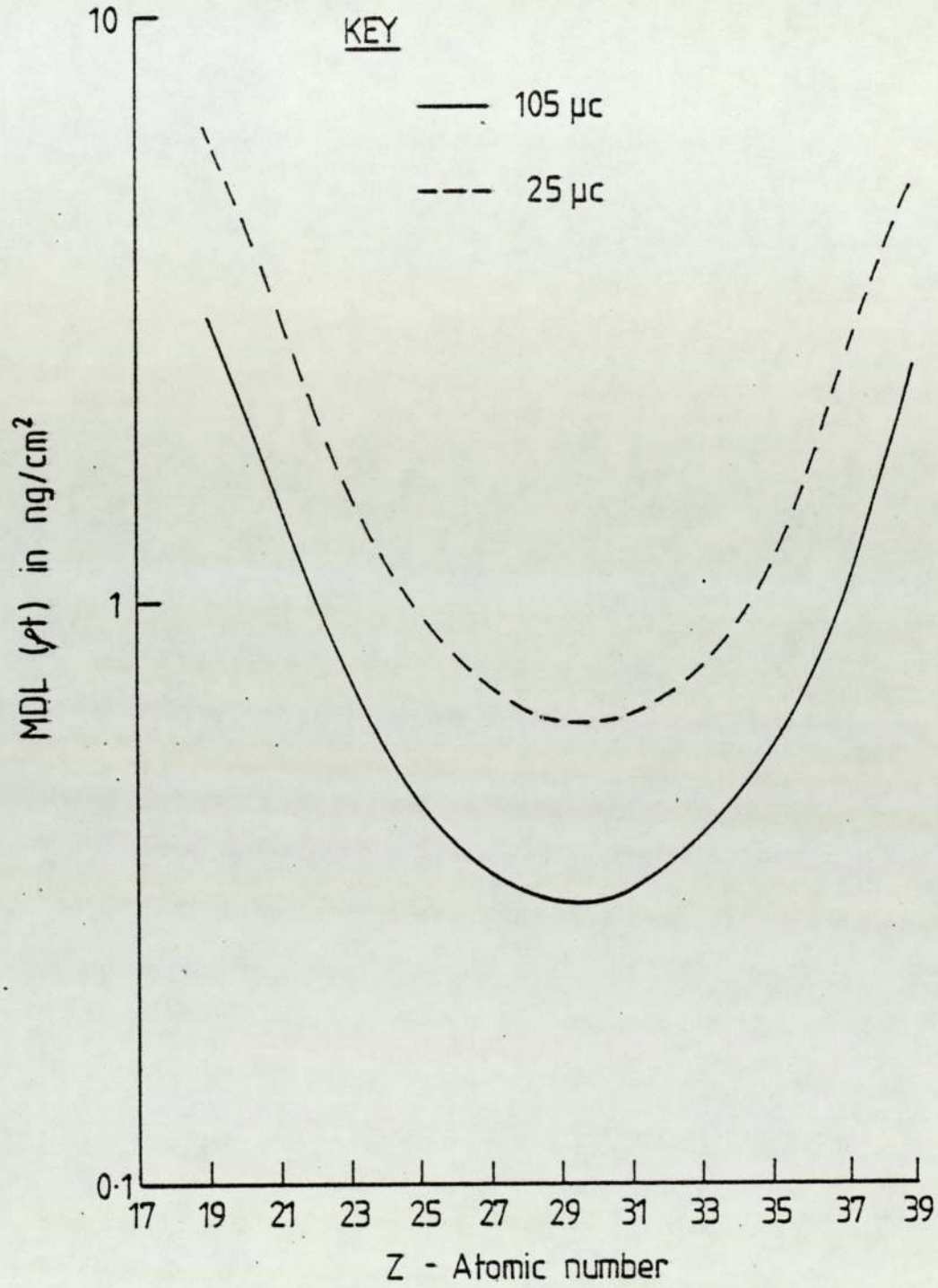

Figure 3.41 Level of detection limits for two different charge on 5 micron Kimfol backing.

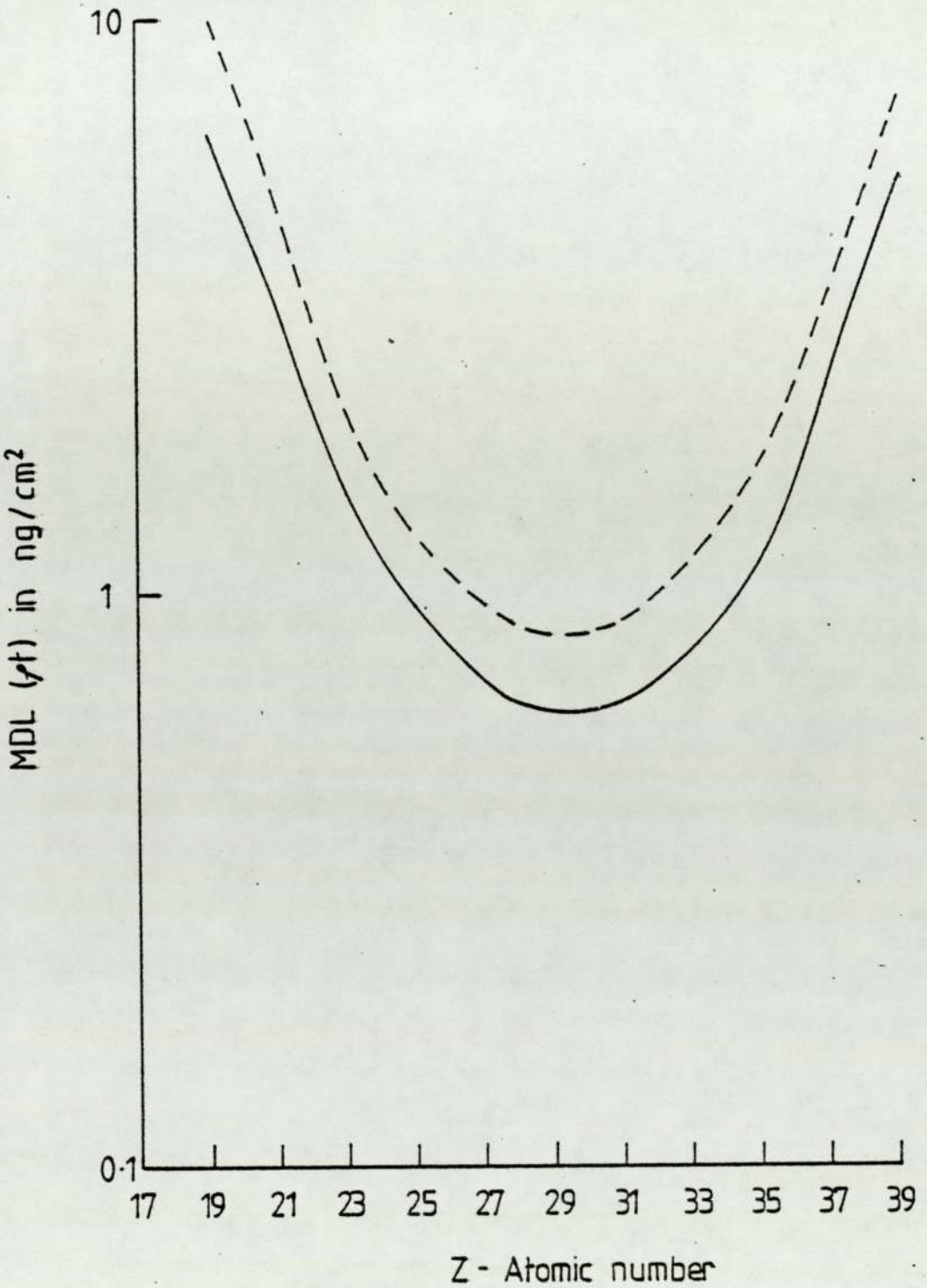

Figure 3.42 Level of detection limits for two different detector solid angles Q = 25 μC
——— Ω = 2·73, 7 μm Al
– – – – Ω = 1·4 , 5 μm Al

and fig.3.42, are immediately obvious, the curves have minima (maximum sensitivity) increasing to larger values (poorer sensitivity) at low-Z and high-Z. This depends on the fact that for high-Z the x-ray cross-sections are decreasing while the background is relatively constant. For lighter elements the sensitivity decreases mainly due to fall-off in fluorescence yield, to relatively large background intensity due to secondary electron bremsstrahlung which reaches a maximum intensity in the low-Z region, to declining detector efficiency, and lastly to the attenuation of low-energy x-ray by the aluminium absorber, Be and melinex windows, and the air passage. Furthermore, it should be noted that the position of the maximum sensitivity depends on the energy of the incident protons. Within certain limits one can therefore adjust the proton beam energy to give maximum sensitivity for a particular trace element.

Several investigators exploring the relative capabilities of various projectile energy have been reported. Barrette et al (1976) evaluated 2.25, 3, and 6.0 MeV protons and 6, 9, 12 and 16 MeV ^{4}He ion and calculated that 3 MeV protons provided the best overall sensitivity, generated lower background, and proved less damaging to the sample than equal velocity ^{4}He ions. Their criterion was that the peak height be equal to three times the square root of the mean background counts per channel. Willis (1977) compared sensitivities for 1.5-4 MeV protons, their results indicate an optimal range of 2-4 MeV for proton

excitation.

Falkmann (1975) discussed 3 different criteria for defining sensitivity based on observations of characteristic x-ray peaks from the trace elements. Analytical sensitivities for 3 MeV protons are compared in different matrices C, Al and Ca. Comparison was also done for different proton energies 1-10 MeV in a carbon matrix. He concluded that the sensitivity limit of the technique lies in the concentration range 10^{-6}-10^{-7} for most elements. Cahill et al (1974) compared equal velocity ^{1}H and ^{4}He ion beams incident on thin deposits from aerosol samples. Normalizing the experimental results to the same characteristic x-ray yields, Cahill found that sensitivities (defined by the $3\sqrt{Y_B}$, detection limit) for both ions are identical for x-rays below 8 keV, above 15 keV the detection limits are approximately 40% higher for ^{4}He ion primarily because of the more intense compton background for ^{4}He excitation.

III.F Accuracy and Precision

III.F.1 Introduction:

The accuracy of an experiment is a measure of how close the result of the experiment comes to the true value. Therefore, it is a measure of correction of the results. It is generally dependent on how well we can control for systematic errors, Bevington (1969).

The precision of an experiment is a measure of how exactly the result is determined, without reference to what that result means. It is also a measure of how reproducible the result is, it is dependent on how well we can overcome or analyse random errors, these are the fluctuations in observations which yield results that differ from experiment to experiment, and that require repeated experimentation to yield precise results, Bevington (1969).

The main function of the analysis in the present work is to identify the various elements in an unknown sample and estimate the amount of each present. This section will discuss the quality and reliability of the results of these analyses. The discussion will consider the factors affecting measurements based on equation 3.12 and ways of minimizing the uncertainties.

III.F.2 Accuracy:

Major factors determining the accuracy of PIXE are:- system calibration, peak statistics, charge integration, target angle, beam energy, beam area, and the effects of excessive heating. The accuracy of the result depends upon how well all the factors mentioned, which would affect the determination, are minimized or accounted for, and is ultimately limited by the accuracy with which the system is calibrated.

III.F.2.1 Accuracy in Calibration Using Thin Standard Foils:

Calibration factors were calculated using equation 3.13, sec.III.C.1, the uncertainties associated with each measurement are the uncertainties in:

a. net counts in the line of interest Y_Z; net counts Y_Z being the difference between the total measured counts, Y_T, at the line position and the background, Y_B, so that $Y_Z = Y_T - Y_B$ with the statistical uncertainty $\sigma(Y_Z) = \sqrt{Y_T+Y_B}$.

b. uncertainties in the total accumulated charge Q; these can arise due to instrumental error or leakage current problems. Leakage current can be avoided by suitable selection of the Keithly resistance, and during the run, the standing current was regularly checked for fluctuations, and the estimated uncertainty introduced into the accumulated charge was approximately 1%.

c. the uncertainty as given by the manufacturers in the areal density of the foils is within 5%.

Based on the results of this the uncertainties in the calibration are better than 6% for all elements measured (table 3.19). This calibration was checked regularly by irradiating one or two foils.

III.F.2.2 Accuracy in Standard Reference Materials:

Independent checks on the system calibration and target preparation have been provided by analysis of NBS Standard Reference Material, bovine liver sec.III.C.3, and the results of the HH-1 interlaboratory comparisons sec.III.C.4. The uncertainty in the analysis includes contributions arising from;

a. Target preparation: the topics considered under the target preparation are; sample digestion, the uncertainties from sample weighing and resulting digested samples were about 2%, sec.III.D.4; target volume, using an Oxford(2-10) Micropipette the uncertainty in the volume was 2.5%; sample location in the frame, a simple device fig.3.23 was used to deliver the digested sample as much as possible at the centre of the backing foil; target thickness, an electrobalance was used, sec.III.D.3, to determine the target thickness to correct for the x-ray absorption and proton energy loss.

b. Peak fitting: data analysis by peak and gaussian

TABLE 3.19

Calibration factor F(z) for thin foils and the uncertainties in each measurement

Element	$Y \pm \sigma(Y_Z)$	Q μc	$\sqrt{2}\rho_Z t$ μg/cm^2	$F(Z) \pm \sigma F(Z)$ Photons/μc.μg. cm^{-2}
Cl	1337 ± 44	0.10	23.53	568 ± 35
K	2620 ± 60	0.10	25.96	1009 ± 56
Ti	3091 ± 58	0.05	57.98	1066 ± 58
Mn	4146 ± 65	0.05	100.41	826 ± 46
Co	2010 ± 46	0.10	35.36	569 ± 33
Cu	2128 ± 47	0.10	56.57	376 ± 21
Ga	1304 ± 37	0.30	20.56	211 ± 12
Ge	1893 ± 45	0.15	76.37	165 ± 9
Rb	1161 ± 36	1.00	23.77	48.9 ± 2.9
Y	1860 ± 44	1.50	48.08	25.8 ± 1.4
Mo	955 ± 33	1.50	52.79	12.1 ± 0.7

routines introduces uncertainties through background determination, peak area calculation sec.III.B. These uncertainties were estimated to be about 2% for large peaks and about 10% for small peaks.

c. Changes in target-detector geometry which may occur after the standard thin foils calibration.

Based on the results of the bovine liver measurements table 3.8, the uncertainties are estimated to be 10% or less for elements between K and Rb with concentrations higher than 10 ppm.

III.F.2.3 Accuracy in Samples Doped with Internal Standard:

For the hair analysis sec.V.A, the concentration in ppm of the unknown elements in the sample, tables 5.10 and 5.11, was calculated using

$$\text{Conc. (ppm)} = \frac{Y_Z \; M_{St} \; F(St) \cdot C_{AL}(St) \cdot C(Z)}{Y_{St} \; M_S \; F(Z) \quad C_{AL}(Z) \quad C(St)} \qquad 3.25$$

taken from equation 3.19, where M_S is the mass of dried hair in grams, and all symbols are as defined in sec.III.C. Based on these calculations, the uncertainties which contribute to the final uncertainty in the concentration of the unknown element are:

a. Statistical uncertainties in the net counts in the line of the unknown element and in the net counts of the standard lines; the uncertainty in the concentration is

mainly due to these statistical uncertainties in the net counts. An example of the calculation of the uncertainties in the lines of elements measured and standard is given in table 3.20, for sample A, one of the hair samples in the group. The smaller the number of counts due to low concentration, the greater the fractional uncertainty especially if a large peak interferes with a very small peak as in the interference of Fe Kβ with Co Kα. The uncertainty from statistical counts in the standard is partly responsible for increasing the uncertainties in the high concentration elements in these groups of hair analysis.

b. Uncertainties in the calibration factors of the elements of interest and the standard are taken from table 3.19.

c. The uncertainty in the hair mass is 3% and in the internal standard mass is 3.8%, sec.V.A.

d. The uncertainty in the calculated correction factors, sec.III.C.3, varies between 7% and 17% depending on the element under investigation.

Using equation 3.25, the concentrations and the uncertainty in the concentrations were calculated for the hair sample A, these are represented in table 3.21.

In the second group of hair analysis sec.V.B. the statistical uncertainty in the counts from the standard was improved by increasing the mass of yttrium in the sample, so that the statistical uncertainty from the counts of

TABLE 3.20

Statistical uncertainties in the counts for the elements measured and in the ratio to the standard, hair sample A, Sec.V.A $Y_{St} = 215 \pm 17$

Element	Total counts Y_T	background counts Y_B	net counts $Y_Z \pm \sigma(Y_Z)$	$\frac{Y_Z}{Y_{St}} \pm \sigma$
S	10359	3390	6970±117	32.48±2.62
K	8054	6610	1393±121	6.49±0.76
Ca	13891	7084	6641±145	30.89±2.51
Co	353	180	14.5±26	0.067±0.122
Ni	103.6	90	11.69±13.98	0.054±0.065
Cu	528	142	385±26	1.79±0.18
Zn	1362	183	1125±40	5.25±0.45
Se	26	20	6.0±6.8	0.028±0.031
Br	37.7	28.1	4.5±8.4	0.021±0.039

TABLE 3.21

Elemental concentration in ppm and the uncertainties in them for one hair sample, sample A.

mass of dried hair = 167.5 ± 5.0 μg

mass of the Y_{39}, internal standard = 0.0739 ± 0.0028 μg

Calibration factor for Y_{39} = 25.9 ± 1.4 counts/μg.μc.cm^{-2}

Correction factor for Y_{39} = 1.10 ± 0.078

Element	$\frac{Y_Z}{Y_{St}} \pm \sigma$	$F(z) \pm \sigma$	$C(z) \pm \sigma$	concentration ppm ± σ
S	32.48±2.62	150±12	1.365±0.226	29848±6709
K	6.49±0.76	1009±56	1.157±0.108	238±45
Ca	30.89±2.51	1070±56	1.130±0.082	750±117
Co	0.067±0.122	569±33	1.085±0.079	1.5±2.7
Ni	0.054±0.065	450±23	1.086±0.079	1.5±1.8
Cu	1.79±0.18	376±21	1.086±0.079	58±10
Zn	5.23±0.45	280±15	1.087±0.079	226±36
Se	0.028±0.031	100±5	1.092±0.080	3.2±3.6
Br	0.021±0.039	76±4	1.094±0.080	3±6

the yttrium improved from about 8% to within 5%. Table 3.22 represents the counts and their statistical uncertainties for the elements measured in one of the hair samples in this group, sample PC3, the equation used in determining the concentration was

$$\text{Conc. (ppm)} = \frac{Y_Z \; M_{St} \; C(Z) \times 10^6}{Y_{St} \; M_S \; RF(Z) \; C(St)} \qquad 3.26$$

where RF(Z) is the relative calibration factor of element Z to the standard Y_{39}, sec.III.C.5. An example of the concentration and uncertainty in the concentration for the elements measured in the hair sample PC3 is represented in table 3.23. The uncertainty in the concentration is ultimately governed by the uncertainty in the net counts of the line of interest, interference increases this uncertainty as discussed previously.

By doping the sample with an internal standard the uncertainties due to charge integration, beam area, target area, and beam energy are eliminated.

One problem it is necessary to try to avoid is excessive heating of the sample during irradiation. This can be done by using a thin target so that the proton energy loss is low, and by keeping the beam current at a low level. The typical current used for all biological thin samples was 10 nA.

The major applications in this work secs.V.A and V.B , is the comparison between two groups in each section,

TABLE 3.22

Statistical uncertainties in the counts for elements measured and in the ratio to the standard, in one of hair sample PC3 sec.V.B.

net counts for the standard Y_{St} = 770 ± 29				
Element	total counts Y_T	background counts Y_B	net counts $Y_Z \pm \sigma$	$\frac{Y_Z}{Y_{St}} \pm \sigma$
S	13934	3368	10566±132	13.72±0.54
K	9320	7355	1965±129	2.55±0.19
Ca	15141	8494	6413±154	8.33±0.37
Fe	751	300	451±27	0.586±0.042
Co	216	117	27.26±18.9	0.035±0.024
Ni	134.7	109	22.0±15.6	0.029±0.02
Cu	262	114	145±19.4	0.192±0.027
Zn	998	131	846±33.6	1.099±0.06
Se	14.0	11.5	2.5±3.74	0.003±0.004
Br	57.9	23.0	30.95±9.21	0.04±0.012

TABLE 3.23

Elemental concentration in ppm and the uncertainties in the concentration for one hair sample, sample PC3,

mass of dried hair = 169.6 ± 5.0 μg

mass of Y_{39} = 0.2913 ± 0.0122 μg

correction factor for Y_{39} = 1.100 ± 0.078

Element	$\frac{Y_Z}{Y_{St}} \pm \sigma$	RF(z) ± σ	C(z) ± σ	concentration ppm ± σ
S	13.72±0.54	0.71±0.05	1.365±0.226	41181±8396
K	2.55±0.19	15.7±1.0	1.157±0.108	294±47
Ca	8.33±0.37	29.6±1.9	1.130±0.082	496±68
Fe	0.586±0.042	25.8±1.7	1.0855±0.079	39±6
Co	0.035±0.024	22.7±1.5	1.085±0.079	2.6±1.8
Ni	0.029±0.02	18.0±1.2	1.086±0.079	2.7±1.9
Cu	0.192±0.027	14.9±0.9	1.086±0.079	21.9±4.2
Zn	1.099±0.06	11.59±0.74	1.087±0.080	161±20
Se	0.003±0.004	3.90±0.25	1.092±0.080	1.3±1.8
Br	0.040±0.012	3.00±0.19	1.094±0.080	23±7

patients and control, and to test if there are any significant differences in the concentration of elements of interest between the two groups. For example in sec.V.B tests of significances were done table 5.21, for the results from agitated demented group in table 5.18 and from control population in table 5.19, using the t-test, where t is given by:

$$t = \frac{\bar{x}_1 - \bar{x}_2}{\sqrt{\frac{\Sigma (x_{i1} - \bar{x}_1)^2}{n_1(n_1-1)} + \frac{\Sigma (x_{i2} - \bar{x}_2)^2}{n_2(n_2-1)}}} \qquad 3.27$$

The suffixes 1 and 2 refer to the two groups, $\bar{x}$ is the mean concentration of the element of interest given by equation 3.26, that is,

$$\text{(mean concentration) } \bar{x} = \frac{M_{St}}{RF[Z]} \cdot \frac{C(Z)}{C(St)} \left[\left(\Sigma \frac{Y_{Zi}}{Y_{Sti}} \frac{}{M_{Si}} \right) / n \right] \qquad 3.28$$

the summation is over the number of samples in each group, substituting for $\bar{x}_1$, $\bar{x}_2$, x_{1i} , and x_{2i} , using equation 3.28, in equation 3.27 and omitting the suffix i for simplicity. Therefore, equation 3.27 gives

$$t = \frac{\left(\Sigma \frac{Y_{Z1}}{M_{St1}} \frac{}{M_{S1}} / n_1 \right) - \left(\Sigma \frac{Y_{Z2}}{Y_{St2}} \frac{}{M_{S2}} / n_2 \right)}{\sqrt{\Sigma \frac{\left(\frac{Y_{Z1}}{Y_{St1}} \frac{}{M_{S1}} - \left[\Sigma \frac{Y_{Z1}}{Y_{St1}} \frac{}{M_{S1}} / n \right] \right)^2}{n_1(n_1-1)} + \Sigma \frac{\left(\frac{Y_{Z2}}{M_{St2}} \frac{}{M_{S2}} - \left[\Sigma \frac{Y_{Z2}}{M_{St2}} \frac{}{M_{S2}} \right] \right)^2}{n_2(n_2-1)}}} \qquad 3.29$$

The only factors which contribute to the t are the counts of the line of interest, which represents the amount of that element in the sample, and the standard line, and

the mass of the hair.

Actually when we compare, concentrations of sets of elements, from patients and control and apply the t-test for each element, the absolute value and how accurate it is does not enter in the comparison, only the difference in the means.

III.F.3 Precision:

Factors affecting the precision of the measurement are; peak statistics, charge integration, target rotation angle, target detector geometry, beam intensity, beam energy, trace fitting, and volatization. A number of these factors were previously discussed as they affect the accuracy, and the precision is ultimately limited by counting statistics and charge integration. The uncertainty in the charge integration was eliminated by doping the sample with the internal standard. Because of the statistical uncertainty of the counts no matter how carefully the same sample is measured, different values for the result will be obtained each time the measurement is repeated.

The analysis of replicate digested bovine liver targets, table 3.8, provided a measure of the overall precision of the PIXE stystem including uncertainty introduced by the target preparation procedures.

CHAPTER IV

GENERAL SURVEY : TRACE ELEMENTS

IV.A Introduction:

Metals at various levels play significant roles in many biological processes and their effects are dictated by the concentration of various elements contained in the organism, and with the improving sensitivities of analytical techniques, knowledge of these roles is continually expanding. The concentration of the element in the organism is often critical since it is possible that at one concentration the metal can be essential while at higher levels this same metal can cause serious metalic imbalance in the organism, Underwood (1977). Often the range between required and excessive concentrations of a metal is not well defined.

Metals are found in air, water, and soil from both natural and manmade sources. Therefore organisms can receive body burdens via various assimulation routes. The symptoms of acute metal toxicity are generally well known, but the symptoms of long-term exposure to low-level concentrations of metals have not been established.

Many elements occur in living tissues in such small amounts that the early workers were unable to measure

their precise concentrations with the analytical methods then available. They therefore frequently described as occurring in "traces" and the term trace elements arose to describe them, Prasad (1976).

IV.B Trace and Major Elements, Essential and Toxic:

At the present time 26 of 92 naturally occurring elements are known to be essential for life. These consist of eleven major elements, known for a long time because their presence was easy to detect, namely hydrogen, carbon, nitrogen, oxygen, sodium, magnesium, phosphorus, sulphur, chlorine, potassium and calcium; and fifteen elements generally accepted as trace elements, these are fluorine, silicon, vanadium, chromium, manganese, iron, cobalt, nickel, copper, zinc, arsenic, selenium, molybdenum, tin, and iodine. In addition, boron is essential for the plants but has not yet been shown to be necessary for animals, Underwood (1977).

An element is considered by Davies (1972) to be essential if it is an element which is necessary for optimal function of the organism. Cotzias (1967) states the position more completely, and Underwood (1977) discussed the classification in detail. The essential trace elements have four major functions, namely as stabilizers, as elements of structure, essential elements for hormonal function, and as co-factors in enzymes, Feinendeger and Kasperek (1980). Examples of stabilizing function are iron

in heme or cobalt in vitamin B_{12}. Silicon in connective tissues is an example of an element of structure. Iodine is essential for the formation of thyroid hormones, and a great number of enzymes rely on trace elements as co-factors, for example Zn in carbonic analydrase.

Some trace elements that are not known to have any beneficial effect occur more or less constantly in variable concentrations in living tissues. They are believed to be acquired by the body as environmental contaminants and to reflect the contact of the organism with its environment, Underwood (1977).

Classification of the trace elements into a further group, known as toxic elements, is perhaps justified for a few elements such as lead, cadmium, and mercury, because their biological significance is so far confined to their toxic properties at relatively low concentrations. Table 4.1 lists these essential and toxic elements.

The classification of metallic elements into essential and toxic is not definite, as the essential elements may become toxic at sufficiently high levels, but there is a wide range of toxicity among the elements which is further complicated by dependence on chemical form. It is important to realize that essential elements such as Co, Cu, Mo and Se can be toxic when ingested in excess, while toxic elements such as As may be essential at low concentration.

Table 4.1: Essential and toxic elements

Major essential elements	Trace essential elements	Major toxic elements
hydrogen	fluorine	cadmium
carbon	silicon	mercury
nitrogen	vanadium	lead
oxygen	cromium	arsenic
sodium	manganese	
magnesium	iron	
phosphorus	cobalt	
sulphur	nickel	
chlorine	copper	
potassium	zinc	
calcium	arsenic	
	selenium	
	molybdenum	
	tin	
	iodine	

Health depends largely on a normal supply and concentration of essential trace elements in tissues and fluids, and lack of essential trace elements will influence the physiological state of the health. Elemental toxicity leads to different disease states including some forms of cancer and disorders of the brain, Prasad (1976).

Relating essential trace elements to disease requires a knowledge of their normal ranges of concentrations. An important review which quotes ranges of composition for many tissues is "Reference Man" Snyder (1975).

IV.C Action and Interaction of Trace Elements:

Interpretation of analytical results of elemental concentration require some understanding of the function of each element and its interaction of other elements.

Most of the elements enter the human organism mainly through the intestinal tract and by the lungs. Once absorbed the element is transported in the blood and taken up to varying extents by tissues. For many metals the liver is the initial place of concentration, redistribution to other tissues then taking place more slowly. Transport in the blood plasma may be by specific proteins such as transferrin (Fe) or caeruloplasmin (Cu).

Summary of the role of some essential elements are given in the following paragraph:

Fe: the role of Fe in blood function is well known, it is a constituent of the haemoglobin in red blood cells upon which the oxygen transport system of the body depends. Fe is absorbed from the diet and is transported to the bone marrow where the red blood cells are manufactured. Iron deficiency depends on the haemoglobin content of whole blood and it is specially common in pre-school children of the poor.

Cu: Cu metalloproteins exist in liver, red cells, and other tissues. Cu deficiency, mostly associated with poor absorption rather than inadequate intake, has been found in a few premature infants, Rechcigle (1978). Cu analysis is useful in diagnosing cirrhosis and nephrosis diseases. From animal studies the role of Cu enzymes in the central nervous system is known to be important, Prasad (1978).

Cr: The biological importance of Cr is established by the beneficial effects of Cr supplementation, as in the Cr sugar in the blood. An improvement in glucose in diabetic patients is claimed as well as lowered insulin requirement in subjects taking Cr supplements for long periods, Shapcott and Hubert (1979).

Zn: Several Zn metalloenzymes are now characterised, most stages of protein production require Zn for full efficiency, Mills (1969). Zn deficiency associated with poor absorption of the element, Prasad (1978), has been shown responsible for dwarfism syndrome in Iranian males. Zn has been shown to be benificial in accelerating the healing of wounds, Davies (1972).

I: The importance of iodine lies in the fact that it is required for the synthesis of thyroxine, a process which is carried out by the thyroid gland. Iodine deficiency can be improved by adding iodide to dietary salt.

Se: Seleno enzyme which is present in tissues, red cells, and plasma, plays a part in cell membrane stabilisation, Prasad and Oberleas (1976). Se present in food, particularly animal and fish protein, this element is generally well absorbed from the gut. Urinary Se excretion reflects dietary levels.

F: Fluoride is absorbed and distributed throughout the body. As much as 95% of the total body fluoride is probably incorporated into skeletal and dental tissues, Prasad (1978). Fluoride deficiency is associated with increased tooth decay in children, Miller (1979).

Co: The chemical form of the element, present in diet, or intravenous fluids, is important. For example, Co must be supplied as vitamin B_{12}, other forms being biologically inactive, Davies (1972).

Mn: Mn is involved in chlosterol synthesis, Davies (1972). The main features in Mn deficiency are skeletal deformities. Excess Mn in urine is an indicator of Mn toxicity, Bowen (1980).

Mo: The molybdenum content of organs depends on the amount in the diet, Davies et al (1960). The liver and kidneys contain a higher concentration of Mo than other tissues. Mo has been shown to reduce the solubility of

teeth in acid and also reduces acid output by the salivary glands, Jenkins (1963), the relation between the lack of Mo and dental caries has been confirmed, Anderson (1969). There is believed to be an additive effect between the benefits of fluoride and Mo, Mo is known to increase the absorption of F from the stomach, Crane (1960).

Si: Schwarz (1974) study has given evidence that Si is an essential element in connective tissues. In addition to a structural function, it is possible that Si may have a function in bone calcification, Carlisle (1974).

Often the effects of a particular element cannot be considered in isolation as the elements interact with each other, so that concentration which, individually would have been safe, become harmful in combination. The interaction of Cu, Mo, and S has been studied, Marcilese et al (1969). Underwood (1977) stated that one and the same copper intake of animals can result in deficiency, a normal state, or toxicity, depending on the occurrence of Mo in the diet. Excess calcium in the diet induces signs of Zn deficiency when Zn intake is normal, Davies (1972). The interaction of Se with As, Cd and Hg is another example, Parizek et al (1974), Se protects experimental animals against Cd poisoning. In the study by Welsh (1974) it is stated that Se can cause increased excretion of Hg. The most striking conclusion from the experiment by Nygaard and Hansen (1978) is that dietary Se influences the distribution of Hg in tissues exposed

to metallic mercury.

It is of value to examine the interaction between metals to which members of a population might well be exposed simultaneously, and the PIXE technique with its capability of multielement analysis with high sensitivity is ideal for this purpose. This enables studies to be made of a wide range of elements in specific pathological states. In this thesis the technique has been applied to mental disorders, hyperactivity in the young and agitation in the elderly. Levels of elements being measured in groups of these patients and in corresponding control groups.

IV.D Use of Hair and Blood in Trace Element Analyses:

To obtain a representative picture of element status, it must be decided which part of the body to take as a specimen for study. In general, a sample must be chosen which although possibly not straight forward to interpret, is readily available. Possible specimens include blood, hair, urine, teeth and nails. The last three can be discounted for gneral use, although circumstances arise where they may be useful: urine gives information only on what the body has lost, not on what it has retained, teeth are not readily available, and nails are likely to be contaminated by external contact. Two possibilities are left; blood and hair. Analysis of these two reflects body trace elements over different scales of time. Trace

element concentrations in blood are transient and related to the supply of element in the previous few hours or days. In contrast while offering no information on immediate levels, hair fixes trace elements, providing a lasting record of levels over the previous few months, Laker (1982). If for instance a factory releases some arsenic compounds into a residential area, and it was some time before residents were examined, blood levels will have declined to normal, Houtman (1978), but hair can be used successfully to determine the release.

Blood is complex in composition, consisting of several parts all of which exhibit different concentrations. Another difficulty is that trace elements are not fixed in each part, but are constantly being transferred from one to another, Valcovic (1977). Concentrations of the trace elements are very low compared with the rest of the body, especially hair. For most techniques they are near the limits for good precision.

Given the difficulties with the use of blood as a specimen, hair offers a number of advantages:

1. hair offers a good way of measuring long-term variations in trace element concentrations and thus reflects past events, Bergmann et al (1980);

2. hair is an inert and chemically homogeneous substance;

3. the concentrations of most trace elements are relatively high, Underwood (1977);

4. specimens can be collected easily, the collection needs no special training or equipment and can be done without pain;

5. samples can be kept without the need of special storage conditions, Lenihan (1979).

These advantages make hair an attractive alternative to blood for trace element testing. Hair was adopted for the major PIXE biomedical applications in the present work, but a number of considerations are discussed in detail in sec.IV.E.

IV.E. Factors to be Considered in Hair Analyses:

There are many factors concerning the data derived from hair analysis which require consideration, these factors are discussed in the following sections:

IV.E.1 Sources of Trace Elements in Hair:

According to Hopps (1977) the sources of hair trace elements are:

a. Trace elements enter hair during its continuous formation, if it were not for other factors, one would find recorded along the length of a hair the whole history of changes in the trace element composition in the blood during the period of hair growth.

b. The sebaceous gland is a source of trace elements

derived from body tissues.

c. Sweat is a source of entry and also a factor in removal. Its quantity and concentrations vary enormously, depending on the individual and environmental conditions.

d. The composition of hair may be affected by the epidermis, since it comes into contact with the hair. Even if sampling is restricted to the first one or two centimeters closest to the scalp, that portion of hair shaft will have been exposed for several weeks.

IV.E.2 Variations with Age:

Deeming and Weber (1978) have reported a decrease in hair Zn levels with samples obtained from donors over fifty years of age, but no significant differences in Fe, Mg, and Cu with age. Klevay (1970) found hair Zn decreased in the first decade of life and increased to a peak in the second decade, over 20 years of age hair Zn again declined but no relationship between hair Cu and age was found. Hamb idge et al (1972) found very low hair Zn concentrations in infants and very young children, in comparison with those of newborn, elder children, and adults. Erten et al (1978) reported increased levels of hair Zn for subjects examined up to 15 years old. Mn, Ni, Cu, Zn, Pb, Hg and Cd were examined, Eads and Lambdin (1973), they found a decrease of Pb, Cd, Zn, Cu and Hg in females aged 37-72. Reeves et al (1975) found no relation of Pb with age for the groups examined.

Significant variations of trace element concentration are probably not simply related with age.

IV.E.3 Variations with Sex:

Variations in hair trace element concentration according to sex have been demonstrated by Schoeder and Nason (1969), Klevay (1970), Petering et al (1971), and Erten et al (1978). Schoeder and Nason (1969) showed that female hair had significantly higher concentrations of Mg, Cu, Co and Ni than male hair, the levels of Zn, Cd, Cr and Pb were not significantly different. Erten et al (1978) found no significant differences with sex. Barlow (1980) found that only Ca and Zn were significantly higher in females.

In general, however, these variations do not appear to be consistent and do not add a significant problem beyond adding to the complexities of selecting the most appropriate control populations.

IV.E.4 Variations with Hair Colour, Location-Diameters:

Significant differences of trace elements concentrations in hair from females had been reported according to colour, Schroeder and Nason (1969), but similar changes were not found in male hair. While Bland (1979) reported that hair metal concentrations were independent of hair colour.

Because of its growth, hair reflects previous elemental

concentrations in body history as well as previous environmental effects. Several measurements of trace element distribution along the hair have been reported, Valcovic (1973), Eads and Lambdin (1973), and Jolley et al (1974). The investigators agree that the variations are characteristic of the subject and that Zn variations, for example, along hair are negligible. Valcovic et al (1975) showed that the elements whose concentrations increase along the hair can be identified as pollutions in the area. Houtman et al (1978) had studied the cross-section of a single hair in the case of suspected arsenic exposure. Variation with location from which scalp hair was sampled, or with the hair diameter do not appear to be of practical importance unless information relating element concentration to hair structure is needed. Most workers overcome this kind of variation by taking hair always from the same part of the head.

IV.E.5 Effects of Hair Treatments:

A variety of hair treatments have been found to alter hair trace element concentrations, Hambidge et al (1972) and McKenzie (1974). Analytical data derived from samples that have been exposed to dyeing, bleaching or other treatments must be considered unreliable. Although shampoos may not remove endogenous trace elements from hair, any trace elements in the product could cause sample contamination with these exogenous sources of trace elements.

IV.E.6 Washing of Hair Samples After Collection:

The composition of hair can be affected substantially by its treatment before analysis. Some authors have not used any treatment at all, as in the present work. In some cases, use has been made of fairly strong detergents, Hammer et al (1971), Deeming and Weber (1977) used one percent nitric acid, but most researchers have used mild washing. Bacsó et al (1982) found calcium varied with different washing processes. Experiments by McKenzie (1974) and Sheared et al (1980) provided a comparison between washing agents, but no conclusion can be drawn as to which provides the best wash. The acceptance of a common washing procedure or no washing would favour compatibility between results obtained by various methods.

IV.E.7 Lack of Clear Definition of Normal Range:

The final problem is the absence of a clear definition of normal range of concentrations in hair. Ascribing a particular group of persons to a normal group may not be regarded as a final judgement, for this can change in light of other facts, and also as a result of comparison of data obtained by different researchers. It is therefore important to define fully the characteristics of any study population

In the present work, in the hair analysis Chapter V, the subjects were selected for the biomedical anaysis with

these factors being considered, tables 5.1 and 5.4. The subjects were drawn from the same place and no hair treatment other than using a specified shampoo was permitted. Sex and age were selected so that the two groups under comparison would match with each other as closely as possible. Since they were drawn from the same place and most of the factors affecting the results were considered, significance in the results will be related to the medical condition.

CHAPTER V

APPLICATION, MAJOR STUDIES

PIXE has been found to be a very useful tool for the analysis of biological and medical specimens. In particular, the ability to detect many elements simultaneously, in small amounts of sample, with good sensitivity makes PIXE valuable.

This chapter describes detailed studies in the use of hair elements analysis by PIXE, in medical applications. Tests of significance are applied to compare hair element contents in a population of hyperactive mentally handicapped children with those of non-hyperactive group used as controls. Similarly the levels of elements in hair from a group of agitated demented elderly were compared with non-agitated demented patients. An attempt is made to investigate the possible correlation between hair elements contents in each population.

V.A Hyperactive Children

V.A.1 Introduction:

The hyperactive child (under various names) was described more than 100 years ago in the medical literature. There are no common diagnostic criteria, so that the term can refer to a number of very different types of behaviour and such children may accordingly exhibit one or more

difficulties, Levine et al (1980). Caroline (1982) has defined the hyperactive child as one whose abnormal behaviour is accentuated as he develops. He is prone to cot-rocking and head banging, and his conduct is consistent and troublesome. He is easily excitable and often in tears, and seems unable to sit still for more than a minute or two. Hyperactive children have learning difficulties, they seem to require little food and less sleep. Boys are affected more than girls.

In the present work 20 hair samples of hyperactive mentally handicapped children and 20 non-hyperactive mentally handicapped as a control population are kindly selected by the Greaves Hall Hospital, Southport. The subjects were drawn from the same institution, the hair samples were selected so that the two groups under comparison would match with each other as closely as possible.

V.A.2 Collection of Hair Samples:

In the determination of hair metal levels it is necessary to consider a number of factors which can influence the concentration of the elements in the samples. Detailed discussion has already been given in sec.IV.E. Effects on trace elements are likely to occur if hair treatments are used on scalp hair. Other factors which must be considered are sex, age, hair colour, hair length, and the medication being taken.

It was in consideration of these factors that the questionnaires shown in table 5.1 were completed, in this way a history for each hair sample was obtained and these are represented in table 5.2 for the hyperactive children and in 5.3 for the control group. Tables 5.2 and 5.3 represent the variable factors only, while other factors are constant in these groups.

The hyperactive children comprise eight females and twelve males. The average age for the group was 14.3 $\pm$ 2.9 years. The control population consisted of children of an average age 11.7 $\pm$ 2.8 years, eight males and twelve females, they are handicapped but not hyperactive.

The position on the head from which the sample was taken might also affect the results, so that all samples should be obtained from corresponding positions on the scalp of the donors. The instructions shown in table 5.4 for the sampling procedure were followed by the person who collected the hair samples from the donors.

When the hair samples arrived at the laboratory they were removed from their paper envelopes, cut into short segments 1-2 cm in length and stored in labelled, plastic, screw capped jars.

Table 5.1

Questionnaire followed by the nurse,
in collecting hair history information

1) Age

2) Male/Female

3) Hair Colour

4) Which shampoo is used?

5) Is any special diet consumed?

6) Are any medicines being taken?

7) When was hair last washed?

8) Diagnosed condition.

Table 5.2

Hair History Information Obtained for the Hyperactive Group for Each Hair Sample Examined						
Sample	Age	Sex	Colour	Type of Shampoo	Medication being taken	Diagnosed condition
A	9	female	fair	Mountain Herv	Melleril-Haldol	deletion of short arm, Edwards syndrome, severely mentally handicapped (SMH) hyperactive
B	19	female	light brown	Nelon natural	Melleril	SMH, Cri du Chat, Hyperactive
C	13	male	blonde	Nelon natural	Nil	SMH, hyperactive
D	18	female	reddish	Nelon natural	Anafranil, Haldol, Disipal	SMH, brain damage
E	15	male	light brown	Nelon natural	Tegretol, Nydrane, Sparine	SMH, epileptic, hyperactive
F	11	male	brown	Nelon natural	Epanutin, Pheno-barb	SMH, hyperactive
G	15	female	brown	Nelon natural	Sparine	SMH, hyperactive
H	14	male	fair	Nelon natural	Diazepam	SMH, hyperactive
I	15	female	fair	Genisol liquid	Tegretol	SMH, epileptic, hyperactive
J	16	male	blonde	Polytar Liquid	Folic acid, Ascorbic acid	SMH, hyperactive

cont.....

Table 5.2 cont.

Sample	Age	Sex	Colour	Type of shampoo	Medication being taken	Diagnosed condition
K	9	male	blonde	Anti-dandruff	Melleril, Folic acid, Ascorbic acid chlorhydrate	blind
L	16	male	brown	Boots Medicated	Mysoline, Tegretol Rivotril	SMH, hyperactive, epileptic
M	16	male	blonde	Boots Family	Milleril	SMH, hyperactive Phentyle Ketonuria
N	16	male	fair	Boots Family	Tegretol	SMH, hyperactive
O	10	male	brown	Boots Family	Phenobarb, Folic acid, Tegretol, Melleril	SMH, hyperactive
P	16	male	brown	Boots Family	Nil	SMH, hyperactive
Q	16	male	brown	Boots Family	Haloperidol, Kenedrine, Dulphalace	Severely subnormal, hyperactive
R	11	female	brown	Boots	Nil	Autism, hyperactive, seldom aggressive, SMH
S	16	female	black	Boots	Epilim, Melleril Fluoride	SMH, hyperactive,epileptic, aggressive tendencies
T	15	female	auburn	Boots	Melleril, Disipal, Orphenadrine	disruptive and aggressive behaviour, SMH, hyperactive

Table 5.3

Hair History Information Obtained for the Non Hyperactive Group for Each Hair Sample Examined

Sample	Age	Sex	Colour	Type of Shampoo	Medication being taken	Diagnosed condition
CA	14	female	black	Boots Family	Fesovit daily	mental handicapneonated Kernictures
CB	8	male	brown	Sunsilk	Atiran, Fenograd, Folic acid	Mental handicap
CC	12	male	brown	Sunsilk	Melleril	Mental handicap
CD	10	female	brown	Sunsilk	Sodium Cromoglyate nasal	Down's Syndrome
CE	9	male	brown	Sunsilk	Anquil, Sparine	Mental handicap
CF	10	male	brown	Sunsilk	Nil	Mental handicap
CG	13	male	mousy	Sunsilk	Nil	Mental handicap
CH	13	female	brown	Boots Family	Dorbanex, Diamox	Mental handicap, Cornell de Long syndrome
CI	14	female	blonde	Boots Family	Melleril, Dupholac	Mental handicap
CJ	17	female	brunette	Sunsilk	Empilim, Tegretol	Subnormal-mild cerebral palsy epileptic
CK	12	male	mousy	Sunsilk	Clopixol, Procyclidine	Mental handicap, partially blind
CL	12	male	brown	Sunsilk	Sinmet, Dulphalac, Melleril	Mental handicap

cont....

Table 5.3 cont.

Sample	Age	Sex	Colour	Type of shampoo	Medication being taken	Diagnosed condition
CM	11	female	brown	Strawberry	Empilim	Severely mentally handicapped, Hemiplegic, Epileptic
CN	18	female	fair	Strawberry	Kemadrin, Tegretol Haloperidol	SMH, epileptic
CO	14	female	brown	Strawberry	Nil	SMH
CP	4	male	fair	Strawberry	Phenobarbitone, Clonazepam Baclofen Dal vit drops	Epileptic, Anoxia at birth
CQ	12	female	black	Strawberry	Tegretol	Hydrocephalic
CR	11	female	red	Strawberry	Tegretol	Microcephally, Epilepsy
CS	12	female	blonde	Strawberry	Tegretol	Severely mentally handicapped Epileptic
CT	11	female	brown	Strawberry	Empilim Nyadrine	Microcephally, Epilepsy

Table 5.4

Instructions for obtaining a hair

1) The hair should be obtained from the back of the head

2) Make a crosswise parting along a line running from the top of one ear to the other

3) Fold the hair up from this parting

4) Below this part gather the hair together and cut it as close to the scalp as possible

5) If the hair is very long cut off the end furthest from the head and discard it, using the remaining 2" or 3" as the sample

6) Place the hair sample in the clean envelope provided and repeat until about 0.5 g have been collected

V.A.3 PIXE Analysis:

The general procedure described in sec.III.D.3, in digesting hair samples and preparing the targets, was followed , only the details are given in this section. For all hair samples 3.5 ml of nitric acid was used in each digestion. The unwashed hair masses used and the resulting digested volumes are given in tables 5.5 and 5.6 for the hyperactive children and their control group respectively. One ml of each digested sample was put in a clean polythene bottle and doped with 15 μL of the internal standard solution containing yttrium of concentration 1 mg/mL. After the sample and the standard were well mixed, 5 μL was used from each hair doped solution to prepare the target, the mass of the dried hair for the 5 μL target was calculated for each hair sample in the two groups and is represented in column four in tables 5.5 and 5.6.

An example of calculating the mass of hair in 5 μl target is given below for sample A:

mass of dried hair used in the digestion = 108.8 ± 0.2 mg

resulting volume of the digested solution = 3.20 ± 0.02 mL

mass of hair in one mL of digested solution

$$= \frac{108.8}{3.2} = 34.00 \pm 0.41 \text{ mg}$$

This one ml having an amount of hair of mass 34.0 mg was doped with 15 μL internal standard solution of concentration 1 mg/mL, and 5 μL of this doped solution

Table 5.5

Masses of hair samples used in the digestion with the resulting volumes and mass of hair in each 5 μL target, Hyperactive group

Sample	hair mass in mg ± 0.2	digested volume in ml ± 0.02	mass of hair in 5 μL target μg ± 3%
A	108.8	3.20	167.5
B	113.9	2.95	190.2
C	110.6	3.16	172.4
D	113.4	3.12	179.0
E	112.6	3.19	173.9
F	108.9	3.06	175.3
G	113.4	3.11	179.6
H	107.8	3.22	164.9
I	110.4	3.13	173.8
J	117.9	3.27	177.6
K	114.5	3.15	179.1
L	117.8	3.19	181.9
M	108.3	3.30	161.7
N	111.7	3.25	169.3
O	113.4	3.24	172.4
P	110.5	3.25	167.5
Q	110.9	3.25	168.1
R	111.1	3.20	171.0
S	109.9	3.25	166.6
T	113.0	3.22	172.9

Table 5.6

Masses of hair samples used in the digestion with the resulting volumes and mass of hair in 5μL target, non-hyperactive control group

Sample	hair mass in mg ±0.2	digested volume in mL ± 0.02	mass of hair in 5μL target μg ± 3%
CA	108.3	3.10	172.1
CB	114.0	3.18	176.6
CC	113.4	3.24	172.4
CD	111.5	3.22	170.6
CE	114.2	3.20	175.8
CF	114.5	3.08	183.1
CG	111.9	3.26	169.1
CH	111.4	3.19	172.0
CI	110.6	3.26	167.1
CJ	110.8	3.20	170.6
CK	110.5	3.21	169.6
CL	111.8	3.22	171.0
CM	113.2	3.19	174.8
CN	107.1	3.20	164.9
CO	111.6	3.20	171.8
CP	109.0	3.21	167.3
CQ	113.7	3.26	171.8
CR	114.0	3.16	177.7
CS	110.1	3.26	166.4
CT	112.1	3.25	169.9

was used to prepare the target, therefore:

mass of hair in 5μL target = $\frac{5 \times 34}{1.015}$ = 167.5 ± 4.9 μg

Using the initial chamber each target was irradiated for 25 μc with a beam current of 10 nA and at a proton energy of 2.37 MeV. An aluminium, x-ray absorber, of 7 μm thickness was inserted between the detector and the irradiated target. Representative spectra of the hyperactive and non-hyperactive groups are shown in figures 5.1 and 5.2 respectively.

V.A.4 Results:

The elemental concentrations were obtained from the 40 samples, twenty hyperactive and twenty control. The calculation was carried out using equation 3.25, sec. III.F, to convert x-ray counts, given in tables 5.7 and 5.8, into ppm for each element measured. The values for the factors used in the calculation are given in table 5.9 all symbols and subscripts are as defined in sec.III.C. The calibration factors, F(z), used in the calculation are the experimental values taken from fig.3.20. Calculation of the peak area and the interference were treated as described in sec.III.B, using figures 3.8 and 3.13 to select the peak size and the peak area. A summary of the elements measured is given below:

1. Sulphur: The Kα line of S is at 2.307 keV. The resolution of the detector in this energy region is

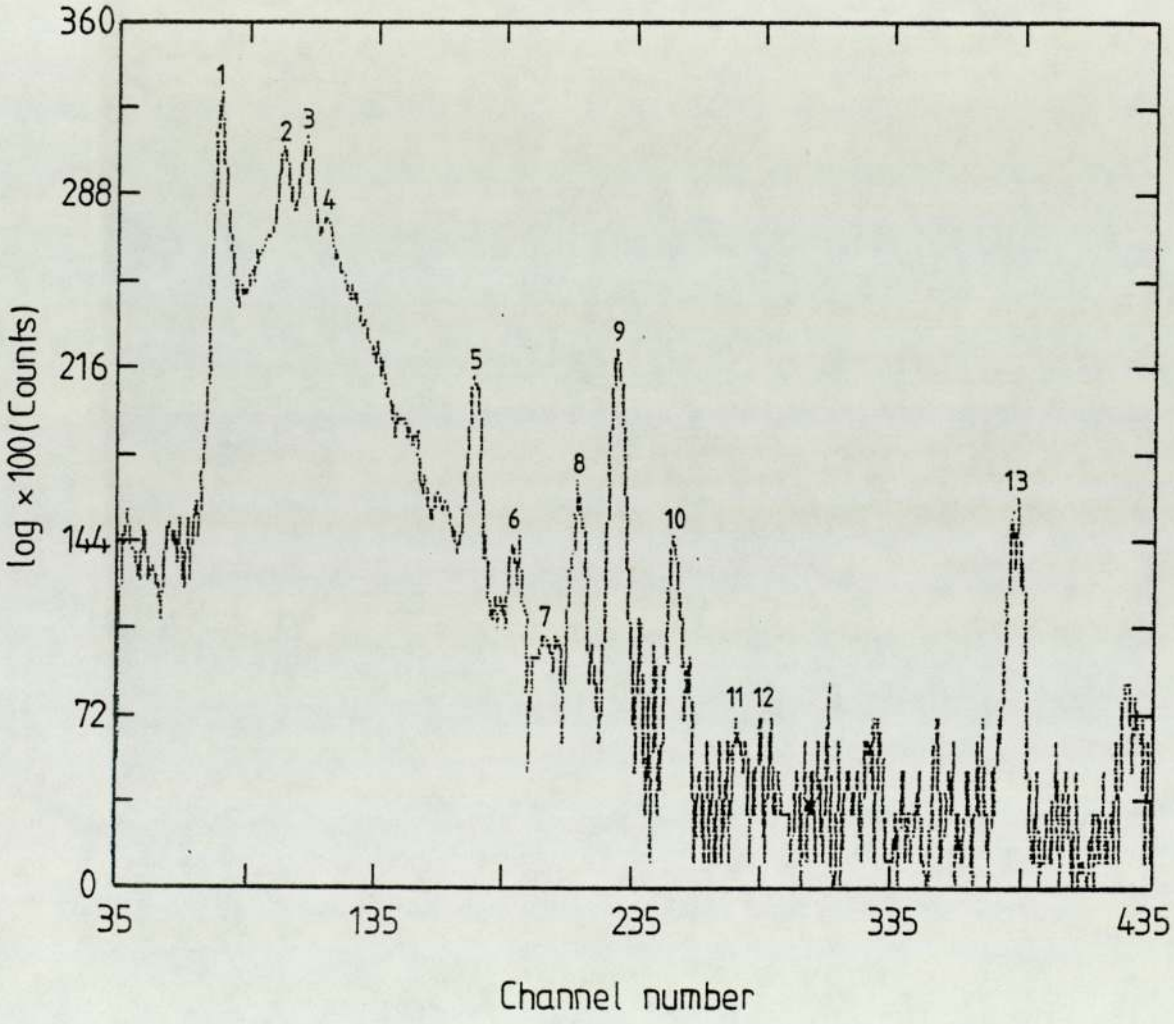

Fig 5.1 Representative PIXE spectrum for one of the hair sample from the hyperactive group.

1 - S (K α + K β)
2 - K (K α)
3 - Ca (K α)
4 - Ca (K β)
5 - Fe (K α)
6 - Fe (K β)
7 - Ni (K α)
8 - Cu (K α)
9 - Zn (K α)
10 - Zn (K β)
11 - Pb (L α)
12 - Se (K α)
13 - Y (K α)

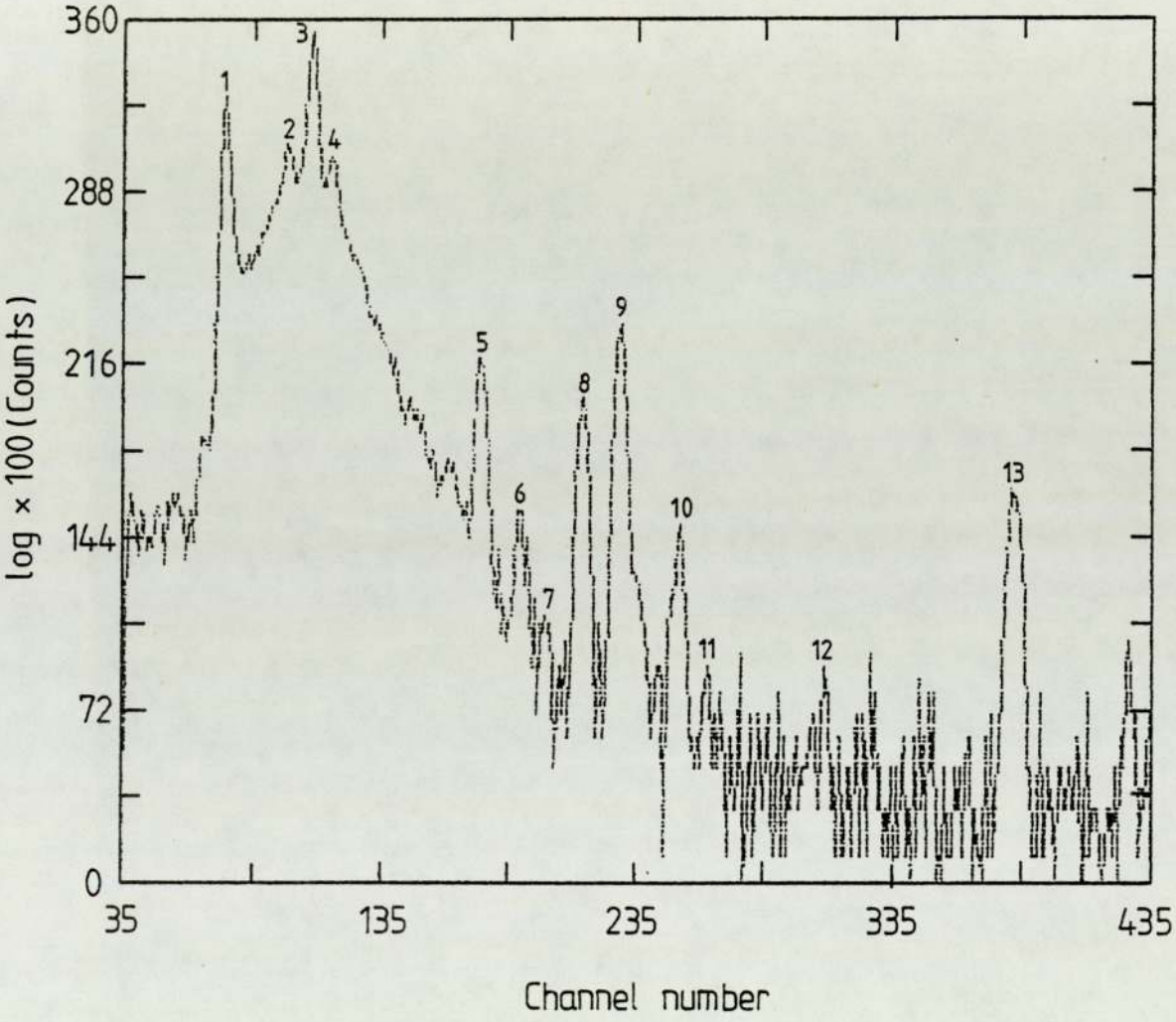

Fig 5.2 Representative PIXE spectrum for one of the hair sample from the non-hyperactive control group.

1 - S (K α + K β)
2 - K (K α)
3 - Ca (K α)
4 - Ca (K β)
5 - Fe (K α)
6 - Fe (K β)
7 - Ni (K α)
8 - Cu (K α)
9 - Zn (K α)
10 - Zn (K β)
11 - Hg (L α)
12 - Br (K α)
13 - Y (K α)

Table 5.7

X-ray counts for the elements measured used in calculating the elemental concentration, hyperactive group (20 targets)

X-ray counts for elements measured												
Sample	S	K	Ca	Co	Ni	Cu	Zn	Se	Br	Y	Hg	Pb
A	6970	1400	6641	15	12	384	1125	6	6	215	7	18
B	11592	761	3411	-	21	241	901	13	7	109	14	11
C	3528	352	2069	-	17	218	808	10	12	213	6	11
D	4774	1673	2692	36	80	557	615	14	6	158	12	23
E	3945	1341	2048	57	46	85	626	23	13	150	3	12
F	5714	1700	4386	22	39	392	500	4	-	210	7	10
G	7949	1412	6077	37	4	761	729	19	5	245	15	28
H	5626	3227	3932	-	24	530	668	16	2	199	12	15
I	7781	1456	4969	9	8	790	1115	12	11	216	13	23
J	1658	439	1816	28	12	101	356	10	6	103	17	16
K	8335	624	3025	50	18	203	1303	19	15	238	15	21
L	4173	999	2449	16	39	112	849	23	8	170	18	16
M	6633	2284	2245	10	36	168	784	14	20	197	9	16
N	4163	450	6447	27	38	263	846	16	5	267	16	26
O	5998	2048	2688	36	18	277	698	7	12	249	32	17
P	4468	364	3509	44	22	118	902	12	13	241	41	19
Q	5814	787	4056	22	36	106	753	12	16	202	7	20
R	7330	3743	6700	30	9	116	1176	14	32	264	-	16
S	3030	264	5459	41	24	114	528	18	19	107	44	22
T	3601	263	5791	23	40	80	700	7	12	162	6	15

Table 5.8

X-ray counts for the elements measured used in calculating the elemental concentration, non hyperactive control group (20 targets)

X-ray counts for elements measured												
Sample	S	K	Ca	Co	Ni	Cu	Zn	Se	Br	Y	Hg	Pb
CA	3471	213	3308	13	11	85	389	55	30	139	10	14
CB	1490	323	1355	54	43	133	257	17	21	111	10	11
CC	4845	492	2564	30	26	152	835	6	13	199	13	6
CD	1335	316	2016	28	29	56	355	7	-	59	20	9
CE	3501	289	2793	-	11	134	653	13	7	180	21	12
CF	2321	321	1977	11	34	129	692	8	3	104	14	11
CG	5835	502	4289	24	26	162	986	12	20	290	17	8
CH	4476	243	4774	36	36	120	824	82	14	174	60	6
CI	8624	420	17293	20	38	169	854	274	-	269	28	23
CJ	7715	287	7718	25	19	165	945	7	1	239	13	11
CK	5072	569	6992	36	22	154	969	14	14	229	-	12
CL	4842	735	4318	17	33	235	1094	6	7	244	11	7
CM	773	302	657	23	13	64	190	17	1	44	30	-
CN	6244	1509	9357	49	32	481	894	9	11	257	17	7
CO	8120	1691	4063	40	27	356	1063	-	9	226	13	8
CP	3621	982	8531	20	38	1903	597	13	2	169	17	13
CQ	2443	405	6762	-	10	761	431	7	5	106	19	23
CR	3814	678	5782	24	21	802	953	12	33	197	4	6
CS	5447	552	6030	6	35	309	676	17	23	196	11	8
CT	4332	617	6218	8	38	1006	837	10	22	174	8	20

Table 5.9

Factors used in the calculation of the ppm mass of internal standard M_{St} = 0.074μg

Element	F(z) counts/μc.μg.cm^{-2}	C(z)	C_{AL}	G(z)
S	150	1.365	0.100	155.95×10^{-3}
K	1009	1.157	0.325	6.05×10^{-3}
Ca	1070	1.130	0.445	4.07×10^{-3}
Co	569	1.085	0.871	3.75×10^{-3}
Ni	450	1.086	0.894	4.63×10^{-3}
Cu	376	1.086	0.910	5.44×10^{-3}
Zn	280	1.087	0.923	7.21×10^{-3}
Se	100	1.092	0.965	19.39×10^{-3}
Br	76	1.094	0.970	25.43×10^{-3}
Hg	130		0.950	15.26×10^{-3}
Pb	106		0.957	18.58×10^{-3}
In.S.Y	25.9	1.100	0.985	

where $$G(z) = \frac{M_{St} \times F(st) \times C(z) \cdot C_{AL}(st)}{F(z) \cdot C(st) \cdot C_{AL}(z)}$$

the symbols and subscripts are as defined in Chapter III. sec.III.C.

115 eV, the 2.464 keV Kβ of S cannot be completely separated from Kα. The counts under Kα + Kβ peak were used to calculate the concentration, no interference was subtracted.

2. Potassium: Counts under the Kα line were measured and Kβ was calculated using the ratio Kβ/Kα, using Khan et al (1980) values fig.2.6, because K Kβ interfere with Ca Kα. No interference was subtracted from K Kα.

3. Calcium: The Ca Kα line overlaps with the K Kβ, the total counts under the Ca Kα + K Kβ was measured and the K Kβ contribution was subtracted to give Ca Kα counts only.

4. Cobalt: Co Kα overlaps with the strong Fe Kβ, this means that Co Kα measurements have high statistical uncertainty, and Co Kβ interfere with Ni Kα. The element Fe in this group was not measured because in this group the target elemental analysis was carried out without subtracting the background from the kimfol and the chamber, which always have a small peak of Fe, Fig.3.16 and Fig.3.17, but the area under Fe Kα was measured and Fe Kβ was calculated. The total peak under Fe Kβ + Co Kα was measured and counts from Fe Kβ were subtracted to give the counts for Co Kα.

5. Nickel and Copper: Interferences of Co Kβ in Ni Kα and Ni Kβ in Cu Kα were very small, nevertheless the corrections were made.

6. Zinc: Zn Kα was calculated after correcting the total counts for Zn Kα + Cu Kβ for the Cu Kβ interference.

7. Selenium: No interference was subtracted in this analysis.

8. Bromine: Lβ of Hg was subtracted and Br Kα was calculated.

9. Mercury: Hg Lα was measured and no interference was subtracted.

10. Lead: Lα of Pb was measured, no interference was subtracted.

The elemental concentration in ppm for eleven elements, obtained from the calculations are represented in tables 5.10 and 5.11 for the hyperactive and the control groups respectively. The mean values and the standard deviations are given in the last row of the tables. Graphical representation of the elemental mean concentration is shown in fig.5.3 for comparison between the two groups.

V.A.5 Statistical Interpretation of Data:

V.A.5.1 Tests of Significance:

When sets of data from the two different groups have been collected and are interpreted, the following question arises: do the groups differ between one another by

Table 5.10

Element levels in ppm for the hyperactive children group

Concentration in ppm											
Sample	S	K	Ca	Co	Ni	Cu	Zn	Se	Br	Hg	Pb
A	30182	235	750	2	2	58	225	3	4	3	9
B	45476	116	349	-	2	33	163	6	5	6	5
C	14983	128	229	-	2	32	159	5	8	3	6
D	26324	358	387	5	13	107	157	10	5	6	12
E	23585	311	319	8	8	18	175	17	13	2	9
F	24206	279	485	2	5	58	98	2	-	3	5
G	28126	194	562	3	-	93	119	8	3	5	12
H	26737	595	487	-	3	88	146	10	1	6	9
I	32332	235	538	1	1	114	214	6	9	5	11
J	14135	145	404	6	3	30	140	10	7	14	16
K	30494	89	289	4	2	26	220	8	16	5	9
L	21045	195	322	2	6	20	198	14	3	9	9
M	32439	434	287	1	5	29	177	9	7	4	9
N	14346	60	580	2	4	32	135	7	8	6	11
O	21816	288	255	3	2	35	117	3	12	11	7
P	17261	55	354	4	3	16	161	6	18	15	9
Q	26702	140	486	3	5	17	157	7	12	3	11
R	25340	501	604	3	1	14	188	6	18	-	7
S	26634	90	1245	9	6	35	213	19	27	38	23
T	20050	57	841	3	7	16	180	5	11	3	10
mean±	25111±	225±	489±	3±	4±	44±	167±	8±	9±	7±	10±
σ	7434	153	241	2	3	32	36	4	7	8	4

Table 5.11

Element levels in ppm for the non-hyperactive control group

Concentration in ppm											
Sample	S	K	Ca	Co	Ni	Cu	Zn	Se	Br	Hg	Pb
CA	22628	54	562	2	2	19	117	45	32	7	11
CB	11833	99	281	10	10	37	94	17	27	7	10
CC	22023	87	422	3	4	20	175	3	9	6	3
CD	20861	191	822	11	14	31	256	13	-	31	17
CE	17254	55	359	-	2	23	149	8	6	10	7
CF	19063	102	423	2	8	37	263	9	4	11	11
CG	18556	62	356	2	3	18	145	5	10	5	3
CH	23323	49	649	5	6	22	198	53	12	30	4
CI	29920	56	1565	2	4	20	137	118	-	9	10
CJ	29508	43	770	2	2	22	167	3	1	5	5
CK	20366	89	732	3	3	22	180	7	9	-	6
CL	18098	107	421	2	4	31	189	3	4	4	3
CM	15673	252	347	11	8	45	178	42	3	60	-
CN	22977	215	895	4	4	62	152	4	7	6	7
CO	32614	263	426	4	3	50	197	-	6	5	4
CP	19972	210	1227	3	6	366	152	9	1	9	9
CQ	20921	134	1510	-	3	227	171	7	7	16	23
CR	16991	117	672	3	3	125	196	7	24	2	3
CS	26045	102	752	1	5	52	149	10	18	5	5
CT	22852	126	855	1	6	185	204	7	19	4	13
mean ±	21898±	121±	702±	4±	5±	71±	173±	18±	10±	12±	8±
1 σ	4576	69	372	3	3	54	41	28	9	14	6

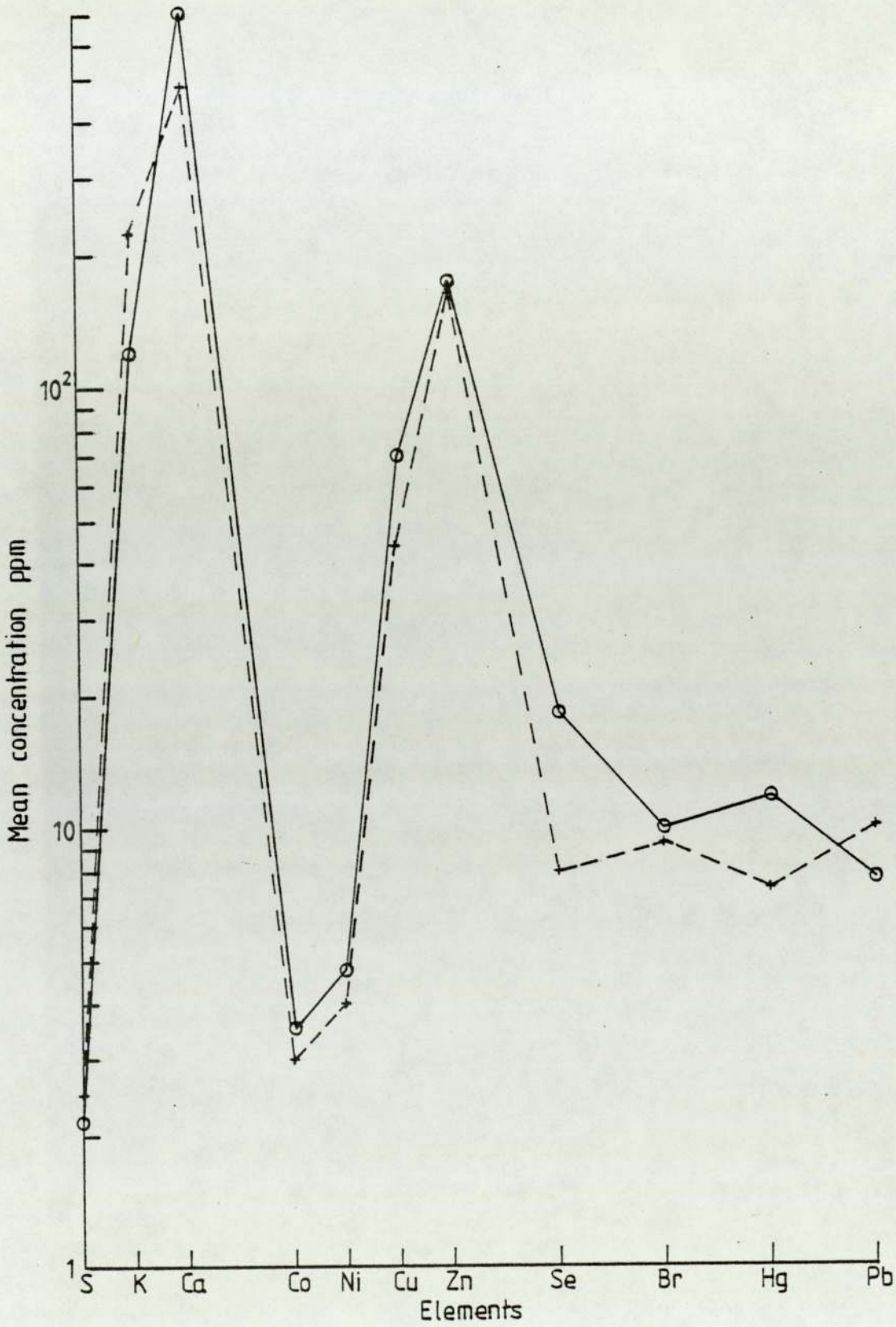

Fig 5.3 Mean concentrations in ppm for elements measured in hyperactive and non-hyperactive control
(+ hyperactive, o control)

more than could reasonably be expected from the experimental error and to biological variation or is there a real difference between the groups. Statistical analysis is required to give a reliable indication, and a test of significance of the means was applied which tests whether two means differ significantly, when both have to be estimated from the data, and there are a limited number, ϕ, degrees of freedom. The ratio of the difference between the two sample means, to the standard error of this difference, gives the test statistic t, equation 3.27.

Referring to the tabulated t values Davies and Goldsmith (1972), for ϕ = 38 values of t lying outside the interval (-2.02, +2.02) are significant at the 0.05 level, 2.02 being the tabulated value of t corresponding to P = 0.025, P is one sided, if the difference is significant we conclude that the true means, are probably different. The appropriate level of significance will depend on the particular problem under consideration. The critical values of t at P = 0.05, P = 0.01 and P = 0.005 are 1.68, 2.42 and 2.7 respectively.

T-tests of significance between the hyperactive group and the non-hyperactive control group for each element mean concentrations were made. All the elements measured were included in the analysis.

Table 5.12 shows the mean concentration and the test of

Table 5.12

Comparison between hyperactive and non hyperactive control groups for elemental levels

Element	mean levels ppm hyperactive group	mean levels ppm non hyperactive group	"t" value	significance 95%
S	25111 ± 7434	21898 ± 4576	1.65	not sig.
K	225 ± 153	121 ± 69	2.77	significant
Ca	489 ± 241	702 ± 372	2.15	significant
Co	3 ± 2	4 ± 3	0.53	not sig.
Ni	4 ± 3	5 ± 3	0.83	not sig.
Cu	44 ± 32	71 ± 54	1.27	not sig.
Zn	167 ± 36	173 ± 41	0.58	not sig.
Se	8 ± 4	18 ± 28	1.65	not sig.
Br	9 ± 7	10 ± 9	0.23	not sig.
Hg	7 ± 8	12 ± 14	1.19	not sig.
Pb	10 ± 4	8 ± 6	0.97	not sig.

significance results for the two groups, it is seen that the only significant differences at the P = 0.05 are for K, Ca and Se, for which the hyperactive children show a higher level in K, and lower levels in Ca and Se. K and Ca levels are also significant at the P = 0.025 but no metal levels were significant at the P = 0.005.

In comparing the individuals in these two groups, there appeared to be no greatly increased or decreased levels of the toxic elements in the hyperactive children examined, but there were a few samples, all in the control group, that did show high levels of Se and Hg. The highest value recorded was 118 ppm for Se, Fig.5.4, and the highest Hg was 59.5 ppm, these were not in the same sample though one sample, fig.5.5, did have high levels of Se with 53 ppm and, Hg with 30 ppm. It was noticed that these individuals are all female, t-tests between males and females in the control group for Se and Hg showed significance in Se at the P = 0.025, but not for Hg.

V.A.5.2 Inter-Element Correlations in Hair:

Concentrations of eleven elements in each group have been measured, tables 5.10 and 5.11. One has to ask, whether, there exist any interrelationships between these elements in each group. What we are asking here is whether or not the variations in the observed values of one element, y, are correlated with the variations in the measured values of another element, x. For example, our

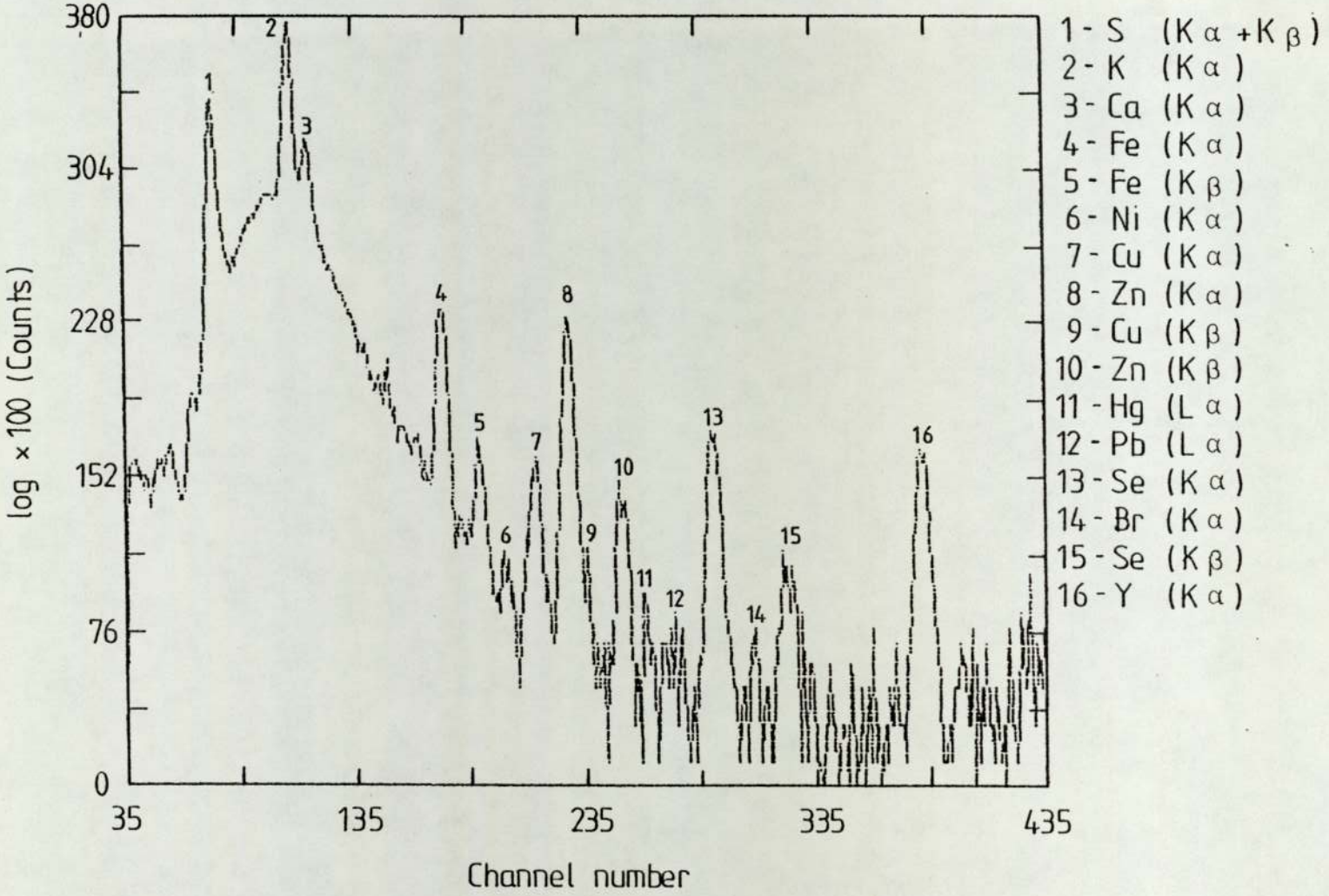

Fig 5.4 PIXE spectrum for the hair sample CI, showed high Se level.

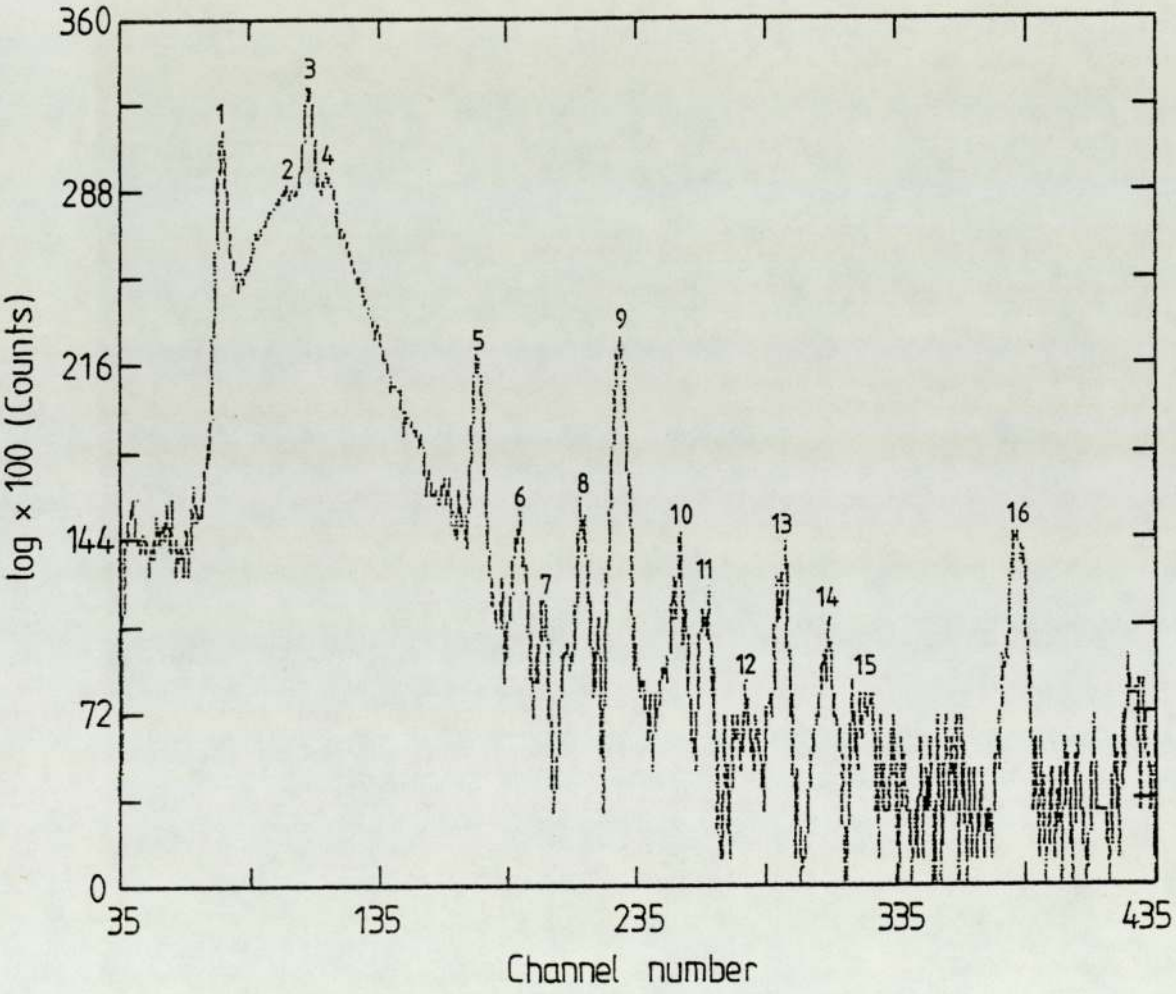

Fig 5.5 PIXE spectrum for the hair sample CH, showed high level in Se and Hg.

1 - S (K α + K β)	9 - Zn (K α)
2 - K (K α)	10 - Zn (K β)
3 - Ca (K α)	11 - Hg (L α)
4 - Ca (K β)	12 - Pb (L α)
5 - Fe (K α)	13 - Se (K α)
6 - Fe (K β)	14 - Br (K α)
7 - Ni (K α)	15 - Se (K β) + Pb (L β)
8 - Cu (K α)	16 - Y (K α)

data can be divided into pairs of measurements (x_i , y_i) for any two elements in the group. If we consider a linear relation between y and x, i.e.

$$y = a + b\,x \qquad 5.1$$

the slope of the line, b, is given by

$$b = \frac{\Sigma (x_i - \bar{x})\,(y_i - \bar{y})}{\Sigma (x_i - \bar{x})^2} \qquad 5.2$$

but the value of b by itself cannot be a good measure of the degree of correlation; and since we are looking for the interrelationship between the variables x and y, we can equally consider x is a function of y, as

$$x = a' + b'\,y \qquad 5.3$$

where

$$b' = \frac{\Sigma (x_i - \bar{x})\,(y_i - \bar{y})}{\Sigma (y_i - \bar{y})^2} \qquad 5.4$$

If there is a complete correlation then $b\,b' = 1$, if there is no correlation, both b and b' are zero.

The measure of the degree of linear correlation, Davies and Goldsmith (1972), is given by

$$r \equiv \sqrt{b\,b'} = \frac{\Sigma (x_i - \bar{x})\,(y_i - \bar{y})}{\sqrt{\Sigma (x_i - \bar{x})^2 \cdot \Sigma (y_i - \bar{y})^2}} \qquad 5.5$$

The value of r, ranges from zero, where there is no correlation, to ± 1, when there is a complete correlation.

A probability distribution of r can be derived from the two-dimensional Gaussian distribution, but its evaluation requires a knowledge of the correlation coefficient "ρ" of the parent population. A more common test of r is to compare its value with the probability distribution of a parent population which is completely uncorrelated, that is, for which $\rho = 0$. Such a comparison will indicate whether or not it is probable that the data points could present a sample derived from an uncorrelated parent population. If this probability is small, then it is more probable that the data points represent a sample from a parent population where the variables are correlated.

The relations between linear-correlation coefficient r, the number of observations N and the corresponding probability of exceeding r in a random sample of observations taken from an uncorrelated parent population ($\rho = 0$) as tabulated by Bevington (1969), were used to check the values of r obtained in this work.

The linear correlation coefficients, r, between the concentration of element y and element x, for all the possible pairs of elements in the data sets for the two groups under study, were calculated using the equation 5.5. The resulting correlation coefficients are represented in table 5.13 for hyperactive children and 5.14 for the non-hyperactive control children. Each table is divided into two triangles, for ease, in the search for

Table 5.13

Correlation coefficients, r, for element/element levels in the hair of hyperactive children (20 samples)

Upper triangle: all correlation coefficients

Lower triangle: only those which are significantly correlated at the 0.05 level

	S	K	Ca	Co	Ni	Cu	Zn	Se	Br	Hg	Pb
S	-	0.215	0.033	-0.261	-0.105	0.288	0.311	-0.022	-0.12	-0.119	-0.15
K		-	-0.181	-0.227	0.088	0.345	-0.104	0.021	-0.281	-0.32	-0.259
Ca			-	0.331	0.061	0.067	0.32	0.248	0.403	0.530	0.645
Co				-	0.436	-0.21	0.113	0.651	0.593	0.575	0.653
Ni				0.436	-	0.046	-0.014	0.452	-0.009	0.116	0.257
Cu						-	-0.113	-0.099	-0.469	-0.082	0.116
Zn							-	0.324	0.424	0.158	0.26
Se				0.651	0.452			-	0.349	0.557	0.639
Br				0.593		-0.469			-	0.571	0.453
Hg			0.530	0.575				0.557	0.571	-	0.796
Pb			0.645	0.653				0.639	0.453	0.796	-

Table 5.14

Correlation coefficients for element/element levels in the hair of the non hyperactive control population (20 samples)

Upper triangle: all calculated correlation coefficients
Lower triangle: only those which are significantly correlated at the 0.05 level

	S	K	Ca	Co	Ni	Cu	Zn	Se	Br	Hg	Pb
S	-	-0.006	0.350	-0.240	-0.23	-0.132	-0.057	0.266	-0.164	-0.275	0.005
K		-	0.041	0.466	0.359	0.377	0.263	-0.243	-0.288	0.388	0.016
Ca			-	-0.307	-0.086	0.548	-0.056	0.387	-0.286	-0.078	0.570
Co		0.466		-	0.749	-0.216	0.090	0.091	-0.023	0.653	-0.068
Ni				0.749	-	0.034	0.386	0.05	-0.10	0.505	0.293
Cu			0.548			-	-0.001	-0.214	-0.055	-0.068	0.394
Zn							-	-0.246	-0.414	0.246	0.115
Se								-	-0.041	0.315	0.017
Br									-	-0.29	-0.002
Hg				0.653	0.505					-	-0.034
Pb			0.570								-

significant values of correlation. The upper triangle gives the correlation coefficients between all pairs of elements whereas the lower triangle shows only those which are correlated at 0.05 level. Table 5.15 represents only the significant correlations at the 0.05 level with the upper triangle for the hyperactive group and the lower triangle for the non hyperactive group, for ease, in the search for any agreement in the significant values.

For N=20 pairs of variables the tabulated values of critical values of r at probabilities P=0.1, 0.05, 0.02 and 0.01 are 0.378, 0.444, 0.516 and 0.561 respectively. In comparing the calculated correlation coefficients with the tabulated values, it can be seen that there are significant correlations in the hyperactive group, at the 0.01 significant level between Ca/Hg, Ca/Pb; Co/Se, Co/Br, Co/Hg, Co/Pb; Se/Hg, Se/Pb; Br/Hg; and Hg/Pb. Also significant at the 0.05 level, are Ni/Se; Cu/Br and Br/Pb. The highest correlation 0.796 is between Hg and Pb.

The results shown in table 5.14 which relates elements in non hyperactive control group, shows, at the 0.01 level, significant correlations between Ca/Cu, Ca/Pb; Co/Ni, Co/Hg; Ni/Hg; and, significant at the 0.05 level, K/Ca; Br/Zn. The highest correlation, 0.749, is between Ni and Co in this group.

From the results shown in table 5.15, there is agreement between some of the significant correlations found in the

Table 5.15

Significant correlation coefficients at 0.05 level for Element/Element in the hair

upper triangle: for hyperactive children

lower triangle: for non hyperactive children

	S	K	Ca	Co	Ni	Cu	Zn	Se	Br	Hg	Pb
S	–										
K		–									
Ca			–							0.53	0.645
Co		0.466		–	0.436			0.651	0.593	0.575	0.653
Ni				0.749	–			0.452			
Cu			0.548			–			0.469		
Zn							–				
Se								–		0.557	0.639
Br									–	0.571	0.453
Hg				0.653	0.505					–	0.796
Pb			0.571								–

two groups. Specifically, the significant correlations for Co/Ni, Co/Hg and Ca/Pb.

Since the number of correlations calculated in the two groups is around 100 values, one would expect about 5 to appear significant at probability 0.05, but the complete significance for the two groups is about twenty, which is represented in table 5.15.

V.B Agitated Demented Elderly Population:

Agitated dementia is a form of severe mental illness, dementia is a largely irreversible disease due to degeneration of the brain cells. There is intellectual impairment with defects in memory, judgement and orientation, together with physical, emotional and personality changes, Koshy (1982). Clothing may be stained with food, they become untidy and unclean; show failing attention and concentration, many have difficulty in speaking, seeing and hearing; or loss of appetite and weight. Demented patients may also be agitated, distinguished by great excitement, motor activity and often continuous hallucinations, which is a similar condition to hyperactivity in the young.

Twenty two hair samples from an agitated demented elderly population and twenty from a non agitated demented control group were kindly selected by staff of the Greaves Hall Hospital, Southport. These groups were all female

subjects, the average age of the agitated group was 83.5 ± 6.5 years and for the non agitated control group 82.7 ± 9.8 years.

The same procedure as described in sec.III.D.3 for target preparation was followed. To improve the yttrium count statistics in these groups, the 1 mL of each digested hair sample was doped with 30 μL of an internal standard solution containing a yttrium concentration of 2 mg/mL. 5 μL of the doped sample was used to prepare the target. Masses of the hair used, resulting digested volumes, and the masses of hair in the 5 μL target are represented in tables 5.16 for the agitated demented group and in 5.17 for the control group.

Representative spectra from the agitated and non agitated demented groups are given in figures 5.6 and 5.7 respectively.

V.B.1 Results:

The calculation for elemental concentrations was carried out using equation 3.28 sec.III.F to convert x-ray counts, tables 5.18 and 5.19, into ppm. All factors used in the calculation are given in table 5.20.

The elemental concentrations obtained from the 42 samples are represented in tables 5.21 for the agitated group and 5.22 for the non agitated group. Graphical represen-

Table 5.16

Mass of hair samples used in the digestion with the resulting volumes and mass of hair in 5µL target, agitated elderly group

Sample	hair mass in mg ± 0.2	resulting digested volume in ml ± 0.02	mass of hair in 5µL target µg ± 3%
PC1	107.9	3.10	169.0
PC2	105.5	3.23	158.6
PC3	111.8	3.20	169.6
PC4	111.7	3.22	168.4
PC5	115.9	3.18	176.9
PC6	108.4	3.13	168.1
PC7	110.4	3.14	170.7
PC8	102.3	3.15	157.7
PC9	112.8	3.16	173.3
PC10	111.1	3.17	170.1
PC11	114.8	3.11	179.2
PC12	114.9	3.12	178.8
PC13	116.9	2.99	189.8
PC14	111.1	3.14	171.8
PC15	111.2	3.02	178.7
PC16	112.4	3.09	176.0
PC17	115.6	3.17	177.0
PC18	116.2	3.16	178.5
PC19	115.5	3.15	178.0
PC20	111.3	3.27	165.0
PC21	113.1	3.15	174.3
PC22	115.8	2.99	188.0

Table 5.17

Mass of hair samples used in the digestion with the resulting volumes and mass of hair in each 5μL target, non agitated elderly group

Sample	hair mass in mg ± 0.2	resulting digested volume in ml ± 0.02	mass of hair in 5μL target in μg ± 3%
PT1	110.7	3.06	175.6
PT2	116.2	3.18	177.4
PT3	112.2	3.12	174.6
PT4	114.1	3.18	174.2
PT5	112.1	3.11	175.0
PT6	110.8	3.10	173.5
PT7	114.8	3.13	178.0
PT8	116.4	3.05	185.3
PT9	115.6	3.14	178.7
PT10	115.2	3.15	177.0
PT11	114.1	3.12	177.5
PT12	108.3	3.14	167.4
PT13	111.6	3.16	171.4
PT14	115.6	3.10	181.0
PT15	114.6	3.25	171.2
PT16	114.2	3.08	180.0
PT17	112.5	3.13	174.5
PT18	113.1	3.05	180.0
PT19	109.0	3.09	171.2
PT20	110.5	3.17	169.2

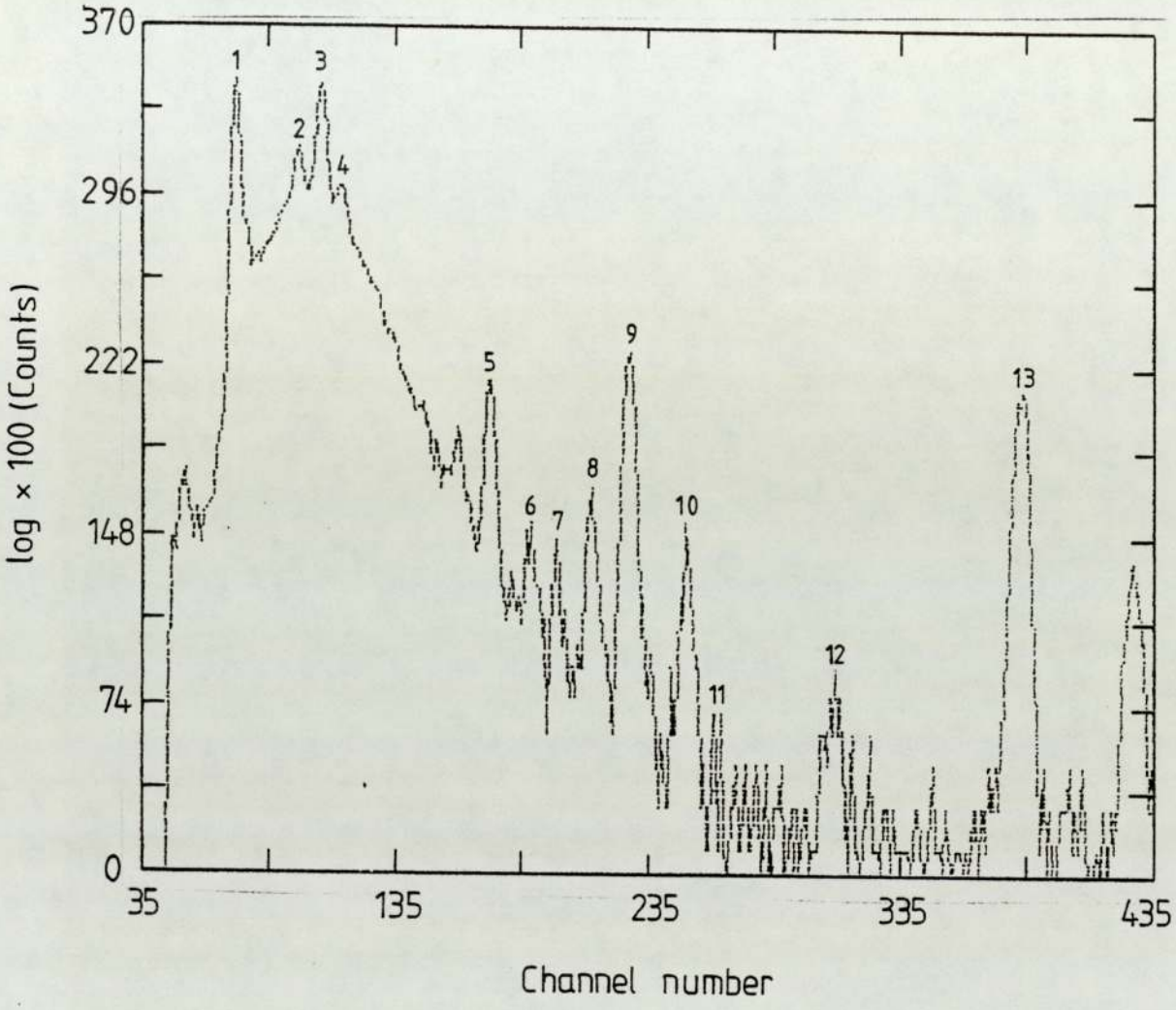

Fig 5.6 Representative spectrum for one sample of the agitated elderly people.

1 - S (K α + K β)
2 - K (K α)
3 - Ca (K α)
4 - Ca (K β)
5 - Fe (K α)
6 - Fe (K β)
7 - Ni (K α)
8 - Cu (K α)
9 - Zn (K α)
10 - Zn (K β)
11 - Hg (L α)
12 - Br (K α)
13 - Y (K α)

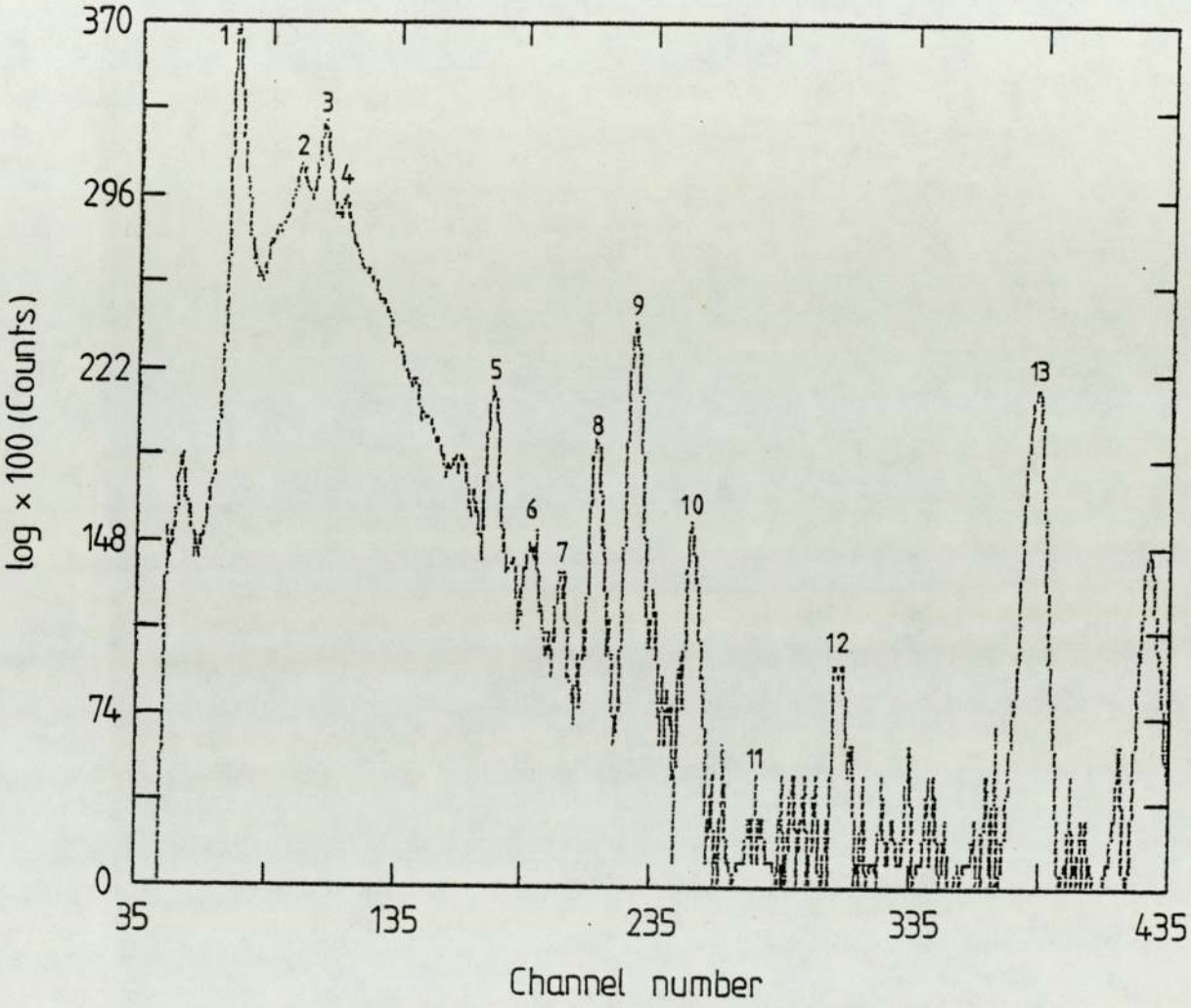

Fig 5.7 Representative spectrum for one sample of the non-agitated control group.

1 - S (K α + K β)
2 - K (K α)
3 - Ca (K α)
4 - Ca (K β)
5 - Fe (K α)
6 - Fe (K β)
7 - Ni (K α)
8 - Cu (K α)
9 - Zn (K α)
10 - Zn (K β)
11 - Pb (L α)
12 - Br (K α)
13 - Y (K α)

Table 5.18

X-ray counts for the elements measured, used in calculating the elemental concentration, for the agitated demented elderly group (22 targets).

	X-ray counts for elements measured												
Sample	S	K	Ca	Fe	Co	Ni	Cu	Zn	Se	Br	Y	Hg	Pb
PC1	7623	297	11293	246	30	27	140	717	5	14	429	12	11
PC2	4931	245	1144	308	39	12	102	536	9	14	378	-	9
PC3	10565	1965	6413	451	27	22	145	846	3	28	770	12	9
PC4	18615	417	3030	317	29	37	167	1091	-	9	807	10	7
PC5	7555	220	2247	299	20	16	158	858	10	7	507	4	12
PC6	9023	852	2009	1080	53	18	108	889	6	11	748	12	10
PC7	8455	312	2797	206	41	36	42	780	6	5	569	9	12
PC8	9303	9740	3612	332	20	14	100	544	6	10	662	8	12
PC9	11634	10197	5234	438	6	19	72	220	12	13	660	5	19
PC10	18530	5411	2257	504	48	23	116	1124	-	17	1022	-	9
PC11	15457	399	2673	325	-	25	162	626	3	8	655	12	5
PC12	19359	1992	33734	730	48	72	418	1390	6	29	1207	7	14
PC13	11637	393	5374	296	37	10	189	1079	7	14	779	4	14
PC14	9016	1825	6154	215	26	17	121	714	11	5	629	10	9
PC15	15218	597	13056	436	-	25	194	874	-	25	681	-	3
PC16	20094	959	9813	374	19	48	117	1023	19	32	861	-	16
PC17	12756	4114	1168	1351	14	20	62	706	9	17	662	-	10
PC18	8834	1148	7742	202	11	28	133	441	6	-	430	11	9
PC19	5918	1002	2394	108	5	18	41	444	2	-	273	6	4
PC20	7790	910	670	369	9	10	61	489	14	6	446	8	8
PC21	10705	873	1530	276	-	30	76	658	5	17	502	2	8
PC22	12153	12153	4620	502	46	20	142	1230	8	10	1107	15	10

Table 5.19

X-ray counts for elements measured, used in calculating the elemental concentration, for the non-agitated demented elderly population (20 targets)

	X-ray counts for elements measured												
Sample	S	K	Ca	Fe	Co	Ni	Cu	Zn	Se	Br	Y	Hg	Pb
PT1	4955	1455	1665	146	14	40	55	252	8	8	401	9	10
PT2	10435	506	13608	230	34	10	247	1048	7	1	768	8	30
PT3	7169	102	1567	144	16	32	96	672	11	7	586	6	10
PT4	8968	1156	9161	210	16	36	231	841	9	12	707	7	12
PT5	11234	1780	3075	549	9	17	211	1252	15	2	876	15	12
PT6	10467	946	2776	444	24	37	121	648	11	14	591	15	12
PT7	8916	1885	5900	278	7	23	118	669	11	22	615	-	15
PT8	9847	521	10169	204	46	16	278	855	6	16	611	15	13
PT9	7274	138	9086	228	21	24	89	607	11	37	506	-	6
PT10	17139	896	1984	232	31	22	112	903	9	3	669	6	11
PT11	12861	4111	10186	634	33	8	347	940	4	12	902	-	13
PT12	8812	500	11658	164	35	19	192	527	7	16	577	5	13
PT13	5780	670	6710	138	-	41	193	281	11	12	365	5	8
PT14	12412	1180	10780	341	57	39	191	1516	9	13	821	6	15
PT15	11650	557	2782	226	15	26	190	705	5	8	573	11	16
PT16	19014	1274	3228	406	19	23	337	1138	16	49	858	-	8
PT17	9218	2466	1171	181	18	20	77	510	7	6	537	10	18
PT18	20077	1236	3258	377	37	32	281	1171	17	19	952	-	14
PT19	20314	2274	3118	183	16	40	182	1118	13	7	863	13	14
PT20	6940	282	670	203	5	2	50	409	11	-	275	11	10

Table 5.20

The factors and their values, used in calculating the elemental concentration using equation 3.28

where $H(z) = \frac{M_{St} \cdot C(z)}{C(st) \cdot RF(z)}$ Factors are as defined in sec.III.C

M_{St} = 0.291 C(st) = 1.100

Element	R F(z)	C(z)	H(z)
S	0.71	1.365	0.509
K	15.71	1.157	0.0195
Ca	29.62	1.130	0.0101
Fe	25.82	1.0855	0.0111
Co	22.5	1.085	0.0128
Ni	18.0	1.086	0.01598
Cu	14.89	1.086	0.0193
Zn	11.59	1.087	0.0248
Se	3.9	1.092	0.0741
Br	3.0	1.094	0.0966
Hg	5.0	-	0.0583
Pb	4.1	-	0.071

Table 5.21

Elemental levels in ppm for the agitated demented elderly population (22 target)

Concentration in ppm												
Sample	S	K	Ca	Fe	Co	Ni	Cu	Zn	Se	Br	Hg	Pb
PC1	53523	80	1573	38	5	6	37	245	5	19	9	11
PC2	41870	80	193	57	8	3	33	222	11	23	-	11
PC3	41183	293	496	38	3	3	21	161	1	21	5	5
PC4	69729	60	225	25	3	4	24	199	-	5	4	4
PC5	37679	41	222	32	3	3	30	208	7	6	2	8
PC6	36530	132	161	95	5	2	17	175	3	9	5	6
PC7	44313	63	291	23	5	6	8	199	4	5	5	8
PC8	45363	1819	349	35	3	2	19	129	4	10	5	8
PC9	51779	1739	462	42	1	3	12	48	8	11	3	12
PC10	54261	607	131	32	4	2	13	160	-	9	-	4
PC11	67037	67	230	30	-	3	27	132	2	7	6	3
PC12	45664	181	1579	37	3	5	38	160	2	13	2	4
PC13	40066	52	367	22	3	1	25	181	4	9	1	7
PC14	42472	330	575	22	3	3	22	162	8	5	5	6
PC15	63658	97	1084	39	-	4	31	172	-	20	-	2
PC16	67502	124	651	27	2	5	15	167	9	21	-	7
PC17	55418	685	101	128	2	3	10	149	6	14	-	6
PC18	58589	292	1019	29	2	6	33	142	6	-	8	8
PC19	61995	403	497	24	1	6	16	226	3	-	7	6
PC20	53822	242	93	55	2	2	16	165	14	8	6	7
PC21	62280	196	177	35	-	6	17	186	4	19	1	7
PC22	29726	1142	224	26	3	2	13	146	3	5	4	3
mean ±	51112±	396±	486±	41±	3±	4±	22±	170±	5±	11±	4±	6±
1 σ	11354	519	443	25	2	2	9	41	4	7	3	3

Table 5.22

Elemental levels in ppm for the non-agitated demented elderly control group (20 targets)

	Concentration in ppm											
Sample	S	K	Ca	Fe	Co	Ni	Cu	Zn	Se	Br	Hg	Pb
PT1	35821	403	239	23	3	9	15	89	8	11	7	10
PT2	38989	72	1009	19	3	1	35	191	4	1	4	16
PT3	35668	19	155	16	2	5	18	163	8	7	3	7
PT4	37068	183	751	19	1	5	36	170	5	9	3	7
PT5	37304	226	203	40	1	2	26	203	7	1	6	5
PT6	52015	180	274	48	3	5	23	157	8	13	8	8
PT7	41461	335	545	28	1	3	21	152	7	19	-	9
PT8	44274	90	907	20	5	2	47	188	4	14	8	8
PT9	40951	30	1015	28	3	4	19	167	9	40	-	5
PT10	73680	147	169	21	3	3	18	189	5	2	3	7
PT11	40892	499	662	44	3	1	41	146	2	7	-	6
PT12	46442	101	1150	19	5	3	38	136	6	16	3	9
PT13	47032	208	1083	24	-	10	60	112	13	19	5	9
PT14	42519	155	733	26	5	4	25	253	4	8	2	7
PT15	60455	111	286	26	2	4	37	178	3	8	7	12
PT16	62673	161	211	29	2	2	42	183	8	30	-	3
PT17	50076	512	126	22	2	3	16	135	6	6	6	13
PT18	59642	141	192	25	3	3	32	170	8	11	-	6
PT19	69992	299	213	14	1	4	24	188	6	5	4	7
PT20	75926	118	145	49	1	2	20	219	18	-	14	15
mean ±	49644±	200±	503±	27±	2±	4±	30±	170±	7±	11±	4±	8±
1σ	12998	142	370	10	1	1	6	37	4	10	4	3

tation for the mean elemental concentration for the elements measured in the two groups are given in fig.5.8.

The frequency distributions of hair elemental concentrations from 22 agitated demented subjects are represented in the upper half of figures 5.9 to 5.20. For comparison the frequency distribution for the 20 non agitated individuals forming the control group are represented in the lower parts of these figures.

Tests of significance of differences between agitated demented samples and the non agitated control group for each mean elemental concentration using the t-test, equation 3.27, were performed. Table 5.23 shows the results of the test, as discussed in sec.V.A.5.1. the results of the calculated t, were compared with the tabulated critical values, and it is seen that the only significant difference at the P = 0.005 is for Cu for which the agitated demented sample shows a lower level than the control group. Fe and Pb levels were significantly different at P = 0.025 for which the agitated group shows a higher level in Fe and lower level in Pb. Graphical representation of all the individuals, arranged in increasing order, for these elements Cu, Fe, and Pb are shown in figures 5.21, 5.22 and 5.23 respectively, where Cu curves show clearly the significant difference.

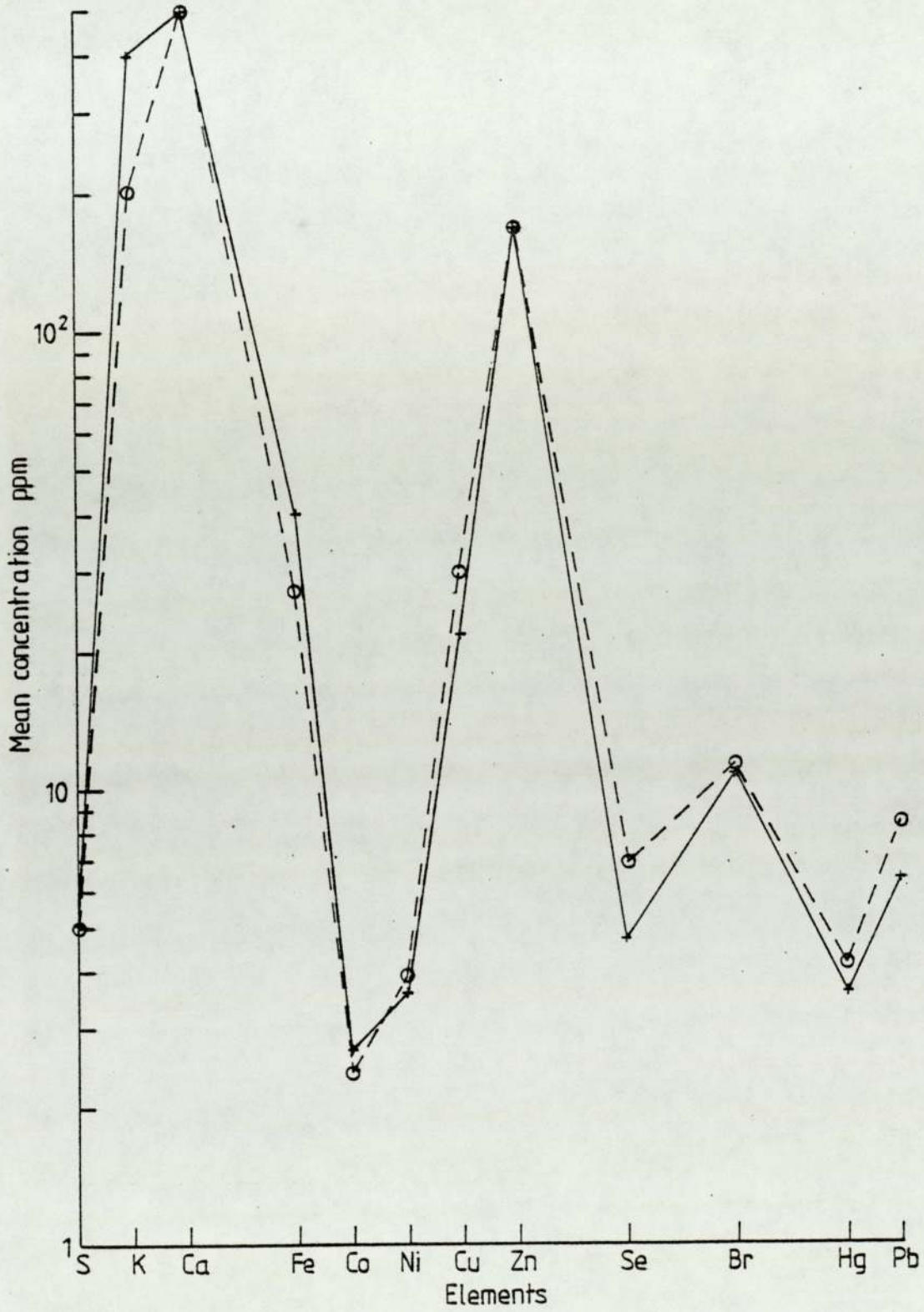

Fig 5.8 Mean concentration for hair elements measured from 22 agitated and 20 non-agitated individuals hair metal concentration.
(+ agitated, o non - agitated)

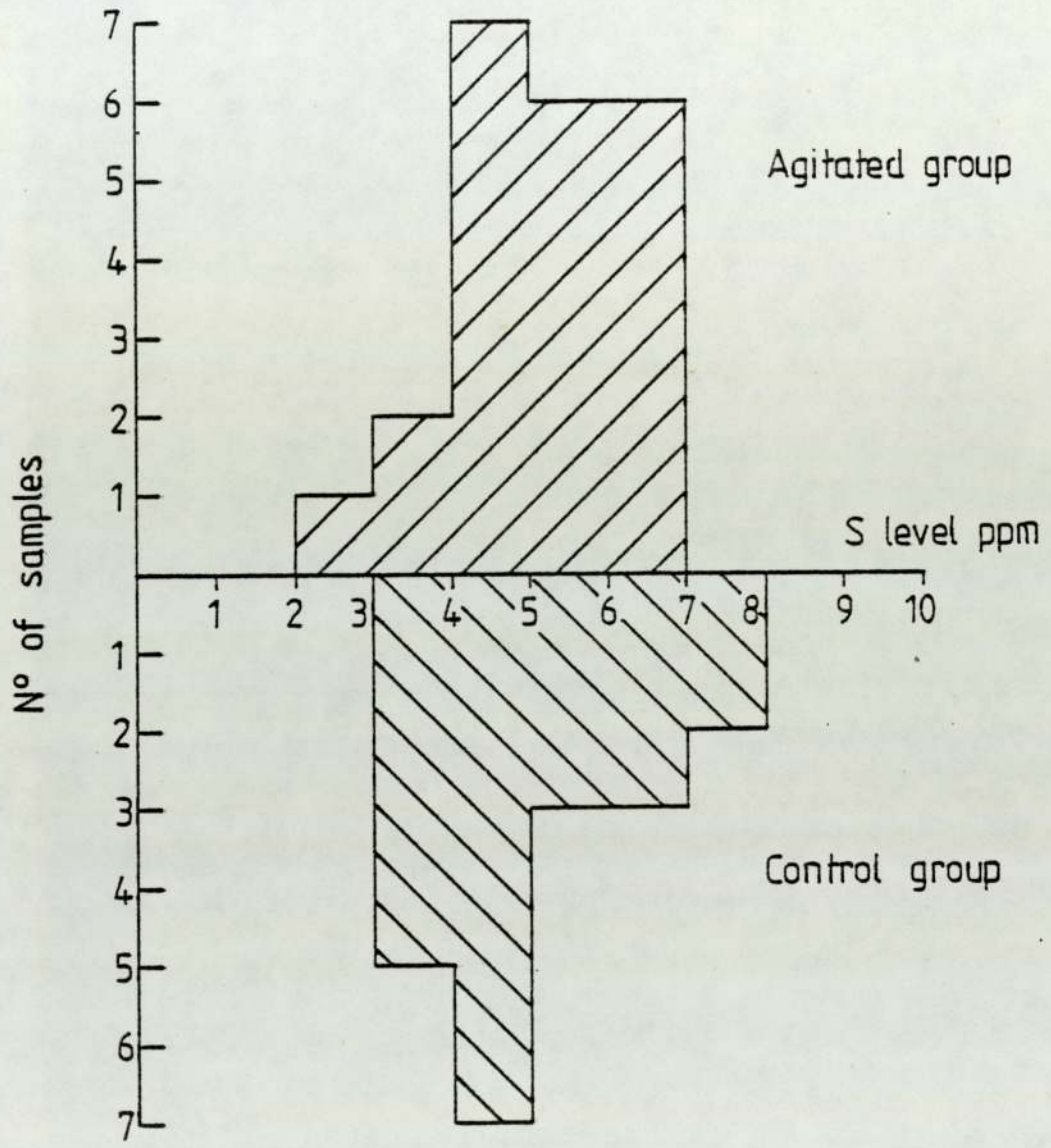

Fig 5.9 Frequency distribution for hair S level, upper half for agitated and lower half for control group

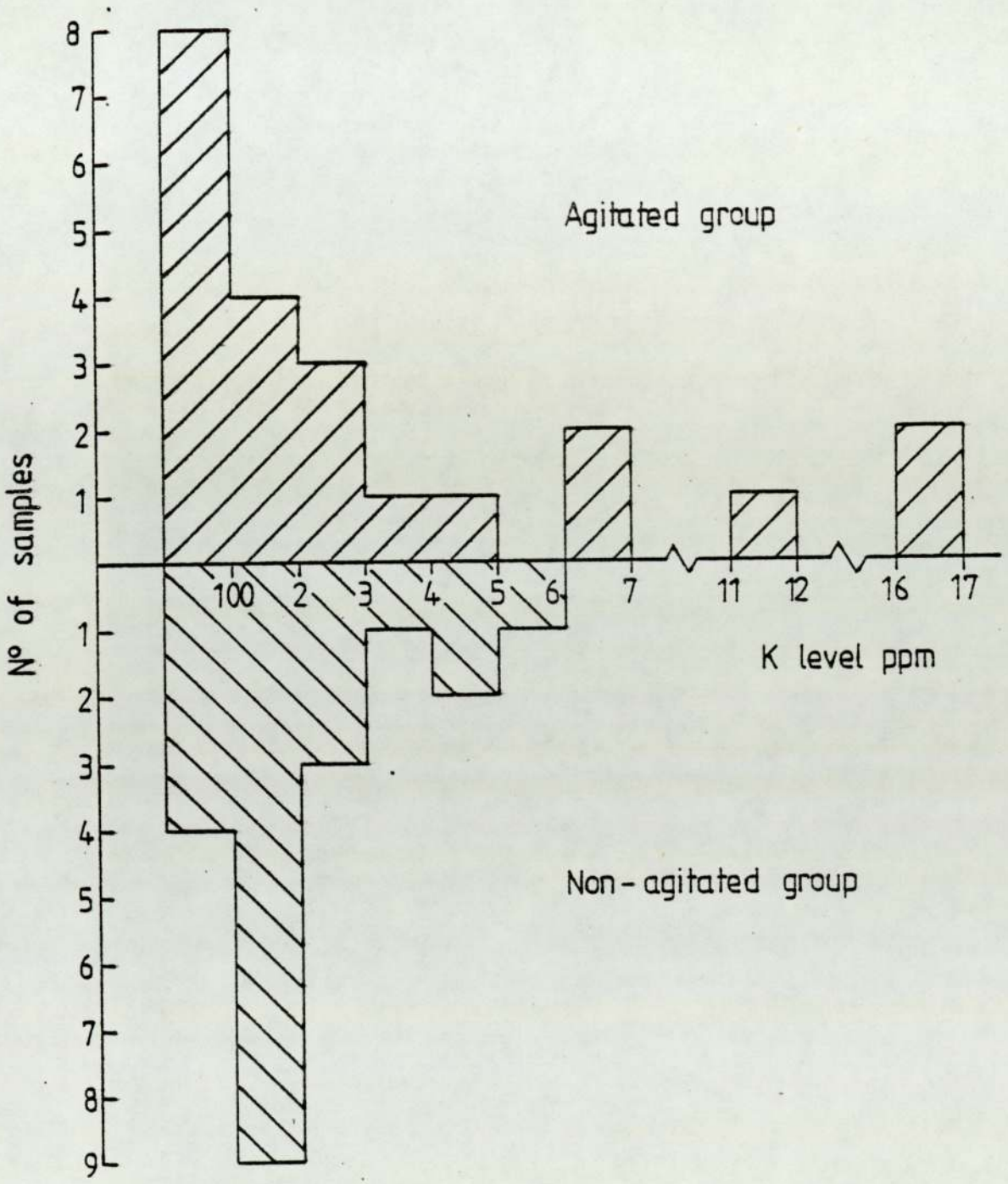

Fig 5.10 Frequency distribution for hair K level, upper half for agitated and lower half for non-agitated group.

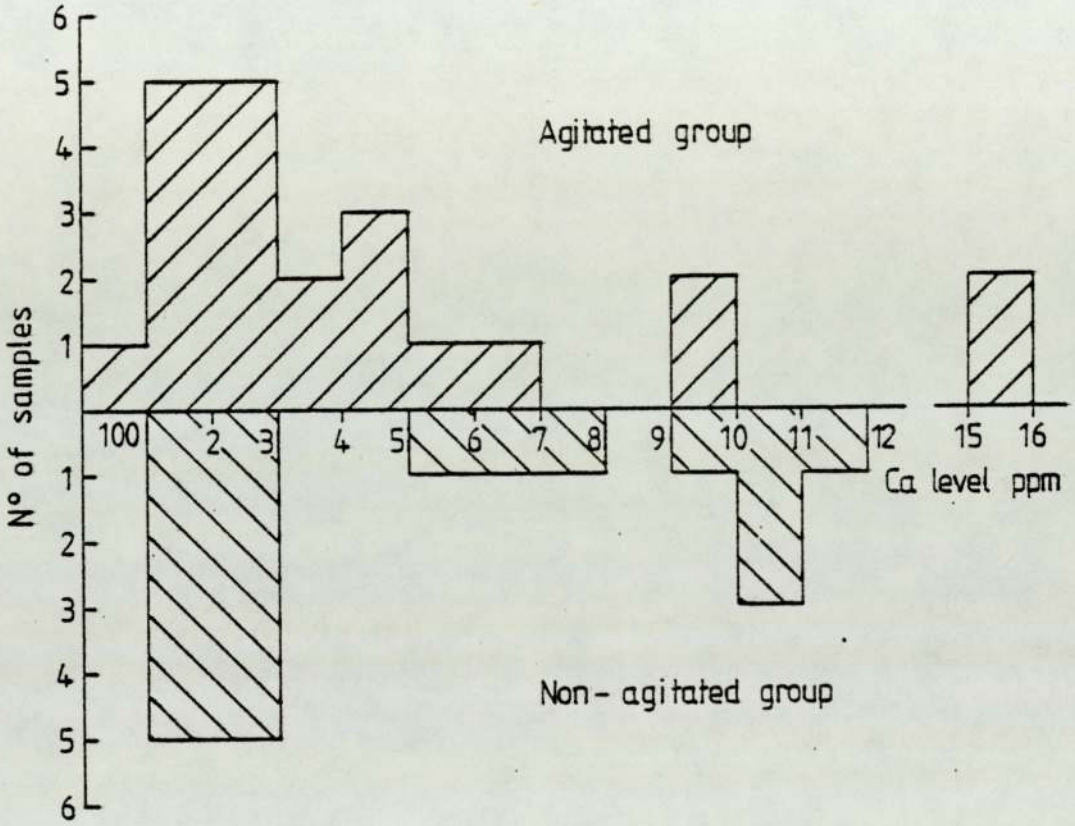

Fig 5.11 Frequency distribution for hair Ca level, upper half for agitated and lower half for non-agitated group.

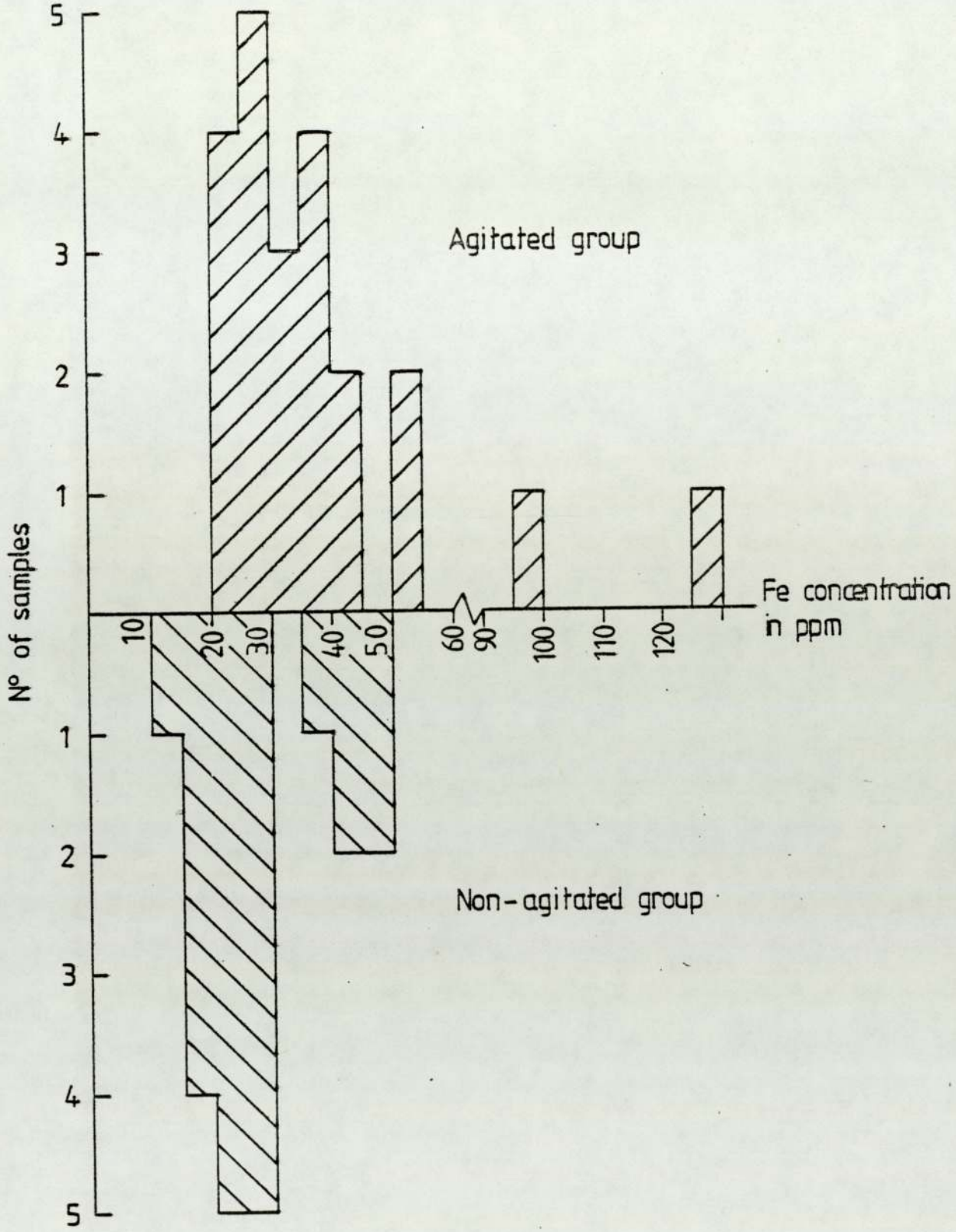

Fig 5.12 Frequency distribution of hair Fe concentration in agitated and control groups.

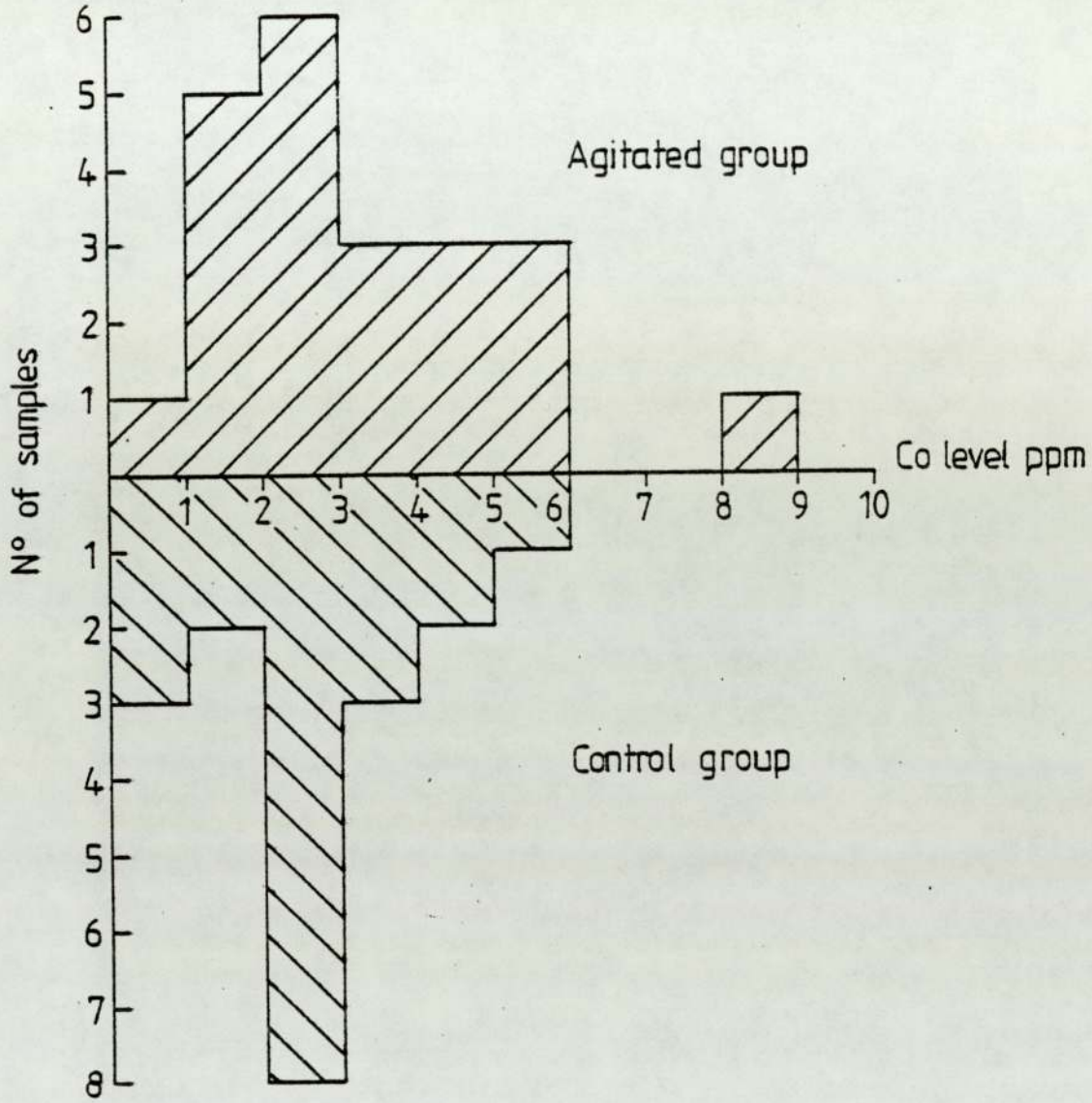

Fig 5.13 Frequency distribution of hair Co concentration in agitated and control groups.

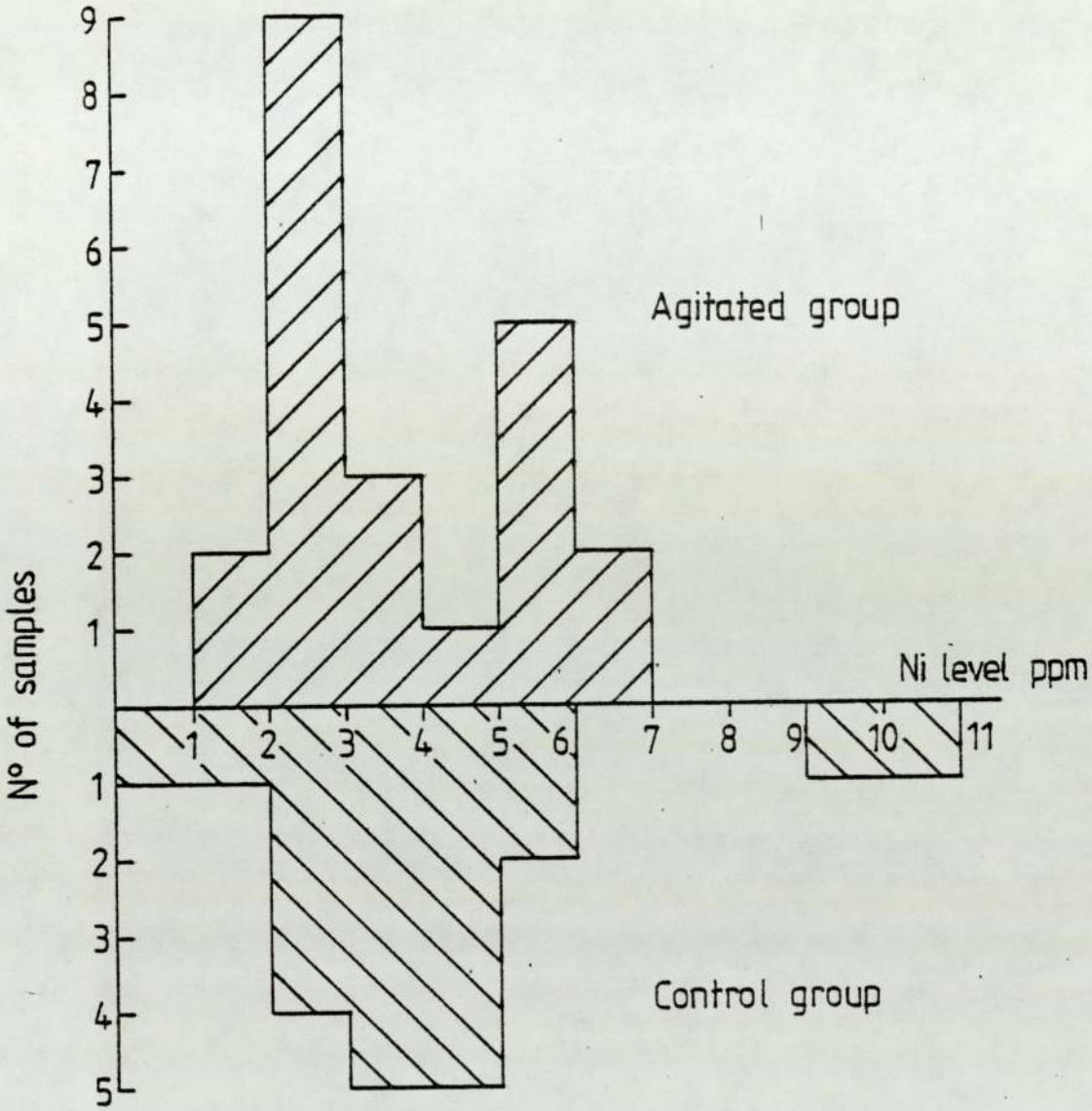

Fig 5 . 14 Frequency distribution of hair Ni concentration in agitated and control groups.

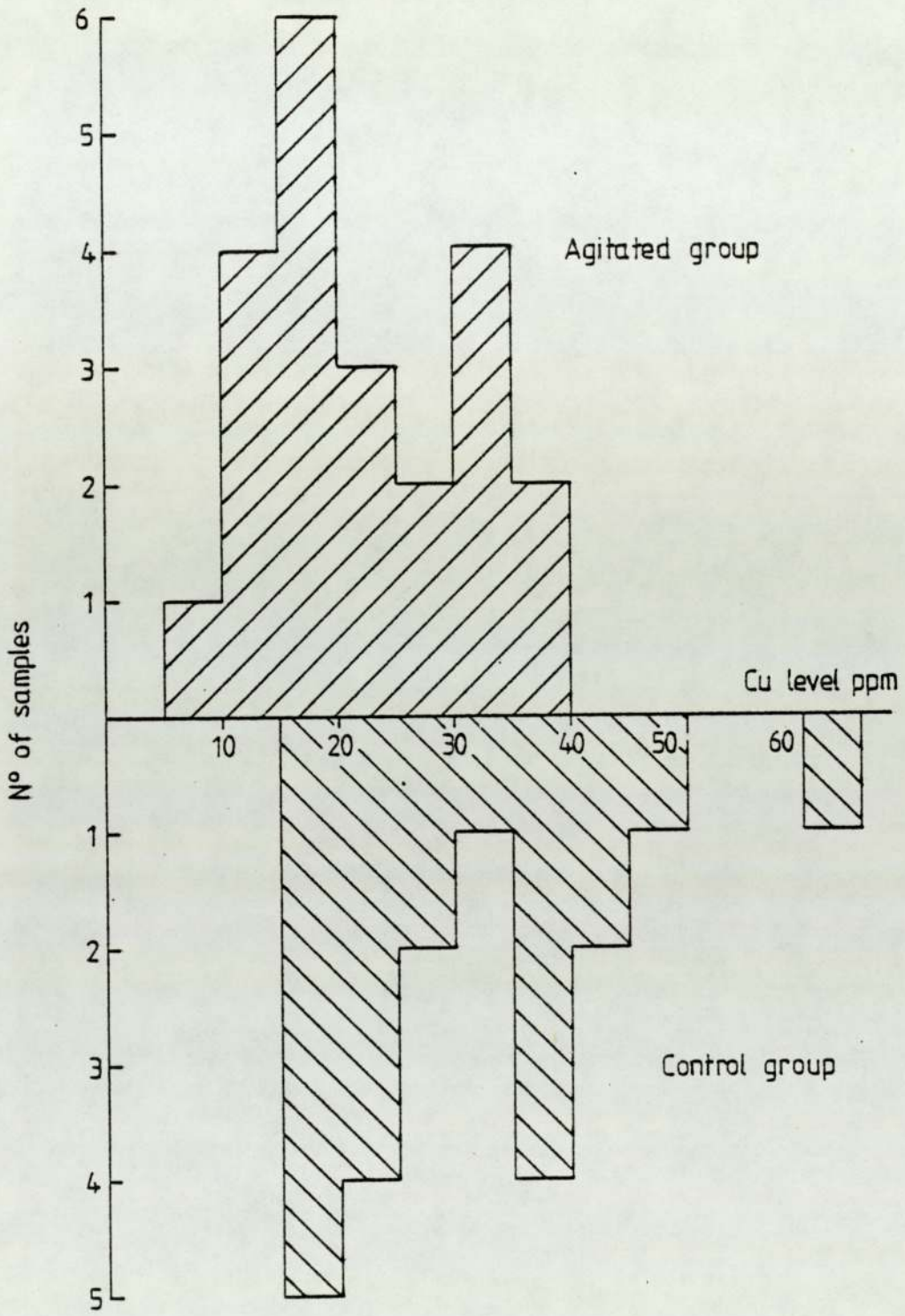

Fig 5.15 Frequency distribution of hair Cu concentration of agitated and control groups.

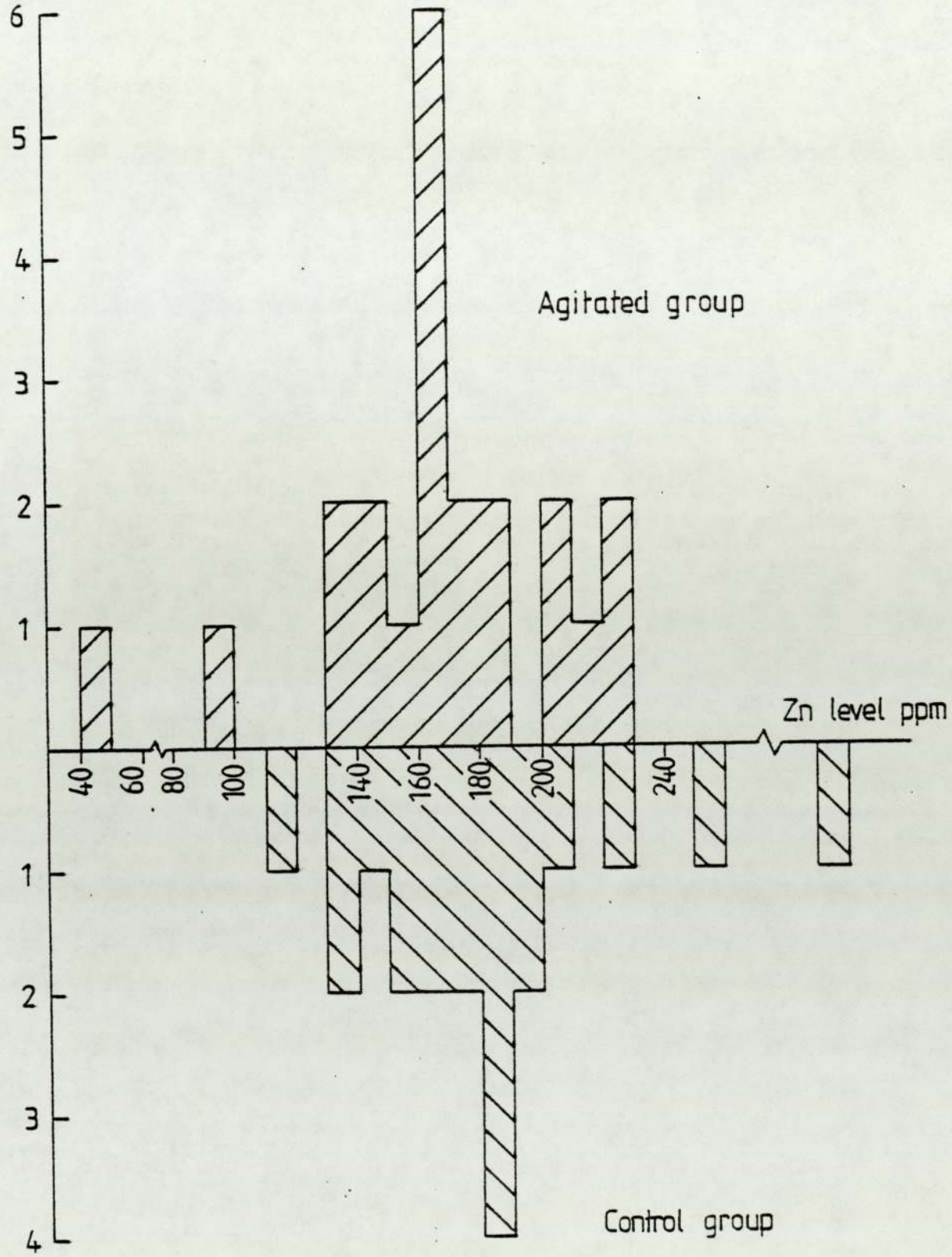

Fig 5.16 Frequency distribution of hair Zn concentration of agitated and control groups.

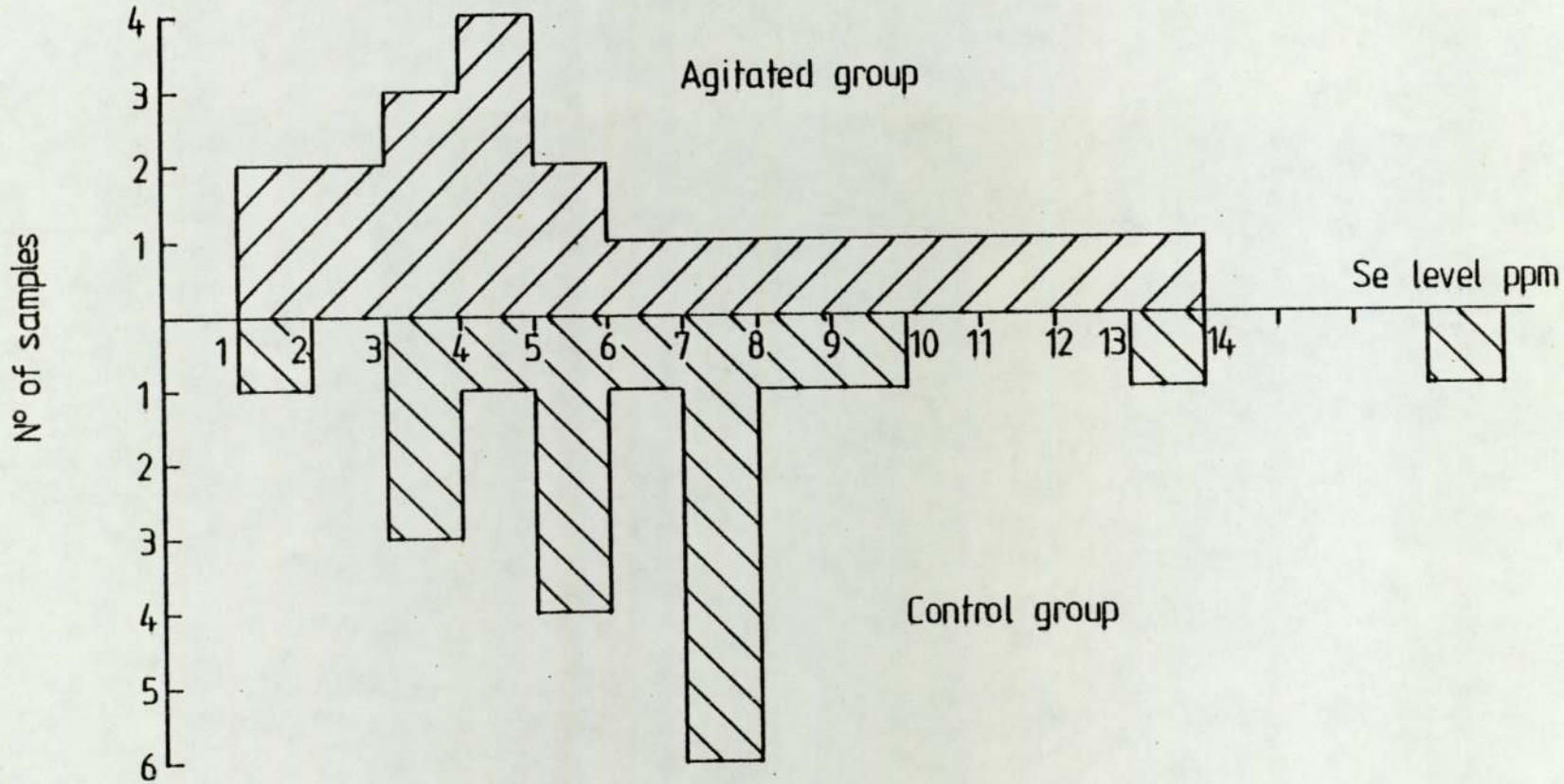

Fig 5.17 Frequency distribution of hair Se concentration of agitated and control groups.

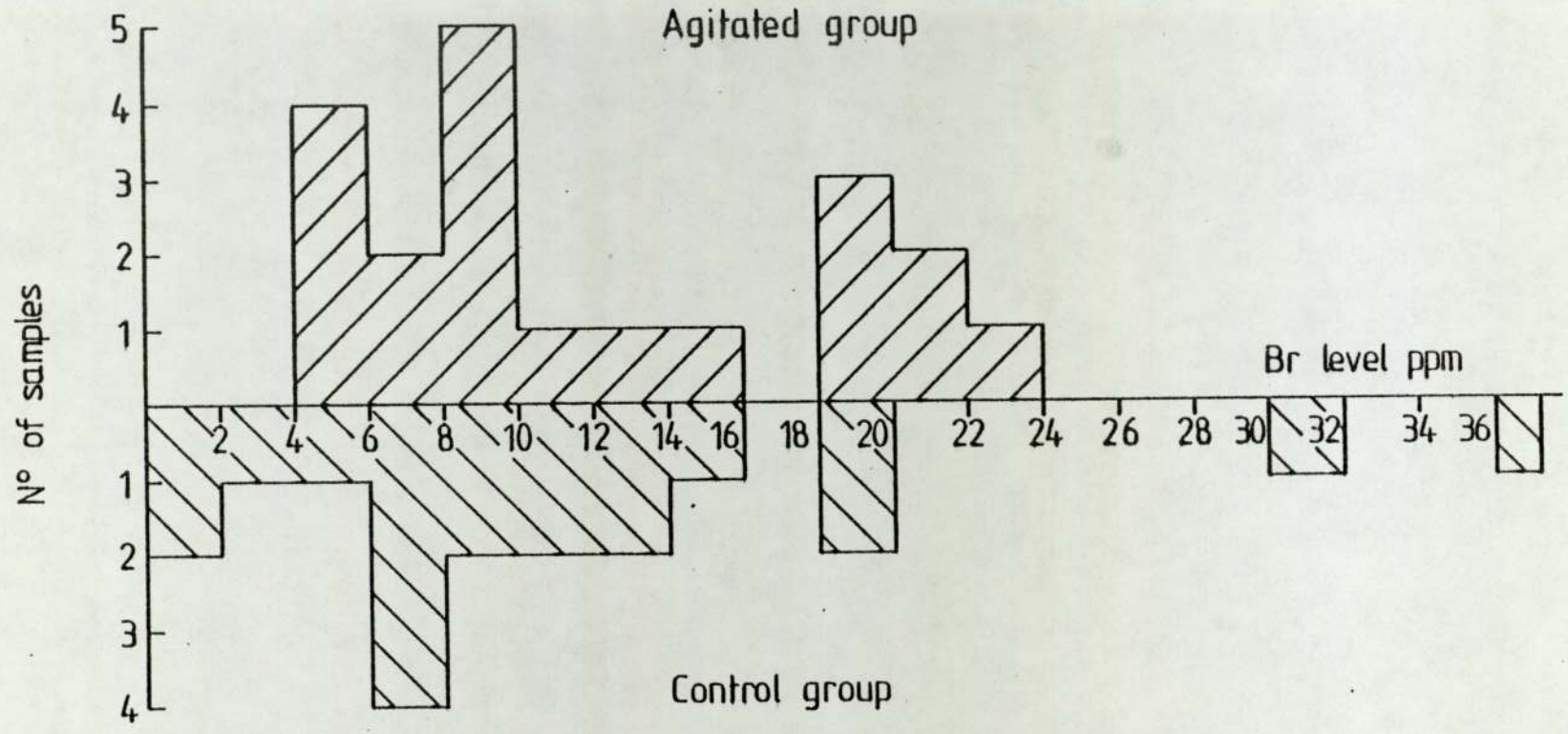

Fig 5.18 Frequency distribution of hair Br concentration of agitated and control groups.

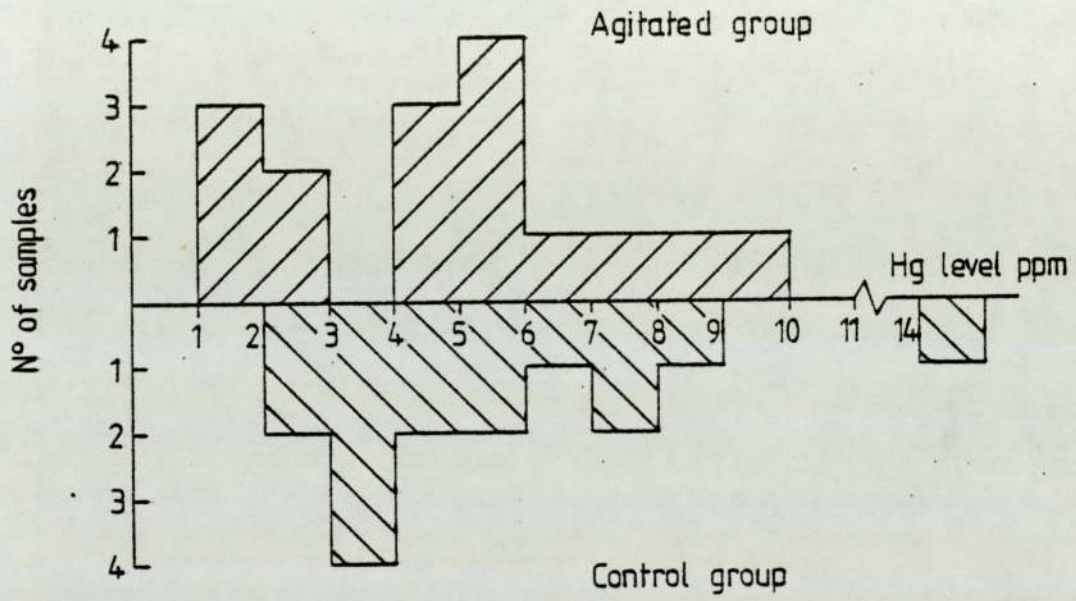

Fig 5.19 Frequency distribution of hair Hg concentration of agitated and control groups.

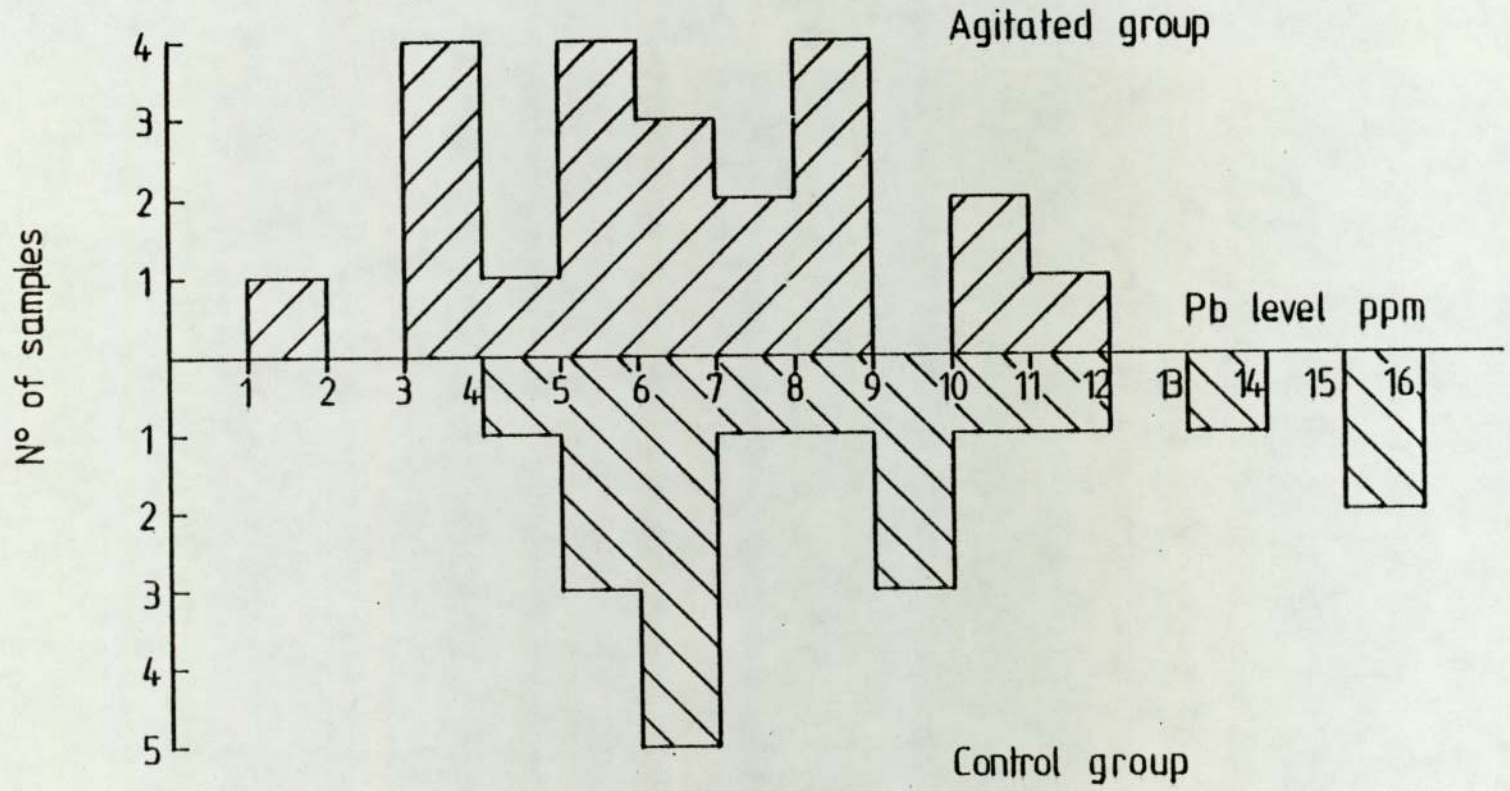

Fig 5.20 Frequency distribution of hair Pb concentration of agitated and contrd groups.

Table 5.23

Hair element levels and the significance between agitated demented and non agitated control groups

Element	mean conc. ppm agitated patients	mean conc.ppm non agitated patients	"t" value	significance 95 %
S	51112 ± 11354	49644 ± 12998	0.40	not sig.
K	396 ± 519	200 ± 142	1.70	not sig.
Ca	486 ± 443	503 ± 370	0.13	not sig.
Fe	41 ± 25	27 ± 10	2.31	significant
Co	3 ± 2	2 ± 1	0.56	not sig.
Ni	4 ± 2	4 ± 2	0.48	not sig.
Cu	22 ± 9	30 ± 6	3.36	significant
Zn	170 ± 41	170 ± 37	0.04	not sig.
Se	5 ± 4	7 ± 4	2.01	not sig.
Br	11 ± 7	11 ± 10	0.24	not sig.
Hg	4 ± 3	4 ± 4	0.52	not sig.
Pb	6 ± 3	8 ± 3	2.14	significant

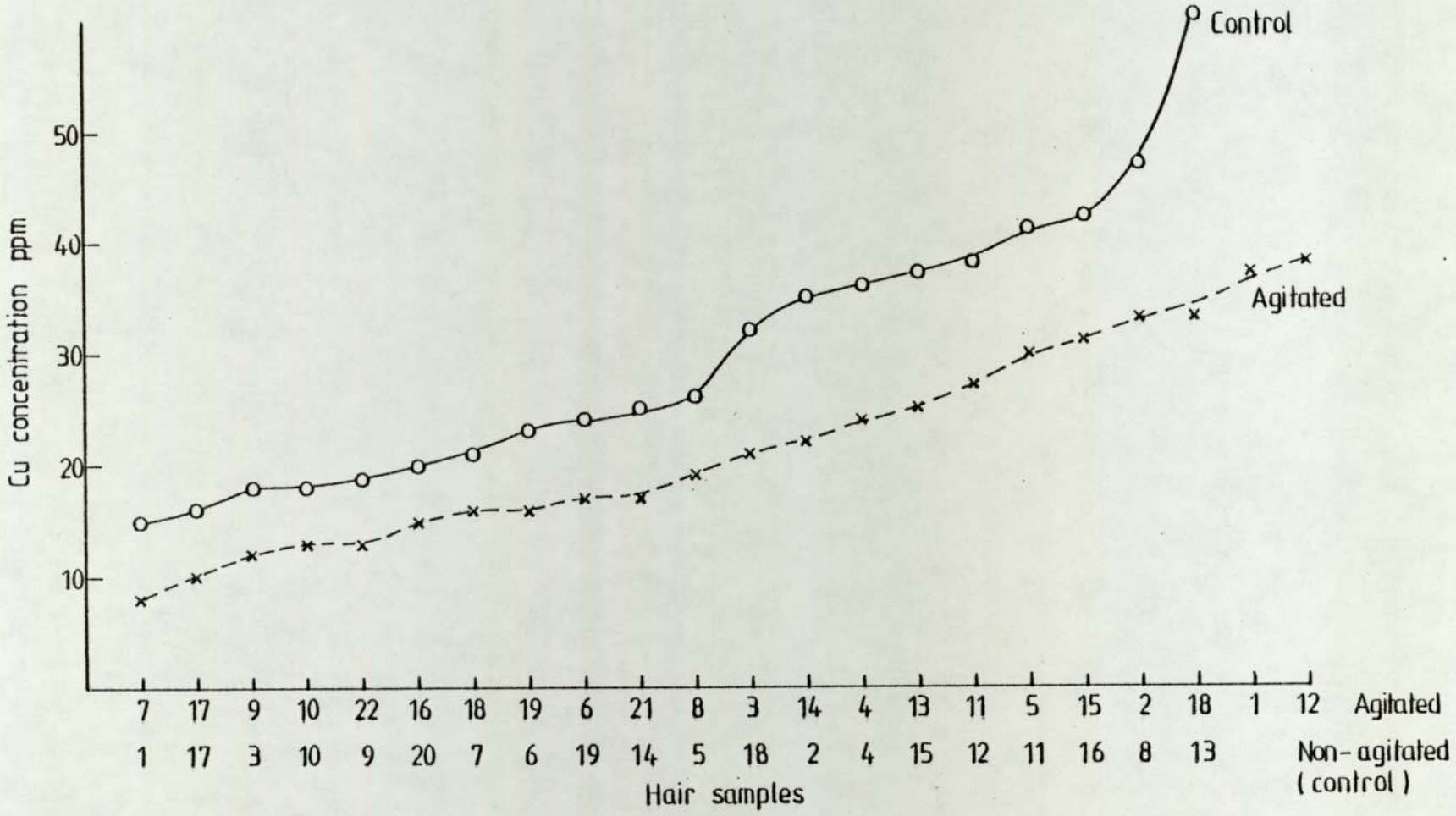

Fig 5.21 Cu level ppm arranged in increasing order

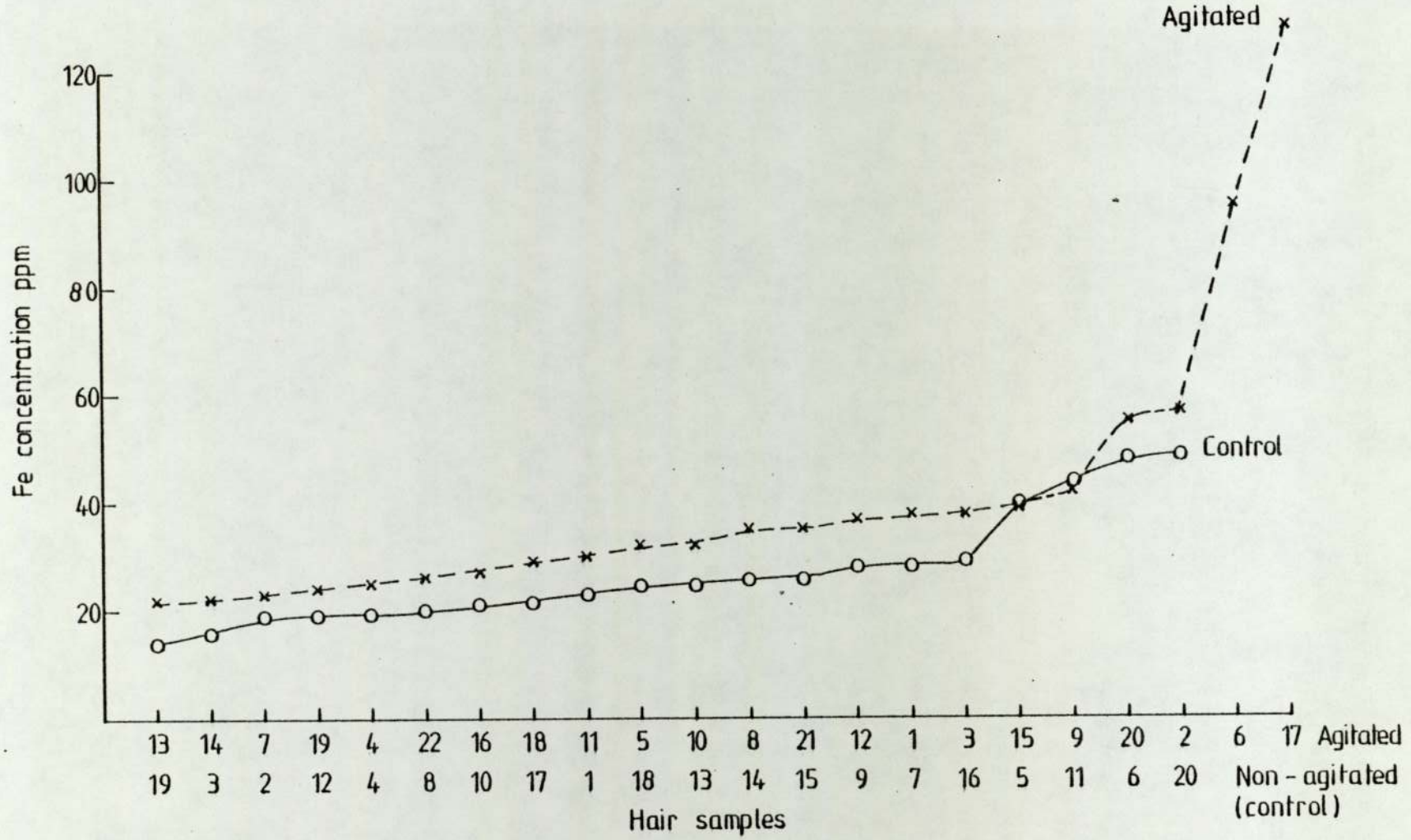

Fig 5.22 Fe level ppm arranged in increasing order

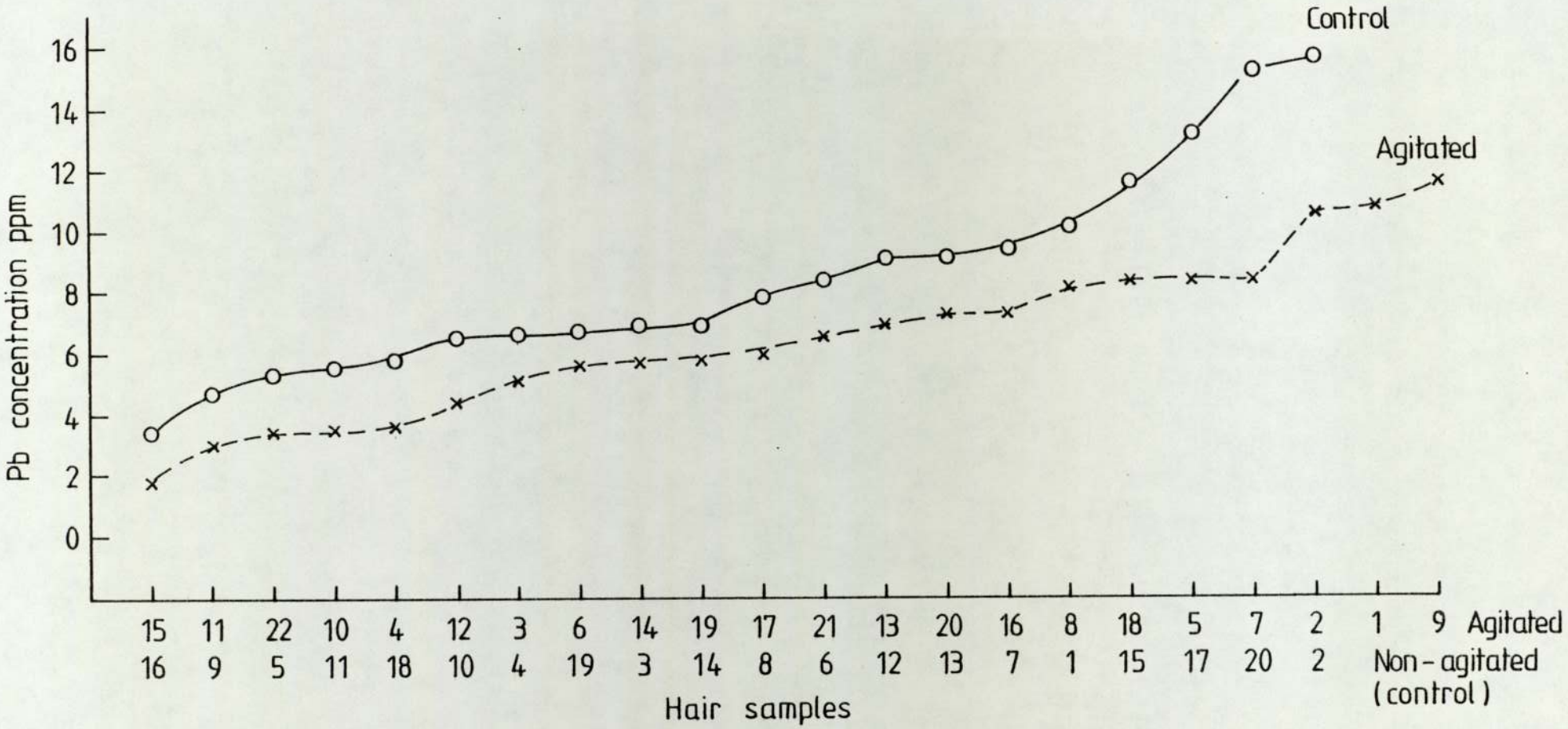

Fig 5.23 Pb level ppm arranged in increasing order.

V.B.2 Inter-Element Correlations:

The linear correlation coefficients between concentration of elements, for all possible pairs of elements in the data set for the agitated population, was calculated using equation 5.5. The resulting correlation coefficients are represented in table 5.24. Table 5.25 represents similar calculations of the correlation coefficients for the non agitated demented control group.

For the N=22 pairs of variables the tabulated critical values of r at probabilities P=0.10, 0.05, 0.02 and 0.01 are 0.360, 0.423, 0.492 and 0.537 respectively. In comparing the calculated r values with the tabulated ones, it can be seen that the only coefficients significant at the 0.01 level, for the agitated demented elderly group, are between S/Co, K/Zn; and these two correlations are negative, while between Ca/Cu, Se/Pb these are positive correlations. Significant at 0.05 level are the correlations between S/Ni, K/Cu, Ca/Ni, Co/Zn and Br/Hg. These significant correlations are given in the lower triangle of table 5.24.

For the non agitated demented control group, the only significant correlations, at 0.01 level, are Ca/Cu, Ca/Ni and Ca/Zn; Pb/Hg. However, significant at the 0.05 level are negative correlations between K/Zn, Co/Se, Br/Hg, Br/Pb; and positive correlation between Se/Hg. These are represented in the lower triangle of table 5.25. The

Table 5.24

Correlation coefficients for element/element levels in the hair of the agitated demented elderly group (22 samples)

	S	K	Ca	Fe	Co	Ni	Cu	Zn	Se	Br	Hg	Pb
S	-	-0.200	0.132	-0.100	-0.549	0.518	0.031	0.003	-0.117	0.088	-0.016	-0.197
K		-	-0.166	0.066	-0.029	-0.364	-0.428	-0.693	0.043	-0.149	-0.041	0.201
Ca			-	-0.237	-0.017	0.515	0.666	0.126	-0.165	0.221	0.238	0.076
Fe				-	0.126	-0.241	-0.21	-0.093	0.181	0.245	-0.21	0.059
Co	-0.549				-	-0.049	0.174	0.484	0.176	0.139	0.058	0.389
Ni	0.518		0.515			-	0.216	0.382	-0.076	0.026	0.303	0.162
Cu		-0.428	0.666				-	0.335	-0.077	0.207	0.149	0.051
Zn		-0.693			0.484			-	-0.044	0.135	0.144	0.036
Se									-	0.110	0.007	0.666
Br										-	-0.479	0.139
Hg										-0.479	-	0.168
Pb												-

Table 5.25

Correlation coefficients for element/element levels in the hair of the non agitated demented (control) group (20 samples)

	S	K	Ca	Fe	Co	Ni	Cu	Zn	Se	Br	Hg	Pb
S	-	-0.098	-0.473	0.135	-0.042	-0.184	-0.079	0.317	0.32	-0.168	0.288	0.102
K		-	-0.262	0.172	-0.25	0.078	-0.14	-0.446	-0.174	-0.181	-0.036	0.061
Ca	-0.473		-	-0.217	0.274	0.073	0.565	-0.114	-0.16	0.373	-0.277	0.027
Fe				-	-0.159	0.066	-0.067	0.143	0.351	0.027	0.315	0.024
Co					-	-0.361	-0.032	0.234	-0.445	0.064	-0.076	-0.031
Ni						-	0.064	-0.585	0.38	0.216	0.167	0.007
Cu			0.565				-	-0.114	-0.115	0.191	-0.152	-0.118
Zn		-0.446				-0.585		-	-0.056	-0.27	0.079	-0.066
Se					-0.445				-	0.12	0.478	0.231
Br										-	0.468	-0.453
Hg									0.478	-0.468	-	0.612
Pb										-0.453	0.612	-

significant coefficients, at 0.05 level, for the two groups are given in one table, table 5.26. The agreement in the significant correlations between the two groups are for Ca/Cu, K/Zn and Hg/Br and these significances are negative in the two groups. As mentioned before, since the number of correlations calculated in the two groups is around 100 values, one would expect about 5 to appear significant at probability 0.05, but the complete significance for the two groups is about 18, which is represented in table 5.26.

The highest correlation coefficient in the agitated group was negative between K/Zn at -0.693, the second highest correlation 0.67 is between Ca/Cu and Se/Pb, these are significant at $P < 0.001$. While the highest correlation in the non agitated group is 0.61 between Pb/Hg.

As mentioned before, by measuring the correlations one can observe if certain trends exist between the elements under investigation. Where a significant correlation coefficient is found this implies there is a real interaction between the elements.

V.B.3 Regression Equation and Multiple Correlation Coefficients:

The use of PIXE analysis for biomedical applications faces one with an enormous amount of quantitative data.

Table 5.26

Significant correlation coefficients for element/element at 0.05 level

upper half: agitated population

lower half: control group

	S	K	Ca	Fe	Co	Ni	Cu	Zn	Se	Br	Hg	Pb
S	-				-0.549	0.518						
K		-					-0.428	-0.693				
Ca	-0.473		-			0.515	0.666					
Fe				-								
Co					-			0.484				
Ni						-						
Cu			0.565				-					
Zn		-0.446				-0.565		-				
Se					-0.445				-			0.666
Br										-	-0.479	
Hg									0.478	-0.468	-	
Pb										-0.453	0.612	-

One way to deal with this is to ignore all data except those believed to be of primary interest in a given problem. Another way is to use methods provided by bivariate and multivariate statistical procedures to make more effective use of the wide elemental range determined by the proton beam analysis. This in turn can greatly increase the value of the technique and allows one to proceed without prejudgment of the elements of critical interest.

If, for example, the dependent variable y is a function of more than one variable x_j, i.e

$$y = a + b_1 x_1 + b_2 x_2 + \ldots\ldots\ldots + b_n x_n \qquad 5.6$$

One might investigate the possibility of correlation between y and the various different variables x_j. One can extrapolate the concept of the linear correlation, r which characterizes the correlation between two variables at a time, to include multiple correlation, between groups of variables taken simultaneously.

The multiple-correlation coefficient R is defined, Bevington (1969), to be the sum over variances, S_j, S_y, and the terms b_j of equation 5.6

$$R^2 \equiv \sum_{j=1}^{n} \left(b_j \frac{S_j}{S_y} r_{jy} \right) \qquad 5.7$$

where

$$S_j = \sqrt{\frac{\sum_{i=1}^{N} (x_{ij} - \bar{x}_j)^2}{N - 1}}$$

$$S_y = \sqrt{\frac{\sum_{i=1}^{N} (Y_i - \bar{y})^2}{N - 1}} \qquad 5.8$$

where n is the number of variables, and N is the number of individuals in one variable.

The linear correlation coefficient, r, is useful for testing whether one particular variable should be included in the theoretical function to which the data are fitted. In the method of multiple correlation and regression, the variable y stands for an element one wishes to predict. We also have information on n other elements, represented by variables x_1 through x_n. The combination of the values x_1 through x_n that will predict the value y for any individual in an optimal way, i.e. the best possible values for a, b_1, b_2,..., b_n, is provided by the criterion of least squares. However, in this instance, the least squares procedure does not yield the required values directly, but instead gives a set of n equations (called the normal equations):

$$\begin{aligned}
B_1 r_{11} + B_2 r_{12} + \ldots\ldots\ldots + B_n r_{1n} &= r_{y1} \\
B_1 r_{21} + B_2 r_{22} + \ldots\ldots\ldots + B_n r_{2n} &= r_{y2} \\
&\vdots \\
B_1 r_{n1} + B_2 r_{n2} + \ldots\ldots\ldots + B_n r_{nn} &= r_{yn}
\end{aligned} \qquad 5.9$$

where the coefficient B_j are related to the coefficients b_j of equation 5.6 by

$$B_j = b_j \frac{S_j}{S_y} \qquad 5.10$$

and the diagonal terms in r are unity $r_{jj} = 1$.
The solution of the normal equations gives the values of B.

The results of significant linear correlation, table 5.26, were used to , for selecting the variable element x_j to be included in the regression equation to which the data are fit. The resulting regression equations for non agitated group elemental results are:

$$y(Hg) = 0.548\ x_1(Se) - 0.192\ x_2(Br) + 2.503 \qquad 5.11$$

$$y(Pb) = 0.482\ x_1(Hg) - 0.0725\ x_2(Br) + 7.22 \qquad 5.12$$

$$y(Se) = 0.466\ x_1(Pb) + 0.666\ x_2(Hg) + 0.007\ x_3(Br) + 0.199 \qquad 5.13$$

$$y(Ca) = 17.5\ x_1(Cu) - 0.506\ x_2(Zn) + 69.3 \qquad 5.14$$

To test the entire fit, the F-test is applied which can be related to the multiple correlation coefficient R, Bevington (1969), as

$$F_R = \frac{R^2\ (N - n - 1)}{(1 - R^2)\ n} \qquad 5.15$$

From the definition of F_R in terms of the multiple-correlation coefficient R, equation 5.15, large values of F_R correspond to a good fit, where the multiple correlation is good. The F-test for this statistic is,

in fact, a test that the coefficient are zero; $b_j = 0$. So long as F_R exceeds the test value for F, we can be fairly confident that our coefficients are non zero.

F_R was calculated to test the fit of equations 5.11-5.14, the results are 8.777, 5.904, 3.967 and 4.14 respectively which are significant at levels < 0.05 when compared with the tabulated critical values of F (Bevington 1969), which are $F \simeq 3.6$ at N=20 and n=2; $F \simeq 3.4$ at N=20 and n=3.

On the other hand, other fit as

$$Y(K) = 0.055\, x_1(Cu) - 0.013\, x_2(Ca) - 0.187\, x_3(Zn) + 236.2 \qquad 5.16$$

which shows $F_R = 2.25 < F$, one can conclude that at least one of the terms in the fitting function is not valid, thus decreasing the multiple correlation coefficient by its inclusion.

For the agitated group the fitted regression equations are

$$Y(Pb) = 0.474\, x_1(Se) + 0.223\, x_2(Hg) + 0.064\, x_3(Br) + 2.721 \qquad 5.17$$

$$Y(Ca) = 108.3\, x_1(Ni) + 28.8\, x_2(Cu) - 525 \qquad 5.18$$

$$Y(K) = 7.85\, x_1(Zn) - 36.9\, x_2(Cu) - 134.4 \qquad 5.19$$

with $F_R = 6.1$, 9.5 and 18.05 respectively.

From the above results the following conclusions may be drawn:

1. When differences between means of the elemental concentrations, for hair from agitated demented elderly and non agitated demented groups were tested for significance, it was found that Cu, Fe and Pb differ significantly at 0.05 level, whereas only Cu differ at 0.01 level.

2. The linear correlation coefficients between pairs of elements in each group showed significant correlations at the 0.01 level between S/Co, K/Zn, Ca/Cu, Se/Pb and at the 0.05 level between S/Ni, K/Cu, Ca/Ni, Co/Zn and Br/Hg for the agitated elderly group. And significant interaction at 0.01 level between Ca/Cu, Ca/Ni, Ca/Zn, Pb/Hg, while at 0.05 level between K/Zn, Co/Se, Br/Hg, Br/Pb and Se/Hg for the non agitated group. Similar significant correlations were found in the two groups between Ca/Cu, K/Zn and Hg/Br.

3. Significant multiple correlations were found between Hg with (Se+Br); Pb with (Hg+Br); Se with (Pb+Hg+Br) and Ca with (Cu+Zn) in the non agitated group, while in the agitated group significance was found between Pb with (Se+Hg+Br), Ca with (Ni+Cu) and K with (Zn+Cu).

Similar observations to the low Cu observed in the agitated demented group compared with the control group, have been reported by Barlow (1980) in hair from three different types of mental abnormalities. The concentration of copper may be particularly relevant, because copper is

involved in DNA repair mechanisms, Hough (1978). The role of Cu enzymes in the central nervous system is known to be important O'Dell (1976), Prasad (1978), Yunica (1979).

As was mentioned in sec.IV.C the effect of a particular element cannot be considered in isolation as the elements interact with each other, Underwood (1977). Examples of the interactionship between elements are Ca and Pb, Barlow (1980), and Cu, Mo and S, Marcilese (1969) and Dick et al (1975). There is agreement between some significant correlations found in this work and relevant literature, sec.VI.B. The interaction between elements may be important from the point of view of therapy and/or the prevention of side effects, Barlow (1980). Therefore, the examination of interactions using linear and multiple correlations, between these elements which have been measured simultaneously is of particular value, and further investigations are desirable.

V.C Comparison of Results of PIXE and AAS Analysis:

All hair samples measured (secs.V.A and V.B) were analysed by atomic absorption spectroscopy (AAS) for comparison with the results obtained by PIXE. The AAS elemental concentrations for some elements are made in collaboration with the Environmental Health Department at the University. Hair samples were digested prior to analysis by AAS, by adding concentrated sulphuric acid to the hair sample, Barlow and Kopel (1982). The mixture was heated until fumes of sulphuric acid appeared. The flask was then removed from the hot plate and 25% hydrogen peroxide was added until a clear solution was obtained. The sample was heated further until no more peroxide was present. The samples were diluted with distilled water and used for the analysis. The results of these analyses, for the elements measured, together with PIXE results in the present work are represented in tables 5.27, 5.28 for the hyperactive and control groups, and in tables 5.29 and 5.30 for the agitated demented and non agitated groups respectively. Scatter diagrams are shown as examples in figures 5.24, 5.25 and 5.26 for hyperactive analysis; and 5.27, 5.28 and 5.29 for the agitated group. An example of the comparison between the individual measurements is shown in figures 5.30 for Ca, 5.31 for Cu, and 5.32 for Zn in the hyperactive group.

Although results of PIXE and AAS are related to different sample preparation and analytical methods, very good

Table 5.27

Results of PIXE and AAS measurements in hair of some elements in the hyperactive group.

Sample	Ca in ppm		Cu in ppm		Zn in ppm	
	PIXE	AAS	PIXE	AAS	PIXE	AAS
A	750	520	58	34	225	100
B	349	320	33	37	163	85
C	229	320	32	42	159	120
D	387	320	107	69	157	90
E	319	320	18	20	175	100
F	485	440	58	68	98	70
G	562	500	94	70	119	80
H	487	500	88	63	146	80
I	538	450	114	71	214	90
J	404	200	30	21	140	100
K	289	250	26	26	220	110
L	322	300	20	14	198	100
M	287	200	29	21	177	85
N	580	800	32	53	135	120
O	255	200	35	45	117	80
P	354	320	16	18	161	110
Q	486	520	17	19	157	100
R	604	520	14	18	188	100
S	1245	960	35	35	213	120
T	841	640	16	20	180	110
mean $\pm \sigma$	489±242	430±201	44±32	38±23	167±36	98±15
PIXE/ASS	1.14		1.16		1.7	
r	0.89		0.87		0.52	

Table 5.28

Results of PIXE and AAS measurements in hair elements in the non hyperactive control group

Sample	Ca in ppm		Cu in ppm		Zn in ppm	
	PIXE	AAS	PIXE	AAS	PIXE	AAS
CA	562	640	19	14	117	120
CB	281	320	37	38	94	120
CC	422	320	20	24	175	110
CD	822	720	31	34	256	120
CE	359	400	23	22	149	120
CF	423	400	37	22	263	100
CG	356	400	18	24	145	120
CH	649	720	22	32	158	120
CI	1565	1040	20	21	137	120
CJ	770	1440	22	38	167	120
CK	732	640	22	24	180	120
CL	421	360	31	25	189	120
CM	347	360	45	43	178	120
CN	895	720	62	80	152	120
CO	426	400	50	50	197	120
CP	1227	1040	366	120	152	120
CQ	1510	1360	227	100	171	150
CR	672	560	125	80	196	150
CS	752	1040	52	65	149	120
CT	855	1000	185	100	204	150
mean $\pm \sigma$	702±372	694±350	71±83	48±32	173±41	123±13
PIXE/AAS	1.01		1.47		1.41	
r	0.81		0.92		0.01	

Table 5.29

Results of PIXE nad AAS measurements in hair elements in agitated demented elderly population

Sample	Ca in ppm		Cu in ppm		Zn in ppm		Fe in ppm	
	PIXE	AAS	PIXE	AAS	PIXE	AAS	PIXE	AAS
PC1	1573	1357	37	26	245	120	38	16
PC2	193	320	33	33	222	135	57	16
PC3	496	616	21	23	161	108	38	51
PC4	225	317	24	25	199	127	25	22
PC5	222	338	30	43	208	134	32	31
PC6	1161	1190	17	21	175	127	95	16
PC7	291	439	8	45	199	102	23	17
PC8	349	994	19	24	129	90	35	29
PC9	462	860	12	20	48	60	42	15
PC10	131	239	13	13	160	104	32	29
PC11	230	301	27	29	132	100	30	41
PC12	1579	1546	38	41	160	131	37	15
PC13	367	-	25	-	181	-	22	-
PC14	567	1540	22	29	162	135	22	55
PC15	1084	1749	31	32	172	116	39	13
PC16	651	860	15	16	167	130	27	21
PC17	101	259	10	15	149	116	128	42
PC18	1019	1793	33	120	142	116	29	16
PC19	497	681	16	15	226	135	24	31
PC20	93	100	16	17	165	106	55	17
PC21	177	259	17	19	186	116	35	22
PC22	224	321	13	15	146	108	26	28
mean±S.D	486±442	591	22±9	24	170±41	111±	41±25	36
PIXE/AAS	0.82		0.92		1.53		1.14	
r	0.8		0.8		0.71			

Table 5.30

Results of PIXE and AAS measurements in hair elements in the non agitated demented elderly population.

Sample	Ca		Cu		Zn		Fe	
	PIXE	ASS	PIXE	AAS	PIXE	AAS	PIXE	AAS
PT1	239	361	15	24	89	80	23	21
PT2	1009	1537	35	32	191	106	19	18
PT3	155	260	18	22	163	108	16	17
PT4	751	321	36	24	170	125	19	13
PT5	203	200	26	24	203	110	40	24
PT6	274	262	23	35	157	141	48	29
PT7	545	1060	21	13	152	95	28	60
PT8	907	924	47	54	188	122	20	31
PT9	1015	2000	19	34	167	110	28	43
PT10	169	198	18	19	189	114	21	21
PT11	662	1000	41	55	146	100	44	9
PT12	1150	1120	38	40	136	106	19	8
PT13	1083	934	60	42	112	99	24	31
PT14	733	996	25	30	253	147	26	46
PT15	286	299	37	30	178	114	25	43
PT16	211	238	42	42	183	119	29	22
PT17	126	199	16	19.5	135	95	22	33
PT18	192	240	32	33	170	128	24	47
PT19	213	319	24	25	188	106	14	29
PT20	145	436	20	27	219	121	49	49
mean±S.D.	503±370	645	30±12	31	169±37	112	27±10	30
PIXE/AAS	0.78		0.97		1.51		0.9	
r	0.88		0.74		0.71			

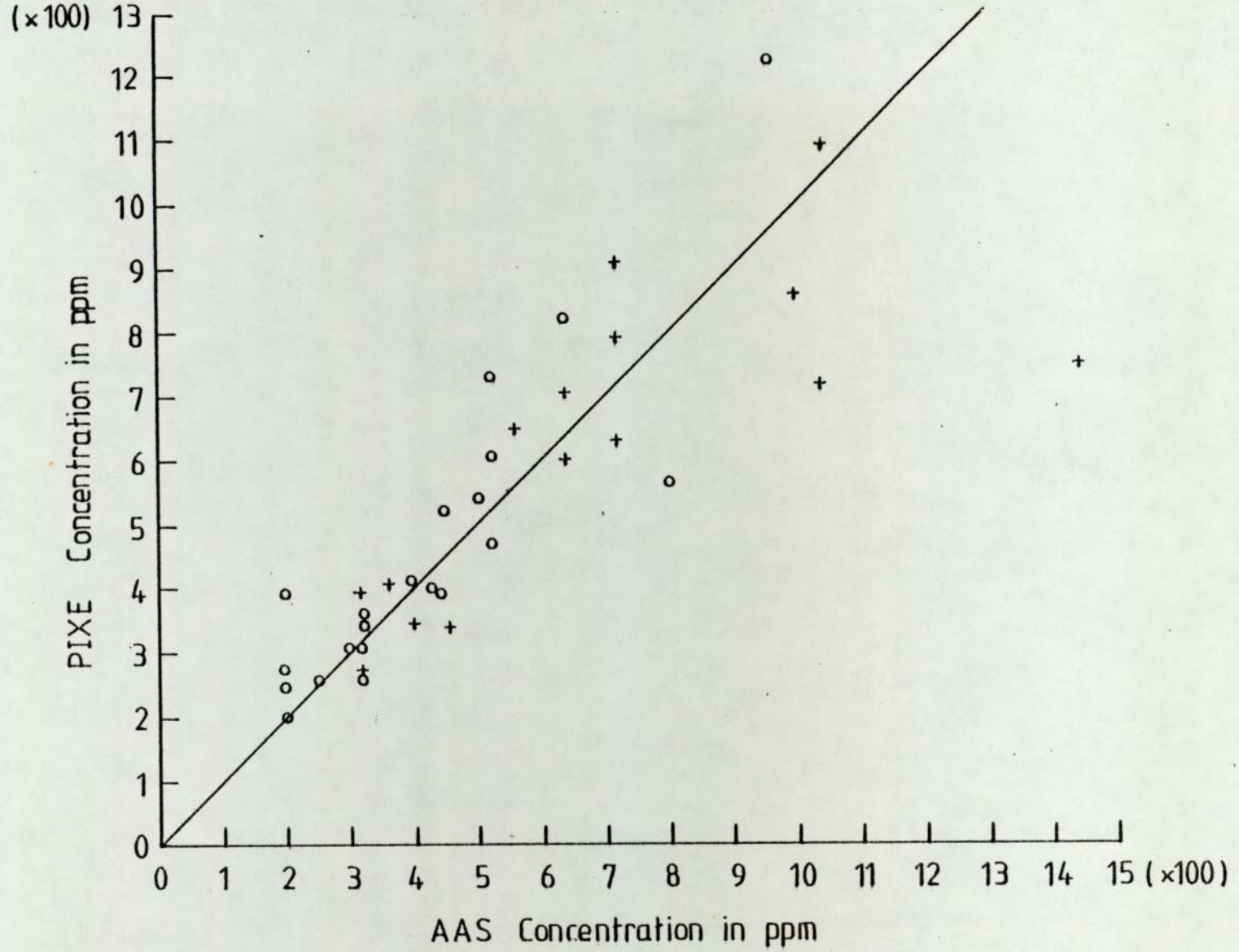

Fig 5.24 Scatter diagram for Ca between PIXE and AAS results in the hyperactive and control groups. (∘ hyperactive, + control)

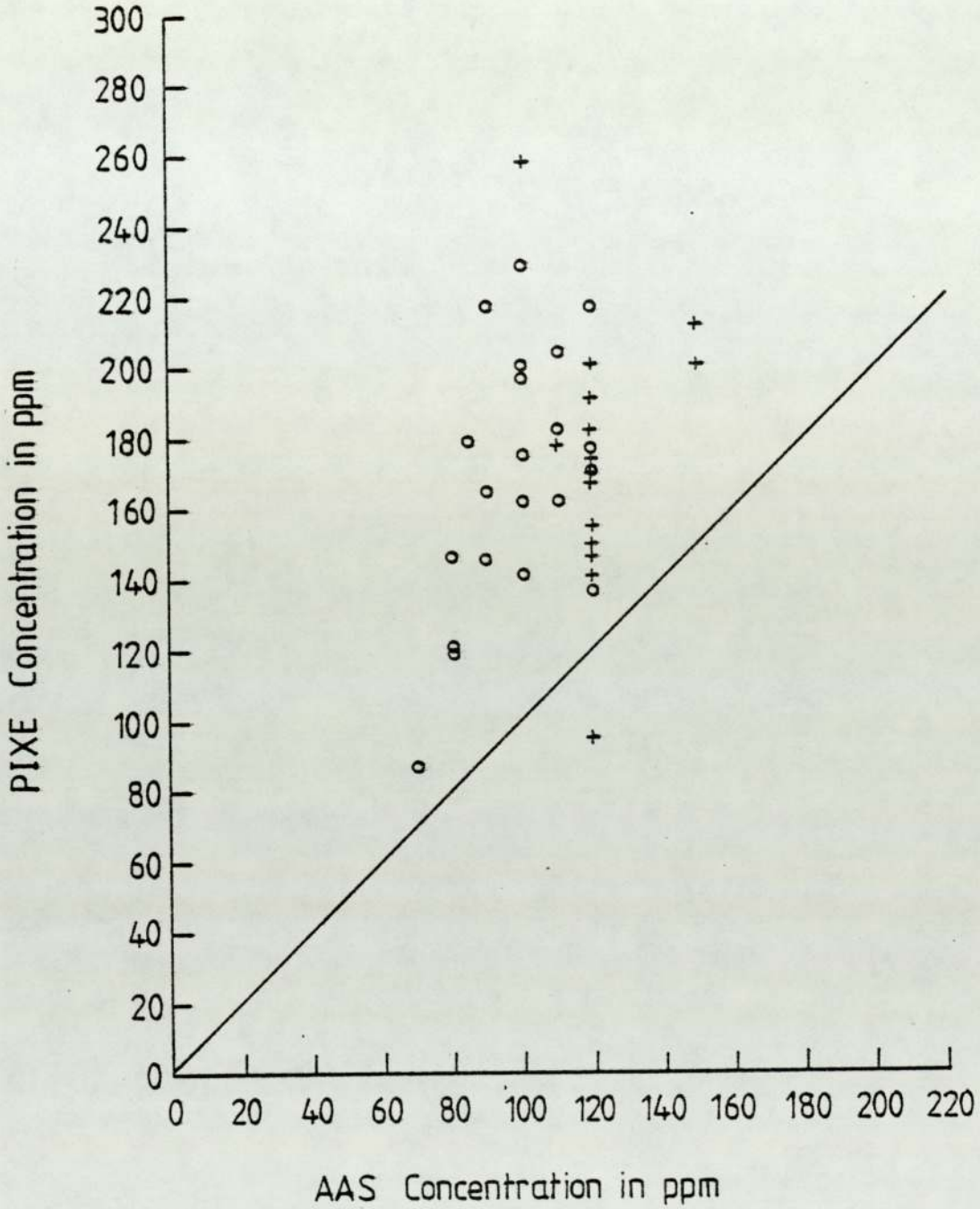

Fig 5.25 Scatter diagram for Zn between PIXE and AAS results in the hyperactive and control groups. (∘ hyperactive, + control)

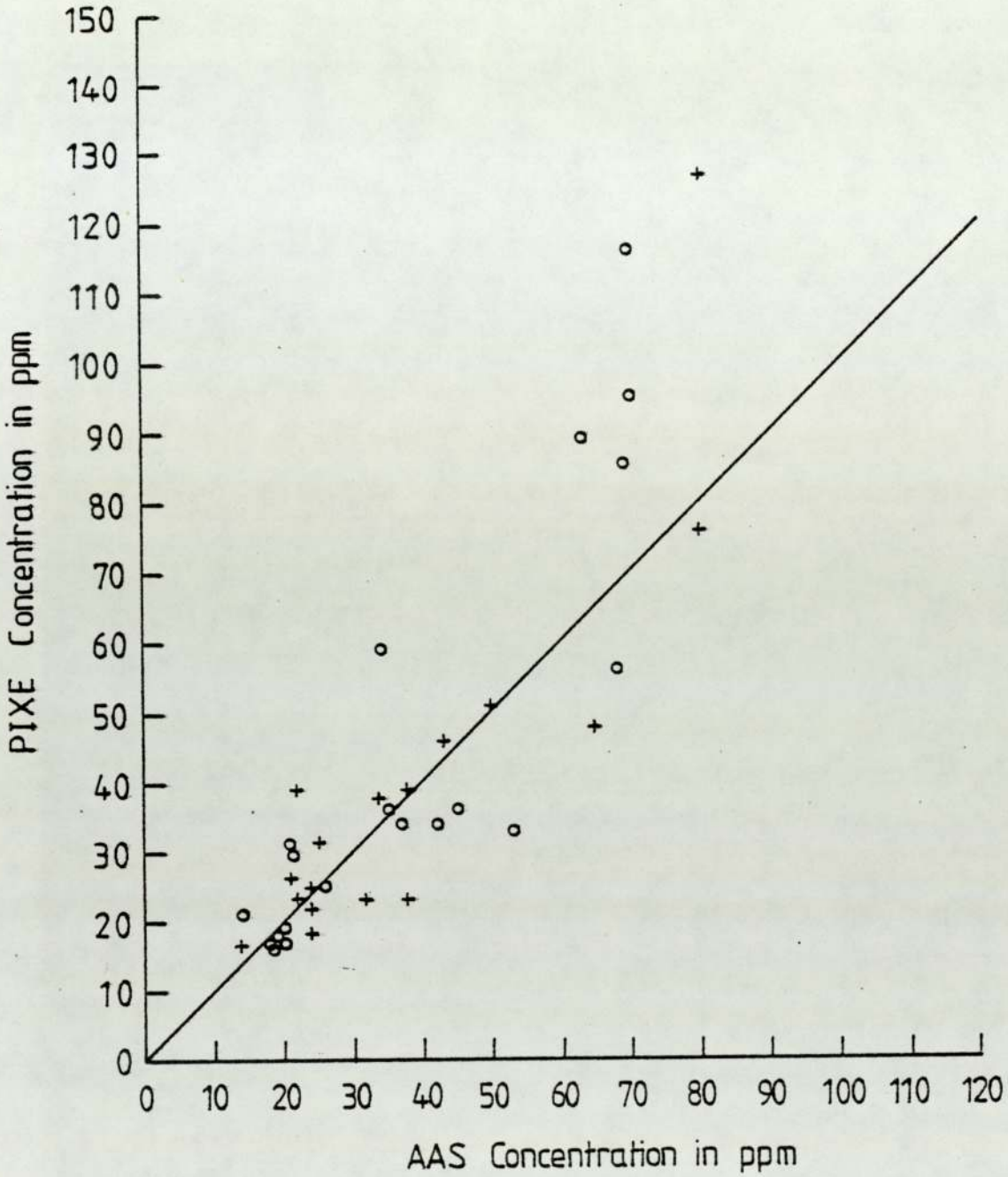

Fig 5.26 Scatter diagram for Cu between PIXE and AAS results, the hyperactive and control groups.
(∘ hyperactive , + control)

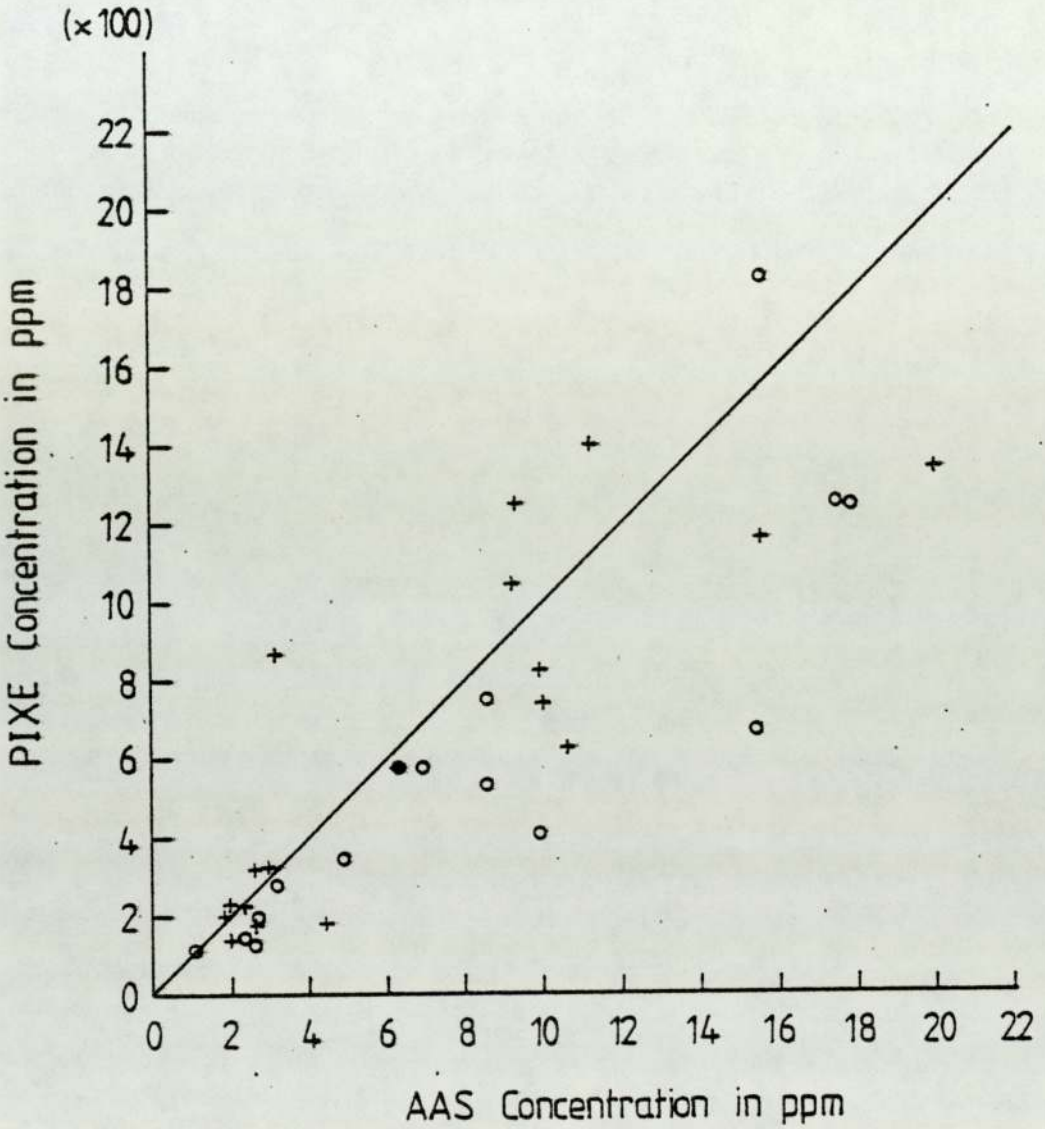

Fig 5.27 Scatter diagram between PIXE and AAS for Ca in the agitated and non-agitated groups. (∘ agitated, + non-agitated)

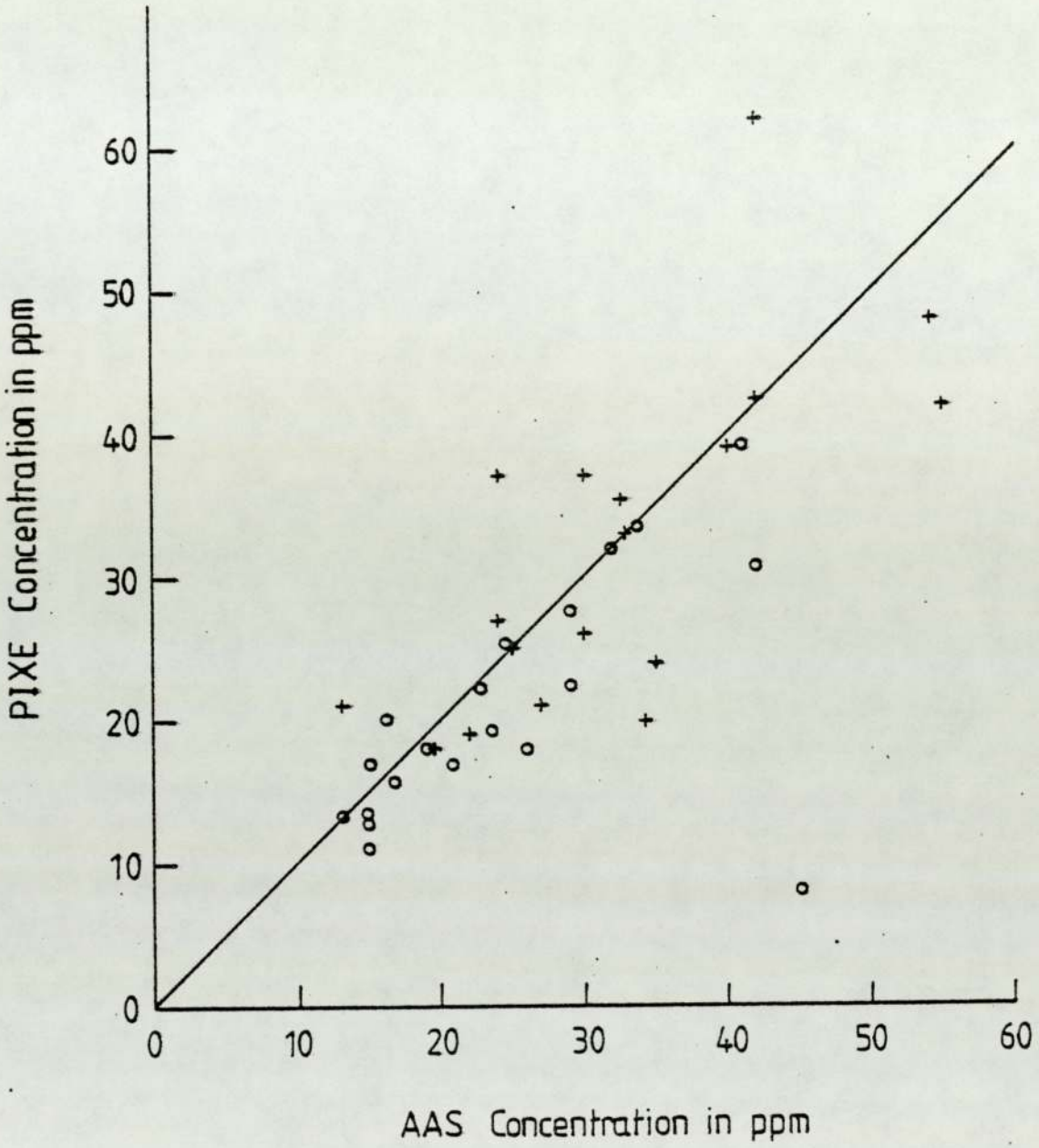

Fig 5.28 Scatter diagram between PIXE and AAS for Cu in the agitated and non-agitated control groups. (∘ agitated, + non-agitated)

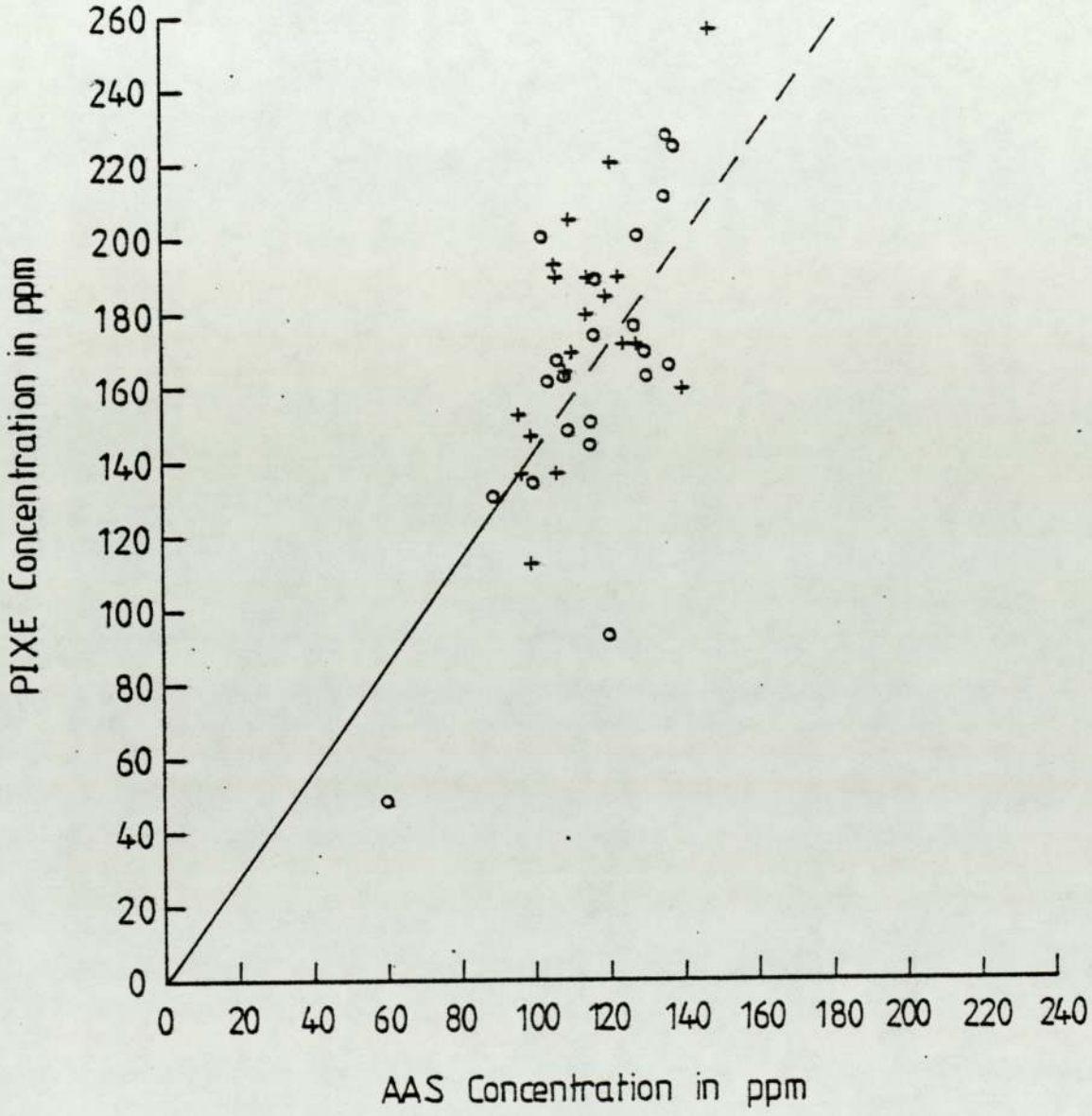

Fig 5.29 Scatter diagram for Zn between PIXE and AAS results in the agitated and non-agitated groups. (∘ agitated, + control)

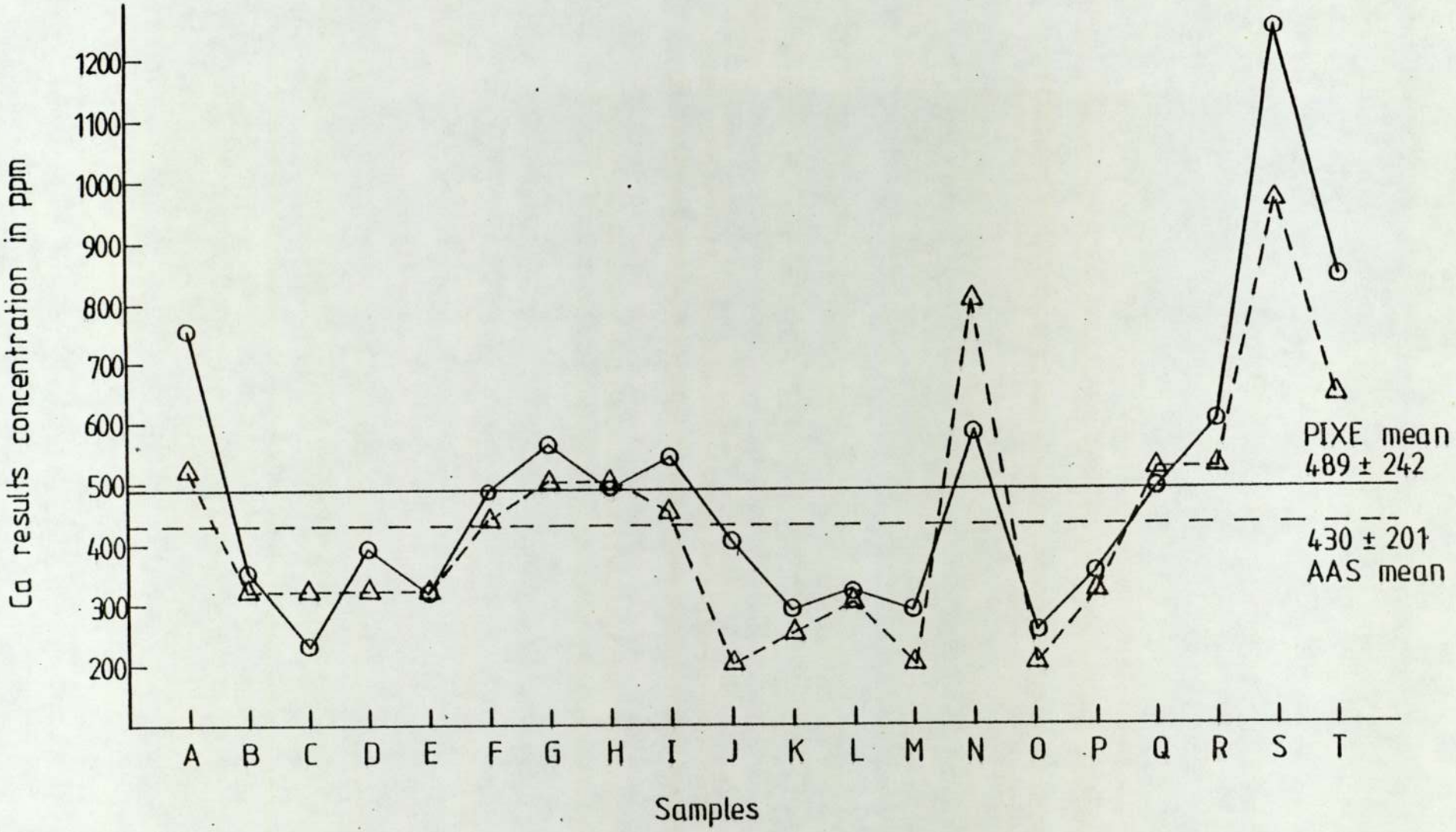

Fig 5.30 Comparison between PIXE and AAS in the individuals of Ca measurements for hyperactive group. (O PIXE, Δ AAS)

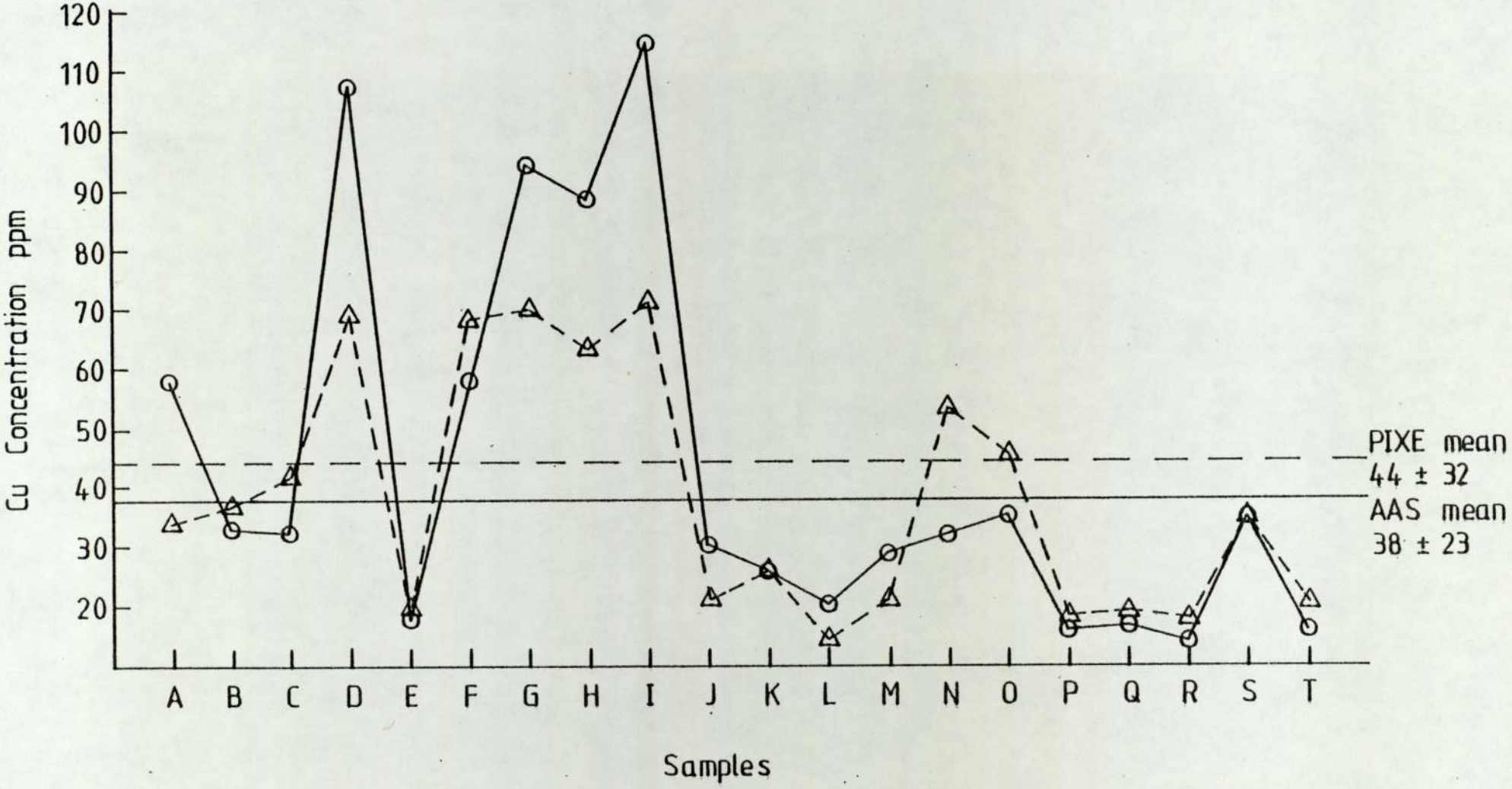

Fig 5.31 Comparison between PIXE and AAS in the individuals of the Cu measurements for the hyperactive group. (O PIXE, Δ AAS)

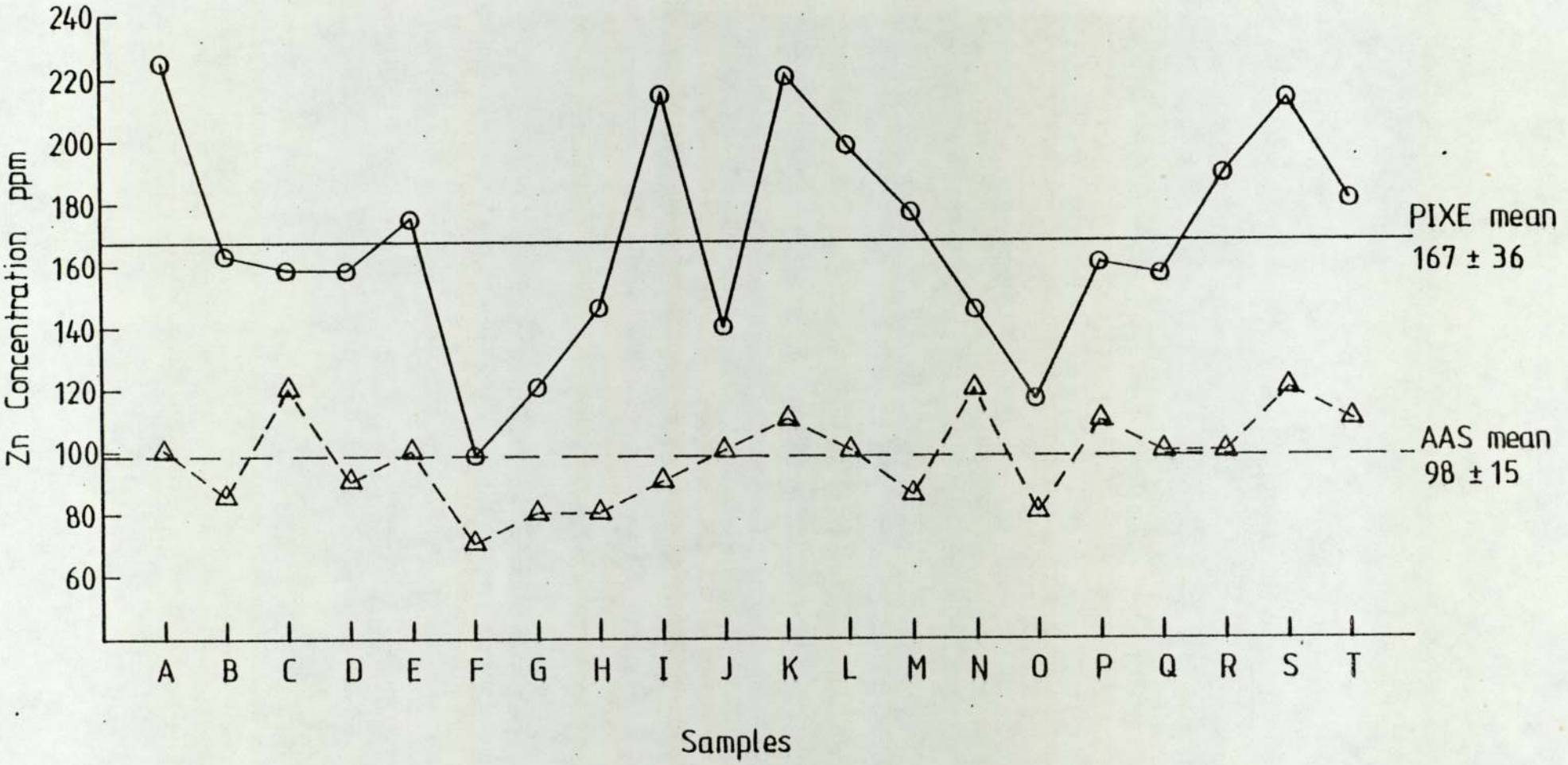

Fig 5.32 Comparison between PIXE and AAS in the individuals of the Zn measurements for the hyperactive group. (O PIXE, Δ AAS)

agreement was found in Ca, and Cu with correlation coefficients 0.81 and 0.92 in the hyperactive control group, 0.89, 0.87 for hyperactive, 0.88, 0.74 for agitated control, and 0.8 , 0.9 for agitated, which are highly significant at probability < 0.001.

From the diagrams 5.25 and 5.29 the consistently higher Zn found by PIXE is probably related to the sample preparation methods involved. Since the standard bovine liver sample described earlier, sec.III.C, was prepared and analysed by identical methods with those used for the hair samples, errors due to sample preparation or calibration should be similar for both. While PIXE results for Zn were higher than the AAS results, PIXE Zn levels in the bovine livers standard were in very good agreement with the NBS value, while AAS Zn levels in the bovine liver showed lower levels than the NBS values, Saied (1981). Comparison between AAS done in the University of Aston and the results from Mineralab Inc., U.S.A., who also used AAS, but a nitric acid digestion, showed higher levels of Zn for the Mineralab (Barlow 1980), as did PIXE. Nielson(1975), in comparison with different sample preparation methods, noted higher levels of Zn when nitric acid was used in the digestion.

The reason for the disagreement sometimes seen in Fe individual absolute measurements is not known, the AAS has strong interference with this element. The PIXE measurements of Fe for bovine liver showed good agreement

with NBS certified values.

The main application of the hair analysis is to compare between hyperactive and control children, likewise between agitated demented and control elderly groups. The averages of the elemental concentrations are represented in table 5.31 with the averages from AAS. The ratio of the results, which represents the comparison between the groups, are also given for PIXE and AAS. The differences in this comparison is found to be 6% for Ca, 12% for Cu and 9% for Zn, these figures are for the case in hyperactive comparison, which are within the accuracy of PIXE for this group, table 3.21 sec.III.F.

In the agitated the differences are down to 2.8% for Ca, 2.6% for Cu, 1% for Zn and 11% for Fe. Which are within the accuracy of PIXE table 3.28. This is perhaps not surprising since the accuracy was improved in the agitated analysis by improving the statistical accuracy, by increasing the counts in the internal standard sec.III.F, and improving the counts statistics using the new PIXE system sec.III.A.

It is worth noting that PIXE measurement in the present work is the result of only one target measurement per sample.

The agreement obtained by the two different techniques is obviously somewhat of an advantage, it does evaluate the usefulness of the results. It does mean, however, that

Table 5.31

Ratio of the results in hair analysis for PIXE and AAS

Groups	mean elemental concentration in ppm and the ratio							
	Ca		Cu		Zn		Fe	
	PIXE	AAS	PIXE	AAS	PIXE	AAS	PIXE	AAS
hyperactive	489	430	44	38	167	98		
control	702	694	71	48	173	123		
ratio hyper/ cont.	0.7	0.62	0.62	0.79	0.96	0.80		
difference	6%		12%		9%			
agitated	503	645	30	31	169	112	27	30
non agitated	486	591	22	24	170	111	41	36
ratio agit/ cont.	1.03	1.09	1.36	1.29	0.99	1.01	0.66	0.83
difference	2.8%		2.6%		1%		11%	

the PIXE technique is highly reliable and can be used for one target analysis with confidence. It could give quicker analysis if it is automatized and computerized.

CHAPTER VI

CONCLUSIONS AND SUGGESTIONS FOR FUTURE WORK

In the fourteen years since the initial studies of Johansson et al (1970), PIXE researchers have made remarkable progress in optimizing the technique, discovering new areas of applications and in demonstrating to the analytical community that PIXE is a powerful and quantitative tool. The studies in this thesis have demonstrated the usefulness of PIXE for multielemental analysis in a major study of biomedical interest - particularly of hair sample analysis from mentally retarded groups. It is worthwhile at this point to briefly summarize the work done, conclusions and the future suggestions.

VI.A Summary:

A proton induced x-ray emission analysis system, Sec.III.A, has been successfully used to give, quantitative, multi-element analysis of elements S, K, Ca, Fe, Co, Ni, Cu, Zn, Se, Br, Hg and Pb. Calibration was accomplished using thin targets of standard foils, sec.III.C, and this is in good agreement with the calculated calibration, using tabulated cross sections data. Calibration accuracy was also established in two independent comparisons using bovine liver Standard Reference Material 1577 and Standard hair powder HH-1, sec.III.C. Quantitative measurements were normalized to a single yttrium internal standard which

eliminated small daily calibration fluctuations, uncertainties in charge collection and beam area. All results are corrected for target thickness effects using a computed correction factor,Sec.III.C.

The PIXE analysis system was applied to mental disorders using hair samples taken from patients suffering from hyperactivity in the young and agitation in the elderly. Including controls four hair sets were involved in the study, each set being of 20 or more samples. One target was analysed from each sample. Elemental concentrations for the elements mentioned above were tabulated for the hair analysis. Detection limits for the different elements have been calculated for hair samples and are reported in sec.III.E.

Analysis of the significance of differences, using the t-test, was applied to the elemental concentrations between the groups under investigation. The t-test indicated significant differences between hyperactive children and non-hyperactive control group, in K and Ca at the P=0.025 level. The hyperactive group showed higher levels of K, and lower levels of Ca. Extremely high Se and Hg levels were observed in a few female samples in the control group only. Significance tests showed higher Se for females than males in this group. Three differences were observed to be significant at the P=0.025 between agitated and non agitated control groups. Cu and Pb levels in the agitated were lower than

in the non agitated, while the Fe level showed higher levels in the agitated than in the non agitated.

Statistical techniques of correlation and multiple linear regression were then used to find the inter-relationships of all the measured elements.

All hair samples were also analysed by AAS for Ca, Fe, Cu and Zn to compare with the PIXE results. Although comparison of PIXE and AAS results involved comparison of sample preparation methods as well as analytical methods, results of Ca and Cu are encouraging. Consistently higher concentrations were noted in PIXE for Zn, but Zn analysis in the bovine liver SRM showed good agreement between PIXE and the NBS certified values. The differences between PIXE and AAS (table 5.31) in the hair element ratios, i.e. elemental concentration in the agitated group to that of the control group, were within 2.8% for Ca, 2.6% for Cu, 1% for Zn and 11% for Fe, which are within the experimental accuracy of the PIXE measurements.

VI.B Conclusions:

It is apparent, from the previous part of this thesis, that a good deal of information may be obtained on the levels of elements in hair using PIXE analysis. PIXE has the advantages of being a multielement technique, where reasonable sensitivities are obtained, but interelement

interferences can limit PIXE sensitivity, as well as the accuracy, and precision of the results. Measurements of a set of elements in one target at the same time has the advantage of looking at the possibility of interaction between elements by calculating linear and multiple correlation coefficients, and where a significant correlation coefficient is found this implies there is a real interaction between the elements. Using hair samples has the advantages, sec.IV.D, that specimens can be collected easily without pain to the donors, the collection needs no special training, equipment, or storage facilities. Moreover, the concentration of many elements is relatively high, a factor which makes the analysis more practicable. It is important to collect a full history as well as other information for each sample examined to ensure that the groups are comparable. The concentration values are influenced by several factors discussed in detail in sec.IV.E. Thus the analysis of an untreated hair sample, taken as close as possible to the scalp, and unwashed should give results truly reflecting the levels present in the body. The measurements of hair trace elements does have the advantage of looking at the mean level of a set of elements over a period of time (dependent upon the length of hair digested) rather than at an instant of time as in the case of blood analysis.

All the samples examined in the present study were obtained from patients whose histories were known, and who come from the same institution. However, when all

the various factors that can affect the hair elemental levels are considered, the following relationships appear to exist:

1. There is a significant difference between the levels of K and Ca in child hyperactive patients and those in controls, with levels in the control being lower in K and higher in Ca than in the hyperactive group.

2. In the group of hyperactive children examined there is no evidence of high levels of the elements Se and Hg. However, in the control group some samples do show very high levels of one or both of these elements, sec.V.A.3.

3. There is a significant difference between the levels of Se in the female to those of the male in this control group.

4. There is a significant difference between the levels of Fe, Cu and Pb in the agitated demented elderly people compared with non agitated demented control group with lower levels of Cu and Pb, and higher Fe in the agitated group.

The significant differences found in the present study seem to confirm that the differences in hair elemental levels do exist for certain groups suffering from particular pathological conditions. These elemental imbalances may be related directly to the pathological conditions present in the donors, and continued clinical studies will give more precise answers.

5. Several elements tended to increase and decrease together in the hair specimens. From table 5.15 there are 14 significant correlations for the hyperactive children and 6 significant correlations for the control group at $P < 0.05$. All significant correlations showed positive trends for these two groups. Agreement between some of the significant correlations was found in the two groups for Co/Ni, Co/Hg and Ca/Pb. From table 5.26, there are nine significant correlations for the agitated group and nine significant in the non agitated control group. Ten of the total significant correlations showed a negative, or inverse trend. Agreement between significant correlations was found in the two groups for Ca/Cu, K/Zn and Hg/Br.

Some significant correlations do support the previous demonstration of elemental interaction in hair analysis. These are significant correlations between K/Zn and Ca/Cu in both agitated and the control groups, a similar finding in disabled subjects was reported by Pihl et al (1980). The significant correlations between Ca/Pb in the hyperactive and Cu/Pb in the control, are similar to findings reported by Barlow (1980) in a control group.

6. Multiple linear regression was applied to the correlated elements and significant multiple correlations were found between Pb/Hg+Br; Se/Br+Hg+Pb; Hg/Se+Br; Ca/Cu+Zn in the agitated group and significant multiple correlations between Ca/Ni+Cu; K/Cu+Zn; Pb/Se+Hg+Br in the non agitated control group.

VI.C Suggestions For Future Work:

1. Some further work relative to agitated demented patients is needed to examine more fully the significance of the low levels of Cu.

2. For hair tissues to give a complete picture of the body burden of a particular element, it is necessary to show some relationship between the level in the hair and in other organs or tissues, further analysis of fluids or tissues in the agitated group is needed, to study more fully the significance of the low levels of Cu.

3. It is important to measure the "normal levels" for normal subjects selected under the same consideration as the patients group, using the same technique for sample preparation and analysis.

4. A more detailed investigation into the elemental interactions using the statistical techniques of correlation coefficients and multiple linear regression.

5. All analysis results should be validated by the use of certified Standard Reference Materials, and if possible to be compared with the data from at least two methods, which differ in basic procedures (including digestion).

6. In biomedical applications, where large numbers of

samples are analysed, the development of fully automated, computerised PIXE analysis system is needed.

7. One can make use of nuclear reactions induced in the target by the incident proton beam to extend the analytical capability of the system to atomic number Z less than 13.

8. Finally, the closest possible collaboration between individual laboratories should be encouraged, and in particular between the analytical physicist and the clinical biochemist.

Appendix

Correction Factor Program

The purpose of this program is to calculate the correction factors, in moderately thick targets, for the reduction in x-ray yields due to proton energy loss and x-ray absorption effects (refer to fig.3.22).

i) Introduction

The number of x-ray counts Y_z generated by element Z in a thin target is given by

$$Y_Z(t) = N_p \, \varepsilon_{int} \frac{\Omega}{4\pi} \cdot \left(\frac{N_o \, t \, n_z}{M}\right) \sigma_z(0) \qquad \text{A.1}$$

where

$\sigma_z(0)$ = x-ray production cross section (cm^2/atom)

N_p = number of protons which pass through the target

ε_{int} = detector efficiency including absorption through windows, air space, and absorbing filters

N_o = Avogadro's number (molecules/mole)

t = effective target thickness (g/cm^2)

n_z = number of atoms of element Z per molecule of matrix

M = molecular weight of matrix (g/mole)

Ω = solid angle subtended by the detector

For thicker targets, the detected x-ray Y'_Z is given by:

$$Y'_Z = N_p \cdot \varepsilon_{int} \frac{\Omega}{4\pi} \cdot \frac{N_o \, n_z}{M} \int_o^t \sigma_z(x) . U_z(x) dx \qquad A.2$$

where

$\sigma_z(x)$ = x-ray production cross section for element Z at thickness x(cm^2/atom)

$U_Z(x)$ = transmission factor for characteristic x-ray of element Z at depth X(E)

$$= \exp \left[-\int_o^t \mu_Z \cot \phi \, dx \right]$$

$$= \exp \left[-\int_o^t \mu_Z \, dx \right] \qquad \text{where } \phi = 45^o \text{ in this work}$$

where $\mu_Z = \sum_j \frac{\mu_{zj} C_j}{M}$ where $\sum_j$ represents the sum over all elements in the matrix and

μ_{zj} = attenuation coefficient (cm^2/g) for x-rays of element Z in sample matrix

$\frac{C_j}{M}$ = fraction by weight of element j in matrix

ϕ = target angle

The depth X in this integral is related to the decreasing proton energy E by the stopping power formula

$S(E) = -(dE/dx)$ where

$S(E)$ = composite stopping power of a matrix (keV.cm^2/g)

$$= \sum_j \frac{C_j \, S_j(E)}{M}$$

$S_j(E)$ = stopping power of matrix element j for protons of energy E (keV.cm^2/g)

ii) Correction Factors

The quantities of interest in PIXE analysis are the absolute abundances M (gram) of element Z in the target where:

$$M_Z(\text{gram}) = C(Z).Y_Z'.A_B/F(Z).Q.C_{AL} \qquad A.3$$

from equation 3.7

Here, $F(Z)$ = thin-target detection efficiency for element Z (Counts/$\mu c.\mu g.cm^{-2}$).

Q = total integrated charge (μc)

$C(Z)$ = thick-target yield correction factor

A_B = proton beam area (cm^2)

C_{AL} = x-ray absorption in the Al absorber

The values Y_Z, Q, F(Z), A_B, and C_{AL} all known or measured. In order to calculate expected values for M_Z, the correction factor C(Z) must be determined.

The correction factor is defined as the ratio of the thin-target x-ray yield $Y_Z(t)$ to the detected thick-target yield Y_Z' :

$$C(Z) = \frac{Y_Z(t)}{Y_Z'} = \sigma_z(0).t. \left[\int_0^t \sigma_z(x).U_z(x)\, dx\right]^{-1} \qquad A.4$$

if the target is thick so that the beam stop in the target then t is replaced by the proton range R .

iii) The Approximation Used

The approximations used for the calculation of equation A.4 are:

a) The slowing down of the proton energy as a function of the proton penetration depth was calculated using the atomic stopping power formula, by Andersen and Ziegler(1977), in the energy range of interest.

b) The production of the analyte x-rays, i.e. the characteristic x-ray production cross section $\sigma_z(E)$, which becomes a function of X by slowing down via

$$\sigma_z(X) = \sigma_z(E)$$

The semi empirical function by Akselsson and Johansson(1974) was used for the ionization cross-section calculation.

c) The self absorption of the emitted x-rays, i.e. the differential yield which emerges from the different depth layers of the target.

The x-ray mass absorption coefficients are calculated using, Montenegro et al polynomial (1978), the fitted third degree polynomial to the values tabulated by Storm and Israel.

iv) Numerical Calculations

The integration in equation A.4 was carried out stepwise using a selected finite thickness stepsize ΔX. In essence, the thick target is treated as a composite of many thin slabs each of which causes a loss of energy ΔE in the proton beam.

A computer program was written for calculating C(Z), the correction factor for 21 elements K-lines emitter, Fig.A.1 represents the flow-chart for this program.

The program was provided by:

1. incident proton energy
2. target thickness
3. the number of layers composing the target
4. the stepsize ΔX
5. tables of x-ray energies for the reference line of the 21 elements
6. tables of ionization energies for the elements.

A useful secondary function of the program is to calculate selected K-shell x-ray ionization cross sections at arbitrary energies.

The final calculation output by this program include correction factors C(Z) for 21 K-line elements, the proton energies, the ionization cross sections, and the

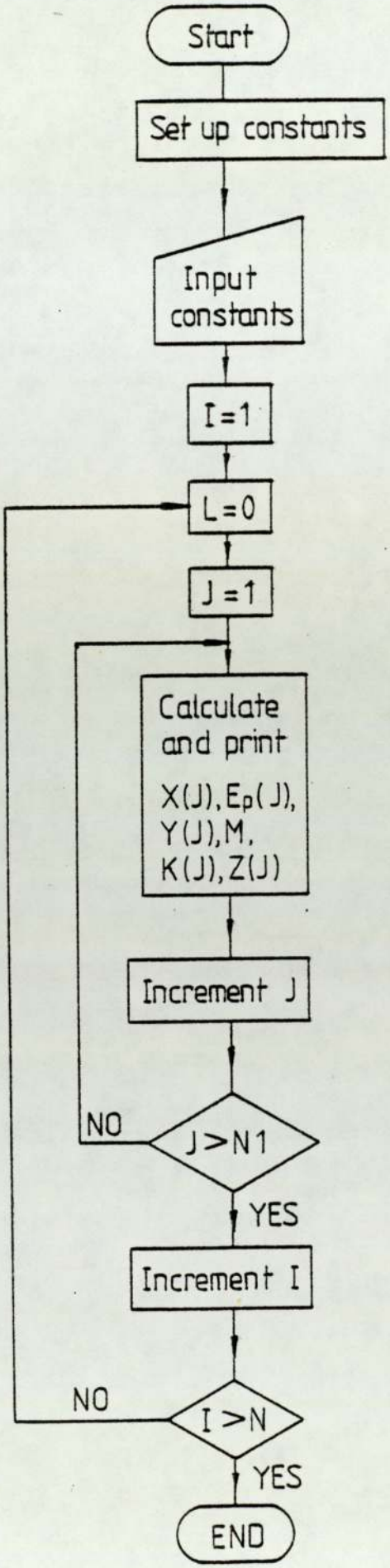

X(J) Thickness of J
$E_p(J)$ Proton energy J
Y(J) X-ray ionization cross section at J
M Mass absorption coefficient
K(J) Attenuation of x-ray in the thickness
Z(J) Correction factor at J

Fig A:1 Flow-chart for the computer program used in calculating the correction factor

x-ray attenuation. Examples of such calculations are represented in table A.1 for Cu in 6 mg/cm^2 NO_3 matrix.

Table A1

Output of the computer program for calculating correction factor for Cu in No_3 matrix

Target thickness mg/cm^2	Proton energy keV	Ionization cross-section of order 10^{-24} cm^2/atom	X-ray attenuation	Correction factor C(Z)
0.1	2358.27	136.78	0.999	1.011
0.3	2334.74	134.10	0.997	1.022
0.5	2311.03	131.40	0.995	1.033
0.7	2287.14	128.70	0.993	1.044
0.9	2263.08	126.00	0.992	1.056
1.1	2238.83	123.30	0.990	1.067
1.3	2214.39	120.59	0.988	1.080
1.5	2189.75	117.88	0.986	1.092
1.7	2164.92	115.17	0.984	1.105
1.9	2139.88	112.46	0.982	1.118
2.1	2114.63	109.74	0.980	1.131
2.3	2089.16	107.03	0.978	1.145
2.5	2063.47	104.31	0.977	1.159
2.7	2037.55	101.59	0.975	1.173
2.9	2011.40	98.88	0.973	1.187
3.1	1985.00	96.16	0.971	1.202
3.3	1958.36	93.45	0.969	1.217
3.5	1931.45	90.74	0.967	1.233
3.7	1904.28	88.03	0.966	1.249
3.9	1876.83	85.33	0.964	1.265
4.1	1849.10	82.63	0.962	1.282
4.3	1821.07	79.93	0.960	1.299
4.5	1792.74	77.24	0.958	1.316
4.9	1735.11	71.89	0.955	1.352
5.1	1705.80	69.22	0.953	1.371
5.5	1646.09	63.91	0.949	1.409
5.9	1584.85	58.66	0.946	1.450

REFERENCES

1. U.Abondanno, A.Boiti and F.Demanins, The application of a non iterative method for fitting a gaussian peak from Ge(Li) and Si detectors, Nucl. Inst. Meth. 142, (1977), 605-607

2. M.Agarwal, R.B.Bennett, I.B.Stump, J.M.D'Auria, Analysis of urine for trace elements by energy dispersive x-ray fluorescence spectrometry with a pre-concentrating chelating resin, Anal. Chem. 47, (1975), 924-927

3. M.Ahlberg, G.Johansson and K.Malnqvist, Elimination of charging the PIXE analysis of insulating samples, Nucl. Inst. Meth., 131, (1975), 377-379

4. M.Ahlberg, Enhancement in PIXE analysis, Nucl. Inst. Meth. 142, (1977), 61-65

5. R.Akselsson, and T.B.Johansson, X-ray production by 1.5-11 MeV protons, Z. Physik., 266, (1974), 245-255

6. K.R.Akselsson and S.A.E.Johansson, PIXE analysis research in Lund , IEEE trans. on nucl. sci. Vol.NS-26 No.1, (1979), 1358-1362

7. K.Alder, A.Bohr, T.Huus, B.Mottelson and A.Winther, Study of nuclear structure by electromagnetic excitation with accelerated ions, Rev. Mod. Phys. 28, (1956), 432-542

8. M.E.Alexander, E.K.Biegert, J.K.Jones, R.S.Thurston, V.Valcovic, R.M.Wheeler, C.A.Wingate and T.Zabel, Trace element analysis of sea-water and fish samples by protons induced x-ray emission spectroscopy, Int. J. Appl. Rad. Isotops. 25, (1974), 229-233

9. R.J.Anderson, Caries. Res., 3, (1969), 75

10. H.H.Anderson and J.F.Ziegler, Hydrogen stopping powers and ranges in all elements, Vol.3, (1977), Pergamon Press Inc., New York.

11. H.Baba, S.Baba and T.Suzuki, Effect of the base line shape on the unfolding of peaks in the Ge(Li) γ-ray spectrum analysis, Nucl. Inst. Meth., 145, (1977), 517-523

12. J.Bacso, L.Sarkadi and E.Koltay, Endogenous and Exogenous calcium content of hair samples used in XRF and PIXE measurements, Int. J. Appl. Radiant Isotop, 33, (1982), 5-11.

13. P.A.Baedecker, Digital methods of photopeak integration in activation analysis, Anal. Chem. 43, (1971), 405-410

14. W.Bambynek, B.Crasemann, R.W.Fink, H.U.Freund, H.Mark, C.D.Swift, R.E.Price and P.V.Rao, X-ray fluorescence yields, Auger and Coster-Kronig transition probabilities, Re. Phys. 44, (1972), 716-813

15. J.Bang, J.M.Hansteen, Kgl. Dansk. Videnskab, Selskab. Mat.-Fys. Medd., 31, (1959), No.13

16. S.E.Bouman, E.T.Williams, H.L.Finston, A.H.Bond Jr., and P.M.S.Lesser, Quantitative analysis by proton induced x-ray emission utilising and inexpensive external-Beam system, Nucl. Inst. Meth. 165, (1979) 57-62

17. G.B.Baptista, E.C.Montenegro, A.C.Paschoa and C.V.Barrosleite, Analysis of trace elements in human hair by PIXE, Nucl. Inst. Meth. 181, (1981), 263-267

18. P.J.Barlow, Ph.D. Thesis, University of Leeds (1980)

19. P.J.Barlow and M.Kopel, Metal levels in the hair of hyperactive children, to be published (1982)

20. P.J.Barlow and M.Kopel, Chapter seven in Hair analysis elements and human illness, by Brown, Poeger Publishers (1980)

21. P.J.Barlow, P.E.Sylvester and J.W.T.Dickerson, Hair trace metal levels in Downs Syndrome patients, J. Ment. Defic. Res. 25 (1981), 161-168

22. M.Barrette, G.Lamoureux, E.Lebel and R.LeComte, P.Paradis and S.Sonaro, Trace element analysis of freeze dried blood serum by proton and alpha induced x-rays, Nucl. Inst. Meth. 134, (1976), 189-196

23. M.Barrette, G.Lamoureux, R.LeComte, P.Paradis, S.Monaro and H.A.Menard, Trace element determination in serum by proton induced x-ray emission, J. Rheumatology Supp. No.5,6 (1979 a), 40-44

24. M.Barrette, H.A.Menard, G.Lamoureux, R.LeComte, P.Paradis, S.Monaro and G.Drapoan, Trace elements and acute phase reactants in gold treatment Rheumatoid Arthritis patients, the Journal of Rheumatology Supplements No.5 (1979 b), 143-148

25. M.Barrette, R.LeComte, P.Paradis, S.Monaro, G.Lamoureux and H.A.Menard, Trace element analysis in rheumatoid arthritis under chrysotherapy, Nucl. Inst. Meth. 181, (1981), 301-303

26. G.Basbas, W.Brandt and R.Lambert, Universal cross-section for K-shell ionization by heavy charged particles. I.Low particle velocities, Phys. Rev.A 7, (1973), 983-1001

27. R.M.Baum, R.D.Willis, R.L.Walter, W.F.Guthnecht, and A.R.Stiles, X-ray fluorescence analysis of environmental samples, Edt., Dgubay,T.G., (Ann Arbor Sci., Ann Arbor, (1977), 165

28. R.C.Bearse, D.A.Close, J.J.Malanify and C.J.Umberger, Elemental analysis of whole blood using proton induced x-ray emission, Anal. Chem. 46, (1974), 499-503

29. K.F.Bergmann, G.Makosch, K.H.Tems, Abnormalities of hair Zn concentration in matters of new born infants with spina bifida, Am. J. Clin. Nutr., 33, (1980), 2145-2150

30. M.Berti, G.Buso, P.Calautti, G.Maschini, B.M.Stievano and C.Tregnaghi, Determination of Se in blood serum by proton induced x-ray emission, Anal. Chem. 49, (1977), 1313-1315

31. E.P.Bertin, Introduction to x-ray spectrometric analysis, Plenum Press, New York and London (1978).

32. P.R.Bevington, Data reduction and error analysis for the physical sciences, by McGraw-Hill, Inc. Printed in the USA (1969).

33. J.Bland, Trace elements in human health and disease, University of Puget Sound, Tacome, Washington (1979).

34. Bodart, Report of the coordinated research meeting on nuclear based methods for the analysis of pollutants in human hair, C E N - Saclay (IAEA, Vienna 1978)

35. H.J.M.Bowen, Problems in the elementary analysis of standard biological meterials, J.Radional. Chem. 19, (1974), 215-226

36. H.J.M.Bowen, The requirement of medicine for trace element analysis in the 21st Century, Trace elements analytical chemistry in medicine, editors P.Bratter, P.Schramel, Walter de Gruyter, New York (1980)

37. W.Brandt and G.Lapicki, L-shell coulomb ionization by heavy charged particles, Phys. Rev. A 20, (1979), 463-480

38. A.C.Brown, Hair trace elements and human illness, Edited by A.C.Brown and R.G.Crounse, Publ. by Proeger Publishers (1980)

39. E.H.S.Burhop and W.N.Asaad, "The Auger Effect", Adv. At. Mol. Physics, 8, (1972), 163-284

40. T.A.Cahill, R.G.Flochini, P.J.Feeney and D.J.Shadoan, Comparison of equal-velocity ion beam for elemental analysis by ion excited x-ray emission, Nucl. Inst. Meth. 120, (1974), 193-195

41. T.A.Cahill, New uses of ion accelerators, Ed. J.F.Ziegler Plenum, New York, (1975), 1-71

42. J.L.Campbell, B.H.Orr, A.W.Herman, L.A.McNelles, J.A.Thompson and W.C.Brian, Trace element analysis of fluids by PIXE fluorescence spectrometry, Anal. Chem. 47, (1975), 1542-1553

43. J.L.Campbell, Specimen preparation in PIXE analysis Nucl. Inst. Meth. 142, (1977), 263-273

44. J.L.Campbell, S.B.Russell, S.Faign, C.W.Schulte, R.W.Olterhead and R.R.Gingerich, Optimization of PIXE sensitivity for biomedical applications, Nucl. Inst. Meth., 181, (1981), 285-292

45. E.M.Carlisle, Silicon: a possible factor in bone calcification, Science. 167, (1970), 279-280

46. Caroline M.Shreeve, A state of perpetual motion hyperactivity, World Medicine, May 1 (1982), 87-93

47. M.A.Chandhri and A.Crawford, A simple method for elimination of charging, and for current integration in PIXE analysis of thick insulating samples, Nucl. Inst. Meth., 181, (1981), 31-35

48. J.R.Chen and J.M.Anderson, Legionnaires disease: Concentrations of Se and other elements, Science, Vol.206, (1979), 1426-1427

49. J.R.Chen, An application of PIXE in medicine; Legionnaires disease, Nucl. Inst. Meth., 181 (1981), 337-343

50. T.C.Chu, V.R.Navarrete, H.Kaki, G.Izama, T.Shiokawa, K.Isha, S.Morita and H.Tawara, A study of proton induced x-ray analysis and its application to environmental samples, J. Radional Chem. 36, (1977), 195-207

51. F.H.Chung, A new approach to quantitative multi-elemental fluorescence analysis, Adv. X-rays Anal. 19, (1978), 181-190

52. J.A.Cookson and F.D.Pilling, Trace element distribution across the diameter of human hair, Phys. Med. Biol. Vol.20 No.6, (1975), 1015-1020

53. J.A.Cookson, The production and use of a nuclear microprobe ions at MeV energies, Nucl. Inst. Meth, 165, (1979), 477-508

54. J.A.Cookson, The use of the PIXE technique with nuclear microprobes, Nucl. Inst. Meth. 181, (1981), 115-124

55. G.C.Cotzias, Trace Subs. Environ. Health-Proc. Univ. Mo Anna Conf. 1st (1967)

56. C.B.Crane, J. Dent. Res. 39, (1960), 704

57. L.A.Curie, Limitation for quantitative detection and quantitative determination, Anal. Chem., Vol.40, (1968), 586-593

58. R.E.Davies, B.L.Reid, A.A.Kurnick and J.R.Couch, The effect of sulfate on molybdenum toxicity in the Chick, J. Nutr., 70, (1960), 193-198

59. I.J.L.Davies, The clinical significance of the essential biological metals, William Heinmann Medical Books Ltd., London (1972)

60. O.L.Davies and P.L.Goldsmith, Statistical methods in research and production, Publisher for Imperical Chemical Industries Limited by Oliver and Boyd, Edinburgh, U.K. (1972)

61. S.B.Deeming and C.W.Weber, Evaluation of hair analysis for determination of Zn status using rats, Am. J. Clin. Nutr. 30, (1977), 2047-2052

62. S.B.Deeming and C.W.Weber, Hair analysis of trace minerals in human subjects as influenced by age, sex, and contraceptive drugs, Am. J. Clin. Nutr., 31, (1978), 1175-1180

63. A.T.Dick, D.W.Dewey amd J.M.Gawthorne, J. Agric. Sci. Camb., 85, (1975), 567-568

64. E.A.Eads and C.E.Lambdin, A survey of trace metals in human hair, Env.-Research., 6, (1973), 247-252

65. J.Erten, A.Arcasoy, A.R.Cavdar and S.Cin, Hair Zn levels in healthy and malnourished children, Amer. J. Clin. Nutr., 31, (1978), 1172-1174

66. F.Folkmann, C.Gaards, T.Huus and K.Kemp, Proton induces x-ray as a tool for trace element analysis, Nucl. Inst. Meth. 116, (1974a), 487-499

67. F.Folkmann, J.Borggreen and A.Kjeldgaard, Sensitivity in trace analysis by P, , and O induced x-rays, Nucl. Inst. Meth. 119, (1974b), 117-123

68. F.Folkmann, Analytical use of ion induced x-rays J. Phys. E.8, (1975), 429-444

69. F.Folkmann, Ion beam surface layer analysis, Eds. O.Mayer, G.Linker and F.Kappeler, Plenum, New York, Vol.2 (1976)

70. L.E.Feinendeger and K.Kasperek, Medical aspects of trace element research, Trace element analytical chemistry in medicine and biology, Eds. P.Bratter, P.Schramel, 1-36, 1980.

71. R.W.Fink, R.C.Jopson, H.Mark and C.D.Swift, Atomic fluorescence yields, Rev. Mod. Phys. 38, (1966), 513-540

72. La Fleur, Biological matrix Standard Reference Materials for trace element determinations, J. Radional Chem. 19, (1974), 227-232

73. R.G.Flochini, P.J.Feeney, R.J.Sommerville and T.A.Cahill, Sensitivity versus target backing for elemental analysis by alpha excited x-ray emission, Nucl. Inst. Meth. 100, (1972), 397-403

74. H.U.Freund, J.S.Hansen, E.Karthinen and R.W.Fink, Proc. Intern. Conf. Radioactivity in Nuclear Spectroscopy, Nashville, Golden and Breach Publ., New York, (1972)

75. G.Friedlander, J.W.Kennedy, E.S.Macias and J.M.Miller, Nuclear and Radiochemistry 3rd Edition, John Wiley and Sons Inc. (1981)

76. J.D.Garcia, Inner shell ionization by proton impact, Phys. Rev. A1, (1970), 280-285

77. J.D.Garcia, R.J.Fortner, T.M.Kavanagh, Inner shell vacancy production in Ion Atom collisions, Rev. Mod. Phys. 45, (1973), 111-177

78. R.P.H.Garten, K.O.Groeneveld and K.H.Kong, A semiempirical procedure for the simple calculation of the signal intensity in PIXE analysis of thick samples, Nucl. Inst. Meth. 181, (1981), 185-188

79. J.V.Gilfrich, P.G.Burkhalter and L.S.Birks, X-ray spectroscopy for particulare air polution - A quantitative comparison of techniques, Anal. Chem. 45, (1973), 2002-2009

80. J.Glazur, L.Jarczyk, E.Rokita, D.Stominska, A.Strzalkowski and M.Sych, A PIXE method for investigating the time changes of holothane content during anaesthesia, Nucl. Inst. Meth, 181, (1981a) 315-317

81. J.Glazur, L.Jarczyk, E.Rokita, D.Stominska, A.Strazalkowski and M.Sych, Determination of circulating blood volume using PIXE, Nucl. Inst. Meth. 181, (1981 b), 319-321

82. B.M.Gordon and H.W.Kraner, On the development of a system for trace element analysis in the environment by charged particle x-ray fluorescence, J. Radional. Chem. 12, (1972), 181-188

83. T.T.Gorsuch, The destruction of organic matter, Pergamon Press (1970)

84. F.S.Goulding, Some aspects of detectors and electronics for x-ray fluorescence analysis, Nucl. Inst. Meth. 142, (1977), 213-223

85. F.S.Goulding and J.M.Jaklevic, XRF analysis - some sensitivity comparison between charged particle and photon excitation, Nucl. Inst. Meth., 142, (1977), 323-332

86. R.J.Grader, R.W.Hill, C.W.McGoff, D.S.Salim and J.P.Stoering, Rev. Sci. Instr., 42, (1971) 499

87. L.Grodzins, P.Horowitz and J.Ryan, Proc. Conf. on Sci. and Indust. Appl. of small accs. Denton, Eds. J.L.Duggan and I.L.Morgan (IEEE, New York, 1976)

88. D.J.Hammer, J.F.Finklea, R.H.Hendricks, C.M.Sly, R.J.M.Horton: Hair trace elemental levels and environmental exposure, Am. J. Epidemiol, 93, (1972), 84-92

89. J.S.Hansen, Formulation of BEA in configuration space and its application to ionization by light ions, Phys. Rev. A8, (1973), 822-839

90. J.S.Hansen, J.C.McGeorge, D.Nix, W.D.Schmitt-ott, I.Uhus and R.W.Fink, Accurate efficiency calibration and properties of semiconductor detectors for low energy photons, Nucl. Inst. Meth. 106, (1973), 365-379

91. J.M.Hansteen and O.P.Mosebekk, Atomic Coulomb agitation by heavy charged particles, Nucl. Phys. A 201, (1973), 541-560

92. J.M.Hansteen, Advances in atomic and nuclear physics Eds. D.R.Bates and B.Bederson, Academic, New York, (1975), Vol.II

93. K.M.Hambidge, F.L.Franklin and M.A.Jacobs, Hair Chromium concentration: Effects of sample washing and external environment, Amer. J. Clin. Nutr. 25, (1972), 384-389

94. E.C.Henley, The Florida State University School of Home Economics, Ph.D. Thesis (1976)

95. E.C.Henley, M.E.Kassouny and J.W.Nelson, Proton induced x-ray emission analysis of single human hair roots, Science, 197, (1977), 277-278

96. A.W.Herman, L.A.McNelles and J.L.Campbell, Target backing for charged particle induced x-ray fluorescence analysis, Nucl. Inst. Meth. 109, (1973 a), 429-437

97. A.W.Herman, L.A.McNelles and J.L.Campbell, Choice of physical parameters in charged particle induced x-ray fluorescence analysis, Int. J. Appl. Radiat. Isot. 24, (1973 b), 677-688

98. J.Hertogen, J.De Doner and R.Gijbels, Experimental data of photo peak integration methods in activation analysis, Nucl. Inst. Meth. 115, (1974), 197-212

99. M.W.Hill, N.F.Mangelson and J.F.Ryder, Proc. 4th Conf. on nuclear mathods in environment and energy research, Colombia (1980)

100. J.S.Hislop, Choice of the analytical method, Trace element analytical chemistry in medicine and biology (1980), Editors P.Bratter and P.Scharamel, Walter de Gruyter

101. H.C.Hopps, The biological basis for using hair and nails for analysis of trace elements, Sci. Tot. Environ. 7, (1977), 71-78

102. P.Horwitz, M.Aronson, I.Grodzins, W.Ladd, J.Ryan, G.Marriam and C.Lechene, Elemental analysis of biological specimens in air with a proton microprobe, Science, 194 (1976), 1162-1165

103. J.P.Houtman, M.de Bruin, J.J.M.de Goeij and P.S.Tjioe, Proc. Int. Symp. Nucl. Activ. in Life Science, Vienna, IAEA (1978)

104. J.H.Hubbell, W.H.McMaster, N.Kerr Del Grand and I.H.Mallett, International Tables for X-ray Crystallography (Kynoch Press Birmingham (1974) Vol.4).

105 W.Huda, Proton induced x-ray fluorescence of thick samples in air for trace element analysis, Nucl. Inst. Meth. 158, (1979), 587-594

106. K.Ishii, S.Morita, H.Tawara, T.C.Chu, H.Kaji and T.Shiokawa, Quantitative trace element analysis by proton induced x-rays, Nucl. Inst. Meth. 126, (1975), 75-80

107. J.M.Jaklevic and F.S.Goulding, Semiconductor detector x-ray fluorescence spectrometry applied to environmental and biological analysis, IAEA, Trans. Nucl. Sci., NS-19, No.3, (1972), 384-391

108. J.M.Jaklevic and R.L.Walter, X-ray fluorescence analysis of environmental samples, Ed. T.G.Dgubay (Ann Arbor Science, Ann Arbor Mich., (1977), 63).

109. J.M.Jaklevic and F.S.Goulding, Practical spectroscopy V.2, x-ray spectrometry by H.K.Herglotz and L.S.Birks (1978)

110. G.N.Jenkins,
J. Dent. Res. 42, (1963), 1102

111. C.Jian-Xin, G.Yuan-Zhuang, L.Hong-Kou, R.Chi-gang, T.Guo-Lun, W.Xi-de, Y-Fu-Chia, Trace element analysis of human hair by PIXE, Nucl. Inst. Meth. 181, (1981), 269-273

112. T.B.Johansson, R.K.Akselsson and S.A.E.Johansson, X-ray analysis elemental trace analysis at the 10 g level, Nucl Inst. Meth. 84, (1970), 141-143

113. T.B.Johansson, R.Akselsson and S.A.E.Johansson, Proton induced x-ray emission spectroscopy in elemental trace analysis, Adv. in X-ray Anal. Vol.15, (1972), 373-387

114 T.B.Johansson, R.E.Van Grieken, J.W.Nelson and J.W.Winchester, Elemental trace analysis of small samples by proton induced x-ray emission, Anal. Chem. 47, (1975), 855-860

115. S.H.Johansson and T.B.Johansson, Analytical application of particle induced x-ray emission, Nucl. Inst. Meth. 137, (1976), 473-516

116. T.Johannesson,G.Lunde and E.Steinnes, Mercury, arsinic, cadmium, selenium and zinc in human hair and salmon fries in Iceland, Acta. Pharmacol et Toxical, 48, (1981), 185-189

117. R.K.Jolly, G.Randers-Pherson, S.K.Gubta, D.C.Buckle and H.Aceto Jr., Process of 3rd Conference on application of small accelerators, Texas, Vol.I, (1974), 203-208.

118. R.K.Jolly, J.R.Knae, D.C.Buckle, G.Randers-Pherson, W.Teoh and H.A.Ceto, A target chamber or PIXE analysis using microampere beams, Nucl. Inst. Meth. 142, (1977), 231-242

119. D.Y.Jones, M.E.Kassouny, H.C.Kaufmann and J.W.Nelson, Hair growth phase and mineral content of hair root determined by accelerator techniques, Fe. Proc. 38, (1979), 712.

120. R.C.Jopson, H.Mark and C.D.Swift, Production of characteristic x-rays by low energy protons Phys. Rev. 127, (1962), 1612-1618

121. H.H.Jorch and J.L.Campbell, On the analytic fitting of full energy peaks from Ge(Li), and Si(Li) photon detector, Nucl. Inst. Meth. 143, (1977) 551-559

122. H.Kaji, T.Schickawa, K.Ishi, S.Morita, M.Kamiya, K.Sora and H.Tawara, Application of proton induced x-ray emission to quantitative trace element analysis, Nucl. Inst. Meth. 142, (1977), 21-26

123. M.R.Khan, University of Aston in Birmingham, Ph.D. Thesis (1976).

124. M.R.Khan,A.G.Hopkins and D.Crumpton, Proton induced inner shell ionization, VIII International Conference X-ray Optics and Microanalysis, (1977), 1

125. F.Khan, University of Birmingham, Ph.D. Thesis (1979)

126. M.R.Khan and D.Crumpton, Proton induced x-ray emission analysis Part I and II, CRC, Critical Reviews in Analytical Chemistry, (1981), 103-155 and 161-193

127. M.R.Khan and M.Karimi, K_β/K_α ratios in energy dispersive x-ray emission analysis, x-ray spectrometry, Vol.9, (1980), 32-35

128. L.M.Klevay: Hair as a biopsy material. II assessment of copper nutrition, Am. J. Clin. Nutr. 23, (1970), 284-299

129. G.F.Knoll, Radiation detection and measurement, by John Wiley and Sons Inc. (1979)

130. W.Koening, F.W.Richter, U.Steiner, R.Stock, R.Thielmann and V.Watjen, Trace element analysis by means of particle induced x-ray emission with triggered beam pulsing, Nucl. Inst. Meth. 142, (1977), 225-229

131. W.Koening, F.W.Richter, B.Meinel and J.Chi Bode, Trace element analysis of thin biological tissue samples using PIXE, trace element analytical chemistry in medicine and biology, Walter de Gruyter and Co., Bertin, (1980)

132. L.Kokta, Determination peak area, Nucl. Inst. Meth. 112, (1973), 245-251

133. K.T.Koshy, Revision noted in psychiatry, Hodder and Staughton, London, Second Edition (1982).

134. M.O.Krause, Atomic radiation and radiationless yields for K and L shells, J. Phys. Chem. Ref. Data, Vol.8, No.2, (1979), 307-316

135. H.Kubo, Reproducibility of proton induced elemental analysis in biological tissue sections, Nucl. Inst. Meth. 121, (1974), 541-545

136. M.Laker, On determining trace element levels in man: Lancet, (1982), 260-262

137. J.M.A.Lenihan, Adventure in activation analysis, J. Radional Chem. 48, (1979), 125-134

138. M.D.Levine and F.Oberklaid, Hyperactivity, Amer. J. Dis. Child, 134, (1980), 409-414

139. Ludi et al, Report of the coordinated research meeting, on nuclear based methods for the analysis of pollutants in human hair, C E N - Saclay (IAEA, Vienna, 1978)

140. D.H.Madison and E.Merzbacher, Atomic-inner processes, Vol.I Ionization and transition probabilities, Ed. Bernd Grasemann (1975)

141. N.F.Mangelson, M.W.Hill, K.K.Nielson, R.F.Ryder, Proton induced x-ray emission analysis of biological samples: some approaches and applications, Nucl. Inst. Meth., 142, (1977), 133-142

142 N.F.Mangelson and M.W.Hill, Recent advances in particle induced x-ray emission analysis applied to biological samples, Nucl. Inst. Meth. 181, (1981), 243-254

143. N.A.Marcilese, C.B.Ammerman, R.M.Valsecehi, B.G.Dunarant, G.K.Davies, J. Nutr. 99, (1969), 177-183, Effect of dietary molybdenum and sulfate upon copper metabolism in sheep

144. J.M.McKenzie, Alteration of Zn and Cu concentrations in hair, Am. J. Clin. Nutr. 27, (1974) 505-514

145. L.A.McNelles and J.L.Campbell, Analytical approximations to peak shapes produced by Ge(Li) and Si(Li) spectrometers, Nucl. Inst. Meth. 127, (1975), 73-81

146. W.Meanhaut, L.de Reu, H.A.Van Rinsvelt, J.Cafmayer and P.Van Espin, Particle induced x-ray emission (PIXE) analysis of biological materials: Precision, accuracy and application to cancer tissues, Nucl. Inst. Meth. 168, (1980), 557-562

147. E.Merzbacher and W.H.Lewiss, X-ray production by heavy charged particles, S.Flugg, Ed. Bertin: Spring Verlay (1958)

148. D.S.Miller, Proc. Nutr. Soc. 38, (1979), 197.

149. C.F.Mills, J.Quarterman, J.K.Chesters, R.G.Williams and A.C.Dalgarno, Metabolic role of Zn, Am. J. Clin. Nutr. 22, (1969), 1240-1249

150. L.Ming Chien, Chang Kong-Long, Chin Po-Kang, Chen Zhi-Ziang, Wong Xue-Peng, Chin Jun-Fa, Rong Ting-Wen, Tan Min-Guang and Xu Yao-Liong, A complete automated PIXE analysis system and its application, Nucl. Inst. Meth., 181, (1981 a), 37-41

151. L.Ming Chien, Chang Kong-Long, Chin Po-Kang, Chen Zhi-Xiang, Wong Xue-Peng, Chin Jun-Fa, Rong Ting-Wen, Tan Ming-Guang and Xu Yao-Liong, PIXE analysis of human serum, Nucl. Inst. Meth. 181, (1981 b), 309-313

152. H.Mommsen, K.G.Bauer and Q.Faziy, Sensitivity of high energy PIXE bulk analysis, Nucl. Inst. Meth. 157, (1978), 305-309

153. E.C.Montenegro, G.B.Baptista and P.W.E.P.Duarte, K and L x-ray mass attenuation coefficients for low-z materials, At. Data. and Nucl. Data Tables. Vol.22, No.2, (1978), 131-177

154. E.C.Montenegro, G.B.Baptista, A.S.Baschoa and C.V.Barros Leite, Uncertainties in elemental quantitative analysis by PIXE, Nucl. Inst. Meth. 159, (1979 a), 153-156

155. E.C.Montenegro, G.B.Baptista, C.V.Barros Leite, A.G. de Pinho and S.Paschoa, Study of a proton beam diffusing system for PIXE analysis, Nucl. Inst. Meth. 164, (1979 b), 231-234

156. E.C.Montenegro, G.B.Baptista, L.V.de Castro Faria, and A.S.Paschoa, Correction factor for hair analysis by PIXE, Nucl. Inst. Meth. 168, (1980) 479-483

157. T.H.Maugh, Hair: A diagnostic tool to complement blood, serum and urine, Science, Vol. 202, (1978), 1271-1273

158. T.Mukoyama, Fitting of gaussian to peaks by non-iterative method, Nucl. Inst. Meth. 125, (1975), 289-291

159. T.Mukoyama, Anon - Iterative method for fitting of overlapping guassian peaks, Nucl. Inst. Meth. 180, (1981), 553-556

160. K.K.Nielson, Bingham Young University, Ph.D., (1975)

161. K.K.Nielson, M.W.Hill, N.F.Mangelson and F.W.Nelson, Elemental analysis of obsidean artifacts by proton induced x-ray emission, Anal. Chem. 48, (1976), 1947-1950

162. S.P.Nygaard and J.C.Hansen, Mercury-selenium interaction of concentrations of selenium and mercury vapours as prevalent in nature, Bull, Environ. Contam. toxical, 20, (1978), 20-23

163. B.L.O'Dell, Biochemistry and physiology of copper in vertebrates, in trace element in human health and disease - Zn and Cu, A.S.Prasad Ed. Vol.I, Academic, New York (1976), 381-413

164. P.S.Ong, P.K.Lund, C.E.Litton and B.A.Mitchell, Energy dispersive and system for the analysis of trace elements in human blood serum, Adv. x-ray anal., 16, (1974), 124-133

165. J.Pallon and K.G.Malmqvist, Evaluation of low temperature ashing of biological materials as a preconcentration method for PIXE analysis, Nucl. Inst. Meth., 181, (1981), 71-75

166. C.S.Papper, M.A.Chaudhri and J.L.Rouse, Elementation of charging in the PIXE analysis of thick biological samples, Nucl. Inst. Meth. 154, (1979), 219-221

167. J.Parizek, J.Kalouskora, A.Babicky, J.Benes and L.Povlik, Interaction of Se with Hg, Ca and other toxic metals, in trace element metabolism in animals, W.G.Hoekstra, I.W.Suttie, H.E.Ganthey, W.Mertz, Eds. (1974), 119-131

168. B.K.Patnaik and N.G.Dhere, Trace elemental analysis in thick targets by charged particle induced x-rays, Nucl. Inst. Meth. 131, (1975), 503-509

169. H.G.Petering, D.W.Yeager and S.O.Witherup, Trace metal content of hair : I Zn and Cu content of human hair in relation to age and sex, Arch. Env. Health, 23, (1971), 202-207

170. R.O.Pihl, H.Drake and F.Vrane, Hair analysis in learning and behaviour problems, Hair trace elements and human illness (1980), 128-143, A.C.Brown, R.G.Crounse, Eds. Praeger, New York

171. A.S.Prasad, Trace elements in human health and disease, Academic Press, New York (1976)

172. A.S.Prasad and D.Oberleas, Trace elements in human health and disease, Academic Press (1976)

173. P.A.Prasad, Trace element and iron in human metabolism, John Wiley and Sons (1978), U.S.A.

174. M.Rechcigle: Handbook of nutrition and food, Nutritional disorders III, Chemical Rubber Co., Cleveland, Ohio (1978)

175. R.D.Reeves, K.W.Jolley and P.D.Buckley, Lead in human hair: relation to age, sex, and environmental factors Env. Contam. and toxical, 14, (1975), 579-587

176. D.Rendic, S.Holjevic, V.Valcovic, Z.H.Zobel and G.C.Phillips, Trace element concentrations in human hair measured by proton induced x-ray emission, J. of Invest. Dermatol 66, (1976), 371-375

177. W.Reuter, A.Lurio, F.Gardone and J.F.Ziegler, Quantitative analysis of complex targets by proton induced x-rays, Journal of applied phys. Vol.46, No.7, (1975), 3194-3202

178. F.W.Richter and U.Watjen, PIXE calibration and correction of matrix effect in the case of thick samples, Nucl. Inst. Meth. 181, (1981), 189-194

179. G.Robaye, G.Weber, J.M.Delbrouck-Habarn, M.C.Depauw, Use of liposomes to reduce enhancement-absorption effects in PIXE, Nucl. Inst. Meth. 172, (1980) 535-539

180. G.Robaye, G.Weber, J.M.Delbrouck, I.Roelandts, P.Bortsch and A.Collignon, Attempt to improve PIXE quantitative trace element analysis of biomedical materials, (1981), 181, 59-62

181. B.L.Roberts, R.A.J.Riddle and G.T.A.Squier, Measurements of Lorentzian line widths, Nucl. Inst. Meth., 130, (1975), 559-563

182. F.A.J.De Rooij, H.P.M.Kivits, C.A.M.Castelijns, G.P.J.Wijnhoven and J.J.M.De Goeij, Target preparation techniques for PIXE and XRF, Nucl. Inst. Meth. 181, (1981), 63-67

183. S.B.Russell, R.S.Gibson, S.Faig and J.L.Campbell, proton backscatter as a means of mass normalisation in PIXE scanning of human hair, Nucl. Inst. Meth. 181, (1981 a), 97-98

184. S.B.Russell, C.W.Schulte, Shatha, Falq and J.L.Campbell, Specimen backing for proton induced x-ray emission analysis, Anal. Chem. Vol.53, (1981 b), 571-574

185. Yu,S.Ryabukhin, International coordinated program an activation analysis of trace elements pollutants in human hair, trace elements and human illness, New York Praeger (1980)

186. S.O.Saied, D.Crumpton, P.E.Francois, The validation of a PIXE system for trace element analysis of biological sample, Nucl. Inst. Meth. 181, (1981), 53-57

187. S.O.Saied, Ph.D. Thesis, University of Aston in Birmingham (1981)

188. S.I.Salim, S.L.Paussion, R.A.Krause, Experimental K and L relative x-ray emission rates, Atomic data and Nuclear data tables, 14, (1974), 91-109

189. J.Scheer, L.Voet, U.Watjen, W.Kaening, F.W.Richter and U.Steiner, Comparison of sensitivity in trace element analysis obtained by x-ray excited x-ray fluorescence and proton induced x-ray emission, Nucl. Inst. Meth., 142, (1977), 333-338

190. H.A.Schroeder and A.P.Nason, Trace metals in human hair, J. Invest. Derm. 53, (1969), 71-78

191. K.Schwarz, New essential trace elements (Sn, V, F, Si). Progress report and outlook in "trace element metabolism in animals - 2" W.G.Hoekstra, J.W.Suttie, H.E.Gauther, W.Mertz, Eds., (1974), University Park, Baltimore, 355-380

192. J.H.Scofield, Exchange correlations of K x-ray emission rates, Phys. Rev. A9, (1974), 1041-1049

193. D.Shapcott and J.J.Hubert, Cr in nutrition and metabolism, Elsevier/North Holand Biomedical Press, Amsterdam (1979)

194. W.S.Snyder, M.J.Cook, E.S.Nasset, L.E.Karhausen, G.P.Howells and I.H.Tipton, Report of the task group on Reference man. Pergamon Press, London (1976)

195. B.Spoelstra, J.P.F.Sellschop, H.J.Annegarn and M.J.Renan, Whole blood analysis of kwashiorkor cases by PIXE, Nucl.Inst. Meth. 181, (1981) 305-308

196. E.Storm and H.I.Israel, Photon cross-section from 1 keV to 100 MeV for elements Z=1 to Z=100, Nucl. Data tables, A7, (1970), 563-681

197. Y.Takeda, M.Kitamuza, K.Kawasa and K.Sugiyama, A study of effect of fitting functions on results of -ray peak analysis, Nucl. Inst. Meth, 136, (1976), 369-371

198. C.J.Umberger, R.C.Bearse, D.A.Close and Malanify, Sensitivity and detectability limit for elemental analysis by proton induced x-ray fluorescence with a 3 MeV Van de Graf. Adv. in x-ray Anal. 16, (1973), 102-110

199. E.J.Underwood, Trace elements in human and animal nutrition, Pub. Academic Press (1977)

200. V.Valcovic, D.Miljanic, R.M.Wheeler, R.B.Liebert, T.Zabel and G.C.Phillips, Variation in trace metal concentration along a single hair as measured by proton induced x-ray emission photometry, Nature, 243, (1973), 543-544

201. V.Valcovic, X-ray emission spectroscopy Part I and II, Contemporary physics Vol.14, No.5, (1973), 415-462

202. V.Valcovic, R.B.Liebert, T.Zabel, H.T.Larson, D.Miljanic, R.M.Wheeler and G.C.Phillips, Trace element analysis using proton induced x-ray emission spectroscopy, Nucl. Inst. Meth, 114, (1974), 573-579

203. V.Valcovic, D.Rendic and G.C.Phillips, Elemental ratios along human hair of indication of exposure to environmental pollution, Env. Sci. Tech., 9, (1975), 1150-1152

204. V.Valcovic, PIXE: applications in medicine, Nucl. Inst. Meth., 142, (1977), 151-158

205. Van Der Kam, R.D.Vis and H.Verheul, The influence of matrix on absolute analysis using PIXE, Nucl. Inst. Meth., 142, (1977), 55-60

206. J.B.D.A.Van Zon, J.T.G.M.Hemelaar, J.A.Vander Heide and H.P.M.Kivits, A procedure for optimal determination of trace elements with PIXE Nucl. Inst. Meth. 181, (1981), 49-52

207. J.Versieck, J.Hoste, F.Barbier, H.Steyaert, J.de Rudder and H.Michels, Determination of Cr and Co in human serum by neutron activation analysis, Clin. Chem. 24, (1978), 303-308

208. R.D.Vis, P.M.A.Van Der Kam and H.Verheul, Elemental trace analysis in serum using proton induced x-ray fluorescence. Nucl. Inst. Meth. 142, (1977) 159-162

209. R.L.Walter, R.D.Willis, G.F.Gutknecht and J.M.Joyce, Analysis of biological clinical and environmental samples using proton induced x-ray emission, Anal. Chem. 46, (1974), 843-855

210. D.R.Weaver, Information for users of the Birmingham Radiation Centre, Paper No.BRC-76/01. (1980)

211. G.Weber, G.Robaye, J.M.Delbrouck, I.Roelandts, O.Didberg, P.Bartsch and M.C.De Pauw, Biomedical application of PIXE in University of Liege Nucl. Inst. Meth. 168, (1980) 551-556

212. S.Welsh, Physiological effects of methyl mercury toxicity: Interaction of methyl mercury with selenium, tellurium and vitamin E. University of Maryland (1974)

213. N.E.Whitehead, Methods of hair analysis by (p, x) spectrometry, Nucl. Inst. Meth., 164, (1979) 381-388

214. R.D.Willis, Ph.D. Thesis, Duke University (1977)

215. R.D.Willis, R.L.Walter, R.W.Shaw and W.F.Gutknedit, Proton induced x-ray emission analysis of thick and thin targets, Nucl. Inst. Meth. 142, (1977), 67-77

216. R.D.Willis and R.L.Walter, Computer analysis of proton induced x-ray emission spectra, Nucl. Inst. Meth. 142, (1977), 231-242

217. R.Woldseth, X-ray energy spectrometry, Kevex, Burlinghams, (1973)

218. A.A.Yunice, Serum copper in relation to age, Ultratrace metal analysis in biological sciences and environment, T.H.Risby Edit. American Chemistry Society, Washington (1979)

Addendum

R.H.Miller and J.R.Greening, Experimental x-ray mass attenuation coefficients for materials of low atomic number in the energy range 4-25 keV, J.Phys. B7, (1974), 2332-2354

E.A.Sheared, M.W.Jonson and R.J.Carter, The determination of chromium in hair and other biological materials, Hair trace elements and human illness, edited by A.C.Brown, R.G.Crounse, Pub. by Praeger Publishers (1980).